Parallel Force Assay for Protein Interactions

Daniela Solveig Raphaela Aschenbrenner

München 2015

Parallel Force Assay for Protein Interactions

Daniela Solveig Raphaela Aschenbrenner

Dissertation
an der Fakultät für Physik
der Ludwig–Maximilians–Universität
München

vorgelegt von
Daniela Solveig Raphaela
Aschenbrenner
aus München

München, den 4. März 2015

Erstgutachter: Prof. Dr. H. Gaub
Zweitgutachter: Prof. Dr. T. Liedl
Tag der mündlichen Prüfung: 24. April 2015

Zusammenfassung

Der Schlüssel zur biologischen Funktion eines Proteins liegt in dessen Interaktion mit anderen Molekülen. Da Proteine für die meisten Prozesse verantwortlich sind, die in der Zelle stattfinden oder von ihr durchgeführt werden, wird die Untersuchung dieser Interaktionen dazu beitragen, die komplexen Abläufe biologischen Lebens zu entschlüsseln. Um die Interaktionen von Proteinen mit unterschiedlichen Biomolekülen sowohl identifizieren als auch genauer charakterisieren zu können, ist eine Vielzahl an interdisziplinären Verfahren entwickelt worden. In diesem Zusammenhang sind verschiedene physikalische Methoden entstanden, die eine Bestimmung der Kräfte erlauben, welche die Interaktionen von Proteinen auf Einzelmolekülebene kontrollieren. Das bekannteste Beispiel hierfür ist das Rasterkraftmikroskop (AFM). Betrachtet man die große Anzahl an Proteinen und somit potentieller Interaktionen, stellt der meist geringe Durchsatz dieser Methoden einen Nachteil dar. Die Technik des *Molecular Force Assay* (MFA) hingegen ermöglicht eine Parallelisierung von Einzelmolekülmessungen. Dieses Verfahren bestimmt die mechanische Stabilität eines molekularen Komplexes durch den Vergleich mit einem bekannten Referenzkomplex und wurde bereits zur Untersuchung von Fehlstellen in DNA oder Protein-DNA Interaktionen angewandt. In der vorliegenden Arbeit wurde das Prinzip des MFA angepasst und weiterentwickelt, um die Untersuchung von Protein-Interaktionen nicht nur mit DNA, sondern auch mit RNA sowie anderen Proteinen zu ermöglichen.

Die erste Studie dieser Arbeit demonstriert die grundsätzliche Fähigkeit des MFA, die Bindung von RNA-Liganden sowie die selektive Hemmung der Aktivität des Proteins Dicer durch diese Liganden effektiv zu testen. Das Nukleaseprotein Dicer ist ein Schlüsselelement der RNA Interferenz. Durch das Schneiden von Vorgängermolekülen aus doppelsträngiger RNA aktiviert Dicer kleine regulative RNAs. Die Identifikation von kleinen Molekülen, die als Liganden für spezifische regulative RNAs den Aktivierungsprozess durch Dicer hemmen können, bietet einen vielversprechenden Ansatz für zukünftige Therapien, da erhöhte Werte regulativer RNA mit schweren Krankheiten in Verbindung gebracht werden. Um Protein-Protein-Interaktionen mit der MFA Technik messen zu können, müssen kovalent gekoppelte Protein-DNA Chimäre hergestellt werden. Im Rahmen dieser Arbeit wurde dafür das ybbR-tag/Sfp System als Methode mit sehr hoher Effizienz sowie spezifisch lokalisierbarer Anbindung identifiziert. Diese Chimäre sind auch für viele andere Anwendungen der Bio-Nanotechnologie nützlich, wie beispielsweise für die kontrollierte Anordnung von Proteinen mit Hilfe der *Single-Molecule Cut & Paste* Technik, die eine Genauigkeit im Angström-Bereich erreicht. Anhand des Model-

systems der Bindung des Nanobodies Enhancer an verschiedene Varianten von GFP wird die Charakterisierung von Protein-Protein-Interaktionen mit der MFA Technik demonstriert. Die mechanische Stabilität des Proteinkomplexes wird hierbei mit einem bekannten DNA Referenzkomplex verglichen, der als Kraftsensor dient. Die Unterschiede in der Stabilität der verschiedenen Enhancer-GFP-Komplexe können Veränderungen in den Aminosäuren zugeschrieben werden, die gemäß der Kristallstruktur lokal wechselwirken. Im Allgemeinen ist die Sensitivität der MFA Technik höher, je ähnlicher die mechanische Stabilität der beiden Komplexe ist, die verglichen werden. Da die Proteinkomplexe in diesem Fall eine höhere Stabilität als ein 40 Basenpaare langer DNA Duplex aufweisen, wird die mechanische Stabilität der DNA sowohl intern durch Basenmodifikationen sowie durch die Bindung von externen Liganden erhöht. Dies erlaubt es, die Sensitivität für dieses Modellsystem zu maximieren und erweitert den dynamischen Bereich der Technik für zukünftige Untersuchungen von Protein-Protein-Interaktionen enorm. Mithilfe der komplementären Techniken MFA und AFM kann die interne Stabilisierung von DNA Komplexen durch Pyrimidinbasen, die mit einer Propynylgruppe modifiziert sind, näher untersucht werden. Die Studie zeigt, dass der Stabilisierungseffekt durch die Propynylbasen sehr stark von der Zeit und Temperatur der Inkubation des DNA-Doppelstrangs abhängig ist.

Zusammenfassend zeigt die vorliegende Arbeit, dass die MFA Technik nicht nur ein wertvolles Instrument für die Untersuchung von DNA-Mechanik ist, sondern auch die parallelisierte und kraftbasierte Charakterisierung von Proteininteraktionen mit verschiedenen Biomolekülen ermöglicht.

Abstract

A protein's biological function is reflected in the interactions it forms with other molecules. Proteins can be regarded as the workhorses of the cell and are involved in most tasks performed in and by the cell. Investigation of these interactions will thus contribute to decipher the complex processes of biological life. Due to the variety of biomolecules with which proteins can interact, a range of interdisciplinary methods have been developed to identify and characterize these interactions. Different physical techniques have evolved that are able to determine the forces that control protein interactions on a single-molecule level, the most prominent example being the atomic force microscope (AFM). A common drawback of these techniques is their low troughput contrasting with the excessive number of proteins and thus possible interactions. A method that allows for the parallelization of single-molecule measurements is the Molecular Force Assay (MFA). This technique determines the mechanical stability of a molecular complex by comparing it to a known reference complex and has been applied *e.g.* to the investigation of DNA mechanics and protein-DNA interaction. In the present thesis, the principle of the MFA is adapted and developed further to enable targeting of protein interactions with the other major classes of biomolecules besides DNA, namely RNA and other proteins.

The ability of MFA to act as a screening assay for the binding of RNA ligands and the selective inhibition of the activity of protein Dicer by these ligands is demonstrated in a proof-of-principle study. The nuclease Dicer is a key element of the RNA interference pathway as it matures small regulatory RNAs by cleaving their precursor molecules into pieces. The identification of small molecule ligands for specific regulatory RNAs that are able to interfere with Dicer cleavage can pave the way for future therapies, as elevated levels of such matured functional RNAs have been related to severe diseases. In order to measure protein-protein interactions with the MFA, covalently coupled protein-DNA chimeras have to be generated. Here, the ybbR-tag/Sfp system has been identified to provide very high efficiency and variable site-specificity. Those chimeras are useful for many other applications in bionanotechnology, such as for the controlled arrangement of proteins at angstrom level by Single-Molecule Cut & Paste. With the model system of the nanobody Enhancer binding to different variants of GFP, the adaption of the MFA technique for the characterization of protein-protein interactions is established. The mechanical stability of the protein complex is hereby compared to a

known DNA reference duplex acting as the force sensor. The different stabilities of the respective Enhancer-GFP complexes can be attributed to alterations in the amino acids that form contacts according to data from crystal structures. In general, the sensitivity of the MFA is dependent on the similarity of mechanical stability of the complexes that are compared. As the protein complexes in this case have a higher stability than a 40 base pair DNA duplex, the DNA's mechanical stability is increased internally by base modifications as well as by binding of external ligands. This allows to adjust the window of maximum sensitivity for this model system and broadens the dynamic range of the assay tremendously for future investigations of protein-protein interactions. A study with the complementary techniques of MFA and AFM investigates the stabilization of DNA complexes harboring pyrimidines internally modified with an additional propynyl group. The stabilization effect is found to depend strongly on time and temperature of the incubation of the DNA duplex.

In summary, this thesis demonstrates that the MFA is not only a valuable tool for the investigation of DNA mechanics but also capable of quantifying protein interactions with different biomolecules in a parallel and force-based manner.

Contents

1 Introduction

The knowledge about the complex biological processes governing the animate world has grown tremendously over the last decades. After milestones such as the discovery of the double-helix structure of DNA in 1953 [1] or the central dogma of molecular biology [2, 3] stating the direction of information flow in the cell - from DNA over RNA to functional proteins - the interdisciplinary efforts of the human genome project even allowed to decipher the human gene code in 2003. In the era of post-genomics, focus is shifting towards identifying the function of the proteins that are synthesized according to the information in the genes. Proteins can be regarded as the workhorses of the cell and are responsible for most processes conducted in or by the cell. As a protein's functionality is reflected in its interaction with other molecules, much of its function can be predicted from the identification of its interacting partners and the characterization of its location in the cell [4, 5], giving rise to the study of interactomes and proteomes. Considering the excessive number of proteins and thus possible interactions with nucleic acids or other proteins, the most promising approach to identify, understand and possibly influence the processes governed by proteins is a combination of interdisciplinary techniques. A large variety of approaches have been developed to target the interaction of proteins with their different, specific ligands. Among many others, examples are chromatin immunoprecipitation [6] for protein-DNA interaction, RNA pull-down assays [7] for protein-RNA interaction or yeast-two-hybrid assays [8] for protein-protein interaction. A generic difficulty in studying proteins in comparison to nucleic acids arises from the infeasibility of easy amplification of proteins for analysis. Additionally, proteins are in general not able to recover their native structure after denaturation. While some techniques focus on the high-troughput identification of interactions, others address the properties of the interactions in more detail. In recent years, physical approaches have been developed that allow for the determination of the forces governing inter- and intramolecular interactions on a single-molecule level. Besides optical tweezers [9], the atomic force microscope (AFM) [10] is hereby the most widely used technique. The AFM allows to measure forces in the piconewton range between a very sharp cantilever tip and a surface, and was originally developed to image the topology of surfaces. In order to detect interaction forces in biological systems, the molecule or interacting molecular complex in question can be clamped between surface and tip. Retraction of the cantilever yields a force load on the molecule(s), which is detected *via* cantilever deflection. From the resulting force-extension curve, different informations such

as the most probable rupture force of an interaction between two molecules or the unfolding of protein domains can be deduced. This principle has already been applied successfully to study different protein-ligand interactions [11, 12, 13] as well as other biological questions such as protein unfolding [14] or the elastic and mechanical behavior of double-stranded DNA [15, 16]. Drawbacks the AFM technique shares with other single-molecule approaches are the high effort needed to gather statistically sufficient data sets or the calibration uncertainties that arise due to the difficulty of measuring different interactions in parallel.

In order to overcome the limitation of low throughput in force-based single-molecule experiments, the Molecular Force Assay (MFA) has recently been developed [17]. Relying on the principle of determining the stability of a molecular complex by comparing it to a known reference complex, single-molecule measurements can be conducted in parallel. In detail, the two complexes to be compared are attached in series to form a so-called Molecular Force Probe (MFP) upon which an external force is applied. This force then directly correlates the mechanical stability of both molecular bonds until, statistically, the weaker one ruptures. In one single measurement, thousands of MFPs can be tested in parallel, thus allowing for a statistically relevant conclusion. Additionally, the technique allows for multiplexing of both sample and reference bond for further parallelization. The outcome of the experiment is analyzed *via* a fluorophore attached to the linker between the two complexes, which stays with the intact complex after force load. As the size of the force sensor in this approach is reduced to a single molecular bond, the force resolution is increased significantly in comparison to the techniques with macroscopic sensors such as the cantilever in an AFM measurement, where the resolution is limited due to thermal fluctuations. Choosing the reference complex to be as close as possible in mechanical stability to the sample complex optimizes the force resolution, allowing the MFA to detect for example single base pair mismatches [17]. MFA has further been applied *e.g.* to detect the binding of small molecule ligands to DNA [18] as well as for the characterization of protein-DNA interaction [19].

The scientific scope of this thesis was to extend and adapt the principle of parallelized force-based MFA measurements towards the characterization of protein-RNA interaction as well as to develop a molecular set-up which enables the measurement of protein-protein interactions with the MFA. These enhancements will allow the MFA to address a large variety of current biological problems regarding the interactions of proteins with DNA, RNA and other proteins. In the course of this thesis, proof-of-principle studies for different model systems were conducted. Due to its straight-forward programming and easy handling, double-stranded DNA was chosen as the reference complex for all different set-ups of the MFA, thus acting as the force sensor.

Although the other nucleic acid, RNA, is chemically relatively similar to DNA, the small differences render RNA prone to degradation. This corresponds to its different tasks in the

cell but makes *in vitro* studies of RNA more challenging. RNA molecules conduct a variety of different functions in a living cell. For example, messengerRNAs act as the carrier of information stored on the DNA genes and transferRNAs are the adopter molecules between the nucleic acid sequence and the amino acid sequence of the protein in the process of translation. The RNA interference mechanism [20] is an endogenous means used by the cell to influence gene expression at the stage of translation. Double-stranded RNA precursor molecules are cleaved into small pieces of 19-22 base pairs by the protein Dicer [21]. Due to this maturation process, one of the RNA strands can now guide a protein complex called RNA induced silencing complex (RISC) to specific messengerRNAs, which in most cases leads to suppression of protein expression. The two main classes of small regulatory RNA that have been identified are short interfering RNA (siRNA) and microRNA (miRNA). They differ in origin and function but share the processing by Dicer. Elevated levels of some miRNAs have been related to severe diseases such as cancer [22]. For that reason, selective inhibition of Dicer activity by the binding of small molecule ligands to specific miRNA precursors might be a promising approach for new therapies. Section 4.1 and publication A.1 describe the proof-of-principle set-up of a MFA-based screening assay for such small molecule ligands. With an RNA aptamer for the aminoglycoside paromomycin integrated into the sample complex, a decrease in Dicer processing upon ligand binding could be verified. Both the minimum amount of ligand necessary for Dicer inhibition as well as the dissociation constant of the ligand to its aptamer could be determined. Due to its parallel format the MFA can be applied to screen for different ligands or miRNA sequences simultaneously.

In order to target protein-protein interactions with the MFA, it is essential to generate covalently coupled protein-DNA chimeras, as they enable to link the protein complex in question to the DNA duplex acting as the force sensor. The coupling is required to be covalent to exclude the case of rupture of this link during the force loading process in MFA, which would render the technique ineffective. Secondly, it needs to be site-specific, as the unbinding force of a molecular complex depends on the pulling geometry and thus the specific position of the attachment [23]. Also, a minimal modification of the protein is desired. As the general methods for covalent protein attachment vary widely in experimental cost, yield and applicability for the coupling to DNA [24], no gold standard exists so far. For the experiments presented in this thesis, the coupling of DNA to proteins *via* an eleven amino acid long protein tag, called ybbR-tag [25], has been identified as a highly robust and efficient means for the generation of such chimeras, as described in detail in section 4.2. On the protein side, the ybbR-tag can be implemented on either the N- or C-terminus or at accessible unstructured regions and thus provides the possibility for site-specific attachment. Mediated by the Phosphopantetheinyl Transferase Sfp [26, 27], the tag couples covalently to Coenzyme A, which can easily be reacted to maleimide-modified DNA. Additionally to MFA experiments, the generation of protein-DNA chimeras with the ybbR-tag has been employed successfully for the controlled

arrangement of proteins at angstrom level with the Single-Molecule Cut & Paste technique, as described in publication A.2. This technique allows to pick up, transfer and deposit single molecules from a depot to a target area with an AFM cantilever. Thereby it relies on a force hierarchy and the binding properties of DNA. Hence, the creation of such chimeras is not only useful for the MFA technique, but offers various advantages as the DNA provides a unique handle *e.g.* for identification and functionalization [24, 28].

The generation of protein-DNA chimeras enables the development of the MFA towards the measurement of protein-protein interactions. The high biological relevance of the detection and characterization of protein-protein interactions is reflected in the increasing interest in the study of proteomes and interactomes [29]. The resulting knowledge of networks of protein interactions will help to better understand the different processes in the cell and the functionality of the individual interaction partners. The MFA technique is able to contribute by its capability to quantify mechanical strengths of protein-protein interactions. Hereby, it relies on the high parallelization of single-molecule experiments and the ability to multiplex both proteins of the complex to be investigated as well as the DNA force sensors. As a model system, the interaction between different types of Green Fluorescence Protein (GFP) to two variants of the nanobody Enhancer is chosen. Enhancer is a camelid-derived, single-domain antibody [30] and the characterization of its binding properties with MFA is described in section 4.3 and publication A.3. The GFP-nanobody complexes hereby display a higher mechanical stability than a 40 base pair DNA duplex. In order to maximize force resolution, the mechanical stability of the DNA duplex is enhanced *via* internal base modification and external binding of a ligand. As ligands, different sequence-specific pyrrole-imidazole hairpin polyamides [31] were employed. For the internal stabilization, pyrimidines were modified with a propynyl group at their C-5 position, which extends into the major groove and increases base-stacking interactions [32].

The need for further quantification of the stabilized DNA force sensors gave the motivation for the study presented in section 4.4 and manuscript B.1. Here, the complementarity of the AFM an MFA techniques is utilized to investigate the impact of the above mentioned C-5 propynyl bases on the mechanical stability of double-stranded DNA. Propynyl-modified DNA offers the advantage of standard base-pairing and easy integration into the DNA during chemical synthesis. The measurements reveal that the degree of stabilization is strongly dependent on the incubation conditions. The duplexes pre-annealed with high temperature for the MFA experiment display significant stabilization. In contrast, the complexes formed during an AFM measurement at room temperature and with short incubation times result in the same most probable rupture force as unmodified DNA duplexes. Due to its property of enhancing the mechanical stability of double-stranded DNA when the corresponding annealing conditions are applied, propynyl modifications broaden the dynamic range of the MFA. Additionally, they can be useful for many other applications in nanotechnology where DNA is used as a

building block.

The biological context of the different studies presented here is sketched in chapter 2, with emphasis on the model systems investigated in the course of this work. In chapter 3, the technique of the MFA is described in detail. Special focus lies on the *status quo* of the possible applications and molecular set-ups that have been realized so far. Chapter 4 summarizes the results of the studies conducted for this thesis. The corresponding publications and a manuscript accepted for publication can be found in the appendix. Finally, a short outlook proposes further developments which could render the technique of the MFA even more efficient for addressing biologically relevant questions.

2 Biological Context

As the physical interaction of a protein with other molecules determines its biological properties, the determination and quantification of those interactions is of utmost importance in order to understand the fundamental processes in the cell. This chapter aims to illustrate the biological context of the studies on protein interactions presented in this thesis. After a short introduction into the forces that govern protein behavior, an overview over protein interactions with the molecules of interest for this thesis is given. Special focus hereby lies on the model systems investigated in the course of this thesis. Finally, the physical properties that enable DNA to act as a force sensor in MFA experiments and methods that allow to increase the force range are sketched.

2.1 Forces Determining Protein Function

Understanding and quantifying the intermolecular forces that control protein behavior is the goal of many biophysical studies [33]. In general, the intermolecular forces between biological molecules do not differ from those between other types of molecules. However, the high degree of complexity of biomolecules and the fact that living systems are never at thermodynamic equilibrium renders the investigation of those biological interactions much more difficult. A detailed picture of intermolecular forces is given *e.g.* in [34]. In short, the forces determining protein interaction involve specific short ranged "lock-and-key" interactions at the binding site as well as nonspecific forces that operate outside the binding pocket. The nonspecific interactions include electrostatic, van der Waals and steric forces. In aqueous solutions, as present in biological systems, the electrostatic interaction between charged particles is mediated by a double layer of ions in the solution between the surfaces of the charged molecules. Besides this electrostatic double-layer force, the second important long-range contribution to protein interaction are the van der Waals forces, which display a longer range for macroscopic bodies than for atoms and small molecules. Steric Pauli repulsion forces operate at short intermolecular distances. Additionally, high spacial and chemical complementarity during molecular recognition allows to form a set of weak, non-covalent but specific "lock-and-key" interactions. The simultaneous formation of multiple hydrogen bonds, hydrophobic interactions and/or van der Waals interactions can lead to a large binding free energy. Those interctions are short-ranged

and determined by the local geometry [35, 33]. As a consequence, every protein interaction will result from a superposition of all or some of these different forces [33, 36]. The biological properties of proteins are determined by those physical interactions with other molecules. For example, the interaction with a ligand can cause an allosteric change in the structure or dynamic of the protein, resulting in a switch to an active or inactive state [37]. Recently, it has become more and more acknowledged that also external mechanical forces such as tension, shearing or compression are able to tune the state of proteins [38, 37].

Different examples illustrate the manifold ways forces determine the function of proteins. A prominent shear-sensing protein is the von Willebrand factor, a blood coagulation factor. The hydrodynamic forces in shear flow of arteriolar bleeding induce a conformational change that activates the protein by exposing an active site [39]. The autoproteolyzed domains of Adhesion-GPCRs are hypothesized to unbind at a certain force threshold acting as a protective mechanism upon exposure to mechanical stress [40]. Mechanical load can decrease the stability of a molecular interaction, which is important *e.g.* in signaling processes such as cell differentiation and immunological recognition. At the other extreme, so called "catch bonds" are stabilized by exerted forces. Here, cell adhesion proteins like integrins [41] and cadherins [42] are prominent examples. Other proteins like molecular motors are able to generate forces and can in turn also be regulated by them in their activity [43].

The forces controlling protein behavior for enzymatic, regulatory, or motor function can indirectly be derived from thermodynamic or kinetic measurements. More recently, the development of techniques such as the single-molecule force spectroscopy with the atomic force microscope (AFM) [10, 44] or optical tweezers [9] render the inter- and intramolecular forces and underlying energy landscapes directly accessible [33, 13, 12]. One of the first protein-protein interactions to be analyzed with the AFM was the well-known Biotin-Avidin complex [11]. As stated by Seifert and Gräter [37], all external perturbation of the protein, not only mechanical stretching but also the binding of a ligand, can be regarded as an external force acting on the protein. Hence, single-molecule force spectroscopy methods are very general tools to address questions such as allosteric mechanisms.

In addition, external forces exerted by force spectroscopy techniques can be employed to differentiate specifically from non-specifically bound ligands due to the different forces needed to separate them. Also, complete unfolding of a protein under external force provides informations on the different domains and thereby on the structure and functionality of the protein. Furthermore, external forces can be used to measure the change in mechanical stability of a molecular complex arising for example from the binding of a protein ligand to a DNA helix. Rather than studying the forces of the interaction, the aim in this case is to use the external force as a tool to test indirectly if an interaction takes place, and, if yes, to quantify it. The Molecular Force Assay, the technique primarily used for the studies presented in this thesis,

is capable both of the direct and indirect use of the external force, as will be explained in more detail in chapter 3.

2.2 Protein Interactions

Proteins are synthesized according to the information stored in the genomic DNA. Initially, a RNA copy of the DNA coding sequence is produced during the transcription process. The information now given in the RNA copy is then translated into an amino acid polypeptide chain, which gains its functionality as a protein by folding into a three-dimensional structure. In both parts of this process of gene expression, a variety of proteins play again a crucial functional and regulatory role. But as the workhorses of the cell, proteins are also needed for most other processes such as signaling, transport or metabolism. In order to perform these different tasks, proteins need to interact with molecules such as DNA, RNA or other proteins. In order to understand the processes in the cell, and, one step further, influence them, it is necessary to target those interactions between proteins and the different biomolecules.

This section wants to give a short overview over the purposes of the interactions that proteins undergo with other DNA, RNA or protein molecules. In particular, the model systems studied in the context of this thesis are introduced.

2.2.1 Protein-DNA Interactions

Proteins are synthesized in the gene expression process according to the information coded in the DNA. But proteins also interact with DNA in manifold ways. A vast network of proteins is responsible for processes altering the cell's DNA such as replication, detection of damage, repair or degradation. Depending on the task, a protein interacts alone or in complexes with other proteins with the DNA. For instance in epigenetics, binding of histone proteins to DNA influences gene expression depending on the modification of the histones, as it determines the accessibility of different parts of the genomic DNA for transcription [45]. Protein-DNA interactions also perform, control and regulate all other processes in the transcription, the first part of gene expression. Examples are helicases opening the double helix and the RNA polymerase adding the matching RNA nucleotides to the complementary DNA strand. One of the most studied classes of DNA binding proteins are transcription factors, which are important means of the cell to regulate the gene expression. By binding to the DNA mostly close to the promoter region of a gene, either alone or in complex with other proteins, transcription factors are able to activate or repress the binding of the RNA polymerase and thus regulate the expression level. Many transcription factors are able to interact with different binding sequences with varying strength. All these regulatory interactions are responsible

for a very fine-tuned level of protein expression which allows the cell to react flexibly and rapidly upon demand [36]. In order to be able to bind to DNA, the proteins possess one or more DNA binding domains. Generally, it can be distinguished between proteins that bind DNA either with a general affinity or only to specific binding sequences as well as between proteins binding to single- or double-stranded DNA. Depending on the binding domain, the proteins mostly bind into the major groove of B-DNA as it exposes more functional groups. Examples of common motifs in the binding domains are the helix-turn-helix, leucine zipper or zinc finger domains (for details see *e.g.* [36]).

The interaction of proteins with DNA can be detected indirectly as it alters the mechanical stability of the DNA under external load depending on the chosen protein. One example for the study of protein-DNA interaction with the MFA in this indirect way can be found in [19]. Here, the stabilization effects of the DNA upon binding of the type II restriction endonuclease Eco-RI and the transcription factor p53 are compared and quantified. In order to determine the binding strength of a transcription factor directly, another set-up of the MFA is employed in [46]. In this study, the binding of an artificial six zinc finger fusion protein to different DNA binding motifs is investigated. Due to the abundant occurrence in eukaryotic transcription factors, zinc finger proteins are very interesting model systems. Details on the zinc finger study can be found in publication A.4 [47], but will not be discussed further in this thesis. More information on the different set-ups of the MFA is given in section 3.3.

2.2.2 Protein-RNA Interactions

Far from being only the intermediate carrier of the information stored in DNA, functional RNA molecules are more prevalent than previously imagined. Beside the messengerRNA (mRNA), the copy of a gene encoded on the DNA, so-called non-coding RNAs are functional units that are not translated into proteins. In translation, transferRNAs act as adaptor molecules between the nucleic acid code of the mRNA and the amino acid sequence of the protein. The ribosome, where the translation takes place, is a protein-RNA complex which consists of more than 60% ribosomal RNA. Other examples are enzymes build from ribosomal RNA, called Ribozymes, or microRNAs (miRNAs) that play a role in gene expression regulation. What the different coding and non-coding RNAs have in common is that their function is almost always mediated through the interaction with proteins, making the study of RNA binding proteins and thus protein-RNA interaction a rapidly expanding field [48]. RNA-binding proteins are for example key players in the regulation of gene expression as they allow for the post-transcriptional control of mRNAs such as alternative splicing, RNA editing, mRNA localization or the control of the recruitment of ribosomes for the translation. The protein-RNA interaction is in general similar to the interaction with DNA, although the discrepancy in the helix structure of RNA leads to differences in interaction motifs. As the

major groove of RNA is deeper and narrower than in DNA, it is relatively inaccessible and prevents *e.g.* the binding of an alpha helix, which is very common in DNA binding motifs [49]. So far, the "Double-stranded RNA-binding motif" and the "RNA-recognition motif" for single stranded RNA have been discovered, and recently it has been shown that the common DNA-binding zinc finger motif is also capable of recognizing RNA [50]. Due to the different functions and tasks of RNA molecules in comparison to DNA, RNA is very susceptible to degradation and displays shorter half-lives. This makes it experimentally more challenging to study the interaction of proteins with RNA than with DNA and special care has to be taken in the handling of the samples in *in vitro* experiments such as the MFA.

Model System: Nuclease Dicer Cleaves Double-Stranded RNA to Start the RNAi Pathway

One example for a protein interacting with double stranded RNA that has increasingly been attracting attention is the endoribonuclease Dicer, which plays a central role in the RNA interference (RNAi) pathway. RNAi is a mechanism of gene regulation in the cell, during which suppression of gene activity is triggered by double-stranded RNA in a homology-dependent manner [51]. Dicer cleaves double stranded RNA (dsRNA) precursor molecules into pieces of 19-23 nucleotides. After unwinding, one of the single short RNA strands is incorporated in a multi protein complex to form the RNA-induced silencing complex (RISC). RISC then employs the RNA template to identify target mRNA *via* Watson-Crick base-pairing and usually inhibits translation. Two main classes of single-stranded RNA involved in metazoan RNA interference have been identified. They differ in their origin and function but share processing by Dicer: short-interfering RNA (siRNA) and microRNA (miRNA) (see figure 2.1). The precursors of siRNA are long dsRNA, which are taken up into the cytoplasm from the environment or originate from sources like the transposons and seem to act as defenders of genome integrity in response to foreign or invasive nucleic acids [52]. In contrast, miRNAs are believed to function as regulators of endogenous genes. They are transcribed and pre-processed in the nucleus into incomplete base-paired stem-loop structures. Those so-called pre-microRNAs are then processed in the cytoplasm by Dicer, which cuts off the loop structures in order to activate the miRNAs. Whereas in most cases siRNA binds to fully complementary target mRNA, leading to the degradation of the mRNA, complete homology is not required for miRNA. The degree of base-pairing governs the resulting downstream process. Mostly, incomplete hybridization due to base pair mismatches leads rather to translation inhibition than degradation of the mRNA [53]. In humans, more than 400 different miRNAs are expressed that are believed to be involved in the regulation of at least 30% of all genes [36].

The multidomain ribonuclease Dicer [54] is found in several variants, sometimes with different tasks, in the cytoplasm of all eukaryotes studied to date. However, the L-shape of the protein

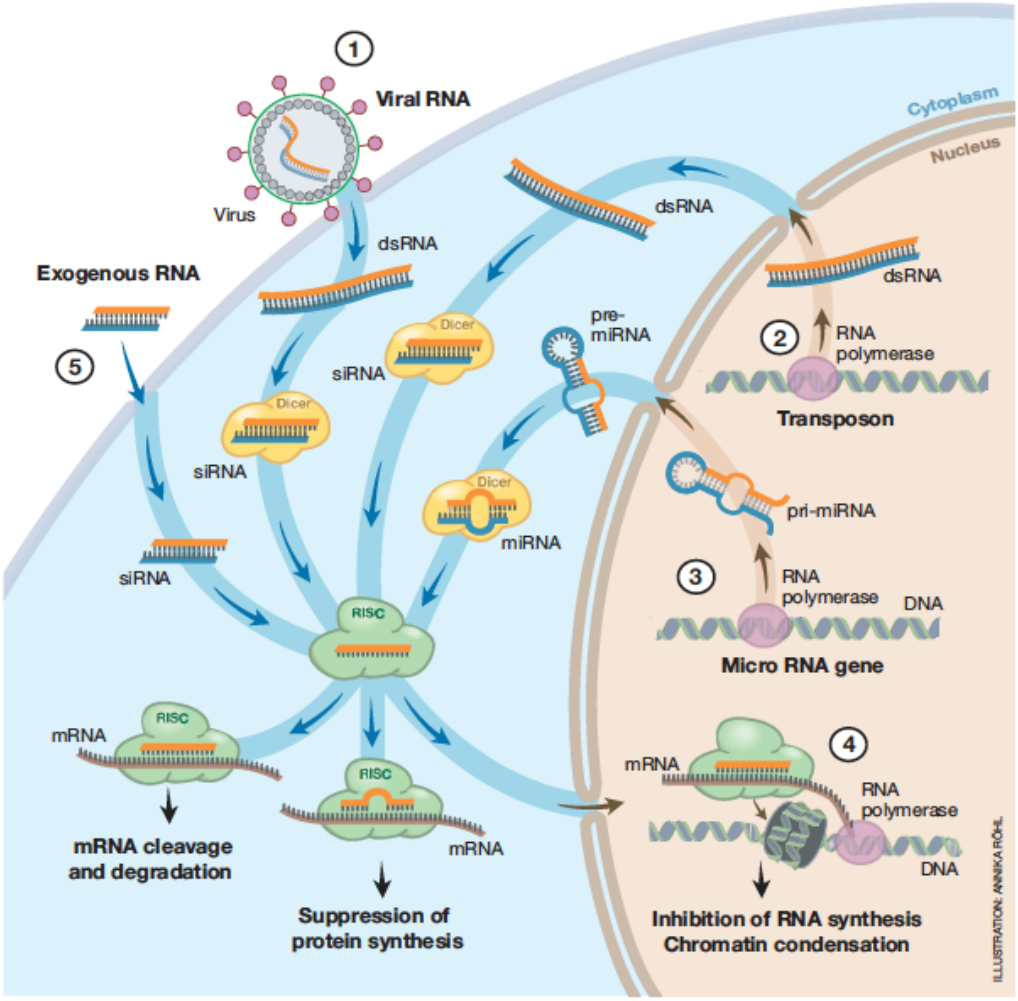

Figure 2.1: The endonuclease Dicer (highlighted in yellow) plays a central role in the RNA interference pathway. It is responsible for the processing of double stranded RNA precursor molecules from endo- and exogenous sources to pieces of 19-23 nucleotides. The matured short-interfering RNA and microRNA are subsequently integrated into the RNA-induced silencing complex (RISC) in order to guide it to target mRNA, mostly for the inhibition of translation. Reproduced from [51].

seems to be well-conserved. A PAZ domain in the head of Dicer is responsible for the recognition of dsRNA. Connected to the PAZ domain by a ruler domain, two RNAse III domains sit adjacent to each other and catalyze the hydrolysis of the dsRNA. A helicase forms the base of the L-shape. The distinct length of the ruler domain enables the processing of the dsRNA into pieces of equal length [55, 21]. Dicer cleaves RNA strands with different lengths (but more than 30 nucleotides) with equal efficiency, but a 3' 2-nucleotide long overhang, as present in pre-miRNAs, increases Dicer's efficiency compared to blunt ends [56].

Severe illnesses like cancer can result from malfunctions in the RNAi pathway. As shown in section 4.1, the MFA technique is capable of measuring Dicer activity. This can be utilized to test means of influencing its ability to activate specific RNA substrates in order to correct for malfunctions.

2.2.3 Protein-Protein Interactions

The ability of proteins to interact with other proteins is essential for most reactions in a living cell and thus one key element for its normal functioning. A protein's function is reflected in its interaction with others so that much of its tasks in the cell can be predicted from the identification of its interaction partners. Hence, the characterization of protein-protein interactions is crucial in order to gain a better understanding of many fundamental processes in nature [5]. Proteins interact through their surfaces with a set of weak, non-covalent bonds and hydrophobic interactions as described in section 2.1. Since each individual bond is weak, effective binding occurs *via* many of them simultaneously when the contours of the binding epitopes match very closely like a hand in a glove. This enables the interaction between proteins to be very specific in location, affinity and kinetics [36, 57]. Similar to the interaction with nucleic acids, typical protein domains involved in the recognition of other proteins have been discovered, although in a larger variety due to the high complexity of the proteins' molecular architecture [58]. Protein-protein interactions are usually classified and devided into permanent and transient interactions [59]. They allow proteins to form either homo- or heterocomplexes, assemble pair-wise or as complex molecular machines with a high number of molecules. Regarding the central role of protein-protein interactions for the processes in the cell, it is not surprising that aberrant interactions *e.g.* due to misfoldings of proteins have been related to various diseases such as Alzheimer's disease, Creutzfeld-Jacob, and cancer [60, 61]. Determining the protein-protein interactions that occur in the cell and form the so-called interactome is thus at the center of current research in order to understand, and, in a second step, influence the processes that lead to diseases. The key problem herein lies in the extensive number of interactions in any given organism. The size of the human interactome is estimated to be in the order of $650,000$ interactions [62]. Presently, the processes that control protein-protein interactions are mostly described in terms of pair-wise interactions. However,

in vivo, the interactions are more often than not part of complex molecular networks that are highly dynamic in time and space [5, 63]. The fact that, in contrast to DNA and RNA, proteins can not be easily amplified for analyzation and the high complexity of the networks render the investigation of protein-protein interactions challenging.

Different experimental techniques for the study of protein-protein interactions have been developed [64]. Prominent examples for high-throughput techniques tackling the high number of interactions are yeast-two-hybrid assays [8], protein microarrays [65], or microfluidic-based techniques [66]. Furthermore, other methods exist that are able to characterize the interactions in greater detail such as X-ray crystallography [67], fluorescence resonance energy transfer (FRET) [68], or surface plasmon resonance [69]. The studies in this thesis focus on the interaction forces that control the interactions. To this end, the MFA technique was adapted in order to be able to quantify protein-protein interaction strength in a parallel manner, as shown in section 4.3. Generally, computational means are employed to predict possible interactions and functions in addition to experimental techniques [57].

Model System: GFP-Nanobody Interaction

The model system for protein-protein interaction investigated in the course of this thesis is the binding of three variants of Green Fluorescent Proteins (GFPs) [70] to the GFP-binding nanobody Enhancer [30].

GFPs are well-known fluorescent proteins of about 27 kDa that are commonly used *e.g.* to label cells across organisms or are coexpressed to act as reporter for gene expression. Wild type GFP (wtGFP) and its derivates investigated here, super folder GFP (sfGFP) [71] and enhanced GFP (eGFP) [72], share the same general molecular architecture. An outer barrel structure consisting of beta sheets encases the chromophore in its center. The standard wtGFP is characterized by its dual-peak excitation at 395 and 477 nm which both result in an emission at about 507 nm. By mutagenesis, many variants have been created to ensure for example higher brightness, such as with eGFP, better folding properties, such as with sfGFP, or the emission at other wavelengths [36].

Nanobodies are single-domain antibodies that are derived from camelids. Their advantage in comparison to conventional antibodies lies in their reduced size and enhanced stability while still featuring similar antigen-binding characteristics. The nanobody “Enhancer” (PDB 3K1K, $\approx 13.5\ kDa$) has been generated and selected for its effect on fluorescence emission of wtGFP [30]. Upon binding of Enhancer, the fluorescence of wtGFP is increased by a factor of four. This is attributed to rearrangements in the chromophore environment induced by the binding of Enhancer. The wtGFPs binding epitope for Enhancer lies on the outer beta barrel structure, as determined in the crystal structure (see figure 2.2) [30]. This outer structure is

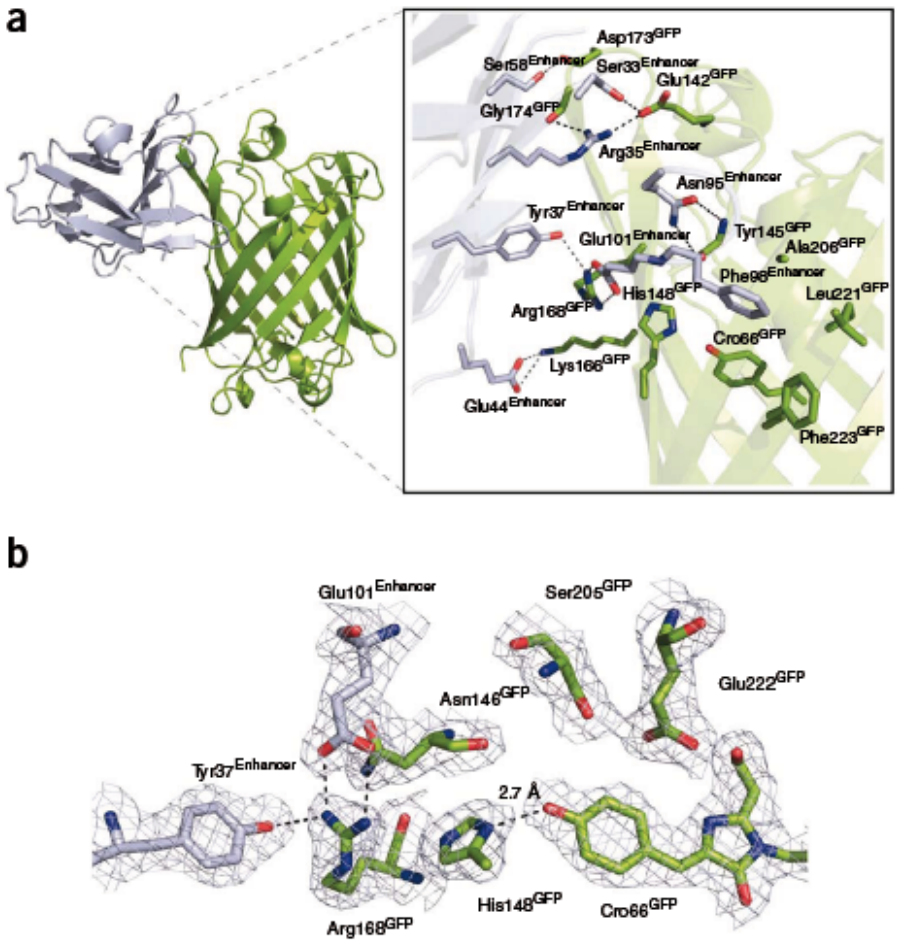

Figure 2.2: (a) Crystal structure of the Enhancer (light blue ribbon model)- wild type GFP (green ribbon model) complex displaying the binding epitope on the GFP beta barrel surface. (b) The chromophore environment of GFP located in the center of the beta barrel is altered upon complexation with Enhancer yielding the change in fluorescence intensity. Reproduced from [30].

conserved for the other mutants investigated here, enabling Enhancer to bind those, too. Due to the nanobodies' excellent binding specificities to GFP and their being stable and functional in living cells, they have been employed for numerous applications. For example, they have been used to monitor protein expression and sub-cellular localization as well as translocation events *in vivo* [30], been employed for high affinity capture of GFP fusion proteins to allow for targeted manipulation of cellular structures [73] or enabled GFP to act as scaffold for the manipulation of gene expression [74].

For the proof-of-principle study presented in this thesis in section 4.3, this model system offers the advantages of being well characterized. Additionally, the GFP can act as an intrinsic fluorescence label for the control of the correct assembly of the MFA.

2.3 DNA as a Force Sensor

The recent technical developments that allow to synthesize DNA strands upon demand in a fast and cheap manner have rendered DNA the perfect candidate for the use as building block in nanotechnology. The DNA's unparalleled properties such as its sequence-specific self-assembly, robustness and simplicity enable to create and build two and three dimensional structures at the nanoscale. Examples are the prominent scaffolded DNA origami [75, 76, 77], small "DNA bricks" which can be assembled to larger structures in a LEGO-like fashion [78] or other molecular devices [79]. *In vivo*, DNA is mostly present double-stranded, with two antiparallel DNA strands forming the famous double helix proposed by Watson and Crick [1]. In the most common and stable conformation, the Watson-Crick base pairing, guanine is bound to cytosine *via* three and adenine to thymine *via* two hydrogen bonds, as shown in the schematic depiction in figure 2.3 (A).

Several factors contribute to the thermal stability of a DNA duplex. Primarily, the helix is stabilized through base-stacking of adjacent bases. Although the hydrogen bonds of the base-pairing also contribute to the overall stability of the helix, their contribution is very small in comparison to the base-stacking. Additionally, the sequence is important for the stability as duplexes with a higher percentage of G-C base pairs melt at higher temperatures. However, the higher stability of guanine-cytosine rich sequences is also mostly due to the dipole-dipole interactions in base-stacking [81]. A DNA duplex is weakened by possible non-Watson-Crick base pairings [82] and bulges. In general, the Coulomb repulsion between the negatively charged phosphate backbones as well as entropic effects act destabilizingly on the DNA. The entropy is reduced upon duplex formation as a DNA duplex has a much longer persistence length than a single strand, and thus less degrees of freedom. In addition, the hydration shell of the double helix is higher than that of two single strands, yielding a destabilizing entropic effect of the solvent. For the experiments conducted for this thesis, DNA duplexes have been applied to act as force sensors. Two ways to unbind a DNA helix under force have been utilized (see figure 2.3 (B)). The DNA strands were always attached at their terminals. In the so-called zipper mode, the DNA is opened from one end, so that one base pair at a time is ruptured in a quasi-equilibrium process. In this mode, the forces needed to melt the DNA duplex are not dependent on the force loading rate but differ for A-T-sequences ($\approx 10\ pN$) and G-C-sequences ($\approx 20\ pN$) [15]. Sequences with mixed content of all bases rupture at medium forces. In contrast, in shear geometry the force is applied parallel to the helix axis to two opposing ends of the DNA, loading all base pairs simultaneously. Thus, the rupture force here depends on the length of the complex, the force loading rate [83] and if the strands were attached at their 5' or 3' termini [84]. Already at duplex lengths of 40 base pairs a rupture force of about 65 pN is reached. Higher average forces can not be achieved with short oligonucleotides, as DNA reaches a force plateau at about 65 pN when sheared due to

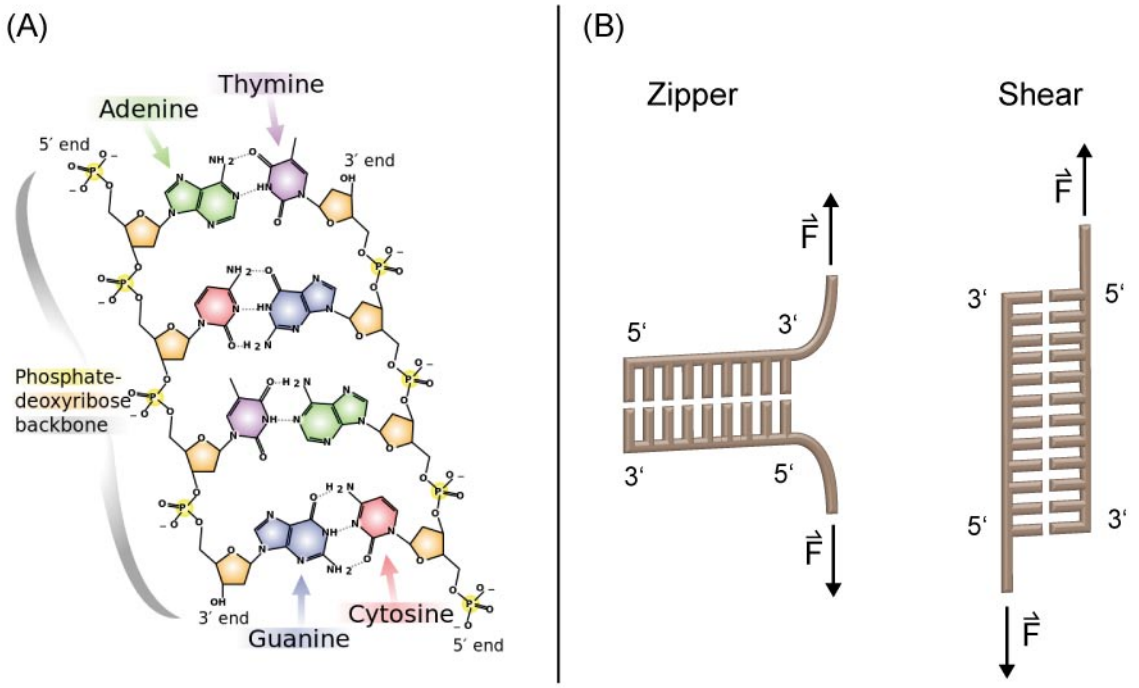

Figure 2.3: (A) Schematic depiction of the chemical structure of DNA with Watson-Crick base-pairing. Adapted from [80]. (B) From its termini, DNA can be melted in two geometries. While in the zipper geometry the force is applied on one end of the helix and one base pair at a time is opened, in shear geometry the force is loaded parallel to the axis of the helix and thus on all base pairs simultaneously.

the so-called BS-transition [16].

The difference in rupture force depending on the geometry permits to establish force hierarchy systems. Relying on this principle, the so-called "Single-Molecule Cut & Paste" technique allows to position individual DNA or protein molecules at nanometer precision [85, 86]. In MFA experiments, both modes of unbinding can be employed and the geometry can be chosen depending on the system to be investigated. In general, the DNA acting as the force sensor in a MFA experiment is mostly designed to be as close as possible in mechanical stability to the complex in question, as this enhances the sensitivity of the assay (see chapter 3).

In order to address some biological systems experimentally, *e.g.* as described in section 4.3, an even higher unbinding force than the 65 pN of the BS-transition is needed. Enhancement of the DNA duplex stability is in general possible intrinsically by nucleobase modification or by binding of an external ligand. A prominent example for a base modification altering thermal and mechanical stability of a DNA duplex is the methylation of the 5' position in cytosines [87, 88], which plays an important role in epigenetics. The modification of the same C-5 position on pyrimidines with a propynyl group [32, 89, 90] (see figure 2.4 (A)) yields an even higher increase in melting temperature than methylation. The apolar propynyl group

is planar with respect to the heterocycle and extends into the major groove. The duplex is thus expected to be stabilized due to enhanced base-stacking. Graham *et al.* [91] determined the thermodynamic parameters for a 12 base pair DNA duplex containing five propynyl bases compared to an unmodified duplex: the significant decrease in enthalpy is attributed to the electronic interactions in the base-stacking and counteracts the entropy decrease likely resulting from more ordered water molecules normally found in the major groove. This results in a decrease in free energy ΔG and thus a stabilized complex [91]. Section 4.4 describes the investigation of the increase in mechanical stability of a DNA duplex due to the integration of propynyl bases with the MFA and AFM technique.

Furthermore, the binding of ligands such as small molecules or proteins can alter the mechanical stability of DNA under force load. An example where an external ligand was used to stabilize the DNA helix is given in section 4.3, where different pyrrole-imidazole hairpin polyamides [31] (see figure 2.4 (B)), binding sequence-specifically into the minor groove of DNA, were utilized to achieve DNA force sensors of different strengths.

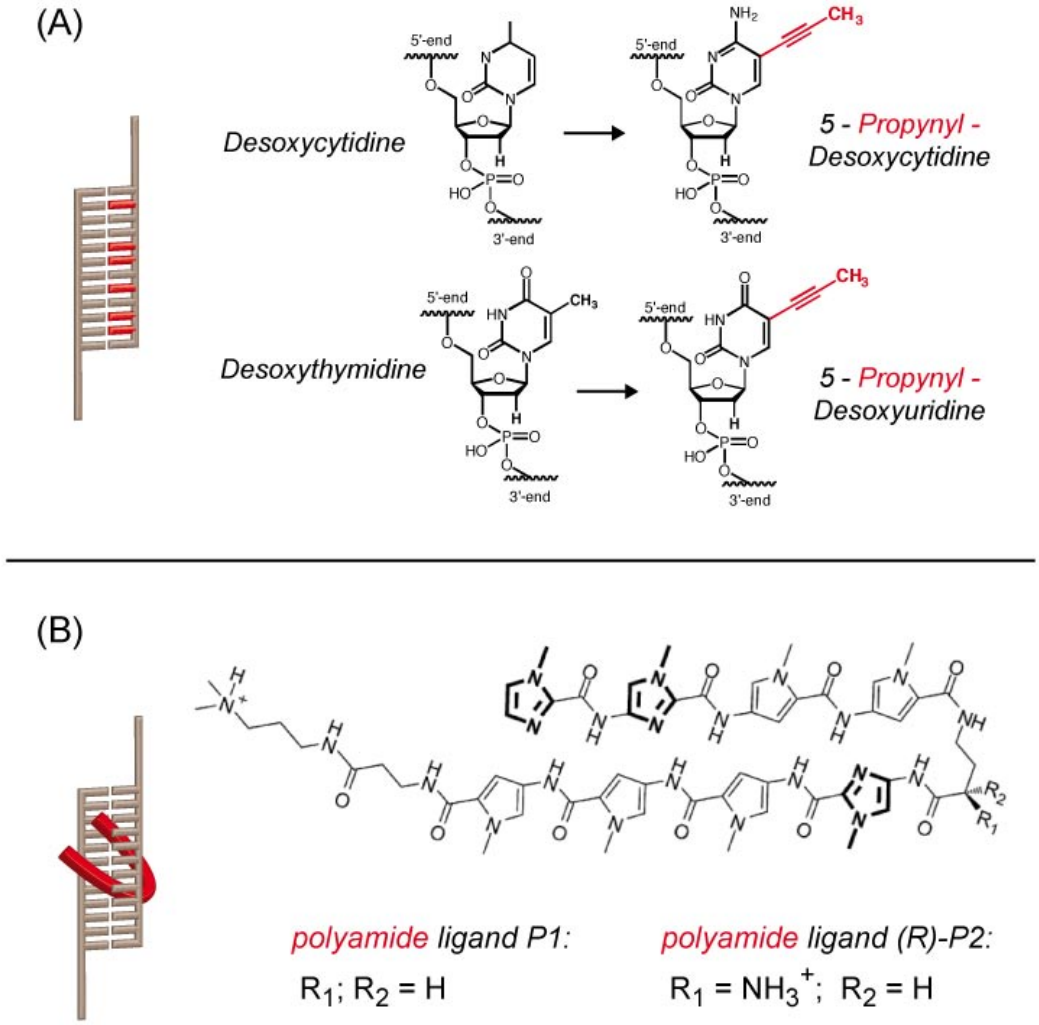

Figure 2.4: In general, the mechanical stability of a DNA duplex can be enhanced either by modification of the DNA itself or binding of an external ligand. (A) An example for internal modification leading to an increase in stability is the replacement of pyrimidines with their corresponding propynyl bases, which harbor the apolar, planar propynyl group at the C-5 position of the base. (B) Externally, DNA stability can for example be variably enhanced upon binding of different site-specific pyrrole-imidazole hairpin polyamides. Polyamide structure adapted from [18].

3 The Molecular Force Assay (MFA)

This chapter introduces the principle of the Molecular Force Assay which allows for the parallelization of force-based single-molecule measurements. The experimental procedure and analysis of the current standard set-up are explained. A detailed overview over the different applications of the MFA enabling it to address various biological problems is given. Finally, the technique of the MFA is set in context to the standard force-spectroscopy technique of the atomic force microscope (AFM).

3.1 Principle of the Molecular Force Assay

The basic principle of the Molecular Force Assay is to determine the mechanical stability of a molecular complex by comparing it to a known reference complex. To this end, a so-called Molecular Force Probe (MFP) is formed by attaching both molecular bonds in series. The application of an external force upon the MFP directly compares the mechanical stability of the two interactions until, statistically, the weaker one unbinds. The intact molecular bond can be determined *via* a fluorophore dye attached to the linker between the two complexes. The main advantage of the MFA technique is its ability to test thousands of MFPs simultaneously, yielding high statistics in one single experiment. As every molecular bond in question is tested against its own reference, MFA enables to parallelize force-based single-molecule experiments. In general, the comparative approach renders the technique very sensitive. Analogous to an old-fashioned scale balance, the MFA has its highest sensitivity if the binding strengths of the bond in question and the reference bond are very similar. This has already been shown when the principle of the MFA was first applied to two DNA duplexes, where single base pair mismatches could be detected [17].

In detail, the actual force assay is realized by clamping the MFPs between two surfaces, which can be separated at a constant velocity building up a force acting on both complexes. Figure 3.1 displays the molecular set-up for the example of two DNA duplexes. The MFP is build up from three DNA oligonucleotide strands forming the sample and the reference complex. The lowermost strand is coupled covalently to the lower surface, a glass slide, while the uppermost strand harbors a biotin modification enabling its coupling to the upper surface,

a soft elasomer PDMS (polydimethylsiloxane) stamp functionalized with streptavidin. A Cy5 fluorophore attached to the poly-thymine linker between the two duplexes stays with the intact bond after force load. By taking fluorescence images of the spots of MFPs on the glass slide before and after force load, the difference of Cy5 signal can be detected and used to determine the outcome of the experiment. A second fluorophore, a Cy3 dye coupled to the uppermost strand forming a FRET pair with the Cy5, is necessary to subtract MFPs from the analysis that did not couple to the stamp. Those MFPs have not been under force load and thus yield a false positive signal of remaining Cy5 dyes on the glass slide.

3.2 Experimental Procedure and Analysis

In the current standard set-up of the MFA technique, the upper surface consists of a PDMS stamp of 1 cm x 1 cm harboring 16 pillars of 1.1 mm in height and a diameter of 1 mm. The PDMS stamp is adhered upside down to a glass block mounted on a closed-loop piezoelectric actuator and a DC motorized translation stage. The pillars of the stamp are microstructured to allow for liquid drainage during the contact and separation process. On the lower surface, the glass slide, a matching 4 x 4 array of MFP spots is assembled (see figure 3.2, center). The standard spot size is about 1.2 mm in diameter. As the density of MFPs on the slide is very high (around 10^4 per μm^2), it is possible to reduce the spot size to about 25 μm^2 for high-troughput applications [19]. But already the standard set-up allows for multiplexing of the reference and/or the sample bond as well as the incubation of every MFP spot with a different ligand concentration.

The contact device is mounted on an inverted epi-fluorescence microscope with an xy DC motorized high-accuracy translation stage. This enables to measure both Cy5 and FRET intensities for each MFP spot on the glass slide at the same position before and after force load. The stamp is adjusted to be planar to the glass slide and then lowered gradually onto it with the piezo using reflection interference contrast microscopy to control the process [92]. After a 10 min incubation step, which allows the biotins of the MFPs to couple to the streptavidins on the stamp, the piezo retracts the stamp with constant velocity. For all experiments conducted for this thesis $v_{piezo} = 1\ \mu m/s$, yielding a force loading rate in the range of $10^5\ pN/s$ [84]. Detailed information about the technical set-up can be found in Severin *et al.* [93].

After the separation process, for those MFPs where the lower complex unbound, the fluorescent Cy5 dye on the linker is transferred to the stamp, yielding a decrease in fluorescence intensity on the glass slide, as shown in figure 3.2. To determine the ratio of still intact lower complexes in comparison to all molecular complexes under force load, the sets of fluorescence

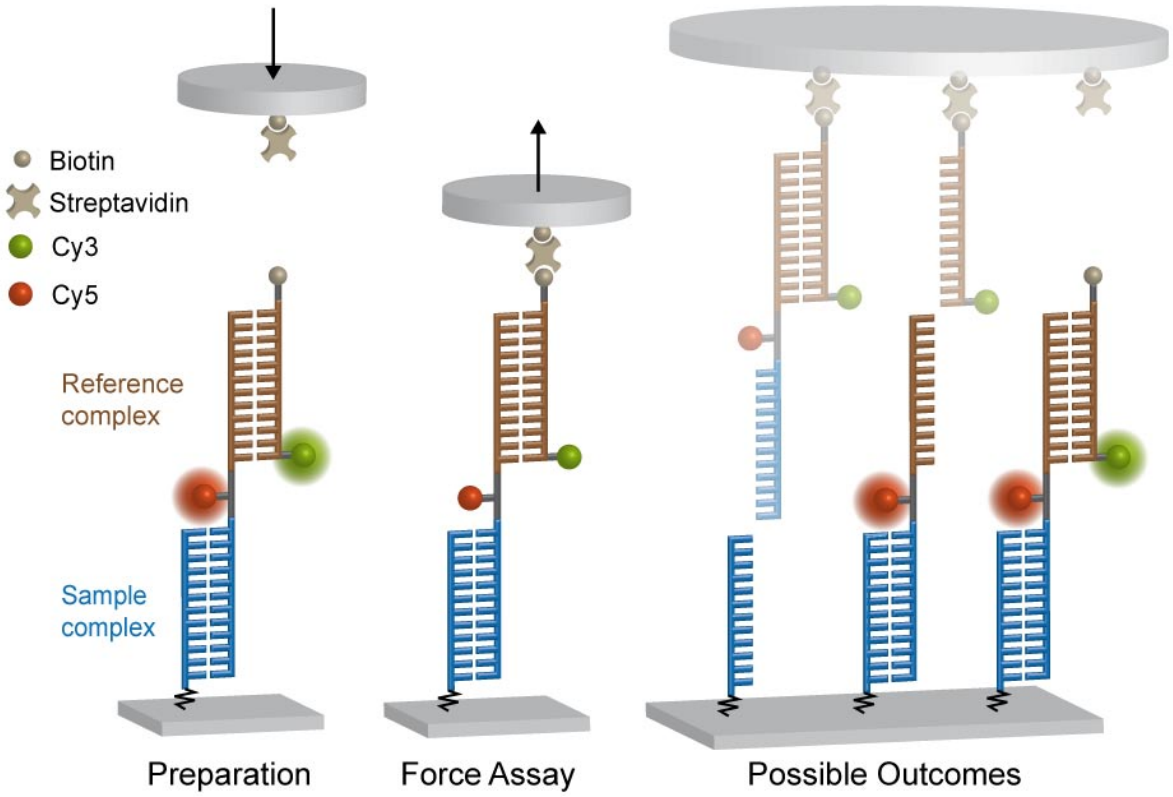

Figure 3.1: In the molecular set-up of the Molecular Force Assay, a sample complex in question is attached in series with a known reference complex to form a so-called Molecular Force Probe (MFP). The MFP is covalently coupled to a lower glass surface, as shown on the left for the example of two DNA duplexes. The fluorescence signal of the Cy5 dye coupled to the linker between the two complexes and a FRET signal obtained *via* the Cy3 dye attached to the uppermost DNA strand give the initial amount of MFPs. The MFPs are then clamped between two surfaces. Coupling to the upper surface, a soft PDMS stamp, is facilitated *via* a biotin on the uppermost strand which binds to the streptavidin on the elastomer. The retraction of the upper surface then leads to a force load on the MFPs which directly compares the mechanical stability of both complexes, until, statistically, the weaker one ruptures. The outcome of the experiment is given by the resulting position of the Cy5 dye on the linker, as its a fluorescence signal only remains on the glass surface if the lower complex is still intact. For the MFPs that did not couple to the upper surface, the Cy5 is also still attached to the lower surface yielding a false positive signal. Those MFPs can be subtracted in the analysis by determining the FRET intensity, as a FRET signal only remains if both complexes are still intact.

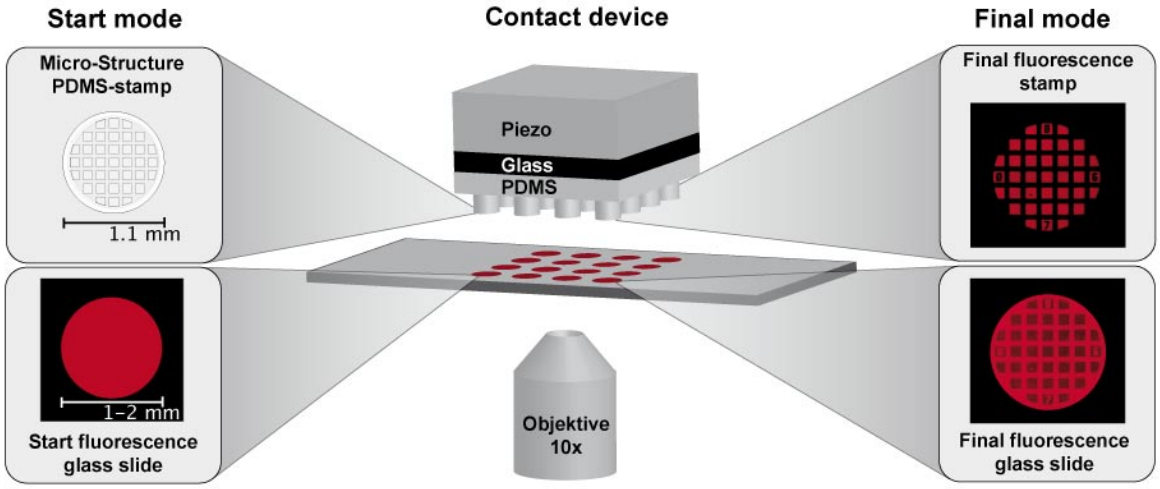

Figure 3.2: The contact device of the current standard set-up is mounted on an inverted epifluorescence microscope. The functionalized PDMS stamp features 16 pillars matching the 4x4 array of MFPs spotted on the lower glass surface. A micro-pattern on the stamp allows for drainage of liquid during the contact and separation process. The resulting fluorescence signal on the glass slide is reduced in comparison to the initially measured intensity, as part of the fluorescence signal is transferred to the stamp. Adapted from [94].

intensity images of every MFP spot on the glass slide before and after contact are processed according to the following equations.

The ratio of residual "RED" signal of the Cy5 dye on the linker to the initial Start intensity gives the ratio of still intact lower bonds in comparison to the initial amount of MFPs

$$\text{Ratio}_{RED} = \frac{RED_{\text{Final}}}{RED_{\text{Start}}}. \tag{3.1}$$

As can be seen in in figure 3.1, MFPs that did not couple to the stamp and thus have not been under force load give a false positive signal as the Cy5 dye stays attached to the surface. The analysis can be corrected for those MFPs by subtracting the ratio of FRET images before and after contact, as a FRET signal only remains if both complexes are still fully assembled

$$\text{Ratio}_{FRET} = \frac{FRET_{\text{Final}}}{FRET_{\text{Start}}}. \tag{3.2}$$

Normalization to the Coupling Efficiency $\text{CE} = 1 - \text{Ratio}_{FRET}$ yields the Normalized Fluorescence NF

$$\text{NF} = \frac{\text{Ratio}_{RED} - \text{Ratio}_{FRET}}{\text{CE}}, \tag{3.3}$$

which denotes the ratio of intact lower bonds to all tested molecular complexes and is given by a number between 0 and 1. Thus, a NF of 0.5 means that both sample and reference complex have the same binding strength, while a NF closer to 0 results from a stronger upper bond and *vice versa* for a NF closer to 1.

As the interaction between the biotin of the MFP and the streptavidin on the PDMS stamp is not covalent, it is possible that this interaction ruptures under force load instead of the sample or reference bond. However, this outcome is not very likely regarding the high rupture force of the biotin-streptavidin complex which lies beyond 100 pN [95, 13] and thus well above many other molecular interactions such as especially the rupture force of short DNA duplexes [16]. Nevertheless, this case is accounted for in the analysis, since it is indistinguishable from the case of a MFP that did not coupled to the stamp. In order to ensure that all MFPs are assembled correctly during the preparation, a 2:1 ratio of the uppermost to the middle strand of the MFP are pre-incubated before use, as it is not possible to identify the false positive signal resulting from molecular constructs missing the uppermost strand and therefore harbor only a Cy5 dye already before force load.

The analysis for the experiments presented in this thesis is conducted automatically using a custom made Labview software which divides the original fluorescence images after background correction pixel-by-pixel according to equation 3.3 and corrects for bleaching. The NF is then determined by fitting of an Gaussian to the resulting histogram of counts. Advantages of this pixel-by-pixel method are that it cancels out inhomogeneities due to the Gaussian illumination profile or coupling density as well as surface defects.

3.3 Different MFA Applications for Protein Interactions

The basic principle of the MFA is applicable to a range of different molecular interactions which allows to address a wide variety of biological problems.

For force spectroscopy experiments in general, the bottleneck is the necessity to anchor the molecules specifically and as strong as possible to enable the build-up of a force load on the molecules in question. DNA and RNA oligonucleotides can easily be modified with chemical groups allowing for attachment. In the standard MFA set-up, a terminal amino-modification is employed for covalent attachment of MFPs consisting of nucleic acids to an aldehyde functionalized glass slide. Here, the site-specific attachment of the molecules is of utmost importance, as the force needed to unbind a molecular interaction is dependent on the pulling geometry. A typical example can be seen in figure 3.3. Whereas the DNA in the MFP in (A) is implemented in the shear mode, meaning that the force is applied parallel to the long axis and thus to all base pairs simultaneously, in the zipper conformation displayed in (B) the force

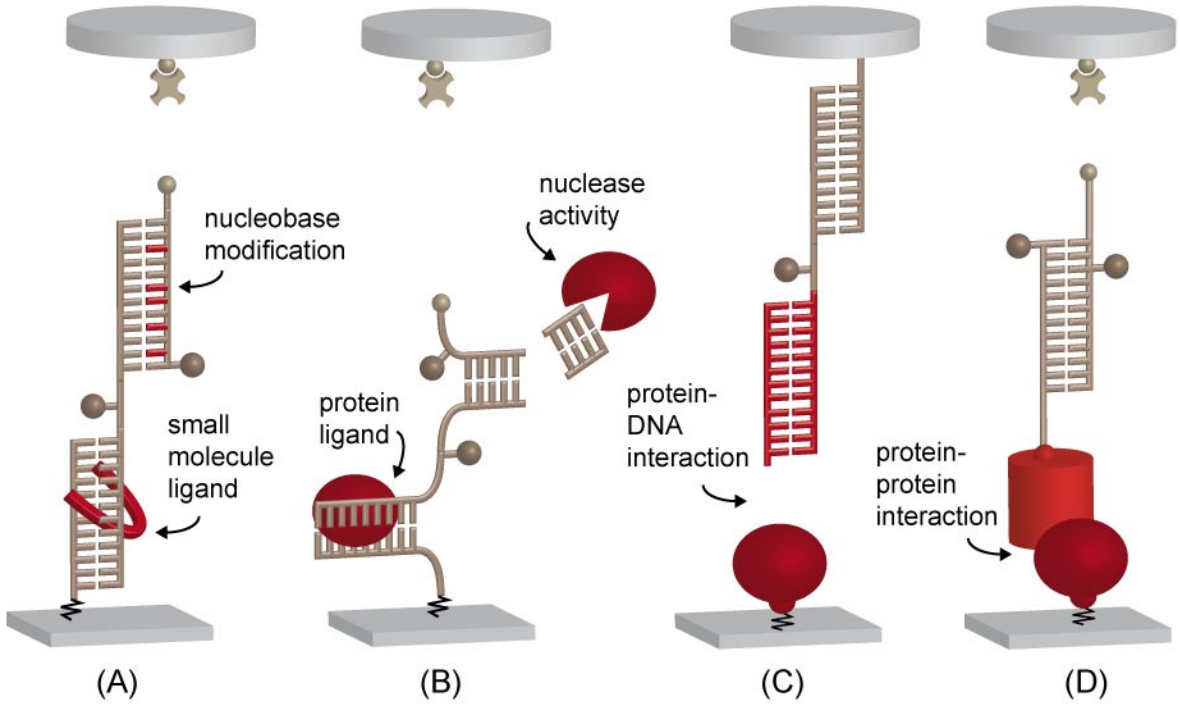

Figure 3.3: An overview of the different applications of the MFA is displayed, with the possible interactions and ligands highlighted in red. DNA and/or RNA can be implemented in shear (A) or zipper (B) mode. A variety of nucleobase modifications (A, upper part) and interacting ligands (A, lower part) can be characterized with the MFA. Proteins interacting with DNA or RNA can be measured if acting as nuclease (B, upper part), ligand (B, lower part) or directly as implemented in (C). The MFA even allows for the study of protein-protein interaction in a parallelized way, as shown in (D).

only acts on one base pair at a time. This leads to higher rupture forces in the shear mode, depending on the number of base pairs (see also section 2.3).

The application modes of the MFA can be divided into two subgroups. First, the MFA can determine modifications in the sample complex exploiting the fact that the modifications change the mechanical stability of the sample complex under force load. Examples for modifications that have been detected with this indirect detection method are nucleobase modifications such as single base pair mismatches [17] (destabilizing the complex), DNA bases modified with an additional propynyl group [32] (stabilizing the complex, see also manuscript B.1) or the methylation of DNA bases [88] (stabilizing or destabilizing dependent on the number of modifications), as shown in figure 3.3 (A), upper part. Also, the binding of small molecule ligands such as aminoglycosides [94] or polyamides [18] can be determined (figure 3.3 (A), lower part). The measurement of a concentration series with the ligand enables the determination of the dissociation constant K_D. Proteins are very complex molecules and more demanding to handle, but protein interactions can also be addressed by the MFA. DNA binding proteins

such as Eco RI [93] can be detected analogous to small molecule ligands (figure 3.3 (B), lower part). If the sample bond consists of an DNA or RNA duplex implemented in zipper mode, MFA can measure the activity of nucleases such as Dicer [94], as the complex is destabilized (figure 3.3 (B), upper part). The main advantage of those indirect measurements is that the analytes such as ligand or protein do not require any labeling or modification. The necessary labeling of the DNA or RNA with fluorophores occurs only well-removed from the binding sites of ligands. Note that in figure 3.3 (A) and (B) both upper and lower complex are displayed with modifications for simplicity; however, for most applications the reference complex is hold constant to compare the measurements against unmodified and modified sample complex. A proof-of-principle study established the integration of the standard DNA-MFA into a microfluidic device, which increases the throughput tremendously [96]. The second mode of applications has to be employed if not the modification of the sample bond but the mechanical stability of the sample bond itself is in question. As shown in figure 3.3 (C), it is thereby possible to probe protein-DNA interaction directly and not through its stabilization effect on the DNA. For this purpose, the MFP is not build up bottom up from the glass slide, but only the protein is attached to the lower surface and two DNA duplexes in series are directly attached to the upper PDMS surface. An example is the quantification of zinc finger protein interaction with different DNA sequences (given in publication A.4 [46]). The set-up as shown in (C) can also be modified to determine the strength of receptor-ligand interactions on living cells [97]. This second mode also allows to measure the interaction between different proteins. Figure 3.3 (D) shows the integration of a protein pair into the MFA. The protein-protein interaction can be characterized by comparing it against different known references or be compared to other protein complexes by measuring against the same reference. This application of the MFA was first implemented for this thesis and the example of nanobodies binding different GFPs will be explained in detail in section 4.3 and publication A.3 [98]. The key challenge hereby is the covalent site-specific attachment of the proteins, especially to the DNA, and will be discussed in section 4.2. For all implementation modes of the MFA, care has to be taken to avoid surface effects by a sensible choice of spacers between surfaces and the molecular constructs. In general, it has to be noted that rupture forces can depend on the force loading rate [83], which lies in the range of 10^5 pN/s for the MFA experiments conducted for this thesis (see section 3.2).

3.4 Comparison to the Atomic Force Microscope (AFM)

This section serves the purpose to compare the technique of the Molecular Force Assay to the complementary force spectroscopy technique of the atomic force microscope [10]. AFM is one of the most common techniques to measure forces in biological systems besides optical tweezers. In this thesis, it is employed in the study described in section 4.4 together with

MFA to gain a better insight in the behavior of propynyl-modified DNA.

In general, AFM relies on the principle of measuring forces by detecting the deflection they induce acting on a cantilever. The cantilever can be regarded as an elastic spring and its bending is monitored by a laser beam reflected from the top surface of the cantilever into an array of photodiodes. In order to detect the unbinding forces of a DNA duplex as described here, the complex to be investigated is clamped *via* polymer linkers between a glass slide and the sharp tip of the cantilever (see figure 3.4 (A), left). Separation of the cantilever from the surface builds up a force, which stretches the polymer linker and the DNA complex, yielding a deflection of the cantilever until the DNA finally ruptures. Statistically relevant data sets are obtained by repeating the circle of bringing the cantilever in contact with the surface in order to let the complex form and retracting of the cantilever in order to unbind the complex again. The conversion from photodiode voltages of the deflected laser beam into force values can be performed after cantilever spring constant calibration by the thermal method using the equipartition theorem [99]. Thus, force-extension curves (figure 3.4 (A), right) are obtained as the outcome of the AFM experiment. In order to investigate the loading rate dependence of the rupture force, the measurements are performed at different retraction speeds of the cantilever. The rupture forces for each distinct retraction velocity can be plotted in histograms and fitted with the Bell-Evans model [95] to obtain the most probable rupture force. The Bell-Evans model can now be applied to the resulting force versus loading rate dependency yielding the natural dissociation rate at zero force k_{off} and the potential width Δx of the investigated DNA complex. A general overview on the set-up, experimental procedure and analysis of AFM force measurements can *e.g.* be found in [100], more detailed information on the measurement of DNA unbinding forces is given in [16] or the supplement of manuscript B.1.

Comparing the AFM to the MFA technique shows that the two approaches address different aspects of the same problem. Thus, they offer different advantages and complement each other.

First, the different approaches lead to different *outputs* of the experiment. The comparative principle of the MFA yields information about the mechanical strength of the molecular interaction in question relative to the chosen reference. The result is read out for all MFPs simultaneously after bond rupture *via* the position of the fluorophores after force load (figure 3.4 (B)). For the determination of absolute values, the unbinding force of the reference complex has to be known. In contrast, the AFM is able to monitor the stretching and rupture process directly for every single interaction. Thereby, the rupture force and loading rate can be determined for every force curve. Conducting measurements on the same sample complex with different retraction velocities of the cantilever yield different loading rates. As described above, fitting of a polymer model to the resulting force-loading rate plot allows then to

determine the natural dissociation rate k_{off} as well as the potential width Δx characterizing the interaction.

Regarding the *sensitivity*, the MFA approach offers two advantages. First, the comparative technique does not depend on a calibration. Thus, a high force resolution can be obtained as no calibration uncertainties arise. Second, increased force resolution in the MFA results from the small size of its force sensor which consists only of a molecular complex. Due to thermal fluctuations, the force resolution is indirectly proportional to the size of the force sensor [101]. For the AFM, efforts have been made to reduce the size of the cantilevers, but this is only feasible to a certain degree.

Further, the way of obtaining sufficient data for relevant *statistics* differs tremendously. Both AFM and MFA can be regarded as single-molecule techniques as every complex to be investigated is tested against its own force sensor. However, the MFA features bulk read-out and a very high degree of parallelization and thus high statistics in one single contact process. In contrast, the high amount of contact and retraction processes needed to gain similar statistics with AFM render this technique more laborious in both experiment and analysis.

Finally, the differing *sample preparations* of AFM and MFA allow to address different incubation conditions of the complex in question. An AFM experiment depends on its capacity to measure the same interaction repeatedly, so that after every contact and separation process the initial state has to be reached again. This implies that the interaction to be investigated has to be the interaction formed upon contact, which is possible for many biological interactions displaying high on-rates. The time for the contact to be made can be increased by increasing the time of the contact process to a certain degree. A disadvantage here is that a long contact time can also lead to a higher number of unspecific interactions, which also result in force-extension curves but have to be separated in the analysis from the specific interactions. The AFM is thus not suitable to investigate interactions which do not rebind after initial separation. This holds not true for the MFA, where the complex to be investigated is build up bottom-up on the glass slide prior to completing the contact between both surfaces. Hence, due to the single contact and rupture process, the MFA can provide long incubation times of the sample complex. Additionally, it can give high statistics on interactions that do not rebind as in the MFA process the complex is loaded under force only once.

In summary, measuring a complex with both techniques helps to obtain a more detailed picture of the investigated interaction as they provide complementary informations.

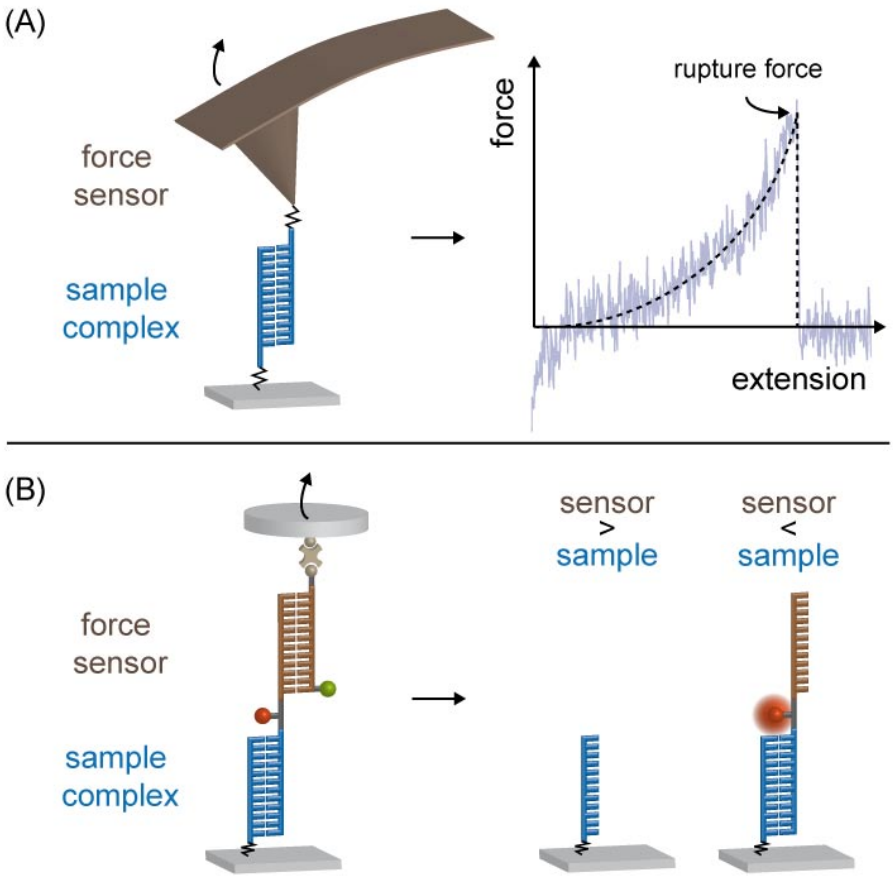

Figure 3.4: A schematic comparison between the experimental set-ups for force measurements with the atomic force microscope (A) and the Molecular Force Assay (B) is displayed. In both cases the sample complex to be investigated (blue) is initially clamped between two surfaces. For the AFM, the force load is applied by retraction of the cantilever (brown), an elastic spring, which acts as the force sensor. In the case of the MFA, the force load is created by the retraction of the stamp, which is connected to the sample complex *via* the second molecular complex (brown) acting as the force sensor. AFM experiments yield force-extension curves as read-out. A schematic example for a single rupture curve for a DNA complex is displayed ((A), right). In contrast, the result of an MFA experiment is read out *via* the position of the fluorophores after the separation process ((B), right).

4 Results and Discussion

After the description of the biological context and the techniques that are employed, this chapter presents the results of the work conducted in the course of this thesis. The results include the studies that demonstrate that both protein-RNA as well as protein-protein interactions can be characterized by MFA. Additional results refer to the prerequisites for the investigation of protein-protein interaction with the MFA, which are the generation of site-specific protein-DNA chimeras and the mechanical stabilization of DNA duplexes with propynyl bases for the use as force sensors. Additional information, especially on the chemical preparation of the experiments conducted in the different studies, can be found in the appendix in the publications A.1, A.2 and A.3, in manuscript B.1 as well as in their corresponding supplements.

4.1 Sequence-Specific Inhibition of Dicer Measured with a Force-Based Microarray for RNA Ligands

As described in section 2.2.2, the nuclease Dicer plays a pivotal role in the RNA interference (RNAi) pathway, which is an endogenous means to regulate protein translation in cells at the post-transcriptional level. Dicer starts the RNAi pathway by cleaving double-stranded RNA into pieces of 19-22 base pairs. Precursor molecules are thus matured into functional small RNAs that are able to influence translation by binding to specific mRNAs. One class of small RNAs are microRNAs (miRNAs) that are involved in the regulation of up to 30% [36] of all genes and, consequently, miRNA dysregulation has been linked to many severe diseases. Due to its central role, direct inhibition of Dicer is not desirable, but blocking the maturation of specific precursor molecules by binding of a small molecule ligand is a promising approach for medical therapeutics. A parallel screening system for ligand binding that is additionally able to determine Dicer inhibition is thus highly desirable. In a proof-of-principle experiment, it was shown that the Molecular Force Assay is well suited for this task as it allows for RNA ligand characterization as well as measurement of Dicer activity. The results of this study are published in publication A.1 [94].

The molecular set-up of the different steps of the experiment is displayed in figure 4.1. The complex in question is given by a RNA duplex, the reference complex by a DNA helix, ensuring

that Dicer can not affect it. Both are implemented in zipper geometry, to allow for Dicer cleavage on the RNA complex and a similar binding strength of both bonds. For the proof-of-principle, a well defined aptamer sequence for the binding of the ligand paromomycin, a 615 *dalton* aminoglycoside, is implemented into the RNA complex (figure 4.1 A). The measurements are performed in two configurations, with the RNA duplex implemented as the upper ("RNA up") or lower complex ("RNA down") of the MFP in order to exclude possible measurement artifacts.

As displayed in figure 4.1 (B) for the "RNA up" configuration, processing of the RNA by Dicer should result in a clear destabilization of the RNA complex and thus higher NF, as Dicer cleaves around 20 of the initially 35 base pairs of the RNA duplex. *Vice versa,* for the "RNA down" configuration the processing by Dicer should yield an decrease in NF. This detection of Dicer activity is clearly given in figure 4.2 (A), where the decrease of the NF value depends on the incubation time of Dicer. As the concentration of the RNA complexes is much higher than that of Dicer, it can be assumed to be constant. Consequently, the reaction rate is only limited by Dicer concentration yielding a linear decrease of the NF with incubation time of Dicer.

The binding of the ligand can be detected with the MFA as displayed in figure 4.1 (C). Ligand binding to the RNA should increase the stability of the duplex, yielding a decrease of the NF value for the "RNA up" configuration. Further characterization of the ligand and the determination of the dissociation constant K_{D} is achieved by the incubation of every spot of MFPs with a different concentration of the ligand paromomycin and fitting of the resulting data with an Hill equation (see figure 4.2 (B)). The resulting K_{D} of $2.55 \pm 2.18\ \mu M$ measured with the RNA complex as the upper bond is in agreement with literature values [102, 103].

The MFA is thus able to detect both Dicer activity and ligand binding to RNA. The combination of both, as displayed in figure 4.1 (D), should thus provide information about the inhibition of Dicer activity upon ligand binding. Figure 4.2 (C) gives the result of the full experiment for the example of RNA implemented as the upper complex. Incubation of 2.5 μl Dicer solution in 1 ml buffer for 1 hour prior to the force assay yields an increase in NF, meaning a destabilization of the RNA complex, in comparison to the initial start value obtained with neither Dicer nor ligand. The addition of 1 mM paromomycin ligand to another sample results in a stabilization effect and thus a decrease of the NF value. Finally, the incubation of first paromomycin and then Dicer for 1 hour yields a NF value close to the ligand only case. This can be attributed to strong but not complete inhibition of Dicer by the ligand bound to the RNA complex. For the RNA down configuration, the same but respectively reverted results are obtained (see publication A.1). Additionally, a minimum concentration of 2.82 μM paromomycin for partial blocking of Dicer could be determined, which agrees with the measured dissociation constant of $2.55 \pm 2.18\ \mu M$.

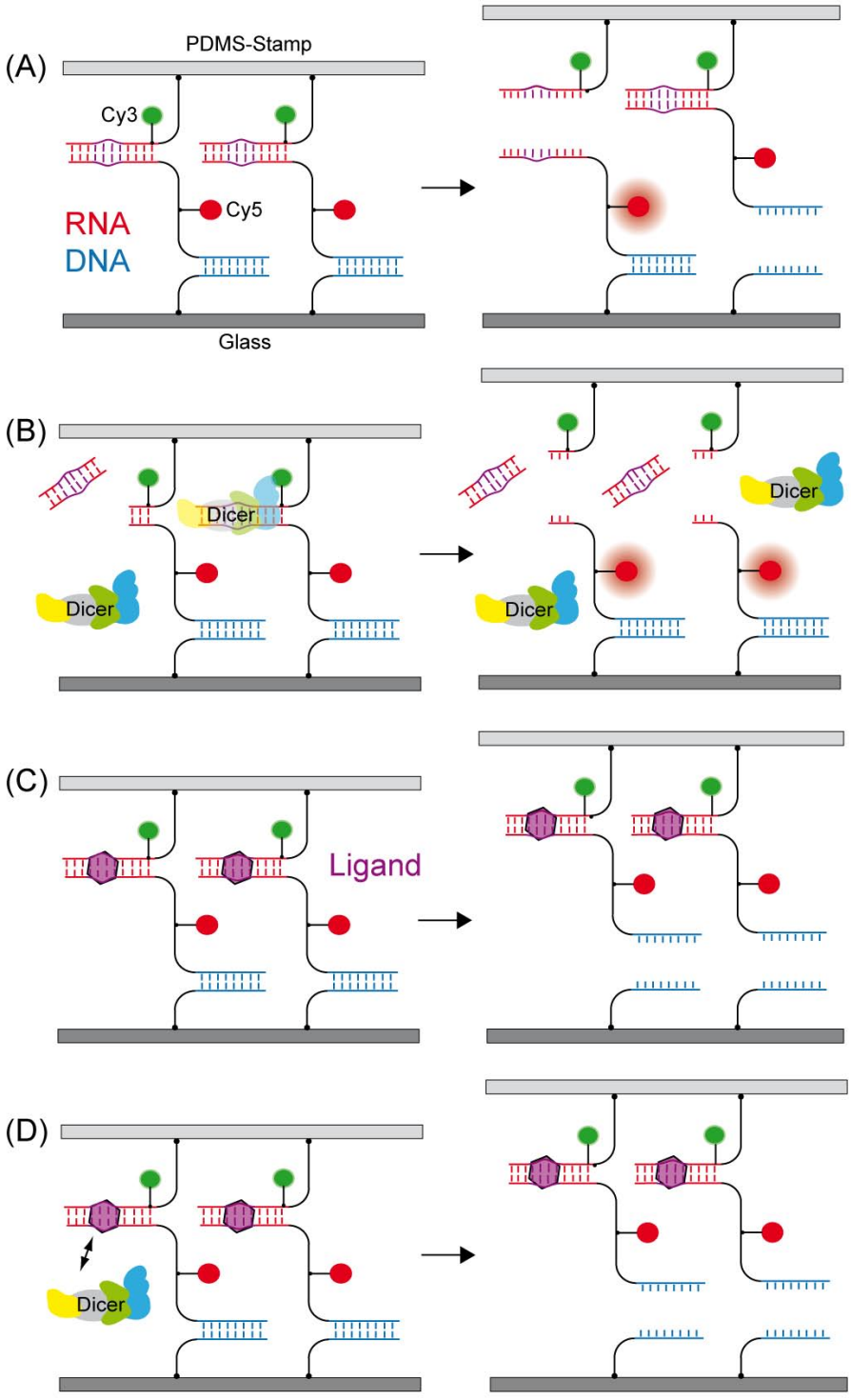

Figure 4.1: For the detection of Dicer inhibition upon binding of a small molecule ligand, first the initial value of the molecular set-up with neither Dicer nor ligand present has to be determined (A). Incubation of the molecular complexes with Dicer leads to a destabilization of the RNA duplex and thus, in the case of RNA constituting the upper complex, to an increase in the Normalized Fluorescence (B). Binding of a ligand stabilizes the RNA duplex and can be detected by a decrease in Normalized Fluorescence for the "RNA up" configuration (C). To detect a possible inhibition of Dicer cleavage, the complexes are first incubated with the ligand and then with Dicer. Blocking of Dicer yields a Normalized Fluorescence close to the ligand only case. Adapted from publication A.1 [94].

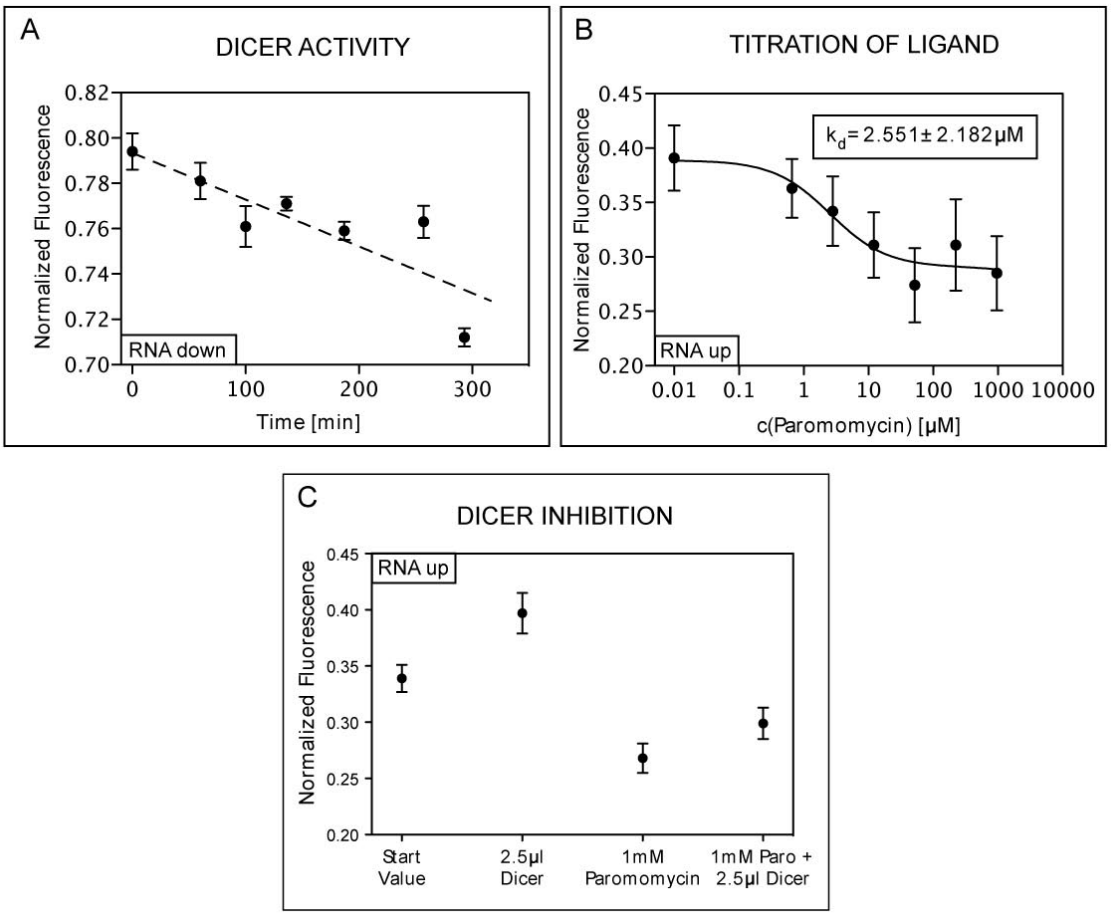

Figure 4.2: Dicer activity is measured in an excess of the RNA substrate. As the processing rate is thus only limited by Dicer concentration (2.5 μl Dicer solution in 1 ml buffer), it is linear with incubation time. Since processing by Dicer destabilizes the RNA complex by cutting of about 20 of the 35 base pairs, this is clearly visible in the linear decrease of the Normalized Fluorescence for the case of the RNA duplex implemented as the lower complex (A). Titration of the ligand paromomycin leads to a gradual stabilization of the RNA complex, leading to a decrease in the Normalized Fluorescence value for the "RNA up" configuration (B). Fitting of an Hill equation isotherm allows for the determination of the dissociation constant of the ligand. (C) For the detection of Dicer inhibition upon ligand binding, four independent measurements are conducted. Incubation with Dicer yields a higher NF compared to the initial start value, as the upper RNA complex is destabilized by Dicer. In contrast, ligand binding leads to decreased NF value. Blocking of Dicer upon ligand binding should result in an NF value close to the ligand only case, which is confirmed in the last data point. Adapted from publication A.1 [94].

In conclusion, the proof-of-principle experiment shows that the cleaving of double-stranded RNA by Dicer can be selectively inhibited by the binding of a small molecule ligand. The technique of the MFA can be employed to reliably detect this blocking of Dicer and be additionally used for the screening of potential RNA ligands. The current standard set-up allows for the parallel screening of 16 different RNA sequences, ligands or ligand concentrations. Further parallelization and miniaturization *e.g.* by implementation of the assay into a microfluidic chip, as described in the outlook of this thesis, would render the MFA high throughput and allow for a more efficient screening for potential therapeutic drugs.

4.2 Preparation of Protein-DNA Chimeras Employing the ybbR-Tag

In order to understand and exploit the diverse functional and structural properties of proteins, they need to be studied in various contexts. Especially in bioanalytical chemistry, molecular diagnostics or nanobiotechnology, *e.g.* for the DNA origami technology, efficient chemical attachment strategies are highly needed. The generation of protein-DNA chimeras offer various advantages as DNA conjugated to a protein of interest provides a unique handle *e.g.* for identification and functionalization [24, 28]. They are also essential in order to characterize protein-protein interactions with the Molecular Force Assay as described in the next section 4.3. Additionally, protein-DNA chimeras allow for the controlled arrangement of proteins at angstrom level precision with Single-Molecule Cut & Paste (SMC&P), as described in publication A.2 [104]. With SMC&P, it is possible to pick up individual molecules from a depot area with an AFM cantilever and to deposit them one by one at defined positions in the target area. It thereby relies on a force hierarchy and the selective binding properties of DNA (as described in section 2.3). Originally developed for DNA only, the efficient coupling of proteins to DNA renders SMC&P with proteins just as robust and effective.

In principle, several possibilities exist for the general attachment of proteins [24], but they vary widely in experimental cost, yield and applicability for the coupling to DNA. For the measurements conducted within the scope of this thesis, as for single-molecule force spectroscopy experiments in general, both site-specific as well as covalent attachment of the molecules is required. Site-specificity is important as the unbinding force of a complex depends on the pulling geometry and thus on the position of the attachment [23]. The covalent attachment ensures that an unbinding process can be clearly attributed to the complex in question and that the protein attachment does not dissociate over time [105]. Additionally, a minimal modification of the protein of interest is desired. Since the different methods for protein-DNA coupling display certain drawbacks, no gold standard exists hitherto [104]. Wild-type proteins without any modification can be attached by methods such as the targeting of lysine

residues on the protein surface, but the need for site-specificity excludes this possibility. Such general techniques harbor the drawback of mostly not being able to control the stoichiometry of the coupling [24]. The problem of site-specificity can be solved by genetical modification of the proteins of interest, which allows *e.g.* for the implementation of a single free Cysteine residue or fusion protein tags, such as the suicide enzyme SNAP-tag (hAGT) [28]. In the case of the SNAP-tag the size of 20 kDa leads to a rather large modification of the protein of interest. In contrast, the additional size of an incorporated Cysteine residue is negligible, and its binding to thiol- or maleimide functionalized DNA is straight forward. On the downside, it can lead to changes in the patterns of disulfide bonds required for proper protein folding. As the Cysteine residues have to be accessible for attachment, the proteins of interest can form unwanted dimers *via* disulfide bonds that have to be broken prior to attachment. For every protein of interest full integrity and functionality under these conditions has to be ensured [105]. The required maleimide group on the DNA offers the advantage of only binding to the thiol group of the Cysteine, while a SH-group on the DNA can also lead to cross linking of the DNA oligonucleotides and thus to a lower yield. However, care has to be taken if a maleimide group is employed due to its time-limited activity in aqueous environments. Other newly presented techniques include light induced DNA-protein conjugation [106] or, for metal-binding proteins, DNA-template directed protein conjugation [107].

For the experiments presented in this thesis we thus chose to employ the 11 amino acid long ybbR-tag [25]. Mediated by the Phosphopantetheinyl Transferase Sfp [27], it couples covalently to Coenzyme A (CoA), which in turn can easily be reacted to maleimide-modified DNA. Upon request, the full DNA-CoA construct is available for purchase from certain companies. In addition to the negligible size, the ybbR technique offers a very high yield, as a coupling efficiency of over 90% can be reached [104]. The ybbR-tag sequence DSLEFIASKLA can be implemented on either the N- or C-terminus or at accessible unstructured regions and is thus very well suited for site-specific attachment. So far, the ybbR-tag is widely used for protein labeling with *e.g.* biotin and fluorescent dyes and has also successfully been employed for the immobilization of proteins on a surface for force spectroscopy experiments [46, 108]. A standard protocol for the ybbR-coupling can be found in [26].

A sample SDS-PAGE gel displaying the efficiency of the ybbR-tag can be found in figure 4.3. Two different proteins, transcription factor Bicoid from *Drosophila melanogaster* [109] labeled with superfolder GFP and a superfolder GFP with a GNC4 peptide handle (as employed in publication A.2 [104]), both harboring a ybbR-tag at the N-terminus, are coupled to a 50 nucleotide DNA strand with a CoA attached on its 5' and a Cy5 fluorophore on its 3' end. Since GFP is still fluorescent in a SDS-PAGE Gel, the colocalization of the protein and the DNA band in the respective lanes 4/5 and 9/10 is clearly visible in the overlay of the fluorescence scans (figure 4.3 (A), purple bands). The efficiency of the coupling can be tuned upon demand. Depending on the desired outcome, a higher concentration of DNA

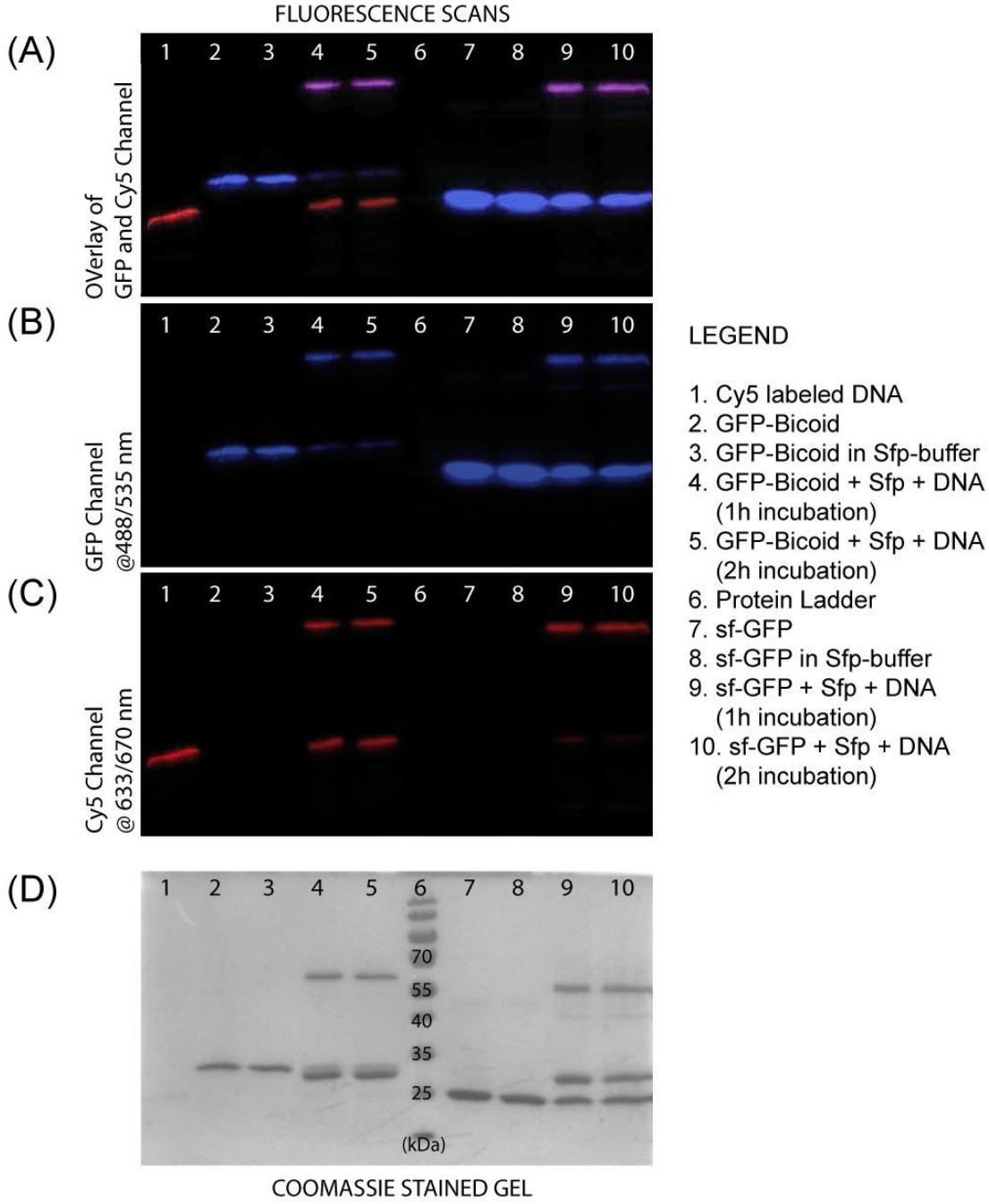

Figure 4.3: The sample SDS-PAGE gel demonstrates the efficiency of the protein-DNA coupling *via* the ybbR-tag. (B) and (C) display fluorescence scans of the sample gel at the corresponding wavelengths for the Cy5 label on the DNA (red bands) and the GFP (blue bands), respectively. Both in lanes 4/5 as well as 9/10 a second band due to the protein-DNA-coupling appears. The colocalization (purple bands) of these bands is clearly visible in the overlay (A). In (D), a coomassie stain image of the same gel is given. Depending on the desired outcome, a higher concentration of DNA than proteins (5 μM to 3.5 μM) leads to a larger fraction of conjugated proteins (lane 4/5). *Vice versa*, a higher concentration of proteins than DNA (15 μM to 5 μM) results in the conjugation of most DNA strands. The different incubation times of 1 or 2 h display no significant difference in coupling yield. A standard protocol for the ybbR-coupling of proteins is given in [26]. Protocols for protein-DNA coupling *via* the ybbR-tag can be found in the publications A.2 and A.3.

than proteins can be chosen to ensure a large fraction of proteins conjugated (see lane 4/5). *Vice versa*, a higher concentration of proteins leads to an almost full saturation of DNAs with protein (see lane 9/10). Standard protocols [26] suggest an incubation time of 30 *min*, and the sample gel displays no significant difference between the duration of the incubation of 1 *h* and 2 *h*. In general, the suitable incubation time can vary for each protein and the progress of conjugation should therefore be followed by analyzation in gels. The coupling reaction takes place at standard buffer conditions, so the protein of interest can also be coupled to double-stranded DNA where one of the DNA strands harbors the CoA. This is highly needed for molecular set-up of the MFA for protein-protein interaction, which will be described in the next section. In summary, ybbR-mediated protein-DNA coupling worked highly robust and efficient for several experiments conducted in our lab. More details on the conjugation process as well as the force spectroscopy experiments that can be conducted with the resulting chimeras can be found in the publications A.2 for Protein-SMC&P and A.3 for Protein-MFA.

4.3 Parallel Force Assay for Protein-Protein Interactions

The need to investigate the intermolecular binding forces that control protein-protein interactions is becoming more and more acknowledged. The development of single-molecule force spectroscopy techniques such as the AFM or optical tweezers have enabled direct quantification of these forces and energy landscapes in biomolecules and biomolecular interactions [33, 13]. However, they suffer from common drawbacks. In order to gain statistically sufficient data sets, high efforts are needed and calibration uncertainties arise from the infeasibility of measuring different interactions in parallel.

As part of this thesis, the characterization of protein-protein interactions with the Molecular Force Assay was demonstrated, meeting the need for parallelization of direct force-based measurements of those interactions. In order to be able to characterize pair-wise protein-protein interactions, the proteins have to be integrated site-specifically and covalently in the molecular set-up of the MFA. As depicted in figure 4.4, one of the proteins is attached to the lower glass slide and the other to one strand of the DNA duplex acting as the reference bond. The proof-of-principle study conducted here aims to test the interaction between three different variants of Green Fluorescent Proteins (GFPs) with the GFP-binding nanobody "Enhancer" as described in section 2.2.3. In order to enable the detection of small differences in binding strengths, the window of high sensitivity of the assay was determined by testing the protein complex against references with different binding strength. Comparison with a second nanobody, a modified variant of Enhancer, highlighted the dependence of the sensitivity on the chosen reference. The results of the study are published in publication A.3 [98].

Nanobodies are small single-domain antibodies derived from camelids. Enhancer is a nanobody

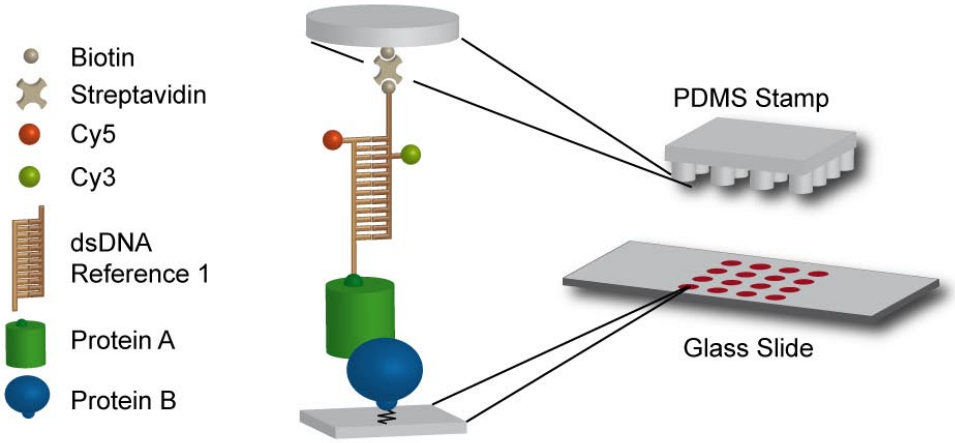

Figure 4.4: In order to enable direct measurement of protein-protein interactions with the MFA, the protein pair is integrated as the lower complex into the molecular setup. It is important to note that both proteins are attached covalently. They are coupled to the lower glass slide and to one of the DNA strands forming the reference duplex, respectively. Two fluorophore dyes forming a FRET pair and a biotin are coupled to the reference DNA, allowing for the readout as well as attachment to the upper PDMS surface as in the standard set-up of the MFA described in chapter 3.

variant that has been generated and selected for its ability to bind wild type GFP (wtGFP), thereby influencing its fluorescence intensity. Upon binding to Enhancer, perturbations in the chromophore environment of wtGFP lead to a fourfold fluorescence enhancement [30]. This effect can be exploited for numerous applications (see section 2.2.3). Since the binding epitopes of the nanobodies lie on the outer beta barrel of wtGFP, binding occurs also to other GFP variants such as enhanced GFP (eGFP) and super folder GFP (sfGFP) for which the general structure is conserved. GFP's ability to act as an intrinsic control for the correct molecular assembly of the assay and the availability of structural data for the Enhancer-wtGFP interaction made the nanobody-GFP system well suited for this proof-of-principle study. For the characterization by means of the MFA, the nanobodies were attached covalently *via* a C-terminal Cysteine to the glass slide. The GFP variants, all harboring a N-terminal ybbR-tag, were coupled to the Coenzyme A-modified DNA. The covalent protein-DNA coupling is discussed in detail in section 4.2. The FRET pair of Cyanine dyes and the biotin on the DNA reference duplex as depicted in figure 4.4 allow for measurement, readout and analysis processes as described for the DNA-only MFA in chapter 3.

Analogous to an old-fashioned scale balance, the MFA has its highest sensitivity to determine small differences in binding strength if well balanced, which in this case means that the binding strength of the protein complex and the DNA reference are similar and lead to a NF value around 0.5. However, initial experiments indicated the Enhancer-GFP interaction to be stronger than a 40 base pair DNA complex in shear conformation with an NF of over

0.9. Due to the force plateau of the BS-transition of DNA at about 65 pN (see section 2.3), higher average forces can not be reached with short oligonucleotides. For higher sensitivity, stabilization of the DNA reference is highly needed. In order to demonstrate the flexibility and robustness as well as to determine the window of high sensitivity of the assay, two different means to enhance the stability of the DNA reference are employed.

As described in section 2.3, several possibilities exist to obtain increased mechanical stability of DNA duplexes. Intrinsic stabilization of the reference duplex can be achieved by the modification of pyrimidines with a propynyl group at their C-5 position. The hydrophobic group extends into the major groove and is expected to stabilize the duplex due to increased base-stacking. In the experiments presented here, 13 cytidines and 9 thymines are replaced by their respective propynyl bases in the biotinylated strand (see supplemental figure S2 of publication A.3). Further information on the stability enhancement through propynyl bases can be found in the next section 4.4. Additionally, it is possible to increase the stability extrinsically by the addition of a DNA binding ligand. Here, three different pyrrole-imidazole sequence-specific hairpin polyamides with different binding affinities for the same DNA sequence are employed. Polyamides P1 ($K_\mathrm{D} = 105\ pM$), P2 ($K_\mathrm{D} = 44\ pM$) and P3 ($K_\mathrm{D} = 1442\ pM$) characterized with the MFA by Ho *et al.* [18] have been used in a concentration of 1 μM, about 1000 times the saturation concentration, to ensure an excess of available ligand.

In figure 4.5 A, the different references used to identify the window of high sensitivity of this application of the MFA are depicted: 40 base pair long double-stranded DNA with and without propynyl modification as well as 20 base pair DNA complexes extrinsically stabilized by the binding of the respective polyamide. Representative data for the different references tested against a Enhancer-sfGFP complex are given in figure 4.5 B. In order to highlight the change in sensitivity depending on the reference stability, the binding of a second nanobody, a modified Enhancer, to sfGFP is investigated as well. The outcome of the experiment, namely the relative higher NF values and thus stronger binding for the modified Enhancer in comparison to Enhancer, stays the same for all references employed. This has to be expected as the reference does not influence the protein complex. The absolute NF values, however, change depending on the chosen reference.

The stronger binding of the modified Enhancer can be attributed to its more positive charge (pI $\approx$ 9.89) in comparison to the original Enhancer (pI $\approx$ 7.85), affecting the binding to the slightly negatively charged sfGFP (pI $\approx$ 6.4) at the given buffer condition (pH 7.4). The differences between the data points for Enhancer and modified Enhancer become significantly larger the closer the mechanical stability of the reference is to the stability of the protein pair. This corresponds to the increased sensitivity the closer the NF values are to 0.5. While the incorporation of the propynyl bases results in a decrease in NF of about 10% in comparison to the unmodified DNA, the effect of the polyamides is stronger and depends on the respective

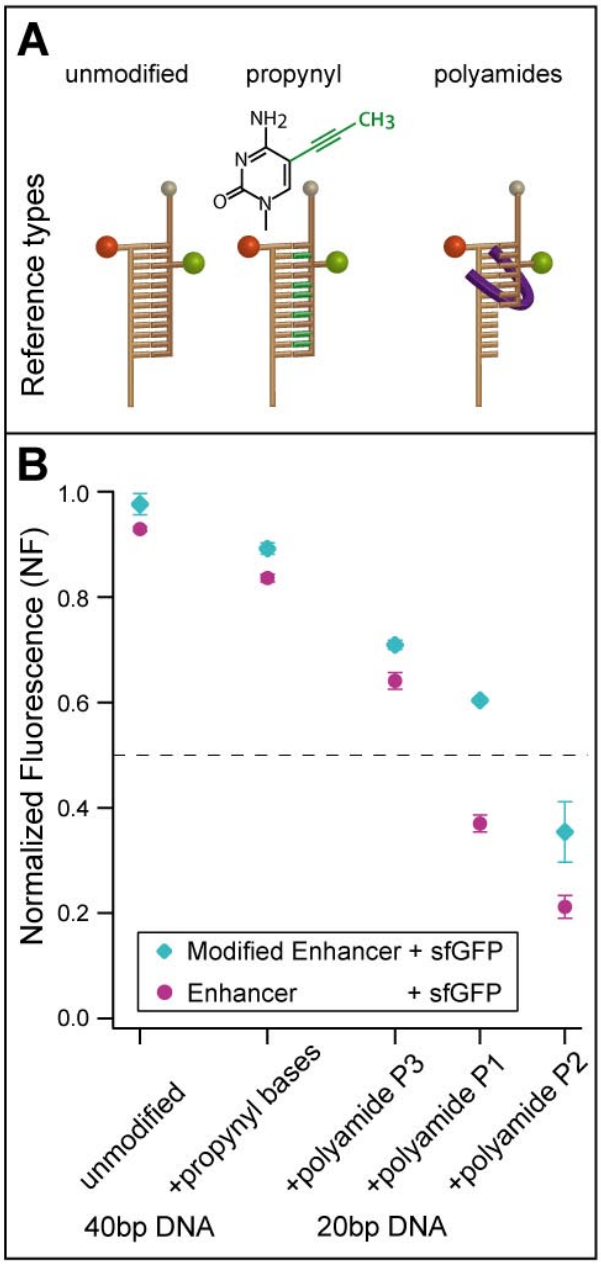

Figure 4.5: (A) The three different types of references employed are unmodified DNA (left, 40 base pairs), DNA intrinsically stabilized by the integration of propynyl bases (center, 40 base pairs) as well as the external stabilization of the DNA duplex upon binding of sequence-specific polyamide ligands (right, 20 base pairs). (B) Representative data of Enhancer and Modified Enhancer binding to sfGFP are given for all different types of references. While the relative order of Modified Enhancer yielding higher NF values than Enhancer is the same for all references, the absolute values are clearly dependent on the chosen reference. The increasing difference between the NF values for Enhancer and Modified Enhancer for absolute values closer to 0.5 display the higher sensitivity in this range. Reproduced from publication A.3 [98].

dissociation constant. As expected, the stabilization effect is higher the lower the K_D of the polyamide. While P3 already has a higher effect on the NF as the internal propynyl modification, the addition of P1 tunes the NF value closest to neutral. P2 reduces the NF even more, which will enable to characterize even stronger protein pairs than the nanobody-GFP complexes at high sensitivity.

In order to determine the difference in binding strength between the three GFP variants, namely eGFP, wtGFP and sfGFP, to Enhancer, the 20 base pair complex stabilized with polyamide P1 is employed as a reference, as it tuned the NF closest to neutral (figure 4.5 B). The result of a representative example measurement is given in figure 4.6 A. While the NF values for eGFP (0.255 ± 0.023) and wtGFP (0.253 ± 0.018) binding to Enhancer are the same within experimental error, both lie distinctively lower than the NF for the sfGFP-Enhancer complex (0.353 ± 0.018). All data points are derived from one single experiment, thus ensuring exactly the same conditions for all complexes and minimizing measurement error. The final NF values are obtained as averages from several spots of identical molecular complexes. However, sample histograms of single protein spots of all three GFPs as depicted in figure 4.6 B display the extensive number of protein-protein interactions tested simultaneously in each single spot.

The higher NF value for the sfGFP-Enhancer interaction corresponds to a higher ratio of intact protein bonds after force load and thus a stronger interaction than for the other GFP-Enhancer complexes. This could result from the mutation of several amino acids for which contacts have been determined for wtGFP by Kirchhofer *et al.* [30], as displayed in the crystal structure given in figure 2.2. Nine amino acids of wtGFP are determined to form 13 direct contacts as well as three amino acids to be responsible for hydrophobic interactions. The alignment of the sequences of all three GFPs (see supplemental figure S3 of publication A.3) shows that all interacting amino acids are conserved for eGFP, which is in good agreement with the observed similar binding strength. However, the difference in binding to sfGFP could result from the mutation of two amino acids forming the direct and all three amino acids forming the hydrophobic interactions.

In summary, the technique of the MFA could successfully be adapted and developed further to allow for the characterization of protein-protein interactions. With the employment of stabilized DNA references, the dynamical range of the assay could be broadened significantly. It now reaches from the lower boundary of DNA implemented in zipper mode, over DNA in shear mode in different lengths to intrinsically and extrinsically stabilized DNA. The upper boundary could even be extended further with stronger ligands such as the DNA binding proteins EcoRI and p53 [19]. Since the binding strength for a random protein pair is not known *a priori*, the variability of references is extremely important in order to enable characterization at high sensitivity. Hence, the Protein-MFA is applicable for many different protein pairs of

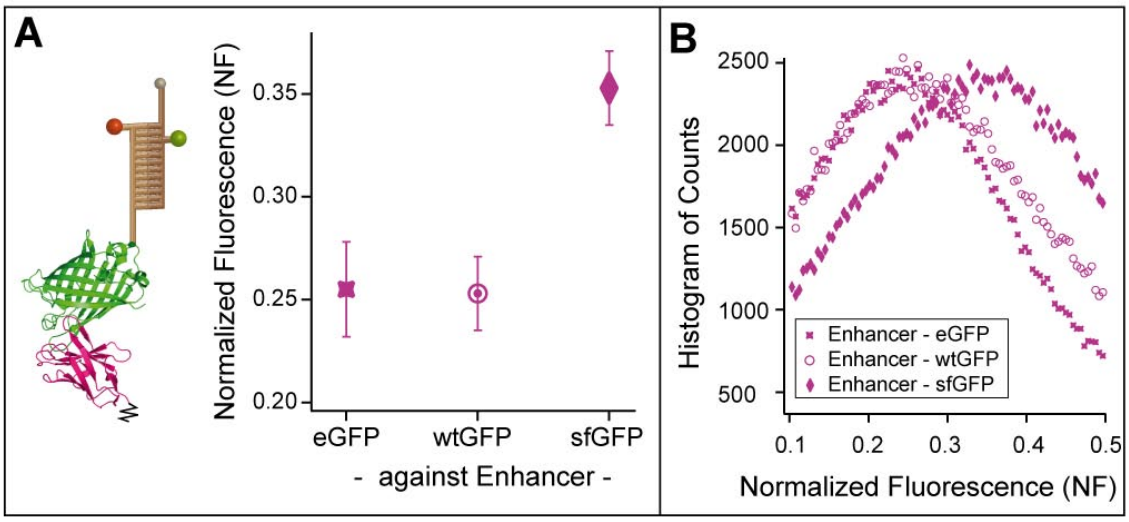

Figure 4.6: (A) A schematic depiction of the molecular set-up with the ribbon model structure of wtGFP (green) - Enhancer (magenta) complex is given. The binding of eGFP, wtGFP as well as sfGFP to Enhancer is directly compared in one example measurement with the Protein-MFA. While the binding strength of eGFP and wtGFP do not differ within experimental error, binding of Enhancer to sfGFP is distinctively stronger. (B) The extensive number of parallelized single-molecule experiments is illustrated by sample histograms of single spots containing one type of protein-protein complex each. Reproduced from publication A.3 [98].

varying bond strength.

More details on the chemical preparation of Protein-MFA and the proof-of-principal study on nanobody-GFP interaction can be found in publication A.3 and its respective supplement [98].

4.4 C-5 Propynyl Modifications Enhance the Mechanical Stability of DNA

The need for short DNA duplexes with higher mechanical stability than can be obtained with unmodified DNA becomes apparent from the study described in the previous section but can also be useful for other applications in nanotechnology and -medicine. Prominent examples where DNA is used as a programmable building block are scaffolded DNA origami which allow to create two and three dimensional defined structures at the nanoscale [75, 76, 77]. Methods to enhance the thermal stability of such DNA structures already exist. An example is photo-cross-linking which improves heat tolerance of origami structures by about 30°C [110]. However, the thermal and mechanical stability are not directly correlated. The reaction to mechanical stress largely depends on the orientation in which an external force is applied, as

outlined for a double-stranded DNA oligonucleotide in section 2.3.

As described in the previous section 4.3, the implementation of propynyl-modified pyrimidines is able to enhance the mechanical strength of DNA duplexes. Here, the complementary techniques of MFA and AFM are employed to characterize the mechanical properties of DNA duplexes harboring propynyl bases in detail. The chemical composition of these bases can be found in figure 2.4 A and section 2.3. In short, the apolar, planar propynyl group is attached to the C-5 position of pyrimidines, extends into the major groove of the DNA helix and is assumed to enhance base-stacking interactions.

For this study, three different 40 base pair long oligonucleotides are investigated in shear mode, harboring no base modification (0P), eight propynyl-desoxycytidines (8P) and 13 propynyl-desoxycytidines as well as 9 propynyl-desoxyuridines (22P), respectively. The modifications are distributed over the same sequence to enable binding to the same complementary, unmodified DNA strand (the sequences can be found in figure 1 of manuscript B.1). The basic principle of measuring rupture forces of DNA duplexes with AFM in comparison with the relative quantification in MFA is depicted in figure 3.4. For the measurements with the AFM, the two DNA strands forming a complex are attached covalently *via* PEG spacers to the cantilever and the lower surface, respectively [16]. The DNA duplex to be investigated is formed when the cantilever is lowered onto the glass slide, retraction of the force-calibrated cantilever stretches both duplex and PEG linker until the DNA duplex finally ruptures. AFM experiments were performed to determine if the integration of propynyl bases leads to higher average rupture forces than for unmodified DNA. All measurements were conducted with the same cantilever harboring the complementary strand to minimize calibration uncertainties. The DNA strands 0P, 8P and 22P were attached covalently to the surface in three distinct populations. Representative histograms for data obtained with a retraction velocity of 1000 nm/s are given in figure 4.7. They are fitted with the Bell-Evans-Model (see [95] or the supplement of manuscript B.1). The most probable rupture forces for the three different possible complexes were determined as 65.1 ± 4.5 pN (0P; N= 705 curves), 65.5 ± 4.4 pN (8P; N= 579) and 64.7 ± 4.5 pN (22P; N= 1079), respectively. Hence, the rupture forces are indistinguishable within error. This holds also true for the other retraction velocities that were tested (the corresponding data can be found in the supplement of manuscript B.1). Pair-wise two-sample Kolmogorov-Smirnov tests were performed to test the hypothesis whether the rupture force distributions were significantly different. As a result, the rupture force distributions for 8P and 22P were found to differ significantly from the 0P distribution with a p-value below 0.05 for all retraction velocities besides 500 nm/s. In detail, the p-values of the 22P distributions are considerably smaller than those of the 8P distributions, when compared against the 0P distributions. This is reflected in the width of the rupture force distributions as they increase with the number of propynyl modifications.

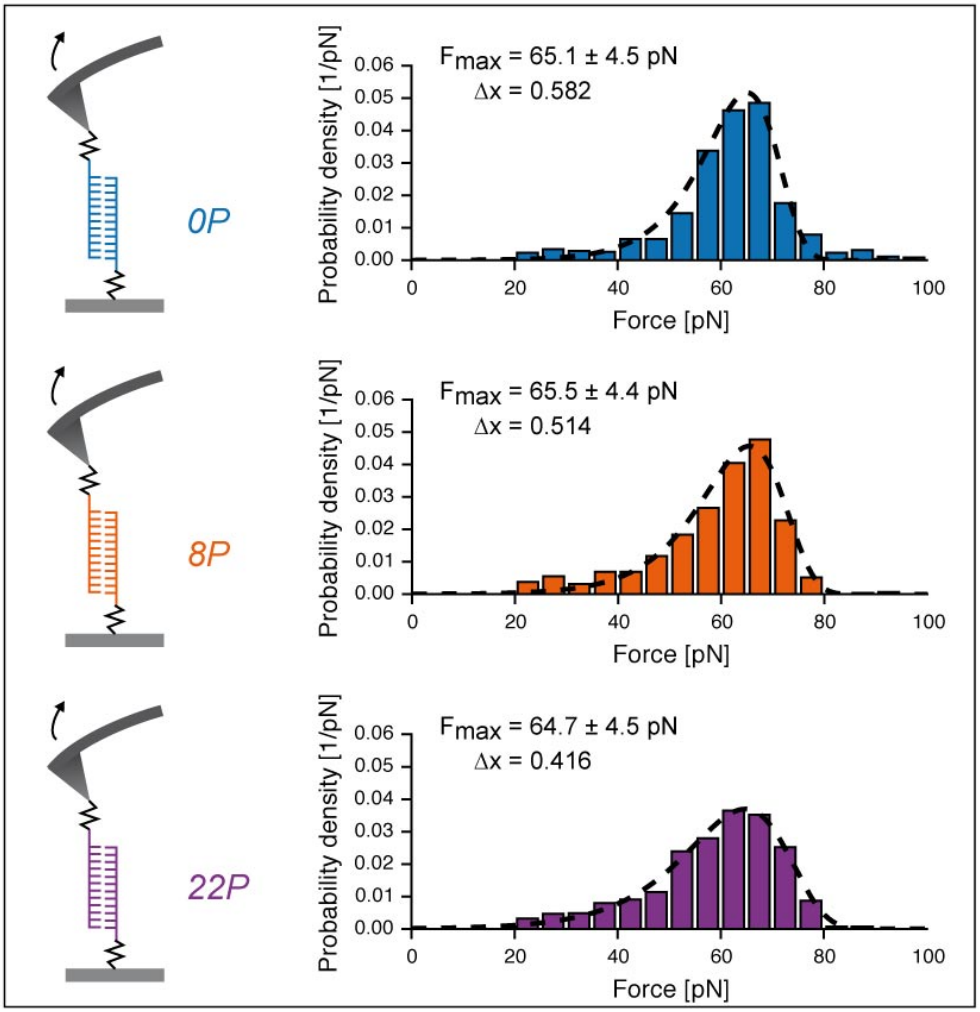

Figure 4.7: Representative histograms of the most probable rupture force for the three investigated DNA duplexes with varying amount of propynyl bases are displayed (retraction velocity of the cantilever: 1000 nm/s). The most probable rupture forces $F_{\max}$ are not distinguishable within error and lie in the vicinity of the BS-transition ($\approx$ 65pN). They were obtained by fitting the histograms within the Bell-Evans formalism.

For the MFA measurement of the same DNA complexes, the Normalized Fluorescence values are determined according to equation 3.3 and the measurement was performed as described in chapter 3. As the DNA duplex in question is implemented as the upper complex, a decrease in NF is equivalent to an increase in stability of this duplex. In contrast to the AFM measurements, where the duplex to be investigated forms when the cantilever is brought into contact with the glass surface, the molecular complexes for the MFA measurements are completely assembled on the glass slide in advance. This allows different modes of pre-incubation of the complex in question. Each of the duplexes with 0P, 8P and 22P oligonucleotides are thus tested after pre-incubation at room temperature (RT) over night or by heating to 95°C and cooling slowly over four hours to 5°C. As displayed in figure 4.8, the corresponding results for the NF values and standard deviation errors are $NF_{RT}(0P) = (0.341 \pm 0.007)$, $NF_{RT}(8P) = (0.327 \pm 0.014)$, and $NF_{RT}(22P) = (0.316 \pm 0.013)$ for incubation at RT as well as $NF_{95}(0P) = (0.344 \pm 0.011)$, $NF_{95}(8P) = (0.306 \pm 0.012)$ and $NF_{95}(22P) = (0.262 \pm 0.017)$ for annealing with high temperature. The complexes formed at RT (right bars) display only a slight stabilization with increasing number of propynyl bases, whereas for the annealed complexes (left bars) this stabilization effect is significant. As expected, the mode of incubation does not influence the stability of the unmodified DNA duplex.

Hence, the probability of strand separation in comparison to the unmodified 0P DNA is reduced about $\frac{NF(8P)-NF(0P)}{NF(0P)} = -11\%$ for the 8P and -24% for the 22P duplex. When characterizing the mechanical stability of methylated DNA, another internal base modification, with both AFM and MFA, Severin *et al.* [88] obtained the same results for stabilizing and destabilizing effects with both techniques. Thus, the differing results of the AFM from the MFA measurements in the case of propynyl-modified DNA can be attributed to different conformations of the DNA resulting from the very different incubation conditions. Both the temperature and time span differ tremendously in AFM and MFA experiments. In AFM, the duplex forms at RT during the contact time of the cantilever to the surface. This time has to be below 0.1 s, as otherwise the probability to obtain single DNA binding events is reduced extremely. Under the chosen conditions, the AFM measurements yield distinct populations of rupture force for all three samples. The oligonucleotide sequences were chosen to allow for one binding mode only. However, the width of the force distributions increases slightly with the number of base modifications resulting from an elevated number of rupture events at lower and higher rupture force. This higher variance of the modified DNA distribution might be attributed to short lived perturbations in duplex formation due to the propynyl bases. In comparison, the samples incubated at RT in the MFA experiments also display only a very small stabilization effect. This leads to the assumption that even though the DNA duplex forms during the AFM measurement, it does not aquire a conformation in which the propynyl group can stabilize the DNA significantly. This indicates a complex energy landscape and a high potential barrier that needs to be overcome in order to form the stabilized complex.

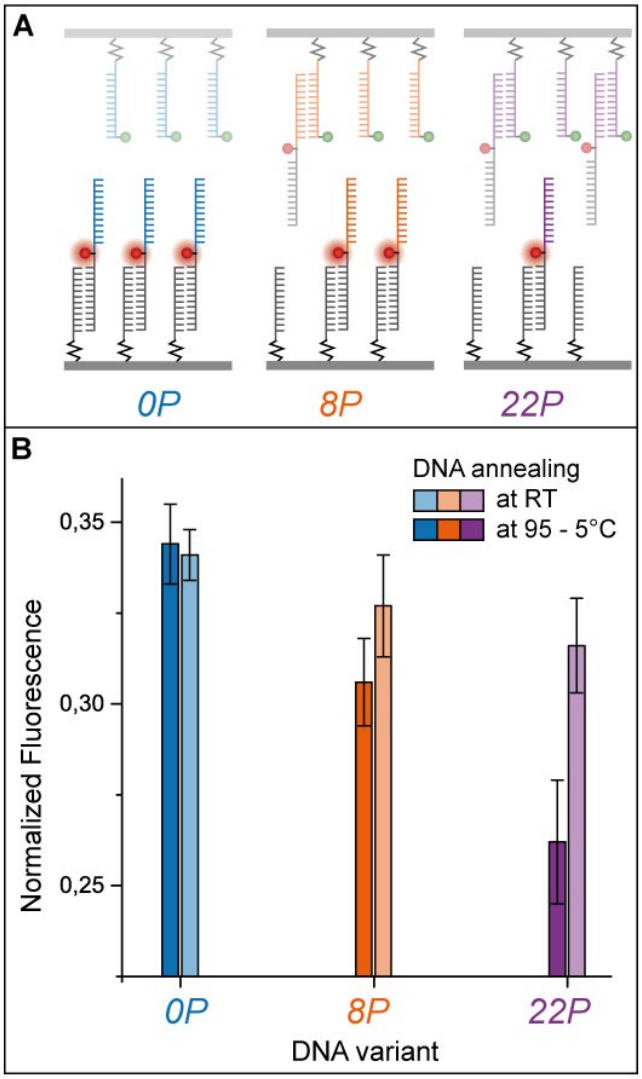

Figure 4.8: The molecular complexes in series for the MFA are fully assembled on the glass slide prior to the actual force load. This allows for pre-incubation of the DNA duplex in question under different conditions. (A) In general, the more stable the upper complex is when compared to the same reference, the less fluorescence signal remains on the glass slide after force load, leading to a smaller Normalized Fluorescence value. (B) The NF values for all three DNA variants are given. Hereby, two different incubation conditions for each duplex are tested. The DNA complexes are pre-annealed either over night at room temperature (RT) or by heating up to 95°C and cooling slowly over four hours to 5°C. The mode of incubation does not influence the stability of the unmodified DNA complex (0P). In contrast, for 8P and 22P a stabilization trend dependent on the number of modifications is discernible, although statistically significant only for the DNA annealed with high temperature.

The fact that the stabilized complex forms upon annealing with high temperature might be due to an increase in kinetic degrees of freedom under these conditions. The assumption that the increased mechanical stability of annealed propynyl DNA is due to enhanced stacking interactions is supported by the comparison with double-stranded DNA harboring a higher number of G-C than A-T base pairs. G-C rich sequences are thermally more stable due to base-stacking interactions [81] but also rupture at a higher external force in shear mode [15].

To summarize, the implementation of propynyl bases has a significant stabilization effect on the mechanical stability of a DNA duplex if the DNA is pre-annealed with high temperature. DNA duplexes with propynyl bases offer the advantage of Watson-Crick base recognition and easy integration during chemical DNA synthesis. Additionally, no other treatments such as irradiation with light are necessary. In general, DNA origami structures are also assembled by annealing with high temperature. However, it has been demonstrated that the folding to the desired structure occurs at a narrow temperature range only [111]. Consequently, the assembly of the origami structures can be achieved at a constant temperature specific for the respective structure. In this context it might be possible to adjust the annealing process for propynyl-modified DNA for samples where heating to 95°C is not feasible.

Notably, the combination of the complementary techniques AFM and MFA was necessary to determine the dependence of the stabilization on the incubation as each technique on its own might have led to false assumptions. More details on the study presented in this section can be found in the corresponding manuscript B.1, which has been accepted for publication.

5 Outlook

In this thesis, it has been demonstrated that the Molecular Force Assay allows to measure protein-RNA as well as protein-protein interactions in a highly parallel and force-based manner. In order to achieve this aim, functional protein-DNA chimeras have been created and the impact of propynyl bases on the mechanical stability of short DNA complexes was investigated in detail. The MFA thus displays a great potential to answer important biological questions regarding the interactions, and with those the functionality, of proteins. This concluding chapter wants to point out promising next steps for future investigations building on the work presented here.

The MFA technique already features intrinsically a very high degree of parallelization as about 10^4 identical molecular constructs are tested per μm^2. In the current standard set-up as employed for the experiments conducted for this thesis, 16 spots of 1 mm in diameter can be functionalized individually. Thus, it is possible to vary the sample complex, the reference complex, the ligands or even the ligand concentration. In order to be able to screen for potential therapeutical drugs binding to specific miRNAs as described in section 4.1, a even higher degree of parallelization of different molecular complexes is needed, especially since not only the binding of a potential drug to its target miRNA has to be detected but it is also necessary to test for possible cross-reactions with other miRNAs. The same need for higher parallelization arises in the investigation of protein-protein interactions described in section 4.3, regarding the extensive number of those interactions in the pathways of the cell. Additionally, a method to facilitate the generation and handling of proteins would improve the usability of the MFA technique considerably.

Thus, the applications of the MFA presented here would profit tremendously from further miniaturization, parallelization and ease of handling of the experimental set-up. As has already been shown [93], reduction of the spot size to 25 μm^2 is sufficient to obtain valid results. This miniaturization has been combined by Otten *et al.* [96] with the integration of the whole MFA set-up into a microfluidic chip (see figure 5.1 (A)). The principle of this double-layered MITOMI chip [112, 113] allows to realize the contact and separation process of the MFA *via* pneumatic pressure with a button valve in the upper layer (see figure 5.1 (B)) and its current 640 chambers enable the needed high throughput testing. Hence, the combination

of the microfluidic chip with the experimental precautions needed for the handling of RNA would allow to screen efficiently for miRNA binding molecules inhibiting Dicer activity.

Also the study of protein-protein interactions could be simplified and parallelized for the simultaneous measurement of a huge number of protein pairs by the use of such a microfluidic chip. As shown only recently [108], the double-chamber architecture of the MITOMI chip (as displayed in figure 5.1 (B)), allows for the *in vitro* expression of a protein in the left chamber and later covalent attachment at a defined spot under the button valve in the right chamber. So far, those proteins have been investigated subsequently with the AFM after removal of the chip. However, the generation of this array of different, covalently attached proteins can now be combined with the MFA technique for protein-protein interactions. With the microfluidic chip, the first step of attachment of the lower protein to the glass slide can be parallelized and facilitated tremendously due to the *in vitro* expression. The molecular set-up can be completed by flushing the protein-DNA chimeras (section 4.2) with the DNA references through the chip. The MFA measurement can then be conducted by contacting the functionalized surface with a suitable PDMS stamp after removal of the chip. If the surface chemistry can be adjusted accordingly, it might even be possible to conduct the whole MFA process in the chip, yielding a highly economic and powerful method for the force-based investigation of protein-protein interactions.

In order to be able to quantify those interactions with high sensitivity, a toolbox of different references with varying mechanical strengths would be of great interest. In this thesis, short DNA duplexes were used as references. The needed variation in stability was achieved by binding of external ligands as well as internally by base modifications. Studied more closely in section 4.4, the internal stabilization through modifications of pyrimidines with a propynyl group was tuned by the number of implemented propynyl bases. This existing toolbox could therefore be expanded by further variation of the number of propynyl modifications, the employment of alternative base modifications, or the use of other DNA binding molecules additionally to the tested pyrrole-imidazole hairpin polyamides. A different but still straight forward concept would be to replace the DNA reference complex by a second protein pair acting as the reference. Here, nanobody-GFP complexes as quantified in section 4.3 would be ideally suited, as many proteins to be investigated already harbor a GFP-tag.

In conclusion, the technique of the Molecular Force Assay has now been developed to a level where it can quantify protein interactions with DNA, RNA as well as other proteins. Due to further parallelization efforts, this valuable bioanalytical tool will be able to handle increasing numbers of different interactions in the future.

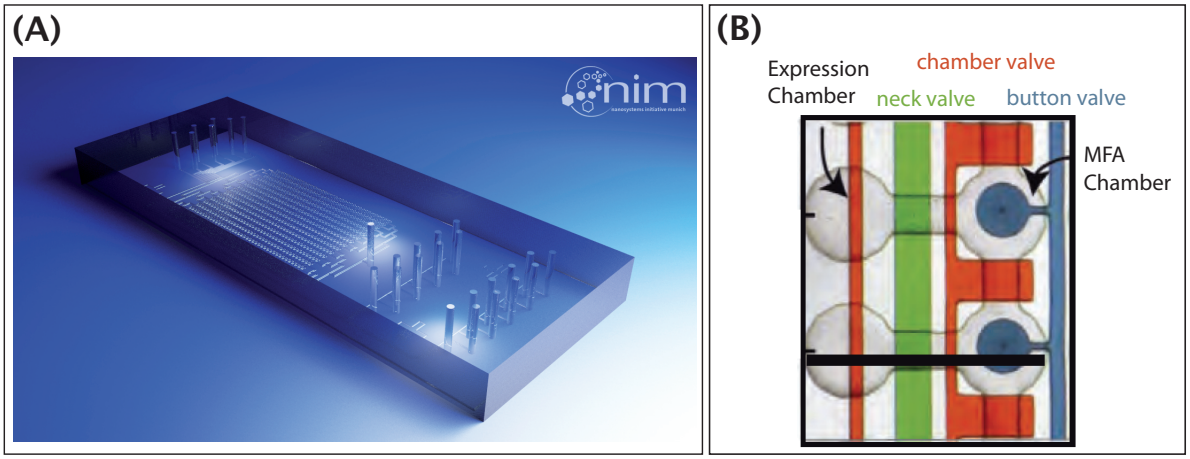

Figure 5.1: The microfluidic MITOMI chip as displayed in (A) provides 640 double chambers. Due to its double-layer architecture, the chambers can be separated *via* pneumatic pressure in the upper layer with different valves (B). The back chamber can be used for *in vitro* protein expression when the chip is placed onto a glass slide with a respectively spotted DNA array. A button valve over the front chamber allows for the contact and separation process of the MFA or for site-specific functionalization for covalent protein attachment. Reproduced and adapted from [114].

A Publications

A.1 Publication 1: Sequence-specific inhibition of Dicer measured with a force-based microarray for RNA ligands

Sequence-specific inhibition of Dicer measured with a force-based microarray for RNA ligands

by

Katja Limmer, Daniela Aschenbrenner and Hermann E. Gaub

published in

Nucleic Acids Research, Vol. 41, No. 6 (2013), e69

Published online 8 January 2013

Nucleic Acids Research, 2013, Vol. 41, No. 6 ***e69***
doi:10.1093/nar/gks1455

Sequence-specific inhibition of Dicer measured with a force-based microarray for RNA ligands

Katja Limmer, Daniela Aschenbrenner and Hermann E. Gaub*

Lehrstuhl für Angewandte Physik and Center for Nanoscience (CeNS), Ludwig-Maximilians-Universität, Amalienstrasse 54, 80799 Munich, Germany

Received September 17, 2012; Revised December 11, 2012; Accepted December 13, 2012

ABSTRACT

Malfunction of protein translation causes many severe diseases, and suitable correction strategies may become the basis of effective therapies. One major regulatory element of protein translation is the nuclease Dicer that cuts double-stranded RNA independently of the sequence into pieces of 19–22 base pairs starting the RNA interference pathway and activating miRNAs. Inhibiting Dicer is not desirable owing to its multifunctional influence on the cell's gene regulation. Blocking specific RNA sequences by small-molecule binding, however, is a promising approach to affect the cell's condition in a controlled manner. A label-free assay for the screening of site-specific interference of small molecules with Dicer activity is thus needed. We used the Molecular Force Assay (MFA), recently developed in our lab, to measure the activity of Dicer. As a model system, we used an RNA sequence that forms an aptamer-binding site for paromomycin, a 615-dalton aminoglycoside. We show that Dicer activity is modulated as a function of concentration and incubation time: the addition of paromomycin leads to a decrease of Dicer activity according to the amount of ligand. The measured dissociation constant of paromomycin to its aptamer was found to agree well with literature values. The parallel format of the MFA allows a large-scale search and analysis for ligands for any RNA sequence.

INTRODUCTION

The enzyme Dicer has increasingly been attracting attention owing to its crucial role in the RNA interference (RNAi) pathway. RNAi is an endogenous means used by cells to regulate protein translation at the post-transcriptional level (1). Single-stranded RNA sequences of 18–25 nucleotides bind to specific mRNAs and hinder protein translation. Although various classes of small regulatory RNA have been identified, two main categories of single-stranded RNA (ssRNA) involved in metazoan RNA interference can be distinguished that differ in their origin and function but share processing by Dicer: short-interfering RNA (siRNA) and microRNA (miRNA). siRNA precursors are long fully complementary dsRNA that are typically introduced directly into the cytoplasm or taken up from the environment, though recent findings suggest that siRNA may also originate from endogenous sources like transposons (2). Hence, the main task of the siRNA-processing machinery seems to be the defense of genome integrity in response to foreign or invasive nucleic acids (3). miRNAs are transcribed and pre-processed in the nucleus into incomplete base-paired stem-loop structures, known as pre-microRNAs. They are then transferred to the cytoplasm, where Dicer matures the pre-miRNA by cleaving the stem loop structure. The mature miRNA strand binds to the mRNA and usually inhibits translation in combination with a protein complex known as RNA-induced silencing complex (RISC) (4), although gene up-regulation by the RISC complex has also been reported (5,6). In contrast to siRNA, which requires total complementarity to its target sequence, miRNAs and their target mRNA do not need to base-pair perfectly so that a certain miRNA can bind and regulate a variety of mRNA sequences. Several miRNAs may also play a role in the regulation of a single mRNA transcript. Thus, miRNA seems to fine-tune protein expression. The amount of the various miRNA strands differs according to cell age, cell type and health status (7). So miR-1 appears to be tissue specific and was only found in heart tissue and somites of mice embryos (8). Evidence is accumulating that miRNAs are critical for many cellular processes such as developmental timing, cell proliferation or stem cell division (9). Consequently, many disease states occur or are sustained by miRNA dysregulation (10). miR-21, for example, was up-regulated in all tumour samples analysed by (11). Therefore, targeting the RNAi pathway at the step of Dicer cleavage is a promising approach for new therapies against illnesses like cancer or metabolic diseases.

*To whom correspondence should be addressed. Tel: +49 89 2180 3172; Fax: +49 89 2180 2050; Email: gaub@physik.uni-muenchen.de

A relatively small protein of <250 kDA, Dicer has been found in the cytoplasm of all eukaryotes studied to date (12), sometimes in several variants with different tasks. For instance in Drosophila, Dicer-1 cuts pre-miRNA while Dicer-2 generates siRNA from long dsRNA precursors (13). The L-shape of the protein seems to be well-conserved for all variants. Recognition of dsRNA by a PAZ domain occurs in the head of Dicer, which is separated from the two RNAse III domains by a ruler domain (Figure 2A). The base of the L is formed by a helicase, whose function is not totally understood (12). Dicer cleaves long and short (>30 nt) dsRNA strands with equal efficiency, whereas duplexes of ≤21 nt are not processed *in vitro*. A 3′ 2-nucleotide-long overhang, a characteristic of pre-microRNA molecules, increases Dicer's efficiency compared with blunt ends (14).

To interfere with RNAi, knocking out Dicer is not advisable owing to Dicer's crucial role for several cellular processes. On the other hand, a small molecule that binds to the pre-miRNA in question with high specificity and hinders Dicer from maturing the miRNA in question is a great drug candidate. The difficulty, herein, lies in finding potential ligands that bind a certain RNA sequence with high selectivity and also interfere with Dicer cleavage. Krützfeldt *et al.* (15) demonstrated that single-stranded cholesterol-conjugated 2′-O-methyl oligoribonucleotides, complementary to a certain miRNA and termed antagomirs, could specifically reduce the level of that miRNA *in vivo*. Elmen *et al.* (16) could reversibly decrease the level of plasma cholesterol by silencing miRNA-122 with a modified antagomir in non-human primates, thus exemplifying the possible therapeutic value of antagomirs. In both studies, already mature miRNAs are silenced, which might impair the potency of these molecules, as mature miRNA are included in the protein complex RISC and are probably less accessible than pre-miRNA. Cellular uptake of oligonucleotides is another difficulty so that Krützfeldt *et al.* needed high doses to see an effect. Thus, targeting pre-miRNA structures with small molecules has several advantages, but the research of small-molecule RNA binding has encountered several problems [for a review see (17)]. Especially an easy high-throughput technique to screen for and characterize RNA binders could speed up the progress of finding suitable molecules.

Our technique of the Molecular Force Assay (MFA) provides a fast and reliable tool to screen for different RNA binders, to characterize them and to quantify their ability to prevent Dicer from cutting. The MFA is a highly parallel technique, described in detail in (18) and (19), to measure unbinding forces comparatively so that small changes in the structural stability of molecular complexes can be detected. Two molecular bonds, a sample and a reference bond, are linked in series between two surfaces. One surface is retracted and a force gradually builds up in the molecular complexes until one of the bonds breaks. A fluorophor attached to the linking sequence between the two molecular complexes stays with the intact bond (Figure 1A) so that a simple fluorescent measurement by means of a commercially available epi-fluorescent microscope may detect the outcome. Thus, the mechanical stability of two molecular interactions can be probed and compared with each other. In contrast to other force-probe techniques like atomic force microscopy (AFM) or optical traps that measure the unbinding force by a spring-like macroscopic object like a cantilever, the MFA reduces the force detector to the microscopic scale of another molecule, a known reference DNA duplex, so that small differences in structural stability like the binding of a ligand may be resolved. The setup of the MFA is designed such that a large number of molecular complexes are tested simultaneously in one experiment on one chip, and the outcome of this experiment gives statistically significant information on the nature of the molecular interaction in question. Furthermore, as the MFA measures the interaction force between the molecules, unspecific binding events or complex backgrounds like serum do not alter the experimental outcome. Thus, the MFA allows us to detect and characterize the binding of a small molecule to a number of different oligonucleotides or of many small molecules to a certain RNA or DNA sequence in a format, where the analytes are not altered, e.g. by labelling. So far, the MFA has been applied to detect single-nucleotide polymorphism (20), study differences in antibody/antigen interactions (21), investigate the chiral selectivity of small peptides (22), characterize the binding properties of an aptamer to its ligand in a molecularly crowded ambient (23) and to analyse protein–DNA interaction (19).

Here, a 35 bp RNA duplex functions as a substrate for Dicer and is tested against a 22 bp or 27 bp DNA double strand that does not interact with Dicer. The two molecular complexes are linked in a zipper configuration so that a force stretching the bonds unzips the two duplexes (Figure 1A). The construct is covalently attached to the glass slide at the bottom and via a biotin–streptavidin–biotin complex to the upper poly(dimethylsiloxane) (PDMS) stamp surface (Figure 1A). The cyanine dye Cy5 between the RNA and DNA duplex stays with the intact bond after the rupture process, while a second fluorophor Cy3, conjugated to the 3′ end of the uppermost strand, constitutes a Fluorescence Resonance Energy Transfer (FRET) pair with the Cy5 and quantifies the constructs that have not properly coupled to the upper surface and, thus, have not been under force load. If Dicer cuts off about 20 bp of the RNA duplex, this bond is weakened and breaks with higher probability. Thus, Dicer activity can be detected and is quantified for different amounts of Dicer and incubation times. As a proof of principle, the RNA double strand incorporates an RNA aptamer specific for the aminoglycoside paromomycin, which we will characterize by measuring the dissociation constant. It is to be expected that the interaction of paromomycin with its aptamer will hinder Dicer from binding to the RNA duplex and, thus, from cutting.

MATERIALS AND METHODS

DNA/RNA constructs

The molecular complexes consist of three strands that are successively hybridized in our laboratory and are shown in

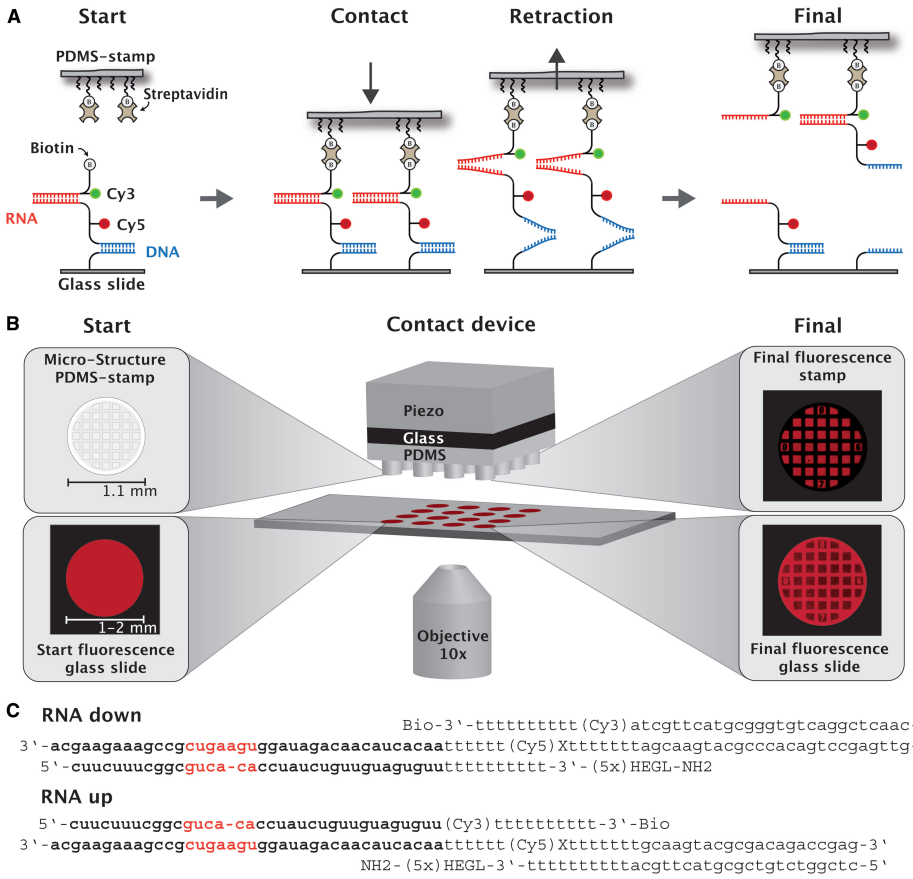

Figure 1. Schematics of the Molecular Force Assay. (**A**) The molecular complex is built up by covalently attaching the lowest strand to a glass slide and, subsequently, binding the pre-hybridized upper duplex to the lowest strand. The fluorophor Cy5 is conjugated to a poly-T sequence connecting the two duplexes. The upper strand is labelled with Cy3 so that a FRET signal provides a measure for a correctly hybridized molecular construct. The 'RNA up' geometry is defined with the DNA complex attached to the glass slide and the RNA duplex constituting the upper part. A biotin–streptavidin–biotin bond links the molecular complex to the upper surface, a soft PDMS stamp. Upon retracting the PDMS stamp, a force builds up in the molecular constructs and unzips the duplexes until the weaker of the two bonds in series ruptures. Note that in this format Cy5 serves as marker for those molecular complexes which remain intact. (**B**) In the setup, the contact device is mounted on an inverted microscope. The PDMS stamp features a micropattern that facilitates leveling and drainage of liquid during the contact and separation process. The oligonucleotide constructs are spotted in a 4×4 pattern, and fluorescence intensities are measured before and after the contact and separation process. After separation the fluorescence intensities of the molecules remaining on the glass and the PDMS surface add up to the total fluorescence intensity measured at the beginning. (**C**) Nucleic acid sequences of the molecular constructs in both configurations.

Figure 1C. The lowermost is modified with an amino group in order to covalenty attach the oligonucleotides to a surface. Avoiding surface effects, 5 HEGL (hexaethyleneglycol) molecules act as an additional spacer between the amino group and the oligonucleotides. Furthermore, poly-T separate the double-stranded sequences from the surfaces and each other. The cyanine dyes Cy5 and Cy3 are attached by a *N*-hydroxysuccinimide ester to the middle and uppermost strand, respectively, at a distance of six nucleobases in the hybridized complex to act as a FRET pair. The medium strand is inverted in the middle by inverse amidites since the force to melt a DNA or RNA double strand depends on the direction of the helix to which the force is applied. The RNA complex features a two nucleotide overhang at the 3′ end in order to maximize Dicer processing (14). Proving the validity of our results, we carried out all experiments in parallel with both possible geometries.

If the RNA target duplex is attached to the glass slide and the DNA complex constitutes the upper part, we call this configuration 'RNA down'. The other geometry with the RNA complex the upper part and the DNA duplex bound to the glass slide we named 'RNA up' (Figure 1C). We bought all oligonucleotides with the modifications from IBA GmbH, Germany.

Slide preparation

All aqueous solutions necessary for the chemical procedures described here were treated with 0.1% Diethyl pyrocarbonate (DEPC) over night and were autoclaved afterwards in order to avoid RNAse contamination. We pipetted 1 µl of the lowermost strand in a concentration of 25 µM in 5× SSC buffer (saline sodium citrate; Sigma-Aldrich GmbH, Germany) on an aldehydesilane-coated glass slide (Nexterion Slide AL, Pequlab, Germany) in a 4 × 4 pattern and incubated it over night in a humid atmosphere. The slide was rinsed thoroughly with ddH_2O and incubated in a 1% aqueous solution of $NaBH_4$ (VWR Scientific GmbH, Germany) for 90 min in order to reduce the Schiff bases and render the linkage of the oligonucleotide to the slide covalent. Unreacted groups were blocked in 1× SSC containing 4% bovine serum albumin (Sigma-Aldrich GmbH; Germany), minimizing unspecific binding. We placed a custom-made 16-well silicone isolator (Grace-Biolabs; USA) on top of the immobilized lowermost oligomer and transferred to each well 3 µl of 0.2 µM of the upper complex in 5× SSC, which had been heated and cooled down over several hours in a thermocycler beforehand to avoid undesired secondary structures. After an hour hybridization, the molecular complexes as diplayed in Figure 1A were completed. Unbound strands were removed by several washing steps with different salt concentrations (2× SSC, 0.2× SSC, 1× SSC). Care was taken that the samples were kept in an aqueous environment at all times.

Incubation of ligands

For all measurements detecting Dicer activity, the glass slide with the molecular bonds was fastened to a custom-made PMMA well with a silicone lip seal. According to the desired incubation time and quantity, the recombinant human Dicer protein in a concentration of 1 U/µl (Life technologies, UK) was directly pipetted into the PMMA well prior to the contact process. We applied amounts between 0.5 and 5 µl Dicer solution. For measurements with paromomycin and Dicer, the appropriate amount of paromomycin (paromomycin sulphate salt, Sigma, Germany) was directly mixed with the solution of 1× SSC of the last washing step and, thus, added before Dicer. The paromomycin titration experiments were executed on one glass slide within the spotted 4 × 4 pattern of oligonucleotides. The custom-made 16-well silicone isolator (Grace-Biolabs; USA) allows the incubation of every spot with a different solution by means of a self-made microfluidic system driven by two 16-channel peristaltic pumps (Ismatec GmbH; Germany). Hence, a whole titration curve can be recorded within a single experiment.

Stamp preparation

Micro- and macrostructured PDMS stamps were fabricated by casting 1:10 crosslinker/base (Sylgard, Dow Corning, MI, USA) into a custom-made Pyrex/silicon wafer (HSG-IMIT, Germany) according to standard procedures (24). The resulting PDMS stamps feature pillars of 1 mm diameter and height with a spacing of 3 mm in a square pattern on a 3-mm-thick basis and are cut in pieces of 4 × 4 pillars. The flat surface of the pillars is microstructured with 100 × 100 µm pads separated by 41 µm wide and 5 µm deep rectangular trenches enabling the drainage of liquid during the contact and separation process (Figure 1B). For the surface functionalization, the cleaned stamp surface was first activated in 12.5% HCl overnight and derivatized with (3-glycidoxypropyl)-trimethoxysilane (ABCR, Germany) in order to generate epoxide groups. 1:1 methoxy-PEG-NH_2 (MW 2000 Dalton) and Biotin-PEG-NH_2 (MW 3400 Dalton) (Rapp-Polymere, Germany) were melted at 80°C, and ~1 µl was transferred to each pillar followed by overnight incubation at 80°C in an Argon atmosphere. The excess polymers were thoroughly removed by rinsing with ddH_2O. Shortly before the experiment, the stamps were incubated in 0.4% BSA in 1× SSC containing 1 µg/µl Streptavidin (Thermo Fisher Scientific, Germany) for 30 min, washed with 0.05% Tween 20 (VWR Scientific GmbH, Germany) in 0.2× SSC and gently dried with N_2 gas.

Contact process and fluorescence read-out

The functionalized stamp adheres upside-down to the glass block glued to a closed-loop piezoelectric actuator (PZ 400, Piezo Systems Jena, Germany) and a DC motorized translation stage (Physik Instrumente GmbH, Germany), as shown in Figure 1B. The slide with the oligonucleotide constructs is fixed beneath the stamp on a stainless steel stage with permanent magnets so that every stamp pillar meets a 1–2 mm diameter spot of oligonuclotides on the glass slide. The whole contact device is mounted on an inverted microscope (Axio Observer Z1, Carl Zeiss MicroImaging GmbH, Germany) with an xy-DC motorized high-accuracy translation stage (Physik Instrumente GmbH, Germany). Contact is made by means of the piezo, and care is taken that each individual pillar is not compressed more than 3 µm. The planar adjustment of stamp and slide as well as the contact process are controlled by reflection interference contrast microscopy (25). To let the biotin of the oligonucleotides bind to the streptavidin coating of the PDMS stamp, the contact between stamp and slide is maintained for 10 min. The piezo retracts the stamp with a velocity of 1 µm/s in all experiments, and a force builds up in the double strands until the weaker one breaks with higher probability. Quantifying the number of intact bonds in relation to total molecular constructs, fluorescence images of the Cy5 intensity are taken before and after the contact process. As it cannot be assumed that all oligonucleotides have bound to the stamp, their contribution has to be substracted. Therefore, a fluorescence picture of the FRET intensity between the Cy3 of

the upper strand and the Cy5 label of the middle strand, being a measure of the integrity of the upper molecular complex, is taken before and after the contact process as well. Three outcomes are possible: First, the lower bond broke so that no fluorescence, neither Cy5 nor FRET signal, can be detected. Second, the upper bond broke so that the Cy5 intensity can be measured but no FRET signal. Third, the molecular construct did not bind to the stamp, which means that the Cy5 and FRET intensity are unchanged except for bleaching. The quotient of the image taken after the contact process to the image taken before, $F_{Cy5} = I_{Cy5}^{Final}/I_{Cy5}^{Start}$ and $F_{FRET} = I_{FRET}^{Final}/I_{FRET}^{Start}$, cancels out inhomogeneities due to the Gaussian illumination profile and surface defects, rendering the MFA rather robust. The normalized fluorescence is given by $NF = \frac{F_{Cy5}-F_{FRET}}{1-F_{FRET}}$. A detailed description can be found in (26). The normalized fluorescence is thus the fraction of intact lower bonds of the total number of molecules under load.

RESULTS AND DISCUSSION

Characterization of Dicer activity

Initially, we developed a platform for analysing the protein Dicer. The schematic outline and RNA sequences are shown in Figure 1. We built a molecular complex comprising a 35 bp double-stranded RNA duplex covalently bound to a glass slide at one end, and covalently attached to a 27 bp reference DNA duplex at the other end. Dicer could be titrated in solution to the completed molecular constructs, and the surfaces were separated after incubation times varying between 60 and 300 min. Figure 2B depicts the results of such a measurement upon addition of 1 µl of Dicer to every sample except the first, which acts as a reference value. The normalized fluorescence at time t = 0 provided a value of $NF = 0.79 \pm 0.01$. An initial value at time t = 0 of $NF = 0.5$, corresponding to two complexes nearly identical in their structural stability, would be desirable to resolve small differences in stability induced through binding of a ligand or mismatch. However, our system was designed to quantify enzymatic RNAse activity. Because Dicer cuts off around 20 bp, we designed our sytem such that the RNA complex before Dicer cleavage was stronger than the DNA, while the RNA complex after Dicer cleavage was weaker than the reference DNA duplex. As in our system the RNA construct is 8 bp longer than the DNA complex, in the absence of Dicer, the weaker DNA reference bond ruptures with higher probability. In the 'RNA down' configuration, the RNA complex is attached directly to the glass slide; therefore, the likelihood for the Cy5 label to be found at the lower surface is higher than at the upper surface, and the normalized fluorescence lies around $NF = 0.8$. If Dicer cleaves off about 20 bp of the RNA double strand, the lower molecular complex is weakened and the normalized fluorescence decreases (Figure 2B). Dicer processes the RNA duplex in multiple enzymatic turnovers. Consequently the normalized fluorescence declined further with increasing incubation time (Figure 2B). Our experimental design provides Dicer with an excess of substrate, dsRNA, so that the substrate concentration can be assumed constant and the reaction rate of Dicer is solely limited by the amount of Dicer present. Thus, a linear relation of the normalized fluorescence to Dicer processing time was expected and verified by our measurement. The slope of the fit was used as a measure of the rate of Dicer processing, allowing us to quantify Dicer activity.

Proof of Principle of the microarray test format for RNA ligands

Next, we analysed the binding properties of the aminoglycoside of the neomycin family, paromomycin, to its RNA aptamer by means of the MFA. The structure of this aptamer and its ligand-binding behaviour are well-known and described in detail in (28) and (29). The aptamer sequence was incorporated into our RNA duplex 11 nucleotides from the 3′ end, and was located within the portion of the RNA duplex cleaved by Dicer. We hypothesized that this position could disrupt Dicer interaction with the RNA duplex. Every second spot in the 16-spot pattern of oligonucleotide constructs bound to the glass slide were incubated for at least 1 h with a different concentration of paromomycin in 1× SSC, ranging from 0 to 1995 µM, so that a single experiment resulted in a full titration curve with two values for every concentration paromomycin. The experiment was carried out several times for both the 'RNA up'and 'RNA down' configurations. From the resulting values for the normalized fluorescence, the mean and standard error of the mean were calculated so that every data point represents between two and four experiments. The data were fitted by a hill equation isotherm that accounts for specific and non-specific binding by means of the software package GraphPad Prism 5 (GraphPad Software, San Diego, CA, USA). The result for the 'RNA up' configuration is shown in Figure 2D, which yielded a dissociation constant of 2.55 ± 2.18 µM and negligible unspecific binding. Literature reports values of 0.2–1 µM depending on the technique (29,30), in agreement with our results. The measurements in the 'RNA down' geometry resulted in dissociation constants of about 100 ± 70 µM (data not shown), which deviated by a factor 50 from our other measurements with the inverted geometry. Non-specific binding of the ligand to the surfaces or molecular complexes would be indentical in both configurations, so we attributed the increase in dissociation constant for the 'RNA down' configuration to the proximity of the RNA construct to the glass slide. Notwithstanding the passivation of the glass slide, the RNA duplex in the 'RNA down' configuration presumably stretches across the surface, which might reduce the accessibility of the RNA aptamer binding pocket for the ligand paromomycin, resulting in an apparent increase in the dissociation constant. Consequently, the 'RNA down' configuration with the ligand-binding part integrated in the lower complex does not seem suited for the characterization of a RNA-binding ligand. In contrast, providing the ligand-binding sequence with a spacer and locating away from the surface by implementing it in the upper RNA duplex yielded reliable values for the dissociation constant

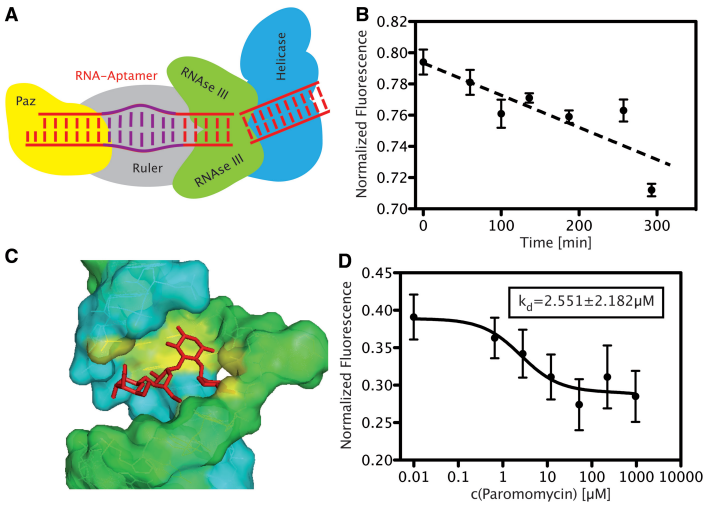

Figure 2. Characterization of molecules in question. (**A**) Schematics of Dicer and its sub-domains. (**B**) The activity of Dicer is measured in an excess of substrate so that the processing rate is constant. Accordingly, the normalized fluorescence decreases linearly with incubation time. The data were measured in the 'RNA down' configuration. (**C**) Schematic picture of paromomycin (red) binding to its RNA aptamer. The two strands of the RNA duplex are displayed in blue and green, while the bases interacting with the ligand are coloured in yellow [PDB: 1J7T by (27)]. (**D**) Titration of the ligand paromomycin to the complexes in the 'RNA up' geometry increasingly stabilizes the upper RNA duplex so that the normalized fluorescence decreases. The fluorescence data were fitted by a Hill equation isotherm.

in agreement with literature values. Although the dissociation constants measured by other more laborious and time-consuming techniques might be more accurate, our assay provides sufficiant accuracy in a parallel screening format for dissociation constants, ranging from the picomolar (26) (chiral polyamides binding to DNA) to the high micromolar scale (23) (DNA-aptamer specific for ATP). Moreover, the current format with 16 spots can be varied to titrate two ligands in parallel (eight spots per ligand) or change the binding sequence in half the spots in order to gain a deeper insight into the ligand-binding sequence interaction in a one-shot experiment.

Hinderance of Dicer processing by ligand binding

In the next step, we prepared four different slides with our oligonulceotide constructs in the 'RNA down' configuration as well as in the 'RNA up' configuration. The initial value for *NF* was determined in pure buffer (Figure 3A). To the second sample, we added 2.5 µl of the Dicer solution and separated the surfaces after 60 min, while we incubated the third sample with 1 mM paromomycin at least 1 h before the measurement (Figure 3B and C). The buffer of the fourth sample contained 1 mM paromomycin, and 2.5 µl Dicer solution was added 60 min before separation of the surfaces (Figure 3D). The first sample acted as reference and gave $NF = 0.34 \pm 0.01$ (standard deviation) in the 'RNA up' configuration. The addition of Dicer weakened the upper RNA double strand by cutting off around 20 basepairs so that the flurophor was found more often on the lower side. Therefore, the *NF* increased to 0.40 ± 0.02, as displayed in Figure 3E. Upon binding of paromomycin, the RNA duplex was stabilized and the *NF* decreased to 0.27 ± 0.01 in the third case. If paromomycin hinders Dicer from cutting the RNA duplex, we expect that the fourth measurement yields *NF* close to the ligand-only case, but at least below the $NF = 0.40$ obtained for measurement with only Dicer in the solution. As shown in Figure 3E, we measured an *NF* of 0.30 ± 0.01, which is close to the result of only paromomycin. From these data, we concluded that Dicer was definitely hindered by binding of paromomycin, but not completely blocked. The 'RNA down' configuration yielded the same outcome (Figure 3F).

Correction of fluorescence data

During the measurments with the 'RNA down' configuration, we found that the quantum yield of the fluorophors, especially of the Cy5, varied slightly owing to the changing local environment. In particular, the fluorescence intensity of Cy5 increased if the upper strand ruptured leaving behind the single-stranded overhang. This leads to the phenomenon that the normalized fluorescence value can adopt values above one in the 'RNA down' configuration (see raw data in the Supplementary Data). Levitus and co-workers reported a change of fluorescence intensity upon interaction of Cy3 with single and double-stranded

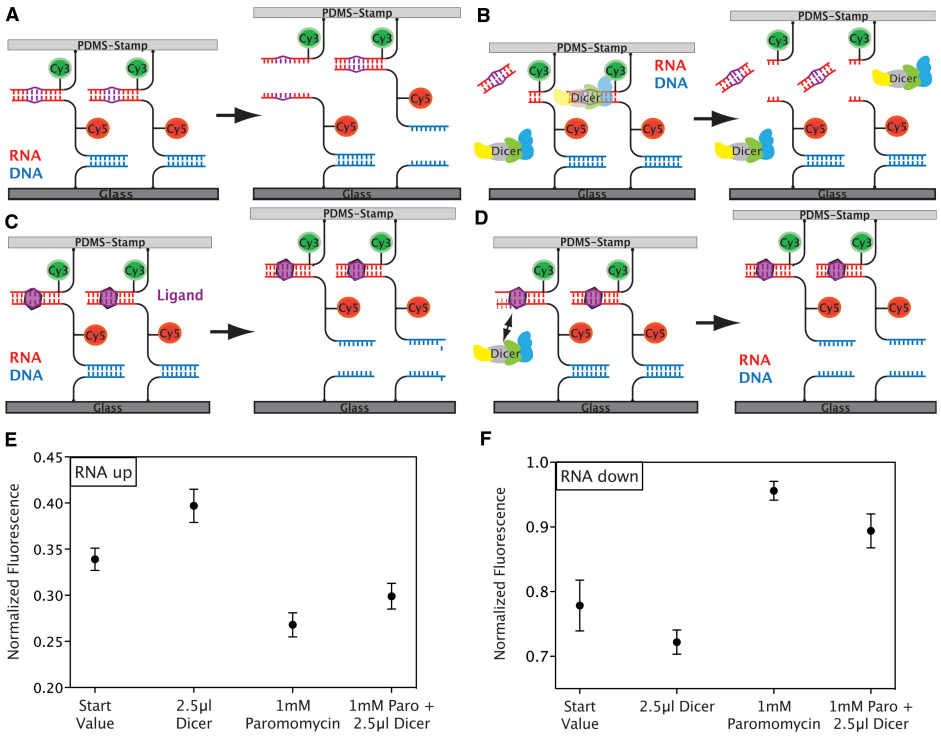

Figure 3. Dicer inhibition. (**A**) Separating the molecular constructs in the absence of Dicer or ligand provides an initial value in the 'RNA up' geometry for the *NF* of 0.34 ± 0.01. (**B**) Upon addition of Dicer, the protein cleaves off around 20 bp of the RNA duplexes and weakens the upper part so that the balance of the fluorophor distribution is shifted towards the lower side and the *NF* increases to 0.40 ± 0.02. (**C**) Binding of the ligand to its aptamer strengthens the RNA complex and the fluorophor distribution after rupture of the molecular complexes is shifted towards the upper surface, decreasing the *NF* to 0.27 ± 0.01. (**D**) Upon addition of Dicer and ligand, binding of the ligand to the RNA duplex blocks Dicer and strengthens the upper complex so that the *NF* yields 0.30 ± 0.01, which is close to the value we measured with ligand only. (**E**) Display of the data measured in the experiment just described. (**F**) Inverting the geometry yields the same result in reverse. From an initial value of 0.78 ± 0.02, the *NF* decreases to 0.72 ± 0.01 through the destabilization by Dicer. Ligand binding strengthens the lower RNA duplex and shifts the *NF* to higher values of 0.96 ± 0.01. If Dicer is hindered from cutting by ligand binding, the *NF* with 0.90 ± 0.01 stays close to the value measured with ligand only.

DNA. They attributed this change to the blocking of non-radiative decay pathways of the excited state fluorophor by steric hindrance (31). In (32), a similar behaviour for Cy5 is described. Although the Cy5 label is, in our case, always conjugated to the middle single strand and six basepairs away from both duplexes, an interaction between the fluorophor and the oligonucleotide duplex seems a plausible explanation for the observed increase in fluorescence intensity. Because the Cy3 is only measured as part of a duplex, any effect due to interactions with the oligonucleotides cancels out in the ratio. To correct the Cy5 fluorescence intensities, we measured the intensity of its emisson spectrum in bulk solution in both cases, the single middle strand and the complete upper duplex, by fluorescence spectroscopy and calculated a quenching factor F (see Supplementary Data). Determining the experimental error for F, we calculated the maximum range of possible factors and re-analysed our data measured by the MFA. Although all measured data points are shifted to smaller *NF* values, the outcome of the experiments and the corresponding conclusions remain unchanged (see Supplementary Figure S1). For further analysis, we therefore chose a medium value for the quenching factor of $F = 1.19$ for the 'RNA down' geometry, and $F = 1.06$ for the 'RNA up' geometry and corrected all measured data accordingly.

Minimum amount of ligand necessary for Dicer inhibition

We investigated what concentration of paromomycin is nessecary to hinder Dicer from cleaving. We incubated samples in the 'RNA down' configuration with

paromomycin, with the concentration ranging from 0.66 to 224 μM, and added 2.5 μl Dicer solution 1 h before the separation. The result is displayed in Figure 4. The lowest concentration of 0.66 μM paromomycin did not affect Dicer processing, but already a concentration of 2.82 μM partially inhibited Dicer, whereas 52 μM paromomycin hindered most of Dicer processing.The dissociation constant, which we had determined in the previous section to be 2.55 ± 2.18 μM, agrees nicely with the finding here, that a paromomycin concentration in this range leads to a partial inhibition of the cleavage process. It points directly towards a close relationship between the dissociation constant of a ligand and its potential to hinder Dicer processing. For ligands that bind thighter to their RNA sequence, we expect a blocking of Dicer at lower concentrations of the ligand.

CONCLUSION

In a proof of principle, we demonstrated that the function of the protein Dicer can be selectively blocked by a ligand that sequence specifically binds to the RNA. Our MFA reliably detected processing of the RNA duplex as well as the binding of a small ligand to RNA, which resulted in an inhibition of Dicer. In contrast to other techniques (33), the MFA requires neither labelling of the target sequence, nor the ligand or protein. It only needs flurophors well-separated from the area of interest so that the interaction of the molecules in question is not disrupted and can be analysed undisturbed. The localization of our molecular constructs between two surfaces is both an advantage and a drawback at the same time. Because we measure interaction forces rather than the mere presence of a ligand, our assay can easily test different ligand–oligonucleotide interactions in parallel without interfering background signals from the bulk or the need for stringent washing procedures. But possible surface effects e.g. non-specific adhesion between ligand or oligonucleotides and surface have to be carefully excluded. Furthermore, our assay allows us to analyse the interaction of Dicer with our RNA construct and the interaction of the ligand to its binding sequence separately without changing the molecular complexes. This ensures that Dicer cleavage is blocked by hindering the protein to bind to its substrate not by any interaction between Dicer and the ligand. In addition, we illustrated the capability of our assay to characterize RNA-binding molecules in a one-shot experiment, enabling examination of the binding behaviour of a large number of molecules with moderate effort. The current setup allows to test 16 different systems in parallel, either one substance against 16 different DNA or RNA sequences or one oligonucleotide construct against 16 different ligands or concentrations of one ligand or a combination of both. To expand the multiplexing capabilities of our setup towards high throughput, the amount of reacting agent has to be reduced to a minimum and the number of RNA sequences have to be increased. Microfluidic devices can drastically diminish the reaction volume, and DNA/RNA spotting techniques allowed us to test eight different systems within $100 \times 100\ \mu m^2$ (19,34). With further standardization and development, our technique of the MFA has the potential to become the first force-based high throughput technique.

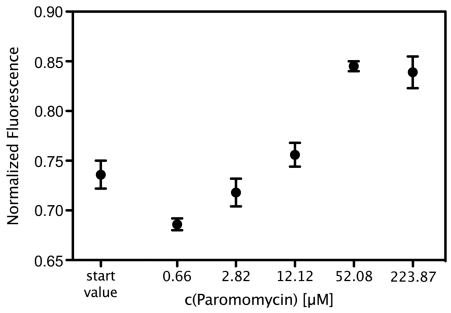

Figure 4. Paromomycin efficiency. To determine the minimum amount of paromomycin necessary to block Dicer, we prepared samples in the 'RNA down' configuration with different amounts of paromomycin and added 2.5 μl Dicer solution 1 h before the measurement. We found that 0.66 μM paromomycin has no effect, but already 2.82 μM paromomycin hinders Dicer processing, while for 52.08 μM paromomycin, all Dicer activity is blocked.

SUPPLEMENTARY DATA

Supplementary Data are available at NAR Online: Supplementary Method and Supplementary Figure 1.

ACKNOWLEDGEMENTS

The authors thank Christoph Arenz from HU Berlin, P. Tinnefeld from TU Braunschweig, Matthias Rief from TU Munich, P. Severin, I. Stein and U. Wienken for helpful discussions. K.L. is grateful to the Elite Network of Bavaria (IDK-NBT) for a doctoral fellowship.

FUNDING

German Science Foundation [SFB 863]; Nanosystems Initiative Munich; European Research Council Advanced Grant. Funding for open access charge: German Science Foundation [SFB 863].

Conflict of interest statement. None declared.

REFERENCES

1. Mello,C.C. and Conte,D. Jr (2004) Revealing the world of RNA interference. *Nature*, **431**, 338–342.
2. Siomi,H. and Siomi,M.C. (2009) On the road to reading the RNA-interference code. *Nature*, **457**, 396–404.
3. Carthew,R.W. and Sontheimer,E.J. (2009) Origins and Mechanisms of miRNAs and siRNAs. *Cell*, **136**, 642–655.
4. Bartel,D.P. (2004) MicroRNAs: genomics, biogenesis, mechanism and function. *Cell*, **116**, 281–297.
5. Vasudevan,S., Tong,Y. and Steitz,J.A. (2007) Switching from repression to activation: microRNAs can up-regulate translation. *Science*, **318**, 1931–1934.

6. Orom,U.A., Nielsen,F.C. and Lund,A.H. (2008) MicroRNA-10a binds the 5'UTR of ribosomal protein mRNAs and enhances their translation. *Mol. Cell*, **30**, 460–471.
7. Ambros,V. (2011) MicroRNAs and developmental timing. *Curr. Opin. Genet. Dev.*, **21**, 511–517.
8. van Rooij,E. (2011) The art of microRNA research. *Cir. Res.*, **108**, 219–234.
9. Shruti,K., Shrey,K. and Vibha,R. (2011) Micro RNAs: tiny sequences with enormous potential. *Biochem. Biophys. Res. Commun.*, **407**, 445–449.
10. Friedman,J.M. and Jones,P.A. (2009) MicroRNAs: critical mediators of differentiation, development and disease. *Swiss Med. Wkly.*, **139**, 466–472.
11. Conti,A., Aguennouz,M., La Torre,D., Tomasello,C., Cardali,S., Angileri,F.F., Maio,F., Cama,A., Germano,A., Vita,G. *et al.* (2009) miR-21 and 221 upregulation and miR-181b downregulation in human grade II-IV astrocytic tumors. *J. Neurooncol.*, **93**, 325–332.
12. Lau,P.W., Guiley,K.Z., De,N., Potter,C.S., Carragher,B. and MacRae,I.J. (2012) The molecular architecture of human Dicer. *Nat. Struct. Mol. Biol.*, **19**, 436–440.
13. Lee,Y.S., Nakahara,K., Pham,J.W., Kim,K., He,Z., Sontheimer,E.J. and Carthew,R.W. (2004) Distinct roles for Drosophila Dicer-1 and Dicer-2 in the siRNA/miRNA silencing pathways. *Cell*, **117**, 69–81.
14. Vermeulen,A., Behlen,L., Reynolds,A., Wolfson,A., Marshall,W.S., Karpilow,J. and Khvorova,A. (2005) The contributions of dsRNA structure to Dicer specificity and efficiency. *RNA*, **11**, 674–682.
15. Krützfeldt,J., Rajewsky,N., Braich,R., Rajeev,K.G., Tuschl,T., Manoharan,M. and Stoffel,M. (2005) Silencing of microRNAs *in vivo* with 'antagomirs'. *Nature*, **438**, 685–689.
16. Elmen,J., Lindow,M., Schutz,S., Lawrence,M., Petri,A., Obad,S., Lindholm,M., Hedtjarn,M., Hansen,H.F., Berger,U. *et al.* (2008) LNA-mediated microRNA silencing in non-human primates. *Nature*, **452**, 896–899.
17. Thomas,J.R. and Hergenrother,P.J. (2008) Targeting RNA with small molecules. *Chem. Rev.*, **108**, 1171–1224.
18. Albrecht,C.H., Clausen-Schaumann,H. and Gaub,H.E. (2006) Differential analysis of biomolecular rupture forces. *J. Phys. Condens. Matter*, **18**, S581–S599.
19. Severin,P.M., Ho,D. and Gaub,H.E. (2011) A high throughput molecular force assay for protein-DNA interactions. *Lab Chip*, **11**, 856–862.
20. Albrecht,C., Blank,K., Lalic-Multhaler,M., Hirler,S., Mai,T., Gilbert,I., Schiffmann,S., Bayer,T., Clausen-Schaumann,H. and Gaub,H.E. (2003) DNA: a programmable force sensor. *Science*, **301**, 367–370.
21. Blank,K., Mai,T., Gilbert,I., Schiffmann,S., Rankl,J., Zivin,R., Tackney,C., Nicolaus,T., Spinnler,K., Oesterhelt,F. *et al.* (2003) A force-based protein biochip. *Proc. Natl Acad. Sci. USA*, **100**, 11356–11360.
22. Dose,C., Ho,D., Gaub,H.E., Dervan,P.B. and Albrecht,C.H. (2007) Recognition of ''mirror-image'' DNA by small molecules. *Angew. Chem. Int. Ed. Engl.*, **46**, 8384–8387.
23. Ho,D., Falter,K., Severin,P. and Gaub,H.E. (2009) DNA as a force sensor in an aptamer-based biochip for adenosine. *Anal. Chem.*, **81**, 3159–3164.
24. Xia,Y. and Whitesides,G.M. (1998) Soft lithography. *Annu. Rev. Mater. Sci.*, **28**, 153–184.
25. Wiegand,G., Neumaier,K.R. and Sackmann,E. (1998) Microinterferometry: three-dimensional reconstruction of surface microtopography for thin-film and wetting studies by interference contrast microscopy (RICM). *Appl. Opt.*, **37**, 6892–6905.
26. Ho,D., Dose,C., Albrecht,C.H., Severin,P., Falter,K., Dervan,P.B. and Gaub,H.E. (2009) Quantitative detection of small molecule/DNA complexes employing a force-based and label-free DNA-microarray. *Biophys. J.*, **96**, 4661–4671.
27. Vicens,Q. and Westhof,E. (2001) Crystal structure of paromomycin docked into the eubacterial ribosomal decoding a site. *Structure*, **9**, 647–658.
28. Fourmy,D., Recht,M.I., Blanchard,S.C. and Puglisi,J.D. (1996) Structure of the A site of *Escherichia coli* 16 S Ribosomal RNA complexed with an aminoglycoside antibiotic. *Science*, **274**, 1367–1371.
29. Anderson,P.C. and Mecozzi,S. (2007) Minimum sequence requirements for the binding of paromomycin to the rRNA decoding site A. *Biopolymers*, **86**, 95–111.
30. Recht,M.I., Fourmy,D., Blanchard,S.C., Dahlquist,K.D. and Puglisi,J.D. (1996) RNA Sequence determinants for aminoglycoside binding to an A-site rRNA model oligonucleotide. *J. Mol. Biol.*, **262**, 421–436.
31. Sanborn,M.E., Connolly,B.K., Gurunathan,K. and Levitus,M. (2007) Fluorescence properties and photophysics of the sulfoindocyanine Cy3 linked covalently to DNA. *J. Phys. Chem. B*, **111**, 11064–11074.
32. Levitus,M. and Ranjit,S. (2011) Cyanine dyes in biophysical research: the photophysics of polymethine fluorescent dyes in biomolecular environments. *Q. Rev. Biophys.*, **44**, 123–151.
33. Davies,B.P. and Arenz,C. (2006) A homogenous assay for micro RNA maturation. *Angew. Chem. Int. Ed. Engl.*, **45**, 5550–5552.
34. Severin,P.M. and Gaub,H.E. (2012) DNA-Protein Binding Force Chip. *Small*, **8**, 3269–3273.

SUPPLEMENTARY DATA

Characterization of fluorophores

In order to quantify the interaction of the fluorophors with the oligonucleotides to which they are conjugated, the fluorescence intensities of the middle strand and and the upper duplex are measured by means of a Fluorometer (Fluorolog3, Horiba Jobin Yvon). The oligonucleotides are diluted in 1xSSC to 0.5 µM and the duplex in a mixture of 1:1 is heated and cooled down over several hours. The excitation wavelength and emission spectra are set according to the parameters of the MFA setup. The resulting intensity curve is integrated and a quenching factor F is calculated by dividing the integrated intensity of the single strand by the integrated intensity of the duplex. Multiplying I_{Cy5}^{Start} by this factor gives the corrected normalized fluorescence.

Several repetitions yielded slightly different factors. Determining a maximum range of possible factors we could prove that the outcome of the experiment is not changed by correcting the NF with the different quenching factors. This is also visible in the Figure S1. Therefore, a medium factor was calculated and used for all analyses.

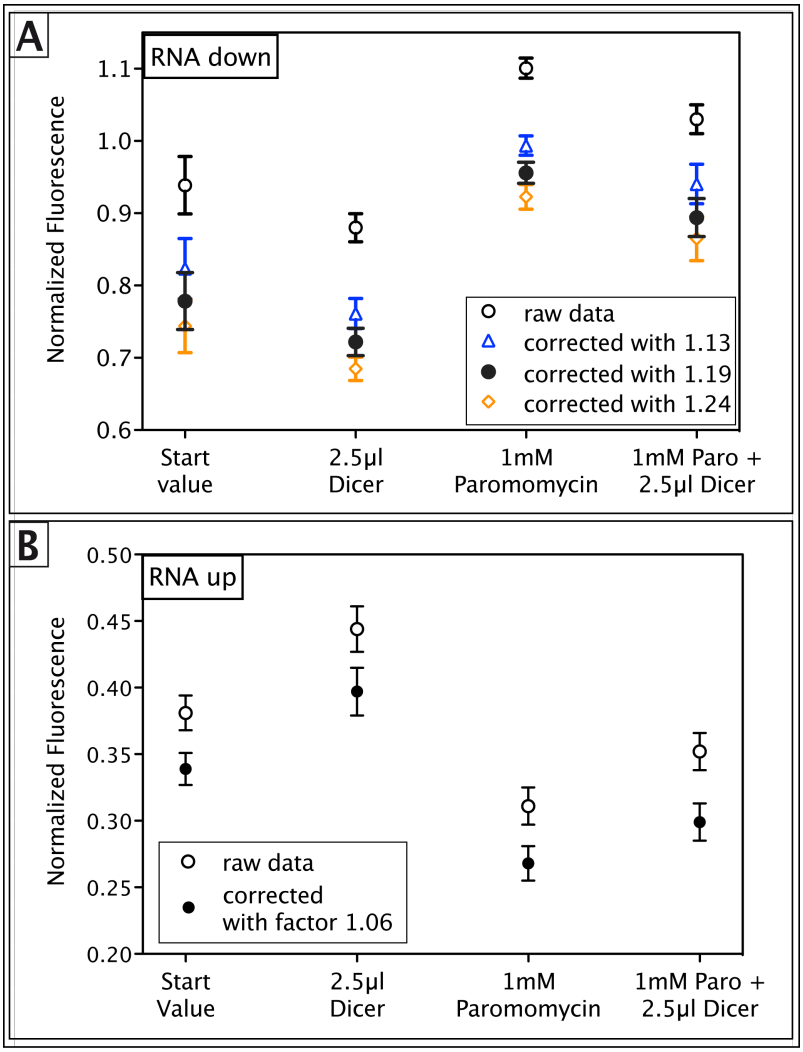

Figure S1: Proximity effects on the fluorescence intensities of Cy5.

The Cy5 with the oligonucleotide bases requires a correction of the measured fluorescence intensity in order to calculate the actual NF. A quenching factor is determined by measuring the fluorescence intensity of Cy5 conjugated to the single, middle strand as well as to the complete upper duplex by means of a fluorometer. Re-analyzing the data with a maximum range of factors does not change the outcome of the experiment. Dicer destabilizes the RNA duplex, while binding of paromomycin strengthens it. Blocking of Dicer leads to NF values close to ones of paromomycin binding. This holds true for both geometries, the RNA complex attached to the glass slide with the DNA duplex constituting the upper part (A) as well as for the inverse (B).

A.2 Publication 2: Protein–DNA Chimeras for Nano Assembly

Protein–DNA Chimeras for Nano Assembly

by

Diana A. Pippig, Fabian Baumann, Mathias Strackharn, Daniela Aschenbrenner and Hermann E. Gaub

published in

ACS Nano, Vol. 8, No. 7, 6551–6555, 2014

ARTICLE

Protein–DNA Chimeras for Nano Assembly

Diana A. Pippig,[†,*] Fabian Baumann,[†] Mathias Strackharn,[†,§] Daniela Aschenbrenner,[†,‡] and Hermann E. Gaub[†,*]

[†]Center for Nanoscience and Department of Physics, University of Munich, Amalienstraße 54, 80799 Munich, Germany and [‡]Center for Integrated Protein Science, 81377 Munich, Germany. [§]Present address: Scanlab AG, Siemensstr. 2a, 82178 Puchheim, Germany.

ABSTRACT In synthetic biology, "understanding by building" requires exquisite control of the molecular constituents and their spatial organization. Site-specific coupling of DNA to proteins allows arrangement of different protein functionalities with emergent properties by self-assembly on origami-like DNA scaffolds or by direct assembly *via* Single-Molecule Cut & Paste (SMC&P). Here, we employed the ybbR-tag/Sfp system to covalently attach Coenzyme A-modified DNA to GFP and, as a proof of principle, arranged the chimera in different patterns by SMC&P. Fluorescence recordings of individual molecules proved that the proteins remained folded and fully functional throughout the assembly process. The high coupling efficiency and specificity as well as the negligible size (11 amino acids) of the ybbR-tag represent a mild, yet versatile, general and robust way of adding a freely programmable and highly selective attachment site to virtually any protein of interest.

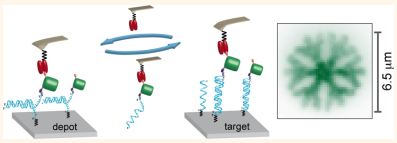

KEYWORDS: protein–DNA chimera · single-molecule cut & paste · AFM · spatial arrangement · patterning · single-molecule fluorescence

To study protein networks at the single molecule level, precise targeting and localization of its constituents are indispensable prerequisites. To this end, we developed the Single-Molecule Cut & Paste (SMC&P) technique,[1,2] which combines the angstrom level precision of the scanning probe microscope with the selectivity of bio–molecular interactions for the assembly of molecules in arbitrary arrangements. It allows individual molecules to be picked up from a depot area and assembled one by one at a chosen position in a "construction site" in the target area (Scheme 1).

SMC&P is based on noncovalent, but thermally stable, bonds for storage (depot), handling (AFM cantilever), and deposition (target). These bonds are chosen such that the force required to release the storage interaction is lower than the force required to overcome the handle attachment, which again is lower than the deposition bond ($F_s < F_h < F_d$). For one-by-one assembly, the functionalized AFM cantilever tip is allowed to bind a transfer molecule in the depot area *via* the specific handle. Upon retraction the storage bond ruptures, the transfer molecule remains attached to the cantilever and is then transferred to the construction site. There, the AFM tip is lowered and the transfer molecule forms a deposition bond and is thus placed at a chosen position in the construction site. Upon retraction of the tip, the handle bond ruptures, while the transfer molecule remains at its position, and the AFM tip is free again to pick up a new transfer molecule from the depot area. Remarkably, the system is now in the same state as prior to the first pick-up so that the SMC&P-process may be repeated with the same tip in a cyclic manner. The rupture forces in this hierarchical system, which allow this cut and paste process to be run over thousands of cycles, may either be programmed by the selection of the binding partners or predetermined by the force loading rates.[3−6] Note that for each of these bond-rupture processes a force *versus* distance curve is recorded to verify that indeed individual molecules were handled or, in the case of high density tip functionalization, to provide an estimate of the number of transferred molecules per cycle.

During recent years, this method was improved and taken from the initial DNA-based stage *via* the functional assembly of RNA aptamers[7] to the much more complex protein level.[8,9] The first approach in protein

* Address correspondence to diana.pippig@physik.lmu.de, gaub@lmu.de.

Received for review March 25, 2014 and accepted June 4, 2014.

Published online June 04, 2014
10.1021/nn501644w

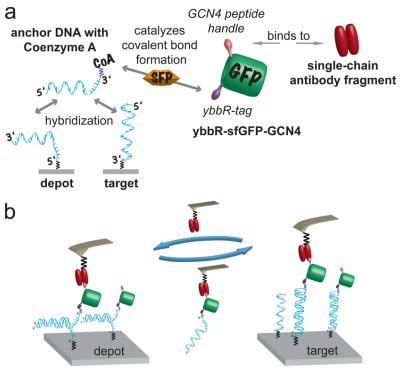

Scheme 1. SMC&P with a chimeric GFP−DNA moiety. (a) To ensure a hierarchical force distribution, DNA duplex interaction is utilized in depot and target region, with the DNA in zipper ($F_{rupture} \sim 20$ pN)[3] and shear conformation ($F_{rupture} \sim 65$ pN),[4] respectively. The intermediate force for the transport handle was achieved using an anti-GCN4-peptide single-chain antibody fragment ($F_{rupture} \sim 50$ pN).[5] (b) Principle of repeatable transfer cycling in protein SMC&P experiments.

SMC&P relied on the use of Zincfinger fusion proteins.[9] The Zincfinger moiety and its specifically bound DNA transfer strand acted as a shuttle for other proteins of interest, combining the advantages and reproducibility of DNA-only SMC&P with the ability to selectively collect and deposit single proteins without loss of functionality. The need for an even more versatile protein transport system arises from the size of the Zincfinger, which imposes a rather big alteration to the protein of interest; its poor solubility, especially in combination with more complex protein candidates; and the noncovalent nature of its DNA interaction.

Minimal modification of the proteins of interest, as well as covalent attachment to the DNA carrier, is greatly desirable. Moreover, there is a general need for robust strategies to selectively couple DNA to proteins. Such chimeras are extremely useful in immunobiological applications[10,11] as well as nanobiotechnology,[12] *e.g.*, for the DNA origami technology.[13] Since the various options to couple DNA-oligonucleotides to proteins harbor certain drawbacks, no gold standard exists hitherto.

Click-chemistry,[14] *e.g.*, while being very specific and selective itself, requires less selective modification of amino acid side chains[15] or the incorporation of non-natural amino acids into proteins.[16,17] The latter is often laborious in terms of expression system and yield.[18] Furthermore, reaction conditions can be rather harsh for proteins or relatively inefficient.[19] Coupling strategies involving bifunctional cross-linkers are less specific. Attachment can be achieved *via* either primary amino groups in proteins or thiol groups, which often requires incorporation of a single accessible cysteine and mutation of others. Thus, full integrity and functionality of the modified proteins is not guaranteed or even unlikely. Furthermore, suicide enzymes, *e.g.*, HaloTag or SNAP-tag (hAGT), could be employed as fusion protein tags for site-specific immobilization reactions.[20−22] However, their respective sizes of 33 and 20 kDa diminish their attractiveness for single-protein manipulation.

We thus chose to employ the 11 amino acid ybbR-tag that, assisted by the Phosphopantetheinyl Transferase Sfp,[23] allows for the site-selective attachment of Coenzyme A (CoA)-modified DNA to proteins of interest[24] (Scheme 1). Coenzyme A is easily reacted to commercially available Maleimide-modified oligonucleotides *via* its intrinsic thiol group, and the already-coupled construct is available upon request for purchase from several companies. The ybbR-tag technology is widely used for labeling proteins with, *e.g.*, biotin or fluorescent dyes and works efficiently on either N- or C-terminus or accessible unstructured regions of proteins.[25] The ybbR-tag/Sfp system can be further employed in the immobilization of proteins on Coenzyme A-functionalized solid carriers or surfaces.[26−28]

RESULTS AND DISCUSSION

We expressed GFP with an N-terminal ybbR-tag and a C-terminal short GCN4-tag and reacted the construct with Coenzyme A-modified transfer-DNA with high yield (Supporting Information Figure S1). The purified chimera was then successfully incorporated in SMC&P experiments. Transport processes were extremely efficient, and the GFP remained intact and fluorescent throughout the SMC&P procedure (Figures 1a,b, and 2). The number of transported molecules can be easily tuned by using either different cantilever sizes and/or varying functionalization densities at the cantilever tip (Figures 1 and 2). Glass surface functionalization is kept as dense as possible to allow for a homogeneous distribution of transfer-DNA:protein complex binding sites in the depot and target area. The number of deposited protein molecules is thus solely dependent on the number of GCN4-binding antibody anchors on the cantilever tip.

To achieve the highest precision possible and to prove that individual molecules can be transported, we performed SMC&P of the GFP-DNA chimera employing BioLever Mini (BLM) cantilevers. Such cantilevers harbor extremely sharp and small, but still functionalizable, tips (10 nm nominal tip radius of curvature; sharpened from the initial pyramidal shape by an oxidation process) and hence, offer the highest accuracy in molecule deposition. Grid patterns of 8 × 8 distinct transfer sites (10.5 × 10.5 μm in size, 1.5 μm in each direction between each grid point) were assembled (Figure 1 and Supporting Information Figure S2). The transport process was followed directly by recording force distance curves with the AFM during SMC&P

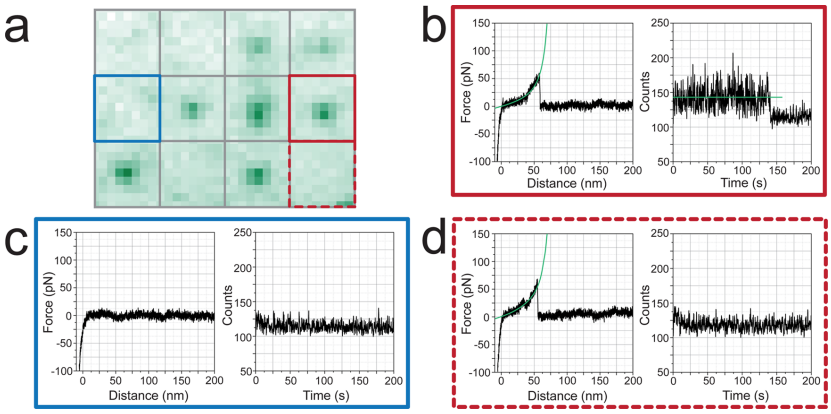

Figure 1. Individual GFP molecules can be transported with AFM cantilevers. (a) Representative 3 × 4 deposition point grid section obtained by SMC&P of GFP molecules employing a BLM cantilever (standard deviation of the fluorescence signal over 100 s, ImageJ) with 7 observable GFP signals out of 12 transfer cycles. (b) Rupture forces around 50 pN (at loading rates around 300 pN/s) correspond to single deposition events in the target area and correlate with a single bleaching step in the fluorescence signal over time at the distinct deposition point (2 × 2 pixel area). (c) Target force curves showing no force built-up correspond to cycles where no molecule could be deposited, which is also evident from the lack of a fluorescence signal at the respective grid position. (d) Due to its limited photostability, a fraction of the GFP molecules is expected to already be bleached throughout the purification and SMC&P preparation process. Yet, the dual mode of transport observation—directly following force–distance curves while performing SMC&P and subsequent fluorescence imaging—allows the detection of single GFP deposition events, even in the absence of a fluorescence signal.

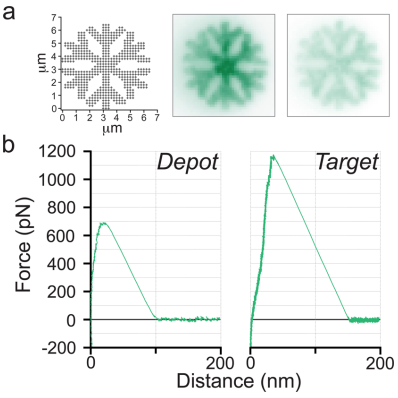

Figure 2. High transport efficiency protein SMC&P. (a) After exposure of the 552-point deposition snowflake pattern for 60 s (0.1 s exposure time at ~10 W/cm^2), it still appears homogeneous and clearly discernible. The pattern template and the average fluorescence over the first (bright) and last (faint) 20 frames of the TIRFM acquisition (600 frames at 0.1 s exposure time) are depicted. (b) Judging from extremely high rupture forces, several (>20) GFP molecules were transported in each cycle.

cycling (Figure 1 and Supporting Information Figure S3). The pattern was subsequently imaged by TIRF microscopy (Figure 1a and Supporting Information Figure S2a). The number of deposited GFP molecules arises from the fluorescence signal over time at a distinct grid point (Figure 1b). We could thus show that indeed single molecules were transferred. Notably, SMC&P utilizing such sharp-tipped cantilevers can also result in force curves devoid of any rupture event and thus no GFP deposition (Figure 1c). In some cases, even though single rupture events were observed, no fluorescence signal could be detected at the corresponding grid position (Figure 1d). A likely cause is the limited photostability of GFP. A fraction of the GFP molecules can be expected to already undergo photobleaching during the purification and SMC&P preparation process. Thus, nonfluorescent GFP molecules would be occasionally transported as well. Furthermore, the rupture events underlying the SMC&P procedure only have a certain probability to lie in the expected force range. In rare cases, the observed rupture event for the deposition process could therefore theoretically originate from a rupture of the shear DNA deposition bond (a most probable rupture force ~65 pN would be expected for the utilized 40 bp duplex at the observed loading rates around 300 pN/s)[4] instead of the desired antibody fragment/GCN4-peptide dissociation ($F_{rupture}$ ~ 50 pN at the observed loading rates around 300 pN/s).[5] This would result in the GFP-DNA chimera remaining on the cantilever and could hence also account for the absence of a fluorescence signal in the respective grid position.

In a typical SMC&P experiment where a 64-point distinct deposition pattern was assembled, an average of 0.89 molecules per cycle were picked up from the

depot area, judging from the according force spectroscopy data. More relevantly, an average of 0.84 molecules were deposited per cycle, based on rupture force evaluation. A fluorescence-based assessment of the number of transported and actually deposited molecules gives rise to an average value of 0.5 molecules per cycle (Supporting Information Figure S2). For comparison, in former DNA-only SMC&P experiments, employing AFM probes with broader tips, around 0.5 molecules per cycle were transported.[29] Further, in earlier Zincfinger-based protein-SMC&P approaches, where larger numbers of molecules should be transferred with densely functionalized broad-tipped cantilevers, efficiencies ranged around 2 molecules per cycle.[9]

Conditions are optimized in a way that mostly individual molecules are transported. Rarely, the transport of two molecules per cycle is observed, whereas SMC&P cycles devoid of a deposition event are much more likely to occur. A transport efficiency of less than one molecule per cycle is acceptable for the benefit of being able to frequently transport truly individual protein constructs. Under the given conditions, one SMC&P cycle takes less than 3 s. This is mainly affected by the chosen pulling speeds that are optimized with respect to apparent loading rates and thus probable rupture forces. These parameters require careful adjustment to ensure functional and structural integrity of the transported protein as well as balancing the hierarchical rupture force "triangle" the SMC&P principle builds-up on. Binding kinetics of the interacting molecules are not expected to be limiting under the experimental conditions (see Supporting Information, p S7).

To further demonstrate the robustness of the SMC&P setup, we additionally utilized a pyramidal shaped MLCT cantilever probe with a nominal tip curvature radius of approximately 20 nm to assemble the pattern of a snowflake in 552 transfer cycles (Figure 2). GFP fluorescence of the pattern was extremely strong, and after laser exposure at 10 W/cm^2 for 60 s, the homogeneous pattern was still clearly discernible (Figure 2). Considering GFP's limited photostability, this indicates high transport efficiency. Judging from AFM rupture force curves of this experiment, more than 20 molecules were transported per cycle.

CONCLUSIONS

In conclusion, we have largely improved protein-based SMC&P in terms of versatility, precision, efficiency and robustness. The adaptability of the system will in the future allow tackling of any protein of interest in single-molecule studies or in complex protein networks, spatially arranged by means of SMC&P. Moreover, protein SMC&P can be utilized to for example place individual enzymes in the center of bow-tie nanoantenna structures[30] or Zero-Mode Waveguides (ZMW), as has been demonstrated for DNA.[31] In favor of this, the applicability of cantilever tips with a high aspect ratio is especially crucial for protein SMC&P as the cantilevers with larger pyramidal shaped tips exceed the dimensions of the nanometer-sized holes of ZMWs. The precision and spatial control achieved with protein SMC&P will thereby significantly improve enzymatic studies in the presence of high concentrations of fluorescent substrates that are unmet by other single-molecule fluorescence methods.[32]

Importantly, the protein–DNA coupling strategy employing Coenzyme A-modified DNA and the ybbR-tag/Sfp system proved to be high-yielding, straightforward (also with other protein constructs, data not shown), and relatively inexpensive in terms of material costs and time. It thus promises to be a useful tool in providing protein–DNA chimeras, which should also be advantageous for other fields of nanobiotechnology and protein engineering.

EXPERIMENTAL SECTION

SMC&P experiments were carried out on a combined AFM/TIRFM setup, as described previously[1] and detailed information can be found in the Supporting Information. In short, GFP harboring an N-terminal Hexa-His-tag, followed by an 11 amino acid ybbR-tag[25] and a C-terminal GCN4-tag[5] was expressed in *Escherichia coli* BL21 DE3 CodonPlus and purified according to standard protocols. The construct was then reacted with Coenzyme A-modified transfer-DNA (biomers.net GmbH, Ulm, Germany) in the presence of Sfp. The progress of the coupling reaction was assessed by SDS-PAGE and subsequent fluorescence scanning as well as Coomassie staining of gels. The GFP–DNA chimera was then purified by anion exchange chromatography. The construct was bound to the DNA-depot area on a functionalized glass surface *via* a custom-built microfluidic system. SMC&P was achieved by means of anti-GCN4 antibody functionalized cantilever tips, delivering GFP–DNA molecules from the depot area to the construction site in the target area. BLM cantilevers were used to transport individual GFP–DNA chimeras. MLCT cantilevers were utilized for comparison and high transport efficiencies. Molecule pick-up and deposition was followed directly by AFM force–distance curves, and the assembled pattern was imaged by TIRF microscopy subsequent to the writing process. Simultaneous detection of AFM curves and fluorescence is also possible; however, it was not feasible for GFP due to its relatively low photostability.

Conflict of Interest: The authors declare no competing financial interest.

Supporting Information Available: Further details on experimental methods and supplementary results. This material is available free of charge *via* the Internet at http://pubs.acs.org.

Acknowledgment. The authors would like to thank Prof. Jens Michaelis for advice concerning protein labeling strategies and the ybbR/Sfp-system in particular and kindly providing the Sfp-Synthase expression vector. We would also like to thank Dr. Christopher Deck of biomers.net GmbH (Ulm, Germany) for technical advice on and custom-synthesis of CoA–DNA constructs, as well as Ms. Katherine Erlich for language proofreading. This work was supported by an Advanced Grant of the European Research Council and the Deutsche Forschungsgemeinschaft through SFB 1032.

REFERENCES AND NOTES

1. Kufer, S. K.; Puchner, E. M.; Gumpp, H.; Liedl, T.; Gaub, H. E. Single-Molecule Cut-and-Paste Surface Assembly. *Science* **2008**, *319*, 594–596.
2. Puchner, E. M.; Kufer, S. K.; Strackharn, M.; Stahl, S. W.; Gaub, H. E. Nanoparticle Self-Assembly on a DNA-Scaffold Written by Single-Molecule Cut-and-Paste. *Nano Lett.* **2008**, *8*, 3692–3695.
3. Rief, M.; Clausen-Schaumann, H.; Gaub, H. E. Sequence-Dependent Mechanics of Single DNA Molecules. *Nat. Struct. Biol.* **1999**, *6*, 346–349.
4. Morfill, J.; Kuhner, F.; Blank, K.; Lugmaier, R. A.; Sedlmair, J.; Gaub, H. E. B-S Transition in Short Oligonucleotides. *Biophys. J.* **2007**, *93*, 2400–2409.
5. Morfill, J.; Blank, K.; Zahnd, C.; Luginbuhl, B.; Kuhner, F.; Gottschalk, K. E.; Pluckthun, A.; Gaub, H. E. Affinity-Matured Recombinant Antibody Fragments Analyzed by Single-Molecule Force Spectroscopy. *Biophys. J.* **2007**, *93*, 3583–3590.
6. Dudko, O. K.; Hummer, G.; Szabo, A. Intrinsic Rates and Activation Free Energies from Single-Molecule Pulling Experiments. *Phys. Rev. Lett.* **2006**, *96*, 108101.
7. Strackharn, M.; Stahl, S. W.; Puchner, E. M.; Gaub, H. E. Functional Assembly of Aptamer Binding Sites by Single-Molecule Cut-and-Paste. *Nano Lett.* **2012**, *12*, 2425–2428.
8. Strackharn, M.; Stahl, S. W.; Severin, P. M.; Nicolaus, T.; Gaub, H. E. Peptide-Antibody Complex as Handle for Single-Molecule Cut & Paste. *ChemPhysChem* **2012**, *13*, 914–917.
9. Strackharn, M.; Pippig, D. A.; Meyer, P.; Stahl, S. W.; Gaub, H. E. Nanoscale Arrangement of Proteins by Single-Molecule Cut-and-Paste. *J. Am. Chem. Soc.* **2012**, *134*, 15193–15196.
10. Akter, F.; Mie, M.; Grimm, S.; Nygren, P. A.; Kobatake, E. Detection of Antigens Using a Protein-DNA Chimera Developed by Enzymatic Covalent Bonding with Phix Gene A. *Anal. Chem.* **2012**, *84*, 5040–5046.
11. Burbulis, I.; Yamaguchi, K.; Gordon, A.; Carlson, R.; Brent, R. Using Protein-DNA Chimeras To Detect and Count Small Numbers of Molecules. *Nat. Methods* **2005**, *2*, 31–37.
12. Cecconi, C.; Shank, E. A.; Dahlquist, F. W.; Marqusee, S.; Bustamante, C. Protein-DNA Chimeras for Single Molecule Mechanical Folding Studies with the Optical Tweezers. *Eur. Biophys. J.* **2008**, *37*, 729–738.
13. Rothemund, P. W. Folding DNA To Create Nanoscale Shapes and Patterns. *Nature* **2006**, *440*, 297–302.
14. Kolb, H. C.; Finn, M. G.; Sharpless, K. B. Click Chemistry: Diverse Chemical Function from a Few Good Reactions. *Angew. Chem., Int. Ed.* **2001**, *40*, 2004–2021.
15. van Dongen, S. F.; Teeuwen, R. L.; Nallani, M.; van Berkel, S. S.; Cornelissen, J. J.; Nolte, R. J.; van Hest, J. C. Single-Step Azide Introduction in Proteins *via* an Aqueous Diazo Transfer. *Bioconjugate Chem.* **2009**, *20*, 20–23.
16. Wang, L.; Schultz, P. G. Expanding the Genetic Code. *Angew. Chem., Int. Ed.* **2004**, *44*, 34–66.
17. Wang, L.; Brock, A.; Herberich, B.; Schultz, P. G. Expanding the Genetic Code of *Escherichia coli*. *Science* **2001**, *292*, 498–500.
18. Cellitti, S. E.; Jones, D. H.; Lagpacan, L.; Hao, X. S.; Zhang, Q.; Hu, H. Y.; Brittain, S. M.; Brinker, A.; Caldwell, J.; Bursulaya, B.; *et al. In Vivo* Incorporation of Unnatural Amino Acids To Probe Structure, Dynamics, and Ligand Binding in a Large Protein by Nuclear Magnetic Resonance Spectroscopy. *J. Am. Chem. Soc.* **2008**, *130*, 9268–9281.
19. Lallana, E.; Riguera, R.; Fernandez-Megia, E. Reliable and Efficient Procedures for the Conjugation of Biomolecules through Huisgen Azide-Alkyne Cycloadditions. *Angew. Chem., Int. Ed.* **2011**, *50*, 8794–8804.
20. Los, G. V.; Encell, L. P.; McDougall, M. G.; Hartzell, D. D.; Karassina, N.; Zimprich, C.; Wood, M. G.; Learish, R.; Ohana, R. F.; Urh, M.; *et al.* Halotag: A Novel Protein Labeling Technology for Cell Imaging and Protein Analysis. *ACS Chem. Biol.* **2008**, *3*, 373–382.
21. Popa, I.; Berkovich, R.; Alegre-Cebollada, J.; Badilla, C. L.; Rivas-Pardo, J. A.; Taniguchi, Y.; Kawakami, M.; Fernandez, J. M. Nanomechanics of Halotag Tethers. *J. Am. Chem. Soc.* **2013**, *135*, 12762–12771.
22. Keppler, A.; Kindermann, M.; Gendreizig, S.; Pick, H.; Vogel, H.; Johnsson, K. Labeling of Fusion Proteins of O6-Alkylguanine-DNA Alkyltransferase with Small Molecules *in Vivo* and *in Vitro*. *Methods* **2004**, *32*, 437–444.
23. Yin, J.; Straight, P. D.; McLoughlin, S. M.; Zhou, Z.; Lin, A. J.; Golan, D. E.; Kelleher, N. L.; Kolter, R.; Walsh, C. T. Genetically Encoded Short Peptide Tag for Versatile Protein Labeling by Sfp Phosphopantetheinyl Transferase. *Proc. Natl. Acad. Sci. U.S.A.* **2005**, *102*, 15815–15820.
24. Maillard, R. A.; Chistol, G.; Sen, M.; Righini, M.; Tan, J.; Kaiser, C. M.; Hodges, C.; Martin, A.; Bustamante, C. Clpx(P) Generates Mechanical Force to Unfold and Translocate Its Protein Substrates. *Cell* **2011**, *145*, 459–469.
25. Yin, J.; Lin, A. J.; Golan, D. E.; Walsh, C. T. Site-Specific Protein Labeling by Sfp Phosphopantetheinyl Transferase. *Nat. Protoc.* **2006**, *1*, 280–285.
26. Wong, L. S.; Thirlway, J.; Micklefield, J. Direct Site-Selective Covalent Protein Immobilization Catalyzed by a Phosphopantetheinyl Transferase. *J. Am. Chem. Soc.* **2008**, *130*, 12456–12464.
27. Wong, L. S.; Karthikeyan, C. V.; Eichelsdoerfer, D. J.; Micklefield, J.; Mirkin, C. A. A Methodology for Preparing Nanostructured Biomolecular Interfaces with High Enzymatic Activity. *Nanoscale* **2012**, *4*, 659–666.
28. Limmer, K.; Pippig, D. A.; Aschenbrenner, D.; Gaub, H. E. A Force-Based, Parallel Assay for the Quantification of Protein-DNA Interactions. *PLoS One* **2014**, *9*, No. e89626.
29. Kufer, S. K.; Strackharn, M.; Stahl, S. W.; Gumpp, H.; Puchner, E. M.; Gaub, H. E. Optically Monitoring the Mechanical Assembly of Single Molecules. *Nat. Nanotechnol.* **2009**, *4*, 45–49.
30. Kinkhabwala, A. A.; Yu, Z. F.; Fan, S. H.; Moerner, W. E. Fluorescence Correlation Spectroscopy at High Concentrations Using Gold Bowtie Nanoantennas. *Chem. Phys.* **2012**, *406*, 3–8.
31. Heucke, S. F.; Baumann, F.; Acuna, G. P.; Severin, P. M.; Stahl, S. W.; Strackharn, M.; Stein, I. H.; Altpeter, P.; Tinnefeld, P.; Gaub, H. E. Placing Individual Molecules in the Center of Nanoapertures. *Nano Lett.* **2014**, *14*, 391–395.
32. Heucke, S. F.; Puchner, E. M.; Stahl, S. W.; Holleitner, A. W.; Gaub, H. E.; Tinnefeld, P. Nanoapertures for AFM-Based Single-Molecule Force Spectroscopy. *Int. J. Nanotechnol.* **2013**, *10*, 607–619.

Supporting Information

Protein-DNA Chimeras for Nano Assembly

Diana A. Pippig[1,*], Fabian Baumann[1], Mathias Strackharn[1], Daniela Aschenbrenner[1,2], Hermann E. Gaub[1]

[1]Center for Nanoscience and Department of Physics, University of Munich, Amalienstraße 54, 80799 Munich, Germany

[2]Center for Integrated Protein Science Munich

[*]diana.pippig@physik.lmu.de

The experiments described in the manuscript were performed on an AFM/TIRFM hybrid, the details of which may be found in Gumpp *et al.*[1] This supporting information specifies methods and materials that are relevant for the conduction of the measurements discussed in the main text.

AFM Measurements

A custom built AFM head and an Asylum Research MFP3D controller (Asylum Research, Santa Barbara, USA), which provides ACD and DAC channels as well as a DSP board for setting up feedback loops, were used. Software for the automated control of the AFM head and xy-piezos during the SMC&P experiments was programmed in Igor Pro (Wave Metrics, Lake Oswego, USA). MLCT-AUHW cantilevers (Bruker, Camarillo, USA; 20 nm nominal tip radius, pyramidal shaped probe) and BioLever Mini (BL-AC40TS, here "BLM") cantilevers (Olympus, Japan; 10 nm nominal tip radius, sharpened probe) were chemically modified (see Preparation of Cantilevers) and calibrated in solution using the equipartition theorem.[2,3] Pulling velocities were set to 2 µm/s in the depot and 0.2 µm/s in the target area. The positioning feedback accuracy is ±3 nm. However, long-term deviations may arise due to thermal drift. Typical times for one Cut & Paste cycle amount to approximately 3 s in these experiments.

TIRF Microscopy

The fluorescence microscope of the hybrid instrument excites the sample through the objective in total internal reflection mode. A 100x/1.49 oil immersion objective (CFI Apochromat TIRF, Nikon, Japan) was employed. Blue excitation for monitoring GFP fluorescence was achieved with a fiber-coupled 473 nm diode laser (iBEAM smart, Toptica Photonics, Gräfelfing, Germany) at an estimated excitation intensity of approximately 10 W/cm^2. The corresponding filter set consists of z 470/10 (Chroma, Bellows Falls, VT, USA), ND10A (for grid experiments, Thorlabs GmbH, Dachau, Germany), z 470 RDC, HQ 525/50, HQ485lp (all of Chroma, Bellows Falls, VT, USA)

and HC 750/SP (AHF, Tübingen, Germany) filters. Images were recorded with a back-illuminated EMCCD camera (DU-860D, Andor, Belfast, Ireland) in frame transfer mode with 1 MHz readout rate at a frame rate of 10 Hz. The camera was water cooled and operated at -75 °C.

Preparation of the C11L34 Single Chain Antibody Fragment

The C11L34 single chain antibody fragment was prepared as described previously.[4] The scFv construct harbored a C-terminal Hexa-His-tag followed by a Cys to allow for site-specific immobilization and was obtained by periplasmic expression in *E. coli* SB536. C11L34 was purified by Ni^{2+} and immobilized antigen affinity chromatography according to standard protocols. The concentration was adjusted to ~1.4 mg/ml in a storage buffer containing 50 mM sodium phosphate, pH 7.2, 50 mM NaCl and 10 mM EDTA.

Preparation of the ybbR-GFP-GCN4 Construct

A superfolderGFP[5] construct was designed to harbor an N-terminal ybbR-tag (DSLEFIASKLA)[6, 7] and a C-terminal GCN4-tag (YHLENEVARLKKL).[8] The sfGFP gene was PCR amplified from a synthetic template (Lifetechnologies, Paisley, UK) with primers containing the respective tag coding sequences. The construct was cloned into a modified pGEX6P2 vector (GE Healthcare, Little Chalfont, UK) that, in addition to the GST-tag, harbors a Hexa-His-Tag and a TEV-Protease cleavage site, by means of NdeI and XhoI restriction sites.

The resulting fusion protein (ybbR-sfGFP-GCN4) harbored a GST- as well as a Hexa-His-tag and was expressed in *E.coli* BL21 DE3 CodonPlus cells (Agilent Technologies, Inc., Santa Clara, CA, USA). For this, one liter of SB medium was inoculated with 10 ml of an overnight culture and grown at 37°C. When an OD_{600} of 0.7 had been reached, over night expression at 18°C was induced by adding 0.25mM IPTG.
Cells were lysed in 50mM Tris HCl pH 7.5, 150 mM NaCl, 2mM DTT, 5% Glycerol, by a French pressure cell press. The ybbR-sfGFP-GCN4 construct was obtained in the soluble fraction and purified by Glutathione affinity chromatography on a GSTrap column (GE Healthcare, Little Chalfont, UK). After over night incubation with PreScission protease the GST-tag was removed and the protein further purified by Ni-IMAC over a HisTrap HP column (GE Healthcare, Little Chalfont, UK). The purified protein was concentrated and the buffer exchanged (50mM Tris HCl pH7.5, 150mM NaCl, 2mM DTT, 5% Glycerol) by ultrafiltration in 10 kDa MWCO Amicon centrifuge filter devices (EMD Millipore Corporation, Billerica, MA, USA). Protein was stored at -80°C at a final concentration of 6.5 µM.

Sfp-mediated Coupling of Coenzyme A-modified DNA to ybbR-GFP-GCN4

3'-Coenzyme A-modified transfer DNA was synthesized by biomers.net GmbH (Ulm, Germany). Lyophilized DNA was dissolved in Sfp-buffer (120 mM TrisHCl pH7.5, 10 mM $MgCl_2$, 150 mM NaCl, 2% Glycerol, 2 mM DTT) to a concentration of 100 mM. The coupling reaction was slightly altered from Yin *et al.*[6] by mixing 10 nmol CoA-DNA with 7.2 nmol ybbR-GFP-GCN4 and 0.75 nmol Sfp in a total volume of 1.5 ml in Sfp-buffer. The mix was incubated at room temperature and the progress of the reaction was

followed by analyzing aliquots in SDS-PAGE. Best coupling efficiency (ca. 90%) was achieved after concentrating the entire reaction mix 10fold by ultrafiltration and over night incubation at room temperature. To remove remaining free DNA, the GFP-DNA construct was further purified by anion exchange chromatography (Suppl. Fig. S1a) on a HiTrap Q HP column (GE Healthcare, Little Chalfont, UK). Fractions were analyzed by SDS-PAGE (Suppl. Fig. S1b) and UV/Vis spectrometry at 260, 280 and 488 nm. Aliquots of 3.8 μM DNA/GFP-GCN4 conjugate were stored at -80°C.

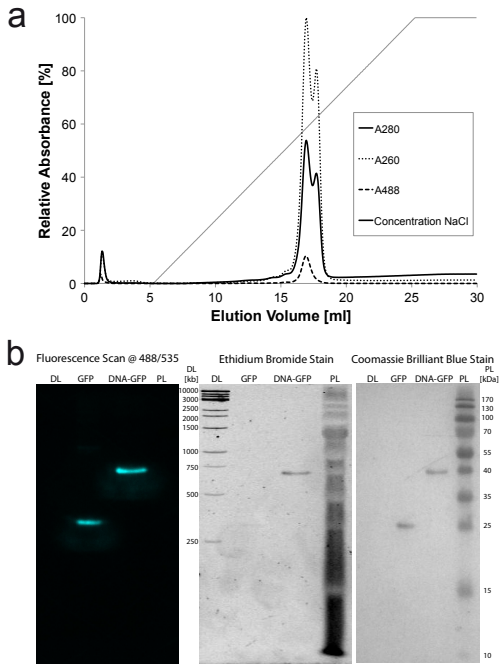

Supplementary Figure S1. Purification of the covalent GFP-DNA complex. (a) Chromatogram of the anion exchange chromatography and (b) SDS-PAGE gel imaged by fluorescence scan (excitation 488 nm, emission 535 nm), after Ethidium Bromide staining and UV detection and after Coomassie Staining. Samples loaded were: "DL" – DNA-ladder 1kb ruler (ThermoFisher Scientific, Waltham, MA, USA), "GFP" – ybbR-sfGFP-GCN4 , "DNA-GFP" – DNA-CoA-ybbR-sfGFP-GCN4, "PL" – Protein ladder PAGERuler Prestained (ThermoFisher Scientific, Waltham, MA, USA).

Preparation of Cantilevers

Cantilevers (MLCT obtained from Asylum Research, Santa Barbara, CA and BioLever Mini obtained from Olympus, Japan) were oxidized in a UV-ozone cleaner (UVOH 150 LAB, FHR Anlagenbau GmbH, Ottendorf-Okrilla, Germany) and silanized by soaking for 2 min in (3-Aminopropyl)dimethylethoxysilane (ABCR, Karlsruhe, Germany; 50% v/v in Ethanol) . Subsequently, they were washed in toluene, 2-propanol and ddH_2O and dried at 80 °C for 30 min. After incubating the cantilevers in sodium borate buffer (pH 8.5), a heterobifunctional PEG crosslinker[9] with N-hydroxy succinimide and maleimide groups (MW 5000, Rapp Polymere, Tübingen, Germany) was applied for 1 h at 25 mM in sodium borate buffer. Afterwards, the C11L34 antibody fragments were bound to the cantilevers at 8 °C for 2-4 h. Finally the cantilevers were washed and stored in PBS.

Preparation of Glass Surfaces

Glass cover slips were sonicated in 50% (v/v) 2-propanol in ddH_20 for 15 min and oxidized in a solution of 50% (v/v) hydrogen peroxide (30%) and sulfuric acid for 30 min. They were then washed in ddH_2O, dried in a nitrogen stream and then silanized by soaking for 1 h in (3-Aminopropyl)dimethylethoxysilane (ABCR, Karlsruhe, Germany, 1.8 % v/v in Ethanol). Subsequently, they were washed twice in 2-propanol and ddH_2O and dried at 80 °C for 40 min. After incubation in sodium borate buffer (pH 8.5), a heterobifunctional PEG crosslinker with N-hydroxy succinimide and maleimide groups (MW 5000, Rapp Polymere, Tübingen, Germany) was applied for 1 h at 50 mM in sodium borate buffer. Depot and Target DNA was reduced with TCEP and then purified by ethanol precipitation. DNA pellets were dissolved in phosphate buffer (pH 7.2, 50 mM

NaCl, 10 mM EDTA). A microfluidic system was fixed on the PEGylated cover glass, and the depot and target DNA oligonucleotides were pumped through the two respective channels and incubated for 1 h. Subsequently both channels were flushed with 1mg/ml BSA and then PBS. The GFP-DNA chimera was pumped into the depot channel and incubated for 60 min. The channel was then rinsed again with PBS and the microfluidic system was removed.

SMC&P Experiment

Grid patterns were written in 64 cycles with 1.5 µm space between each deposition point. The denser snowflake pattern was written in 552 transfer cycles. The pulling speed in the depot was set to 2 µm/s and in the target to 0.2 µm/s. This corresponds to approximate surface contact times[10] (dependent on approach/retraction velocity, indentation force and substrate stiffness) of 8 ms and 80 ms, respectively, and should allow for ligand binding (compare k_{on}(DNA)>10^4 $M^{-1}s^{-1}$ and k_{on}(AB)~10^6 $M^{-1}s^{-1}$).[10-13] Considering a single antibody molecule being bound to the cantilever tip and estimating its localization in a half sphere with r= 30 nm (length of PEG linker), the local concentration of antibody would be in the mM range. This is several orders of magnitude higher than the K_d for the antibody-peptide interaction (pM to nM range - Berger *et al.*; FEBS, 1999). Taking further into account that bond formation is not diffusion-limited for the SMC&P experiment, successful attachment is very likely even at the given, short contact times. In addition, it is crucial for the respective interactions to be thermally stable over a long time span. Especially the DNA storage bonds in the depot site as well as in the construction

site are required to not passively dissociate. Judging from the extremely low expected off-rates (k_{off}(DNA)>10^{-10} s^{-1}, k_{off}(AB)~10^{-4} s^{-1})[4, 14] this prerequisite should be fulfilled. One SMC&P cycle is completed in less than 3 s, this is mainly dependent on the pulling speed, which is optimized with respect to loading rates and thus rupture forces. This warrants that the zipper-DNA storage bond is more likely to rupture during the pickup process than the newly formed antibody – GCN4-peptide bond, whereas the shear-DNA bond formed in the deposition process is more likely to withstand the final retraction. The functionalization density of the cantilever, depot and target region was adjusted to allow for high effectiveness in SMC&P. Transfer efficiencies were determined from rupture events and forces (Fig. 2, 3, Suppl. Fig. S3) as well as fluorescence intensity traces (Fig. 2) of transported GFP molecules over time.

Rupture forces and loading rates were evaluated from AFM force distance curves that were recorded for each pick-up and deposition process (moving average smoothing over 5 data points was employed for improved visualization in Fig. 2, but not evaluation) utilizing a quantum mechanically corrected WLC model[15] (force spectroscopy data was evaluated in Igor Pro).

Fluorescence bleaching of deposited molecules in a 2x2 pixel area (180 nm/pixel), corresponding to the 4 brightest pixels in the expected deposition vicinity, was followed for 200 s at 0.1 s exposure time. Smoothing, by moving average over five data points, for improved bleaching step perceptibility and analysis were performed in ImageJ. Where applicable, *i.e.* with the number of transported GFP molecules being in an, in our hands, resolvable range in the time course experiments (for BLM grids), exact numbers of

deposited GFP molecules could be deduced from bleaching steps in the fluorescence traces (Fig. 2, Suppl. Fig. S2 – traces not shown).

For MLCT cantilevers the transfer efficiency ranged around 20 (as found for the snowflake pattern; deduced from rupture forces Fig. 3) molecules per cycle. For the sharp-tipped BLM cantilevers functionalization conditions were limiting, so that mainly single molecules were transported and not all SMC&P cycles resulted in a deposition (Fig. 2, Suppl. Fig. S2)

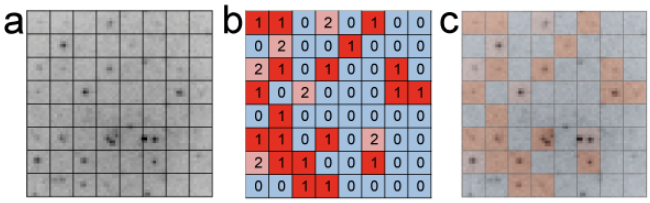

Supplementary Figure S2. Representative 8x8 deposition point grid pattern of a GFP SMC&P experiment employing a BLM cantilever. (a) The TIRFM image represents the standard deviation of the fluorescence within the recorded series as evaluated with ImageJ (exemplary BLM 8x8 grid: first 774 frames at 0.1 s exposure time). (b) The number of deposited GFP molecules in each grid position was determined from fluorescence signals over time in 2x2 pixel areas, representative of the 4 brightest pixels in the approximated deposition vicinity. (c) Superposition of the TIRFM image and the color-coded deposition count panel (blue - 0, red – 1, pale red - 2 GFP molecules).

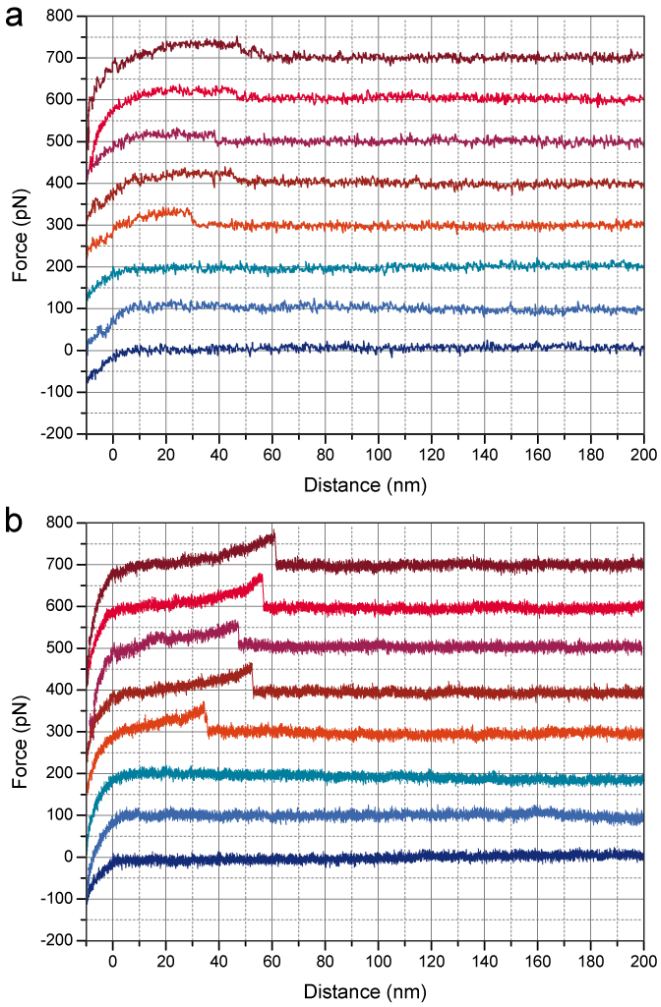

Supplementary Figure S3. Representative example curves of GFP SMC&P experiments employing BLM cantilevers. Curves that represent no rupture, *i.e.* no pick-up or deposition events are depicted in tints of blue. Single-event curves are shown in tints of red. (a) Single-event depot rupture forces range around 20 pN (corresponding with the unzipping of the DNA storage bond)[16], (b) whereas single-event target rupture forces range around 50 pN, which resembles the

rupture of a single anti-GNC4 antibody/GCN4-peptide interaction at the observed loading rates of ~300 pN/s.[4]

Oligomer Sequences

thiolated depot oligomer

5' SH - TTT TTT CAT GCA AGT AGC TAT TCG AAC TAT AGC TTA AGG ACG TCA A

thiolated target oligomer

5' CAT GCA AGT AGC TAT TCG AAC TAT AGC TTA AGG ACG TCA ATT TTT T– SH

CoA-modified transfer oligomer for protein coupling

5' TTG ACG TCC TTA AGC TAT AGT TCG AAT AGC TAC TT G CAT GTT TTT TTT TTT TTT-

CoA 3'

References

1. Gumpp, H.; Stahl, S. W.; Strackharn, M.; Puchner, E. M.; Gaub, H. E. Ultrastable Combined Atomic Force and Total Internal Reflection Fluorescence Microscope [Corrected]. *Rev. Sci. Instrum.* 2009, 80, 063704.
2. Florin, E. Sensing Specific Molecular Interactions with the Atomic Force Microscope. *Biosens. Bioelectron.* 1995, 10, 895-901.
3. Butt, H. J.; Jaschke, M. Calculation of Thermal Noise in Atomic-Force Microscopy. *Nanotechnology* 1995, 6, 1-7.
4. Morfill, J.; Blank, K.; Zahnd, C.; Luginbuhl, B.; Kuhner, F.; Gottschalk, K. E.; Pluckthun, A.; Gaub, H. E. Affinity-Matured Recombinant Antibody Fragments Analyzed by Single-Molecule Force Spectroscopy. *Biophys. J.* 2007, 93, 3583-3590.
5. Pedelacq, J. D.; Cabantous, S.; Tran, T.; Terwilliger, T. C.; Waldo, G. S. Engineering and Characterization of a Superfolder Green Fluorescent Protein. *Nat. Biotechnol.* 2006, 24, 79-88.
6. Yin, J.; Lin, A. J.; Golan, D. E.; Walsh, C. T. Site-Specific Protein Labeling by Sfp Phosphopantetheinyl Transferase. *Nat. Protoc.* 2006, 1, 280-285.
7. Yin, J.; Straight, P. D.; McLoughlin, S. M.; Zhou, Z.; Lin, A. J.; Golan, D. E.; Kelleher, N. L.; Kolter, R.; Walsh, C. T. Genetically Encoded Short Peptide Tag for Versatile Protein Labeling by Sfp Phosphopantetheinyl Transferase. *Proc. Natl. Acad. Sci. USA* 2005, 102, 15815-15820.
8. Strackharn, M.; Stahl, S. W.; Severin, P. M.; Nicolaus, T.; Gaub, H. E. Peptide-Antibody Complex as Handle for Single-Molecule Cut & Paste. *ChemPhysChem* 2012, 13, 914-917.
9. Celik, E.; Moy, V. T. Nonspecific Interactions in Afm Force Spectroscopy Measurements. *J. Mol. Recognit.* 2012, 25, 53-56.
10. Guo, S.; Lad, N.; Ray, C.; Akhremitchev, B. B. Association Kinetics from Single Molecule Force Spectroscopy Measurements. *Biophys. J.* 2009, 96, 3412-3422.
11. Tawa, K.; Yao, D.; Knoll, W. Matching Base-Pair Number Dependence of the Kinetics of DNA-DNA Hybridization Studied by Surface Plasmon Fluorescence Spectroscopy. *Biosens. Bioelectron.* 2005, 21, 322-329.
12. Henry, M. R.; Wilkins Stevens, P.; Sun, J.; Kelso, D. M. Real-Time Measurements of DNA Hybridization on Microparticles with Fluorescence Resonance Energy Transfer. *Anal. Biochem.* 1999, 276, 204-214.
13. Berger, C.; Weber-Bornhauser, S.; Eggenberger, J.; Hanes, J.; Pluckthun, A.; Bosshard, H. R. Antigen Recognition by Conformational Selection. *FEBS Lett.* 1999, 450, 149-153.
14. Strunz, T.; Oroszlan, K.; Schafer, R.; Guntherodt, H. J. Dynamic Force Spectroscopy of Single DNA Molecules. *Proc. Natl. Acad. Sci. USA* 1999, 96, 11277-11282.
15. Hugel, T.; Rief, M.; Seitz, M.; Gaub, H. E.; Netz, R. R. Highly Stretched Single Polymers: Atomic-Force-Microscope Experiments *Versus* Ab-Initio Theory. *Phys. Rev. Lett.* 2005, 94, 048301.
16. Rief, M.; Clausen-Schaumann, H.; Gaub, H. E. Sequence-Dependent Mechanics of Single DNA Molecules. *Nat. Struct. Biol.* 1999, 6, 346-349.

A.3 Publication 3: Parallel Force Assay for Protein-Protein Interactions

Parallel Force Assay for Protein-Protein Interactions

by

Daniela Aschenbrenner, Diana A. Pippig, Kamila Klamecka, Katja Limmer, Heinrich Leonhardt and Hermann E. Gaub

published in

PLOS ONE, Dezember 2014, 9(12):e115049

PLOS | ONE

RESEARCH ARTICLE

Parallel Force Assay for Protein-Protein Interactions

Daniela Aschenbrenner[1,3], Diana A. Pippig[1]*, Kamila Klamecka[1,2], Katja Limmer[1], Heinrich Leonhardt[2,3], Hermann E. Gaub[1]

1. Lehrstuhl für Angewandte Physik and Center for Nanoscience (CeNS), Ludwig-Maximilians-, . Universität, Amalienstrasse 54, 80799 Munich, Germany, **2.** Department of Biology II and Center for Nanoscience (CeNS), Ludwig-Maximilians-Universität, Großhadernerstr. 2, 82152 Planegg-Martinsried, Germany, **3.** Munich Center for Integrated Protein Science (CIPSM), Butenandtstr. 5–13, 81377 Munich, Germany

*diana.pippig@physik.uni-muenchen.de

OPEN ACCESS

Citation: Aschenbrenner D, Pippig DA, Klamecka K, Limmer K, Leonhardt H, et al. (2014) Parallel Force Assay for Protein-Protein Interactions. PLoS ONE 9(12): e115049. doi:10.1371/journal.pone.0115049

Editor: Gideon Schreiber, Weizmann Institute of Science, Israel

Received: July 1, 2014

Accepted: November 18, 2014

Published: December 29, 2014

Data Availability: The authors confirm that all data underlying the findings are fully available without restriction. All relevant data are within the paper and its Supporting Information files.

Funding: Funding was provided by the Deutsche Forschungsgemeinschaft SFB 1032-A01 (HEG) and SPP 1623, LE 721/13-1 (HL) as well as a European Research Council Advanced Grant (HEG). The funders had no role in study design, data collection and analysis, decision to publish, or preparation of the manuscript. KK and KL are grateful to the Elite Network of Bavaria (International Doctorate Program NanoBioTechnology) for doctoral fellowships. DA, KK and KL thank Nanosystems Initiative Munich for support.

Competing Interests: The authors have declared that no competing interests exist.

Abstract

Quantitative proteome research is greatly promoted by high-resolution parallel format assays. A characterization of protein complexes based on binding forces offers an unparalleled dynamic range and allows for the effective discrimination of non-specific interactions. Here we present a DNA-based Molecular Force Assay to quantify protein-protein interactions, namely the bond between different variants of GFP and GFP-binding nanobodies. We present different strategies to adjust the maximum sensitivity window of the assay by influencing the binding strength of the DNA reference duplexes. The binding of the nanobody Enhancer to the different GFP constructs is compared at high sensitivity of the assay. Whereas the binding strength to wild type and enhanced GFP are equal within experimental error, stronger binding to superfolder GFP is observed. This difference in binding strength is attributed to alterations in the amino acids that form contacts according to the crystal structure of the initial wild type GFP-Enhancer complex. Moreover, we outline the potential for large-scale parallelization of the assay.

Introduction

Protein-protein interactions are essential to most reactions in the cell and thus their characterization crucial for a better understanding of many fundamental processes in nature [1]. A key problem herein lies in the extensive number of interactions in any given proteome [2]. Several high-throughput methods have been developed to meet this challenge, such as yeast-two-hybrid assays [3], protein microarrays [4], or microfluidic-based techniques [5]. These are valuable tools for the identification of interacting proteins [1, 6]. In addition, several low-

throughput methods exist that are able to characterize such interactions in greater detail. Prominent examples, providing different information on the structure or the kinetics of an interaction, are X-ray crystallography [7], fluorescence resonance energy transfer (FRET) [8], or surface plasmon resonance [9]. Another parameter becoming more and more acknowledged is the intermolecular binding force that controls the interaction. Mechanical stability of a biomolecular interaction does not necessarily compare to its thermal stability and *vice versa*. However, mechanical load can for example decrease thermal stability and "off-time" of a bond, which plays a pivotal role in receptor-ligand interactions and thus signaling processes in *e.g.* cell differentiation and immunological recognition. At the other extreme, bonds may be stabilized by exerted forces. These so called "catch bonds" are found across various species and in different biological contexts. In those cases interactions that would otherwise be of transient and low affinity nature are stabilized by the shear force the binding partners experience. Prominent examples are adhesion proteins like integrins [10] and cadherins [11] in humans or FimH [12] in bacteria, which tune their binding properties in response to mechanical stress [13]. Another example for potential biological importance of binding forces is in autoproteolyzed domains of Adhesion-GPCRs, where the two parts of the protein are hypothesized to unbind at a certain force threshold. This could serve as a protective mechanism upon exposure to mechanical stress [14]. As the impact of forces in those contexts is challenging to study it can be assumed that other examples will follow.

In order to address questions regarding forces in biomolecules or biomolecular interactions, single-molecule force spectroscopy techniques have been developed, based on *e.g.* the atomic force microscope (AFM) [15, 16] or optical tweezers [17] enabling direct quantification of the forces and energy landscapes underlying protein-protein interactions [18–20]. Common drawbacks of those single-molecule techniques are the high effort needed to gather statistically sufficient data sets or the infeasibility to measure different interactions in parallel, giving rise to calibration uncertainties [21]. Thus, a method able to parallelize force measurements of protein-protein interactions is highly desirable.

As low throughput is a general limitation of force-based single-molecule experiments, our lab has recently developed the Molecular Force Assay (MFA) to overcome this bottleneck. Relying on the principle of comparing the bond in question with a known reference bond, single-molecule measurements can be conducted in parallel. In detail, the two complexes to be compared are attached in series to form a so-called Molecular Force Probe (MFP) upon which a force is applied. The force directly correlates the mechanical stability of both bonds until, statistically, the weaker bond ruptures. In one single experiment thousands of MFPs can be tested simultaneously. Additionally, the sample and reference bond can be multiplexed. This very sensitive method has already been applied successfully to DNA, *e.g.* to resolve single base-pair mismatches [22]. It was further utilized to characterize the binding of ligands like polyamides [23] or proteins [24] to DNA as well as to RNA [25]. In order to enhance the throughput, the capacity of the MFA technique for parallelization, by means of a microfluidic

chip [26], as well as for miniaturization [27] has been demonstrated. In a first approach to determine protein interactions, a force-based sandwich immunoassay relying on the basic principle of two bonds in series was constructed [28]. Here, we introduce parallelized force measurements of protein-protein interactions utilizing site-specific and covalent integration of a protein pair into the MFA. Our proof-of-principle study aims to test the binding of three variants of Green Fluorescent Proteins (GFPs) [29] to the GFP-binding nanobody "Enhancer" [30]. To be able to detect the differences in binding strength, first the window of high sensitivity of the assay is determined by testing against references with different binding strengths. In order to highlight the dependence of the sensitivity on the chosen reference, a modified variant of Enhancer, displaying a different binding strength to GFP, is employed and compared to Enhancer.

Nanobodies are camelid-derived single-domain antibodies. Enhancer has been generated and selected for its modulation of the conformation and the spectral properties of wild type GFP (wtGFP), where its binding leads to a fourfold fluorescence enhancement [30]. The binding epitopes of the nanobodies lie on the outer beta barrel structure, which is conserved for the other GFP variants investigated here, namely superfolder GFP (sfGFP) [31] and enhanced GFP (eGFP) [32]. As GFP binding nanobodies are stable and functional in living cells, they have been used for numerous applications. Examples are the detection of translocation events *in vivo* [30], the high affinity capture of GFP fusion proteins [33], or enabling GFP to act as scaffold for the manipulation of gene expression [34]. All rely on the nanobodies' excellent binding specificities. In addition to being well characterized, this system offers the advantage of GFP acting as an intrinsic fluorescence label to control for the correct assembly of the Protein-MFA.

Results and Discussion

General Functionality of the Protein Molecular Force Assay

Based on the principle of the standard DNA-MFA [24], the Molecular Force Probes of the Protein-MFA consist of two molecular bonds in series, which are attached between two surfaces. The bond to be probed is the protein complex, where both proteins are attached covalently, one to the glass slide, which acts as the lower surface and the other to one strand of a DNA duplex which acts as the reference bond. A Cy5 dye is attached to the DNA strand coupled to the protein. The complementary DNA strand is labeled with a Cy3 dye, forming a FRET pair with the Cy5, as well as with a Biotin, which enables the coupling to the upper surface, a soft PDMS stamp functionalized with Streptavidin (Fig. 1A). The PDMS stamp has a size of 1 cm $\times$ 1 cm and features 16 pillars of 1mm in height and 1.1mm in diameter. A matching 4×4 array of MFPs is assembled on a glass slide, where each spot can be functionalized independently, enabling the measurement of 16 different protein pairs and/or the variation of the reference DNA (Fig. 1A). For the preparation of the measurement, first the lower proteins

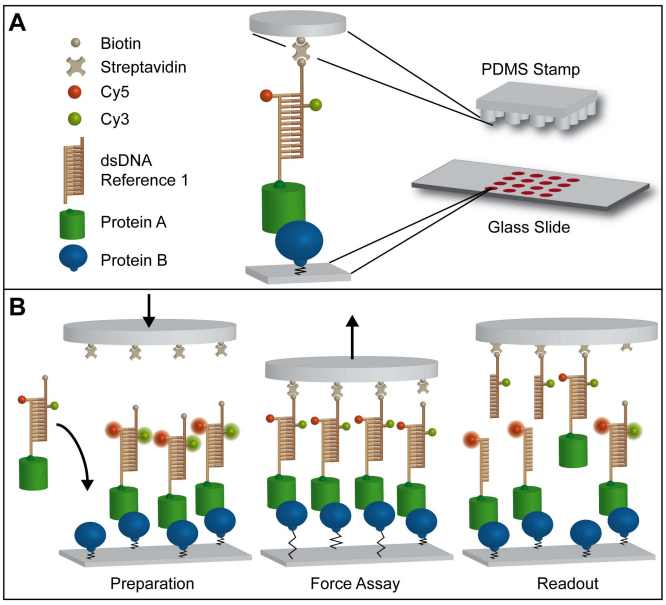

Fig. 1. Basic Principle of the Protein Molecular Force Assay. (A) Molecular Force Probes (MFPs) consist of two bonds in series, a protein complex to be studied and a DNA duplex acting as a reference. Both proteins are attached covalently at their N- or C-terminus, one to the glass slide and the other one to a strand of the DNA duplex. Cy5 and Cy3, coupled to one of the DNA strands each, form a FRET pair. Linkage to the upper surface, a PDMS stamp functionalized with Streptavidin, is facilitated *via* a Biotin on the DNA. In the macroscopic view, the PDMS stamp with 16 pillars as well as the glass slide with a matching 4×4 array of spots of MFPs is displayed. Every spot may be functionalized with a different set of MFPs, allowing for the measurement of 16 different protein pairs and/or the variation of the reference. (B) *Preparation:* After the stepwise assembly of the MFPs on the glass slide, fluorescence "Start" images of the Cy5 signal (with red excitation) as well as the FRET of the MFPs are recorded. Assembly of the assay is completed by lowering the stamp, which enables the Biotins of the MFPs to bind to the Streptavidins on the elastomer. *Force Assay*: Upon retraction of the stamp with constant speed, a force is gradually built up in the MFPs, acting equally on all molecular components in series. As a result, either the DNA reference duplex or the protein-protein interaction unbinds, resulting in the transfer of either Cy3 alone or Cy3 together with Cy5 to the surface of the stamp. *Readout*: Another set of fluorescence "Final" images of the glass surface provides the ratio of broken protein to reference bonds. The ratio of the Cy5 signals on the glass slide provides the surface density of remaining, intact protein complexes in comparison to the initial number of protein pairs. The residual FRET signal accounts for complexes that were not loaded under force and are still fully assembled. The ratio of the FRET signal thus allows for the correction of the analysis.

doi:10.1371/journal.pone.0115049.g001

are attached to the glass slide *via* a PEG linker, then the pre-incubated complex of upper protein and DNA reference is added. Multiple washing steps after each incubation step minimize unspecific binding. Fluorescence "Start" images of the Cy5 (red excitation) and FRET signals are recorded for each spot on the glass slide with an inverted epi-fluorescence microscope. After the stamp is lowered gradually onto the glass slide using reflection interference contrast microscopy

[35], an incubation step of 10 min allows for the coupling of the Biotins to the Streptavidin on the stamp. A piezo actuator enables retraction of the stamp with constant speed, gradually building up a force acting on both complexes of the MFPs until, statistically, the weaker one unbinds. Here, the retraction speed of 1 μm/s yields a force loading rate in the range of 10^5 pN/s [27, 36]. After the retraction of the stamp, another set of "Final" fluorescence images is taken as the ratio of remaining dyes determines the outcome of the experiment.

The Normalized Fluorescence (NF) gives the number of broken upper DNA bonds normalized to the total number of Molecular Force Probes that have been under load. To determine the NF, the "RED" and "FRET" signals recorded of every single spot before and after the actual force assay are processed after background correction. In the analysis, the ratio of RED Final to RED Start gives the density of still intact protein bonds in comparison to the initial amount of protein bonds.

$$Ratio\_RED = RED\_Final / RED\_Start.$$

The ratio of FRET values needs to be determined as well, as a remaining FRET signal after the force assay gives the number of MFPs that have not been under load and are thus still fully assembled (see Fig. 1B). For those MFPs, the Cy5 dye giving the RED signal is still attached to the surface yielding a false positive signal. By determining the FRET ratio *(Ratio_FRET = FRET_Final/FRET_Start)*, those MFPs can be subtracted.

Normalization to the Coupling Efficiency $CE = 1 - Ratio\_FRET$ yields the Normalized Fluorescence:

$$NF = (Ratio\_REDRatio\_FRET)/CE. \quad \text{(Equation 1)}$$

Thus, a NF of 0.5 in this context means that the protein and the DNA complex have the same binding strength, a NF closer to 1 indicates that the protein complex is stronger than its DNA reference and *vice versa* for a NF closer to 0. For the analysis, the assumption is made that all MFPs are correctly assembled in the beginning, meaning that every protein-DNA complex has the second DNA strand attached to it. This is achieved by pre-incubating the DNA in a stoichiometry of 1:2 before coupling to the protein. If only the lower protein is present with nothing bound to it, it does not give a fluorescent signal and can thus be neglected. The RED and FRET signals cannot be compared directly by division, as the fluorescence efficiency of a Cy5 dye is different to that of a Cy3-Cy5 FRET pair. As demonstrated before by Severin *et al.* [24], the pixel-by-pixel method offers the advantage of canceling out inhomogeneities due to the Gaussian illumination profile or coupling density as well as surface defects. Importantly, in the actual force assay all MFPs are tested simultaneously in the moment of the retraction of the stamp while the read-out can take place subsequently without

time constraints [27]. Another very substantial advantage is that the force assay is not disturbed by complex ambients [37] since only fluorescence from the lower surface is measured.

Supporting information on chemical protocols and the measurement process can be found in Materials and Methods in S1 Supplement and S1 Fig.

One of the key challenges in the integration of functional proteins in the MFA was their covalent attachment, especially to the DNA. In principle, different possibilities exist for the coupling of proteins, although differing widely in yield, experimental effort and cost as well as the applicability for attachment to DNA [38, 39]. For the experiments conducted here, as for single-molecule force spectroscopy measurements in general, the site-specific attachment is of utmost importance, as the force needed to unbind a complex depends on the pulling geometry and thus on the position of the attachment [40]. Additionally, to prevent possible mis-assembly, it is reasonable to choose two different strategies for the attachment of the two proteins. In the study presented here, we employed the ybbR-tag [41] on the GFPs' N-termini to covalently attach 5′ Coenzyme A-modified DNA. The coupling is mediated by the Phosphopantetheinyl Transferase Sfp [42, 43] and offers the advantages of very high yield (up to 90%) [44] and a negligible size (11 amino acids) of the protein modification. Further, it has been successfully employed *e.g.* in single-molecule force spectroscopy experiments for the coupling of different proteins in varying experiments to DNA [44, 45] and surfaces [21, 46].

The nanobodies are attached to the glass slide by coupling of the free C-terminal Cysteine to the maleimide group of a heterobifunctional PEG linker [47]. As no extra components are needed, this is a good choice, provided that the protein does not harbor any other accessible or interfering Cysteine residues.

While not needed for the readout of the actual experiment, the use of GFP in this proof-of-principle system offers the advantage of an additional intrinsic control. We observed colocalization of GFP-fluorescence with the fluorescence of the Cy3 and Cy5 dyes, which confirms the specific interaction and correct assembly of the Protein MFPs. The surface density of the Protein MFPs estimated from the Cy5 signal is, similar to previous MFA experiments, about 10^4 MFPs per μm^2 [23, 27]. The results for the NF values are reproducible over numerous experiments conducted independently (see S1 Table). However, the most valid conclusions on very small differences can be drawn from data received by a single experiment since it offers exactly the same environment and treatment such as pressure of the stamp and loading rate.

Adjusting the Sensitivity of the Protein-MFA with Different References

As with an old-fashioned scale, the MFA has its highest sensitivity to discriminate very small differences if it is well balanced, which in our case means that the binding strengths of both complexes are very similar, so that the NF lies close to 0.5. For pure DNA-MFA experiments the strength of the reference could easily be

tuned by varying length, composition and conformation of the DNA duplex, reaching from 15pN for DNA in zipper mode (by opening the DNA like a zipper from the same end) [48] to about 65pN by implementing a 40 base-pair (bp) duplex in shear mode (where the DNA is sheared by applying the force at opposing 5′ termini). Higher average forces cannot be reached with short oligonucleotides as DNA reaches a force plateau at about 65pN when sheared due to the so-called BS-transition [49, 50]. Forces in between can be achieved by varying the number of base pairs in shear mode [51]. For a random protein-protein complex, no information is given about the interaction strength *a priori*.

In the study presented here, the tested protein complexes between nanobodies and GFPs were stronger than a 40bp duplex in shear confirmation, resulting in very high NF-values (see S1 Table). To determine small differences in binding strength, higher sensitivity at NF-values closer to 0.5 is highly desirable, which can be obtained by increasing the strength of the reference. To demonstrate the flexibility and robustness of the Protein-MFA, two different methods to enhance the mechanical stability of the DNA reference are presented here.

The stability of the DNA duplex can be altered intrinsically by nucleobase modification, methylation of the 5′ position in cytosines [52, 53] being a prominent example. Studied primarily in duplex formation with RNA for antisense gene inhibition [54], the modification of the 5′ position of pyrimidines with a propynyl group [55] results in an even higher increase in melting temperature than achieved by 5′ methylation [55-57]. The propynyl group is planar with respect to the heterocycle and extends into the major groove. It is thus expected to stabilize the duplex due to increased base-stacking and a smaller unfavorable entropy change [55, 57, 58]. In the experiments presented here, a 40bp DNA duplex is employed as a reference, where in the biotinylated strand 13 cytidines and 9 thymines are replaced by their corresponding propynyl bases. In comparison to this intrinsic stabilization, the stability can also be altered extrinsically by the addition of a DNA binding ligand. As has been shown in previous studies with the MFA [23, 59], sequence-specific binding of pyrrole-imidazole hairpin polyamides [60, 61] to the minor groove of the DNA helix enhances the stability of the duplex depending on the modification and concentration of the polyamide. For the experiment presented here, three hairpin polyamides with different affinities for the same DNA sequence have been employed. Polyamides P1 (K_D =105pM), (*R*)-P2 (here P2; K_D =44pM) and (R)-P3 (here P3; K_D =1442pM) described in Ho *et al.* [23] have been used in a concentration of 1 μM, approximately 1000 times higher than the saturation concentration, to ensure an excess of available ligand (see S2 Fig. for the DNA sequences as well as the chemical structures of the propynyl bases and the polyamides). P2 displays higher affinity than the sequence-specific binding P1, as it was modified with an amine substituent to introduce chiral selectivity. P3's lower affinity, despite also being chiral, results from a single base-pair mismatch [23].

Fig. 2A depicts the three different reference types used to identify the window of high sensitivity of the assay: unmodified 40 bp double-stranded DNA,

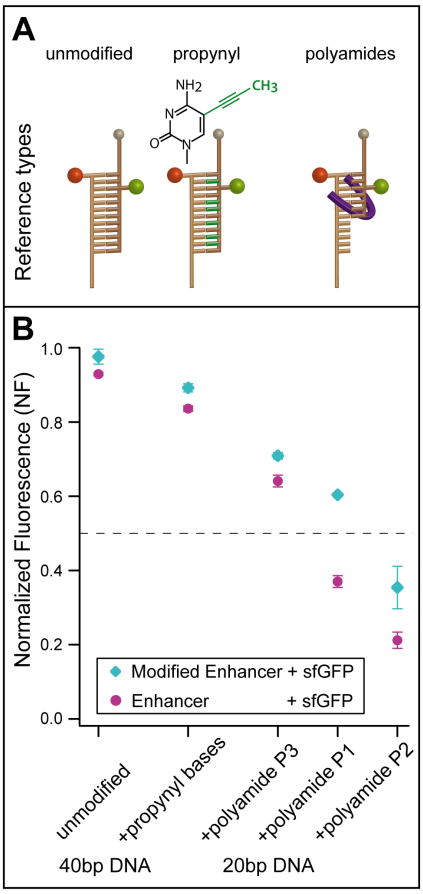

Fig. 2. Utilization of Modified Reference DNA Duplexes to Adjust the Sensitivity Window in a Multiplexed Protein-MFA. (A) Three different reference types are compared: unmodified DNA (left), intrinsically stabilized DNA (center), where a part of the pyrimidine bases is replaced by corresponding propynyl bases, as well as extrinsically stabilized DNA (right), where the addition of a specific polyamide ligand [23] enhances the binding strength. (B) Representative sample measurements of Enhancer and Modified Enhancer binding to sfGFP for all types of references are displayed. The NF shows a clear dependence on the reference strength. The NF is higher for the Modified Enhancer than Enhancer in all cases. Additionally, the difference in NF between Modified Enhancer and Enhancer increases the closer the NFs are to 0.5, displaying the higher sensitivity in this range.

doi:10.1371/journal.pone.0115049.g002

intrinsically stabilized DNA using propynyl bases, and extrinsically stabilized DNA through the binding of sequence-specific polyamide ligands. Representative data

for the different references testing Enhancer and Modified Enhancer against sfGFP are depicted in Fig. 2B with standard deviation. The original values can be found in S2 Table. Small differences in the size of the error bars can be attributed to measurement error. For all three types of reference, the outcome of the experiment – namely the relative higher NF values for the Modified Enhancer in comparison to Enhancer – stays the same, but the absolute NF values change depending on the reference. This was to be expected since the reference does not influence the nanobody-GFP complex itself so that the relative ranking of the stability of the complexes stays preserved. Whereas the incorporation of propynyl bases into a 40 bp DNA duplex reduces the NF values about 10%, employing a 20 bp DNA reference with added polyamide ligand leads to larger drops in NF depending on the polyamide. Notably, the closer the mean of the NF values for one reference is to 0.5, the larger the difference between the data points for Enhancer and Modified Enhancer becomes. This is consistent with the higher sensitivity of a well-balanced MFP.

The stronger binding of the Modified Enhancer can be attributed to its more positive charge (pI ≈9.89) when compared to the original Enhancer (pI ≈7.85), as sfGFP is slightly negatively charged (pI ≈6.4) under the given buffer conditions (pH 7.4). This ranking holds also true for the other GFP variants wtGFP (pI =6.17) and eGFP (pI =6.04), as can be seen in S1 Table. The incorporation of propynyl bases into the 40 bp DNA duplex obviously tunes the molecular balance closer to neutral, but with NF values of approximately 0.8 the result is still not entirely satisfying. Not much is known at present about the molecular mechanisms of the stabilization of the DNA duplex by the propynyl bases. The apolar methyl group is assumed to be buried in the core of the DNA double strand and by means of this contributes to the hybridization energy *via* hydrophobic interaction. Since the increase in stability of the reference depends on number and position of included propynyl bases [62], they represent a versatile tool for fine-tuning the reference bond. Whether this modification of the local interactions results in a change of the potential width or only deepens the potential well is not known yet and will be in the focus of future AFM-based single-molecule force spectroscopy studies.

In comparison to the intrinsic stabilization by propynyl bases, the addition of a polyamide has a much stronger impact on the NF, depending on the chosen polyamide. As expected, the lower the K_D, the higher the stabilization of the DNA reference and thus the lower the NF. While P3 already has a bigger effect on the NF than the incorporation of propynyl-bases, P1 tunes the MFA closest to neutral. In fact the addition of the polyamide P2 tunes the balance towards the other side resulting in an NF between 0.2 and 0.4. This enables to probe even stronger protein bonds than that of nanobody-GFP complexes. The polyamides used for the given study are known to bind into the minor groove of the DNA, thereby enhancing its mechanical stability, as has been found also for other DNA binding molecules [63, 64]. As shown in Ho *et al.* [23], such polyamides can be designed to modulate the stability of a DNA helix in a wide range. Following this principle,

other DNA binding molecules might be candidates to change the DNA reference stability extrinsically as well.

Summarizing, DNA offers the possibility to introduce a very broad range of references with different mechanical and thermal stability, ranging from low forces of about 15 pN with DNA in zipper mode over shear mode DNA in various lengths to enhanced stability *via* intrinsic or extrinsic modification of the DNA. The dynamic range of the mechanical stability of DNA-based references can be extended even further towards higher stabilities by the use of DNA binding proteins such as EcoRI and p53 [27]. Protein-MFA is thus applicable for many different protein pairs of varying bond strength.

Investigation of the Enhancer-GFP System with Protein-MFA

Fig. 3A depicts the result of one representative example measurement, where the binding between the nanobody Enhancer and the three different variants of GFP, namely enhanced GFP, wild type GFP, and superfolder GFP are compared. As shown in the ribbon model structure for wild type GFP [30], all GFP constructs are attached at their N-termini to the DNA reference while Enhancer is coupled to the glass slide *via* its C-terminus. For this measurement, the 20 bp DNA stabilized with polyamide P1 was used as a reference. P1 was chosen as its use could tune the NF in the measurement shown in Fig. 2B closest to neutral. All data points are derived from one contact process with a single stamp ensuring exactly the same conditions and thus minimizing measurement error. As the reference DNA is the same for all protein pairs, comparing the resulting NF values provides information about the differences in the binding strengths of the protein-protein interactions. Displaying the bulk readout of the extensive number of parallelized single-molecule measurements, sample histograms of protein spots with MFPs of all three GFPs are shown in Fig. 3B. In order to evaluate the outcome of the MFA experiment, the Normalized Fluorescence NF is calculated by dividing the fluorescence images according to equation 1. The most-likely NF is then determined by Gaussian fitting of the resulting count histogram.

While the NF values for the Enhancer-eGFP (0.255 ± 0.023) and Enhancer-wtGFP (0.253 ± 0.018) interaction are the same within experimental error, they both lie distinctively lower than the value for the Enhancer-sfGFP (0.353 ± 0.018) construct. This corresponds to a higher ratio of resulting intact Enhancer-sfGFP complexes than Enhancer-eGFP or wtGFP complexes after force application, implying that for this specific pulling geometry the Enhancer-sfGFP interaction is stronger.

From the crystal structure of wtGFP binding Enhancer (PDB 3K1K), Kirchhofer *et al.* [30] determined 9 amino acids that form 13 direct contacts and 3 amino acids forming hydrophobic interactions. The alignment of the amino acid sequences of all three GFP variants (see S3 Fig.) shows that all interacting amino acids of wtGFP are conserved for eGFP, which is in good agreement with the similar binding strength observed in Fig. 3A. The difference in binding strength of sfGFP to Enhancer could result from the mutation of two of the amino acids

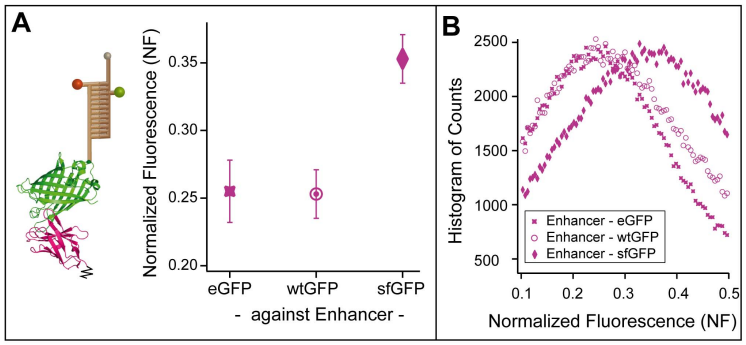

Fig. 3. Analysis of Different GFP Variants for Enhancer Interaction Strength with Protein-MFA. (A) Schematic depiction of the MFP for the measurement of the interaction between GFP and Enhancer with the ribbon model structure of wtGFP (green) with Enhancer (magenta) (crystal structure from [30], PDB file 3K1K). One example measurement depicts the differences in binding strength of Enhancer tested against enhanced, wild type, and superfolder GFP with the same reference DNA (20 bp DNA stabilized with polyamide P1). While the binding to eGFP and wtGFP lie within the same range, binding of Enhancer to sfGFP is distinctively stronger. All data points are determined in one single measurement process, derived as the mean of several protein spots and displayed with standard deviation error bars. (B) Sample histograms of MFP spots of Enhancer measured against all three GFP variants illustrate the extensive number of parallelized single-molecule experiments. The Normalized Fluorescence (NF) is determined by dividing the raw fluorescence images before and after transfer pixel-by-pixel (according to Equation 1), and fitting of a Gaussian to the resulting histogram of all pixel counts.

doi:10.1371/journal.pone.0115049.g003

which form direct contacts to Enhancer and all three amino acids responsible for the hydrophobic interaction. Notably, in force spectroscopy experiments the pulling geometry may have a significant impact on the unbinding force [40].

Conclusion

With the proof-of-principle system of nanobodies binding to GFPs, we successfully demonstrated the implementation of the Molecular Force Assay in parallelized measurements of protein-protein interactions. The reference strength of the DNA duplex can be adjusted as required both intrinsically through modification of the bases or extrinsically by binding of a ligand to ensure high sensitivity of the assay for the investigated interaction. In addition, the assay has a multiplexing capacity for different protein pairs and provides the high sensitivity and versatility of a fluorescence readout. With a moderate experimental effort, high statistics can be achieved in a single experiment with easy and very fast analysis. The parallel format of the assay also offers the advantage of testing the proteins only once, allowing the measurement of proteins that lose their original conformation upon application of force. With the current set-up, protein interactions that dissociate in the time span of the experiment can not be investigated. A solution would be an alternative set-up of the MFA such as presented in [65], where the upper part of the MFP is attached to the stamp. Also, at the moment only a limited number of protein-pairs can be tested simultaneously and to obtain absolute values the binding strength of the reference has to be known. Additional miniaturization and parallelization will further

emphasize the main advantage of the Protein-MFA, namely the high sensitivity due to the comparative approach of the assay. It has already been shown [27], that the results for DNA-MFA do not change when the diameter of the MFP spot is reduced from 1 mm in our current standard set-up to approximately 20 μm. In Otten *et al.* [26] the MFA system was integrated into a microfluidic chip, enabling the measurement of 640 spots of MFPs simultaneously. The next goal will be to combine the parallelization and miniaturization with the expression and direct covalent attachment of the lower protein in a microfluidic chip, as demonstrated recently [21], to turn the Protein-MFA into a high-throughput method. Such a set-up would allow the additional measurement of standardized protein pairs with known rupture force in the same stamping process, which could provide a very robust way to gain even more accurate information about the absolute values of the rupture forces. Creating a "toolbox" of references will render the Protein-MFA applicable to measure an extensive number of protein pairs and a fast way to determine and compare binding strengths.

Supporting Information

S1 Fig. Coupling of CoA-DNA to ybbR-tagged GFP. SDS-PAGE gel displaying the coupling between CoenzymeA-modified DNA to the ybbR-sfGFP construct in both fluorescence scans and Coomassie staining. In this sample gel, both GFP and CoA-DNA were mixed in equal concentrations (5 μM) as in the standard protocol [42].
doi:10.1371/journal.pone.0115049.s001 (PDF)

S2 Fig. DNA References. The reference DNA duplexes are displayed. The strand containing the CoenzymeA and Cy5 modification stays the same for all three types of reference, whereas the complementary strand modified with Cy3 and Biotin varies in length and constitution of bases. Chemical structures of the propynyl bases replacing their corresponding cytidine and thymidine bases are shown (structures provided by biomers.net GmbH, Germany). The polyamide ligands *P1*, *(R)-P2* and *(R)-P3* from [23] bind to the highlighted six base pair long binding sequence in the DNA reference duplex.
doi:10.1371/journal.pone.0115049.s002 (PDF)

S3 Fig. Sequence Alignment of the GFP Variants. The sequence alignment of all three variants of GFP displays the differences in the amino acid sequences and highlights the positions of the direct contacts (pink) and hydrophobic interactions (pale pink) to the nanobody Enhancer obtained for wtGFP by [30]. For eGFP, none of the interacting amino acids are mutated, but for sfGFP two of the contacts sites for Enhancer are different. In addition, all three amino acids forming the hydrophobic interaction are mutated. Sequence Alignment of GFPs was performed using Clustal W2 (http://www.ebi.ac.uk/Tools/msa/clustalw2/).
doi:10.1371/journal.pone.0115049.s003 (PDF)

S1 Supplement. Materials and Methods.

doi:10.1371/journal.pone.0115049.s004 (PDF)

S1 Table. Reproducibility of Data. NF values are best comparable when obtained in a single stamping process, but nonetheless the absolute NF values are reproducible over independent exeriments. Here, mean NF values averaged over several measurements are displayed with their corresponding standard deviation. In measurements against an unmodified 40 bp duplex the nanobody-GFP interaction is much stronger in comparison resulting in very high NF values around 0.9.
doi:10.1371/journal.pone.0115049.s005 (DOCX)

S2 Table. Original NF Data for the Figs. 2 and 3. The orignal Normalized Fluorescence (NF) data with the corresponding standard deviation (SD) are given. For the data of Fig. 2, the difference between the respective NF values for Modified Enhancer and Enhancer is displayed, which increases the closer the NF values are to 0.5. The maximal deviation is calculated as the addition of the absolute values of the corresponding standard deviations.
doi:10.1371/journal.pone.0115049.s006 (DOCX)

Acknowledgments

The authors are grateful to Prof. Peter Dervan for providing the pyrrole-imidazole hairpin polyamides. We would like to thank Dr. Chistopher Deck of biomers.net (Ulm, Germany) for excellent technical advice on and custom-synthesis of DNA modified with propynyl bases and CoA. We would further like to thank Prof. Jan Lipfert, Dr. Marcus Otten and Dr. Philip Severin for helpful discussions.

Author Contributions

Conceived and designed the experiments: DA DAP KK KL HL HEG. Performed the experiments: DA. Analyzed the data: DA. Contributed reagents/materials/analysis tools: DA DAP KK KL. Wrote the paper: DA DAP KK KL HEG.

References

1. **Werther M, Seitz H, editors (2008)** Protein - Protein Interaction. Springer-Verlag Berlin Heidelberg.
2. **Stumpf MPH, Thorne T, de Silva E, Stewart R, An HJ, et al.** (2008) Estimating the size of the human interactome. Proc Natl Acad Sci USA. pp.6959–6964.
3. **Uetz P, Giot L, Cagney G, Mansfield T, Judson R, et al.** (2000) A comprehensive analysis of protein–protein interactions in Saccharomyces cerevisiae. Nature.
4. **Zhu H, Bilgin M, Snyder M** (2003) Proteomics. Annual review of biochemistry. pp.783–812.
5. **Gerber D, Maerkl SJ, Quake SR** (2009) An in vitro microfluidic approach to generating protein-interaction networks. Nat Methods. pp.71–74.
6. **Shoemaker BA, Panchenko AR** (2007) Deciphering protein-protein interactions. Part I. Experimental techniques and databases. PLoS Comput Biol. pp. e42.
7. **Kornreich M, Avinery R, Beck R** (2013) Modern X-ray scattering studies of complex biological systems. Current Opinion in Biotechnology.

8. **Truong K, Ikura M** (2001) The use of FRET imaging microscopy to detect protein–protein interactions and protein conformational changes in vivo. Curr Opin Struct Biol.
9. **Karlsson R** (2004) SPR for molecular interaction analysis: a review of emerging application areas. Journal of Molecular Recognition.
10. **Kong F, García AJ, Mould AP, Humphries MJ, Zhu C** (2009) Demonstration of catch bonds between an integrin and its ligand. The Journal of Cell Biology. pp.1275–1284.
11. **Manibog K, Li H, Rakshit S, Sivasankar S** (2014) Resolving the molecular mechanism of cadherin catch bond formation. Nat Commun. pp.3941.
12. **Thomas W, Trintchina E, Forero M, Vogel V, Sokurenko E** (2002) Bacterial adhesion to target cells enhanced by shear force. Cell.
13. **Rakshit S, Sivasankar S** (2014) Biomechanics of cell adhesion: how force regulates the lifetime of adhesive bonds at the single molecule level. Phys Chem Chem Phys. pp.2211–2223.
14. **Langenhan T, Aust G, Hamann J** (2013) Sticky signaling—adhesion class G protein-coupled receptors take the stage. Science signaling.
15. **Binnig G, Quate C, Gerber C** (1986) Atomic force microscope. Physical review letters.
16. **Hinterdorfer P, Dufrêne Y** (2006) Detection and localization of single molecular recognition events using atomic force microscopy. Nature Methods.
17. **Moffitt J, Chemla Y, Smith S, Bustamante C** (2008) Recent advances in optical tweezers. Biochemistry.
18. **Moy VT, Florin EL, Gaub HE** (1994) Intermolecular forces and energies between ligands and receptors. Science. pp. 257–259.
19. **Leckband D** (2000) Measuring the forces that control protein interactions. Annu Rev Biophys Biomol Struct. pp. 1–26.
20. **Lin S, Chen J, Huang L, Lin H** (2005) Measurements of the forces in protein interactions with atomic force microscopy. Current Proteomics.
21. **Otten M, Ott W, Jobst M, Milles L, Verdorfer T, et al.** (2014) From genes to protein mechanics on a chip. Nature Methods.
22. **Albrecht C, Blank K, Lalic-Mülthaler M, Hirler S, Mai T, et al.** (2003) DNA: a programmable force sensor. Science. pp. 367–370.
23. **Ho D, Dose C, Albrecht CH, Severin P, Falter K, et al.** (2009) Quantitative detection of small molecule/DNA complexes employing a force-based and label-free DNA-microarray. Biophys J. pp. 4661–4671.
24. **Severin PMD, Ho D, Gaub HE** (2011) A high throughput molecular force assay for protein-DNA interactions. Lab Chip. pp. 856–862.
25. **Limmer K, Aschenbrenner D, Gaub H** (2013) Sequence-specific inhibition of Dicer measured with a force-based microarray for RNA ligands. Nucleic Acids Res.
26. **Otten M, Wolf P, Gaub HE** (2013) Protein-DNA force assay in a microfluidic format. Lab Chip. pp. 4198–4204.
27. **Severin PMD, Gaub HE** (2012) DNA-Protein Binding Force Chip. Small.
28. **Blank K, Lankenau A, Mai T, Schiffmann S, Gilbert I, et al.** (2004) Double-chip protein arrays: force-based multiplex sandwich immunoassays with increased specificity. Anal Bioanal Chem. pp. 974–981.
29. **Tsien R** (1998) The green fluorescent protein. Annual review of biochemistry.
30. **Kirchhofer A, Helma J, Schmidthals K, Frauer C, Cui S, et al.** (2010) Modulation of protein properties in living cells using nanobodies. Nat Struct Mol Biol. pp. 133–138.
31. **Pédelacq J-D, Cabantous S, Tran T, Terwilliger TC, Waldo GS** (2006) Engineering and characterization of a superfolder green fluorescent protein. Nat Biotechnol. pp. 79–88.
32. **Heim R, Cubitt A, Tsien R** (1995) Improved green fluorescence. Nature.
33. **Rothbauer U, Zolghadr K, Muyldermans S, Schepers A, Cardoso MC, et al.** (2008) A versatile nanotrap for biochemical and functional studies with fluorescent fusion proteins. Mol Cell Proteomics. pp. 282–289.

34. **Tang JCY, Szikra T, Kozorovitskiy Y, Teixiera M, Sabatini BL, et al.** (2013) A nanobody-based system using fluorescent proteins as scaffolds for cell-specific gene manipulation. Cell. pp. 928–939.

35. **Wiegand G, Neumaier KR, Sackmann E** (1998) Microinterferometry: Three-Dimensional Reconstruction of Surface Microtopography for Thin-Film and Wetting Studies by Reflection Interference Contrast Microscopy (RICM). Appl Opt. pp. 6892–6905.

36. **Albrecht CH, Neuert G, Lugmaier RA, Gaub HE** (2008) Molecular force balance measurements reveal that double-stranded DNA unbinds under force in rate-dependent pathways. Biophys J. pp. 4766–4774.

37. **Ho D, Falter K, Severin P, Gaub HE** (2009) DNA as a force sensor in an aptamer-based biochip for adenosine. Anal Chem. pp.3159–3164.

38. **Stephanopoulos N, Francis MB** (2011) Choosing an effective protein bioconjugation strategy. Nat Chem Biol. pp. 876–884.

39. **Jongsma MA, Litjens RHGM** (2006) Self-assembling protein arrays on DNA chips by auto-labeling fusion proteins with a single DNA address. Proteomics. pp. 2650–2655.

40. **Dietz H, Rief M** (2006) Protein structure by mechanical triangulation. Proc Natl Acad Sci USA. pp. 1244–1247.

41. **Yin J, Straight PD, McLoughlin SM, Zhou Z, Lin AJ, et al.** (2005) Genetically encoded short peptide tag for versatile protein labeling by Sfp phosphopantetheinyl transferase. Proc Natl Acad Sci USA. pp. 15815–15820.

42. **Yin J, Lin AJ, Golan DE, Walsh CT** (2006) Site-specific protein labeling by Sfp phosphopantetheinyl transferase. Nat Protoc. pp. 280–285.

43. **Quadri LE, Weinreb PH, Lei M, Nakano MM, Zuber P, et al.** (1998) Characterization of Sfp, a Bacillus subtilis phosphopantetheinyl transferase for peptidyl carrier protein domains in peptide synthetases. Biochemistry. pp. 1585–1595.

44. **Pippig DA, Baumann F, Strackharn M, Aschenbrenner D, Gaub HE** (2014) Protein-DNA Chimeras for Nano Assembly. ACS Nano.

45. **Maillard RA, Chistol G, Sen M, Righini M, Tan J, et al.** (2011) ClpX(P) generates mechanical force to unfold and translocate its protein substrates. Cell. pp. 459–469.

46. **Limmer K, Pippig DA, Aschenbrenner D, Gaub HE** (2014) A Force-Based, Parallel Assay for the Quantification of Protein-DNA Interactions. PLoS ONE. pp. e89626.

47. **Zimmermann JL, Nicolaus T, Neuert G, Blank K** (2010) Thiol-based, site-specific and covalent immobilization of biomolecules for single-molecule experiments. Nat Protoc. pp. 975–985.

48. **Krautbauer R, Rief M, Gaub H** (2003) Unzipping DNA oligomers. Nano Letters. pp. 493–496.

49. **Morfill J, Kühner F, Blank K, Lugmaier RA, Sedlmair J, et al.** (2007) B-S transition in short oligonucleotides. Biophys J. pp. 2400–2409.

50. **Rief M, Clausen-Schaumann H, Gaub HE** (1999) Sequence-dependent mechanics of single DNA molecules. Nat Struct Biol. pp. 346–349.

51. **Strunz T, Oroszlan K, Schäfer R, Güntherodt H** (1999) Dynamic force spectroscopy of single DNA molecules. Proc Natl Acad Sci USA.

52. **Severin P, Zou X, Gaub H, Schulten K** (2011) Cytosine methylation alters DNA mechanical properties. Nucleic acids Res.

53. **Lefebvre A, Mauffret O, el Antri S, Monnot M, Lescot E, et al.** (1995) Sequence dependent effects of CpG cytosine methylation. Eur J Biochem.

54. **Wagner RW, Matteucci MD, Lewis JG, Gutierrez AJ, Moulds C, et al.** (1993) Antisense gene inhibition by oligonucleotides containing C-5 propyne pyrimidines. Science. pp. 1510–1513.

55. **Froehler B, Wadwani S, Terhorst T, Gerrard S** (1992) Oligodeoxynucleotides containing C-5 propyne analogs of 2′-deoxyuridine and 2′-deoxycytidine. Tetrahedron letters. pp. 5307–5310.

56. **Shen L, Siwkowski A, Wancewicz EV, Lesnik E, Butler M, et al.** (2003) Evaluation of C-5 propynyl pyrimidine-containing oligonucleotides in vitro and in vivo. Antisense and nucelic acid drug development.

57. **Terrazas M, Kool E** (2009) RNA major groove modifications improve siRNA stability and biological activity. Nucleic acids research. pp. 346–353.

58. **Znosko B, Barnes T, Krugh T, Turner D** (2003) NMR Studies of DNA Single Strands and DNA: RNA Hybrids with and without 1-Propynylation at C5 of Oligopyrimidines. Journal of the American Chemical Society. pp. 6090–6097.

59. **Dose C** (2007) Recognition of Mirror-Image DNA by Small Molecules. intersciencewileycom.

60. **Dervan P, Edelson B** (2003) Recognition of the DNA minor groove by pyrrole-imidazole polyamides. Curr Opin Struct Biol.

61. **Dervan P, Poulin-Kerstien A, Fechter E, Edelson B** (2005) Regulation of gene expression by synthetic DNA-binding ligands. Top Curr Chem.

62. **Barnes T, Turner D** (2001) Long-range cooperativity in molecular recognition of RNA by oligodeoxynucleotides with multiple C5-(1-propynyl) pyrimidines. Journal of the American Chemical Society. pp. 4107–4118.

63. **Koch S, Shundrovsky A, Jantzen B, Wang M** (2002) Probing protein-DNA interactions by unzipping a single DNA double helix. Biophys J.

64. **Krautbauer R, Fischerländer S, Allen S, Gaub H** (2002) Mechanical fingerprints of DNA drug complexes. Single Mol.

65. **Wienken U, Gaub H** (2013) Stamping Vital Cells—a Force-Based Ligand Receptor Assay. Biophys J.

Supplement S1. Materials and Methods.

Preparation of Proteins

Preparation of Nanobodies Enhancer and Modified Enhancer

Both nanobody constructs were cloned into a pHEN6 vector and harbor a pelB leader sequence for periplasmic export and a C-terminal Hexa-His-Tag for purification, followed by a terminal Cysteine for covalent, site directed coupling of the protein. For expression, a 5l E. coli JM109 culture was induced with 0.5mM isopropyl β-D-1-thiogalactopyranoside and incubated for 5 hours at 30°C. Cells were lysed by sonification in buffer containing 1xPBS pH 8.0, 0.5M NaCl, 20mM imidazole, 1mM PMSF and 10 g/l lysozyme. After centrifugation, the nanobody constructs in the soluble fraction were purified by immobilized metal affinity chromatography (IMAC) on prepacked 1ml HisTrap HP columns with an Äkta Explorer HPLC system (GE Healthcare, Freiburg, Germany) according to manufacturer's instructions. The elution fractions were analyzed by SDS-PAGE. Purified nanobody fractions were pooled and dialysed overnight into 1xPBS, flash-frozen and stored at -80°C at concentrations of 21µM (Modified Enhancer) and 35µM (Enhancer).

Nanobody Sequences

- Construct of Enhancer (PDB 3K1K) as in [1] with an additional C-terminal Cysteine:

QVQLVESGGALVQPGGSLRLSCAASGFPVNRYSMRWYRQAPGKEREWVAGMSSAGDRSSYEDSV
KGRFTISRDDARNTVYLQMNSLKPEDTAVYYCNVNVGFEYWGQGTQVTVSSHHHHHHC

- The construct of Modified Enhancer harbors an additional N-terminal, very positively charged, 12 amino acid long tag and a C-terminal Cysteine:

GRKKRRQRRRGSQVQLVESGGALVQPGGSLRLSCAASGFPVNRYSMRWYRQAPGKEREWVAGM
SSAGDRSSYEDSVKGRFTISRDDARNTVYLQMNSLKPEDTAVYYCNVNVGFEYWGQGTQVTVSSHH
HHHHC

Preparation of GFPs

All GFP constructs were designed to harbor an N-terminal Hexa-His-Tag for purification, followed by the ybbR-tag (DSLEFIASKLA) [2,3] and the respective GFP type (wtGFP, eGFP and sfGFP; for the sequences see the alignment in Figure S3). All fusion proteins were cloned into pET28a vectors (EMD Group, Merck KGaA, Darmstadt, Germany) and were expressed in *E.coli* BL21 DE3 CodonPlus cells (Agilent Technologies, Inc., Santa Clara, CA, USA). For this, 0.5l of SB medium was inoculated with 5ml of an over night culture and grown at 37°C until an OD_{600} of around 0.7 had been reached. Then, over night expression at 18°C was induced by the addition of 0.25mM IPTG. Cells were lysed by sonification in 50mM Tris pH 7.5, 100mM NaCl, 5% Glycerin, 15mM Imidazole and 10mM β-Mercaptoethanol. After centrifugation the ybbR-GFP constructs in the soluble fraction were purified by immobilized metal affinity chromatography (IMAC) on prepacked 1ml HisTrap HP columns with an Äkta Explorer HPLC system (GE Healthcare, Freiburg, Germany) according to manufacturer's instructions. The elution fractions were analyzed by SDS-PAGE and pooled accordingly. The pooled protein samples were then dialyzed into storage buffer (30mM Tris pH 7,5, 100mM NaCl, 5% Glycerin, 2mM DTT) over night, and stored at -80°C at final concentrations of 50µM for sfGFP, 550µM for eGFP and 200µM for wtGFP.

Protein-DNA coupling

In general, the Phosphopantetheinyl Transferase (Sfp)-mediated coupling of CoenzymeA modified DNA to ybbR-tagged proteins offers a very high yield. A standard protocol for the coupling reaction can be found in [2]. The fraction of reacted GFP or DNA can be tuned by adjusting the respective concentrations. In the experiments conducted here, a high fraction of reacted GFP was desired, so that most GFPs binding to the nanobodies carry a DNA reference and thus form a fully functional Molecular Force Probe. In a slightly altered coupling reaction, first the DNA duplex was hybridized by mixing the CoA strand in a ratio of 1:2 with the biotinylated strand (to again ensure that the CoA strands form a duplex). This pre-incubated mix containing 10µM CoA-DNA was then combined with 5µM of the corresponding GFP sample and 6,65µM Sfp in a final 10µl Ansatz in Sfp buffer (150mM NaCl, 1mM DTT, 10mM MgCl and 50mM Tris) and used after incubation at room temperature for at least 1 hour.

The DNA oligonucleotides were purchased, including all modifications, from biomers.net GmbH, Germany.

Chemical Procedures

Assembly of Protein-MFPs

Microscopy glass slides were aminosilanized in our lab (for a detailed protocol, see eg. [4]) and deprotonated in sodium borate buffer (50mM H_3BO_3, 50mM $Na_2B_4O_7$•10 H_2O pH=8.5) for 45 minutes. For functionalization, 50mM NHS-PEG-Maleimide crosslinker (MW 5000; Rapp-Polymere, Germany) in sodium borate buffer was incubated for 1 hour. After careful drying of the slide with N_2 gas, a custom-made silicone isolator with 16-wells in a 4x4 array (Grace-Biolabs, USA) was placed on the glass slide. To obtain free Cysteines at the C- termini of the nanobodies, possible intermolecular disulfide bonds were reduced with TCEP

beads (Immobilized TCEP Disulfide Reducing Gel, Thermo Fisher Scientific inc., Rockford, IL, USA) for 30 min. After removal of the beads, samples were spun down in a table top centrifuge for 15 min to remove agglomerates. The supernatant with the respective nanobody was pipetted in the wells of the isolator and incubated for 1 hour. The wells were then rinsed thoroughly with 1xPBS and the respective GFP-DNA constructs (for preparation see: Protein-DNA coupling) were spotted into the wells for incubation of 1 hour. To remove unbound free DNA and Protein-DNA constructs, the slide was rinsed in washing steps with 2x, 0.2x and finally 1xPBS, which acts as buffer for the measurement. Care was taken to ensure aqueous buffer environment for the samples at all time during the preparation process. In measurements with polyamide, 1µM of ligand was added to the measurement buffer and left to incubate for 2 hours before measurement. In general, all samples were measured within 3 hours after sample preparation.

Note, that the temporal and spatial delimitation of the probe assembly would also allow for surface immobilization *via* a ybbR-tag, if thiol-chemistry were unfavorable. In this case, a purification of the DNA-protein complexes is necessary to remove the Sfp.

Stamp preparation

Fabrication and functionalization of the PDMS (polydimethylsiloxane) stamp has been described in detail elsewhere (*e.g.* in [5,6]). In brief, 1:10 of crosslinker/base (Sylgard, Dow Corning, MI, USA) was cast in a custom-made micro- and macrostructured Pyrex/silicon wafer (HSG-IMIT, Germany) according to standard procedures. They were then cut into an arrangement of 4x4 pillars, so that the final stamps feature 16 pillars of 1mm in height and 1.1mm in diameter on a 3mm thick basis. The top

of the pillars is microstuctured with pads of 100µm x 100xµm separated by trenches (41 µm in width, 5 µm in depth) to ensure liquid drainage during the contact and separation process.

For the functionalization, the stamps were activated in 12.5% hydrochloric acid over night and derivatized with (3- glycidoxypropyl)-trimethoxysilane (ABCR, Karlsruhe, Germany) for the generation of epoxide groups. A 1:1 mix of NH_2-PEG-Biotin (MW 3400) and NH_2-PEG-CH_3 (MW 2000) (Rapp-Polymere, Germany) was melted at 80°C, about 1µl was spotted to each pillar and incubated over night at 80°C under argon. The excess polymers were thoroughly removed by rinsing with ddH_20. For final functionalization, the stamps were incubated for 60 min with 1xPBS containing 0.4% (w/v) BSA and 1 mg/ml Streptavidin (Thermo Fisher Scientific, Bonn, Germany), rinsed with 0.05% Tween 20 (VWR Scientific GmbH, Germany) in 0.2xPBS and gently dried with N_2 gas.

Measurement and Analysis

As the measurement process and the pixel-by-pixel analysis are identical to that of the original DNA-MFA, additional information to the explanations in the main text can be found in the corresponding publication of Severin *et.al.* [7].

References

1. Kirchhofer A, Helma J, Schmidthals K, Frauer C, Cui S, et al. (2010) Modulation of protein properties in living cells using nanobodies. Nat Struct Mol Biol. pp. 133-138.
2. Yin J, Lin AJ, Golan DE, Walsh CT (2006) Site-specific protein labeling by Sfp phosphopantetheinyl transferase. Nat Protoc. pp. 280-285.
3. Yin J, Straight PD, McLoughlin SM, Zhou Z, Lin AJ, et al. (2005) Genetically encoded short peptide tag for versatile protein labeling by Sfp phosphopantetheinyl transferase. Proc Natl Acad Sci USA. pp. 15815-15820.
4. Limmer K, Pippig DA, Aschenbrenner D, Gaub HE (2014) A Force-Based, Parallel Assay for the Quantification of Protein-DNA Interactions. PLoS ONE. pp. e89626.
5. Limmer K, Aschenbrenner D, Gaub H (2013) Sequence-specific inhibition of Dicer measured with a force-based microarray for RNA ligands. Nucleic Acids Res.
6. Severin PMD, Gaub HE (2012) DNA-Protein Binding Force Chip. Small.
7. Severin PMD, Ho D, Gaub HE (2011) A high throughput molecular force assay for protein-DNA interactions. Lab Chip. pp. 856-862.

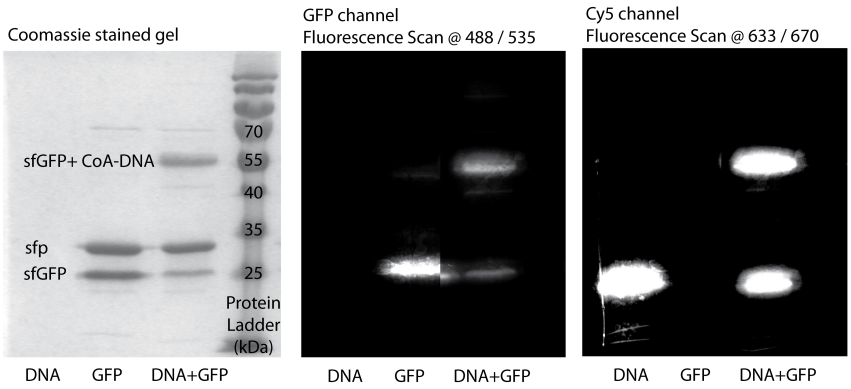

Figure S1. Coupling of CoA-DNA to ybbR-tagged GFP.

SDS-PAGE gel displaying the coupling between CoenzymeA-modified DNA to the ybbR-sfGFP construct in both fluorescence scans and Coomassie staining. In this sample gel, both GFP and CoA-DNA were mixed in equal concentrations (5μM) as in the standard protocol [1].

References

1. Yin J, Lin AJ, Golan DE, Walsh CT (2006) Site-specific protein labeling by Sfp phosphopantetheinyl transferase. Nat Protoc. pp. 280-285.

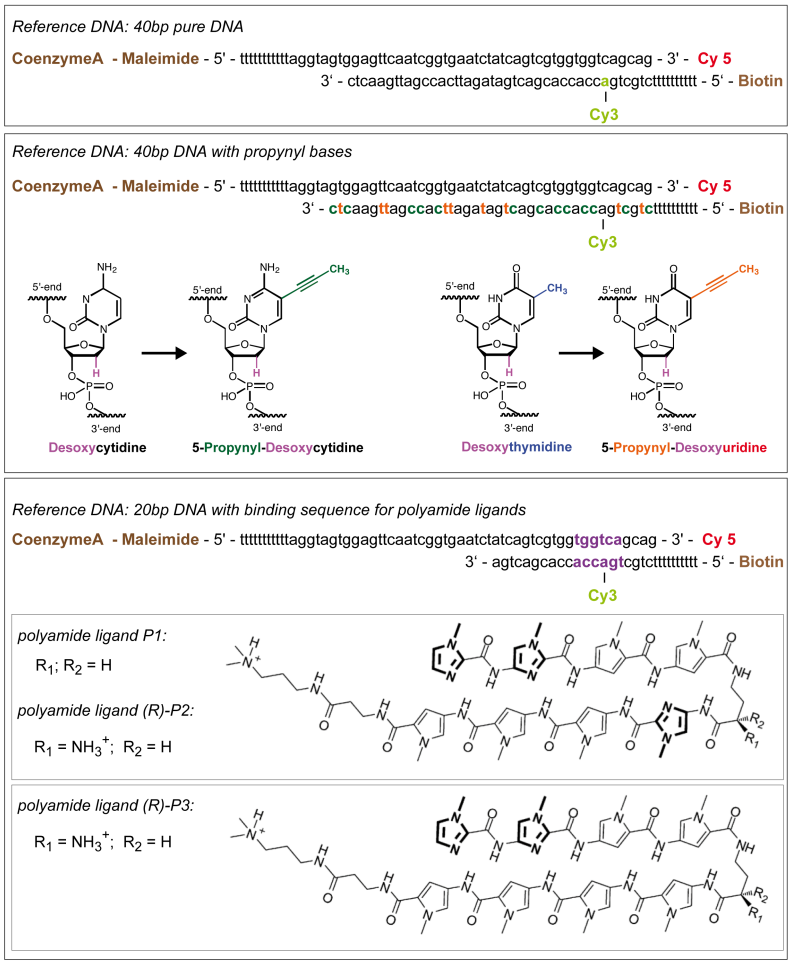

Figure S2. DNA References.

The reference DNA duplexes are displayed. The strand containing the CoenzymeA and Cy5 modification stays the same for all three types of reference, whereas the complementary strand modified with Cy3 and Biotin varies in length and constitution of bases. Chemical structures of the propynyl bases replacing their corresponding cytidine and thymidine bases are shown (structures provided by biomers.net GmbH, Germany). The polyamide ligands *P1*, *(R)-P2* and *(R)-P3* from [1] bind to the highlighted six base pair long binding sequence in the DNA reference duplex.

References

1. Ho D, Dose C, Albrecht CH, Severin P, Falter K, et al. (2009) Quantitative detection of small molecule/DNA complexes employing a force-based and label-free DNA-microarray. Biophys J. pp. 4661-4671.

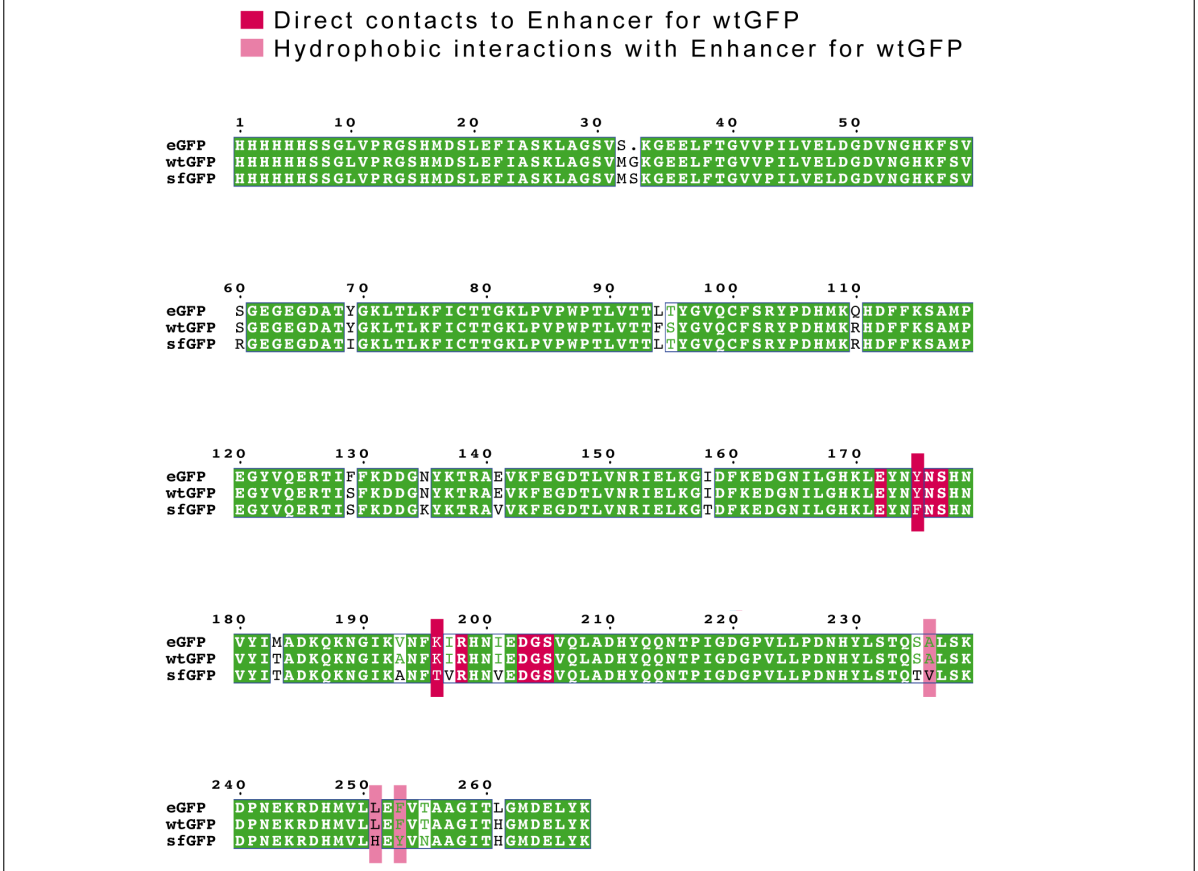

Figure S3. Sequence Alignment of the GFP Variants.

The sequence alignment of all three variants of GFP displays the differences in the amino acid sequences and highlights the positions of the direct contacts (pink) and hydrophobic interactions (pale pink) to the nanobody Enhancer obtained for wtGFP by [1]. For eGFP, none of the interacting amino acids are mutated, but for sfGFP two of the contacts sites for Enhancer are different. In addition, all three amino acids forming the hydrophobic interaction are mutated. Sequence Alignment of GFPs was performed using Clustal W2 (http://www.ebi.ac.uk/Tools/msa/clustalw2/).

References

1. Kirchhofer A, Helma J, Schmidthals K, Frauer C, Cui S, et al. (2010) Modulation of protein properties in living cells using nanobodies. Nat Struct Mol Biol. pp. 133-138.

Protein Pair	Reference DNA	Averaged NF-Values	Standard deviation of the means	Number of Measurements
Enhancer – sfGFP	40 bp	0.928	0.023	9
Modified Enhancer – sfGFP	40 bp	0.944	0.027	9
Enhancer - eGFP	40 bp	0.892	0.04	8
Modified Enhancer - eGFP	40 bp	0.905	0.05	8
Enhancer – sfGFP	40 bp + propynyl	0.854	0.025	2
Modified Enhancer – sfGFP	40 bp + propynyl	0.886	0.08	2
Enhancer - eGFP	40 bp + propynyl	0.863	0.001	2
Modified Enhancer - eGFP	40 bp + propynyl	0.881	0.031	2
Enhancer - wtGFP	40 bp + propynyl	0.892	0.012	2
Modified Enhancer - wtGFP	40 bp + propynyl	0.911	0.012	2
Enhancer – sfGFP	20 bp + polyamide P3	0.636	0.007	2
Modified Enhancer – sfGFP	20 bp + polyamide P3	0.732	0.032	2
Enhancer – eGFP	20 bp + polyamide P1	0.253	0.051	6
Enhancer – wtGFP	20 bp + polyamide P1	0.263	0.047	6
Enhancer – sfGFP	20 bp + polyamide P1	0.359	0.059	8
Modified Enhancer – sfGFP	20 bp + polyamide P1	0.602	0.004	2
Enhancer – sfGFP	20 bp + polyamide P2	0.217	0.008	3
Modified Enhancer – sfGFP	20 bp + polyamide P2	0.266	0.079	3

Table S1. Reproducibility of Data.

NF values are best comparable when obtained in a single stamping process, but nonetheless the absolute NF values are reproducible over independent exeriments. Here, mean NF values averaged over several measurements are displayed with their corresponding standard deviation.

In measurements against an unmodified 40bp duplex the nanobody-GFP interaction is much stronger in comparison resulting in very high NF values around 0.9.

Data for Figure 2

GFP variant	Reference	NF (Modified Enhancer)	SD (Modified Enhancer)	NF (Enhancer)	SD (Enhancer)	Difference of the NFs	Maximal Deviation
sf	40bp DNA unmodified	0.976	0.02	0.929	0.004	0.047	0.024
sf	40bp propynyl-DNA	0.892	0.011	0.836	0.007	0.056	0.018
sf	20bp DNA + polyamide P3	0.709	0.009	0.641	0.016	0.068	0.025
sf	20bp DNA + polyamide P1	0.604	0.005	0.37	0.016	0.234	0.021
sf	20bp DNA + polyamide P2	0.354	0.057	0.212	0.022	0.142	0.079

Data for Figure 3

GFP variant	Reference	NF (Enhancer)	SD (Enhancer)
e	20bp DNA + polyamide P1	0.255	0.023
wt	20bp DNA + polyamide P1	0.253	0.018
sf	20bp DNA + polyamide P1	0.353	0.018

Table S2. Original NF Data for the Figures 2 and 3.

The orignal Normalized Fluorescence (NF) data with the corresponding standard deviation (SD) are given. For the data of Figure 2, the difference between the respective NF values for Modified Enhancer and Enhancer is displayed, which increases the closer the NF values are to 0.5. The maximal deviation is calculated as the addition of the absolute values of the corresponding standard deviations.

A.4 Publication 4: A Force-Based, Parallel Assay for the Quantification of Protein-DNA Interactions

A Force-Based, Parallel Assay for the Quantification of Protein-DNA Interactions

by

Katja Limmer, Diana A. Pippig, Daniela Aschenbrenner and Hermann E. Gaub

published in

PLOS ONE, February 2014, 9(2): e89626

OPEN ACCESS Freely available online

PLOS ONE

A Force-Based, Parallel Assay for the Quantification of Protein-DNA Interactions

Katja Limmer[1,2], Diana A. Pippig[1], Daniela Aschenbrenner[1], Hermann E. Gaub[1]*

1 Lehrstuhl für Angewandte Physik and Center for Nanoscience (CeNS), Ludwig-Maximilians-University, Munich, Germany, **2** Munich Center for Integrated Protein Science (CIPSM), Munich, Germany

Abstract

Analysis of transcription factor binding to DNA sequences is of utmost importance to understand the intricate regulatory mechanisms that underlie gene expression. Several techniques exist that quantify DNA-protein affinity, but they are either very time-consuming or suffer from possible misinterpretation due to complicated algorithms or approximations like many high-throughput techniques. We present a more direct method to quantify DNA-protein interaction in a force-based assay. In contrast to single-molecule force spectroscopy, our technique, the Molecular Force Assay (MFA), parallelizes force measurements so that it can test one or multiple proteins against several DNA sequences in a single experiment. The interaction strength is quantified by comparison to the well-defined rupture stability of different DNA duplexes. As a proof-of-principle, we measured the interaction of the zinc finger construct Zif268/NRE against six different DNA constructs. We could show the specificity of our approach and quantify the strength of the protein-DNA interaction.

Citation: Limmer K, Pippig DA, Aschenbrenner D, Gaub HE (2014) A Force-Based, Parallel Assay for the Quantification of Protein-DNA Interactions. PLoS ONE 9(2): e89626. doi:10.1371/journal.pone.0089626

Editor: Fenfei Leng, Florida International University, United States of America

Received October 28, 2013; **Accepted** January 21, 2014; **Published** February 27, 2014

Funding: Funding provided by German Science Foundation SFB 1032-A01 and a European Research Council Advanced Grant. The funders had no role in study design, data collection and analysis, decision to publish, or preparation of the manuscript.

Competing Interests: The authors have declared that no competing interests exist.

* E-mail: Gaub@lmu.de

Introduction

The sequence-specific interaction of certain proteins with the genomic DNA is prerequisite for the complex task of transcriptional regulation. Those transcription factors bind alone or in clusters to the DNA and can thus activate or impede transcription. Many of the transcription factors can bind to several, different DNA sequence motifs with varying strength [1]. Recent studies suggest that not only strong interactions between transcription factors and the DNA influence gene expression, but that weak interactions significantly contribute to transcriptional regulation and are evolutionary conserved [2]. Quantitative models support the importance of weak interactions and show that correct recapitulation of transcriptional processes is only possible by including low-affinity transcription factor binding sites in their calculations [3]. Hence, in order to get a comprehensive picture of transcriptional regulation, it is essential to quantify the interaction of a broad range of transcription factors with all possible DNA sequences.

Recent developments in high-throughput techniques, for example the *in vivo* method chromatin immunoprecipitation combined with microarray analysis (ChIP-chip) [4,5] or sequencing (ChIP-seq) [6] or *in vitro* techniques like protein binding microarrays (PBM) [7–10] have greatly increased our knowledge about various transcription factor binding sites. However, in most instances these techniques lack the ability to accurately quantify the protein-DNA interaction or require complicated algorithms and approximations to do so. Various methods exist to characterize the protein-DNA interactions by measuring thermodynamic and kinetic constants, for example electrophoretic mobility shift assay (EMSA) or surface plasmon resonance. Yet their common drawback is the low throughput that makes it nearly impossible to analyze a transcription factor against a whole genome. Two techniques have made huge advances in bridging the gap between measuring thermodynamic constants and high throughput, namely mechanically induced trapping of molecular interactions (MITOMI) [11] and high-throughput sequencing - fluorescent ligand interaction profiling (HiTS-FLIP) [12]. Both can determine dissociation constants of several transcription factors against thousands of DNA sequences (MITOMI) or of one protein against millions of DNA motifs (HiTS-FLIP), but require some approximations in order to calculate dissociation constants in a high-throughput format (MITOMI) or need a washing step that interferes with the analysis of transient interactions (HiTS-FLIP).

Importantly, due to the high concentration of DNA in a bacterial cell or eukaryotic nucleus, the dynamic equilibrium between unbound and bound activated transcription factors is shifted towards DNA-protein complexes. Hence, affinity described by the dissociation constant might not be the best measure to characterize the protein-DNA interaction inside a nucleus. The specificity defined as the ability of a transcription factor to discriminate between a regulatory sequence and the vast majority of non-regulating DNA might be a more suitable quantity. But quantification of the specificity in that sense means to determine the complete list of dissociation constants for all possible DNA sequences or a constant calculated from those dissociation constants [13]. Therefore, a method that determines the specificity in a single measurement is highly desirable considering the number of transcription factors and possible genomic sequences. Since the force required to break a bond increases with decreasing potential width, a more localized interaction between protein and

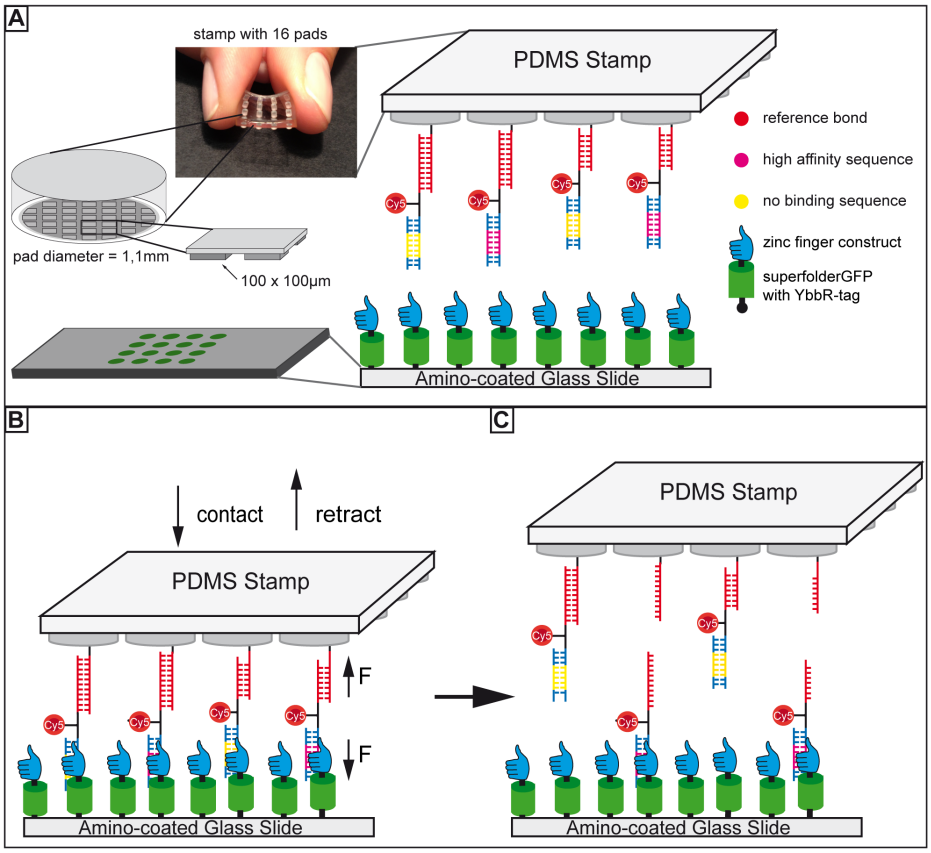

Figure 1. Description of the Molecular Force Assay (MFA). (A) The geometries of the PDMS stamp and the 4x4 pattern of protein spots on the glass slide are displayed. The zinc finger protein is covalently bound to an amino-coated glass slide functionalized with Coenzyme A via a ybbR-tag. A superfolderGFP acts as an additional spacer and helps to adjust the glass slide beneath the pads of the stamp. Different combinations of reference sequences and DNA binding motifs are attached to each pillar. (B) The PDMS stamp is carefully brought into contact with the glass slide and the DNA sample bonds are allowed to bind to the protein. Subsequently, the PDMS stamp is retracted with constant velocity so that a force builds up in the DNA-protein complexes and the reference bonds until the weaker construct ruptures. (C) After the force probe, the fluorescence signal on the glass slide is a measure for the number of intact protein-DNA bonds.
doi:10.1371/journal.pone.0089626.g001

DNA as it is expected for a sequence specific interaction will result in a higher unbinding force. Thus, a possibility for describing the specificity arises out of the binding strength between a protein and a DNA motif that is accessible in force-based measurements. Single-molecule force spectroscopy experiments allow the characterization of a protein-DNA bond in great detail [14–18] but are very time consuming and therefore not the appropriate tool to analyze the binding properties of a transcription factor against a whole genome.

The Molecular Force Assay (MFA) developed in our lab [19,20] parallelizes single-molecule force experiments. It relies on the principle of comparing the interaction in question with a well-defined reference bond. We here describe a new application of the MFA to quantify binding strengths of several DNA-protein complexes directly and in parallel. This should contribute to a more conclusive and complete understanding of transcriptional regulation. In an adaptation of the original setup, we demonstrate in a proof-of principle experiment that we are able to determine the binding strength of a zinc finger protein against several DNA sequences in a single measurement.

Zinc finger motifs are one of the most abundant DNA binding domains in eukaryotic transcription factors [21]. The protein in our experiment Zif268/NRE is an artificial fusion protein of two zinc fingers of the Cys_2-His_2 class [22]. Zif268 is a transcription factor in mouse and a popular model system due to the existence of structural data of the protein-DNA complex [21,23]. NRE is an

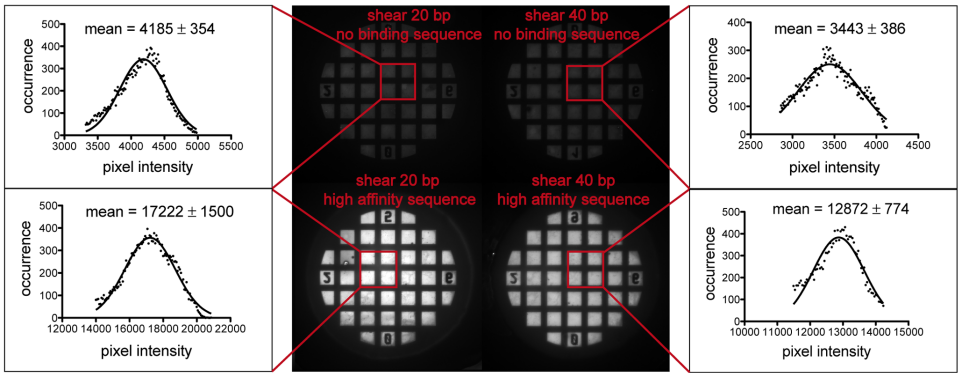

Figure 2. Transfer of Cy5-labeled DNA to the glass slide. After the contact and separation process, the fluorescence intensity of Cy5 on the glass slide is determined. Histograms of selected areas (without prior background subtraction) show a very modest signal slightly above the background signal (1000–2000 counts) for the DNA harboring the no binding sequences for the protein in question. DNA with a high affinity sequence did bind the protein in question and a transfer signal is clearly visible. The images are optimized in contrast to make the transfer of the no binding sequence as well as the difference in fluorescence signal between the no binding sequence and high affinity motif visible. A first assessment of the binding strength is possible by varying the reference bond. The weaker reference of 20 bp shows a higher fluorescence intensity of 17000 counts compared to the stronger reference of 40 bp with 13000 counts.
doi:10.1371/journal.pone.0089626.g002

engineered variant of Zif268 that binds specifically and with high affinity to a nuclear receptor element [24]. Our force-based design allows us to characterize the interaction of this six zinc finger protein with three DNA binding motifs, a high affinity sequence, a low affinity sequence and a no binding sequence, by a single value that can be directly correlated to the binding strength. Additionally, we show that we could gain further information about differences in the binding strength by varying the reference bond between a 20 base pair (bp) DNA sequence and a 40 bp DNA sequence. This demonstrates the possibility to convert the measured binding strength into intuitive units of DNA base pairs binding strength. Hence, this new variant of the MFA can quantify DNA-protein interaction and describe the binding strength in a simple picture by correlating it to the average binding strength of a certain number of DNA base pairs.

Results and Discussion

The standard Molecular Force Assay (MFA) consists of two molecular bonds in series, a reference and a sample bond, clamped between two surfaces. The two surfaces are separated with a constant velocity so that a force builds up in the two molecular bonds until the weaker one ruptures. A fluorophore conjugated to the linker sequence between the two molecular complexes indicates the intact molecular bond. Hence, the ratio of the fluorescence intensity before and after the force loading of the molecular constructs is a measure of the strength of the sample bond in comparison to the reference bond. An alternative view of this assay is that the force greatly enhances the off rate of the bond under investigation and reduces the otherwise extremely long spontaneous dissociation times towards seconds [25]. As every molecular complex is tested against its own reference bond, the measurement is a single-molecule experiment that can be conducted in parallel with several thousand constructs. If oligonucleotide sequences are used for sample and reference complex, different binding sequences for ligands can be introduced in the sample bond so that a strengthening of the sample bond can be detected upon binding. Thus, the dissociation constant for ligands like polyamides [26] or proteins [27] was determined and an ATP-aptamer [28] as well as the interaction of the protein Dicer with double-stranded RNA [29] was characterized. Additionally, the reference bond can be varied in length and thus in the binding strength the sample bond is compared to. Hence, it was possible in former studies to quantify the increase of the sample bond strength upon ligand binding to the stability of 9.5 base pairs for a polyamide and to 27.7 base pairs for the protein EcoRI [30]. In a subsequent experiment integrated in a microfluidic setup, the binding of EcoRI to two sample bonds with different affinity was tested against four different reference bonds in a single measurement and the stabilization of the sample bonds was quantified in units of DNA base pairs. [31].

In the configuration of the MFA used in all former studies, the ligand-DNA interaction is not directly probed, but the ligand stabilizes the molecular bond and is thus detected. We here describe our new variant of the MFA that can probe the protein-DNA interaction directly and compare it to a reference bond. For this purpose, the fusion protein construct consisting of an N-terminal ybbR-tag [32] followed by a superfolderGFP [33] variant and the six zinc finger construct ZIF268/NRE [22] (details can be found in Supplement S1) is covalently attached via the ybbR-tag to a glass slide coated with Coenzyme A in a 4x4 pattern [34]. The two double-stranded DNA complexes in series are covalently attached to the 16 pillars of a soft PDMS surface with the upper one as reference bond and the lower one as sample bond (see Figure 1A). The DNA sequences in shear geometry are separated by a linker sequence to which a Cy5 fluorophore is conjugated. Due to the macrostructure of the PDMS stamp (see Figure 1A) a maximum of 16 combinations of different reference sequences as well as sample sequences can be tested within one experiment (Figure 1A). The PDMS surface is carefully brought into contact with the glass slide so that the sample sequence is able to bind to the protein on the glass slide (Figure 1B). This process is controlled via reflection interference contrast microscopy [35]. The GFP

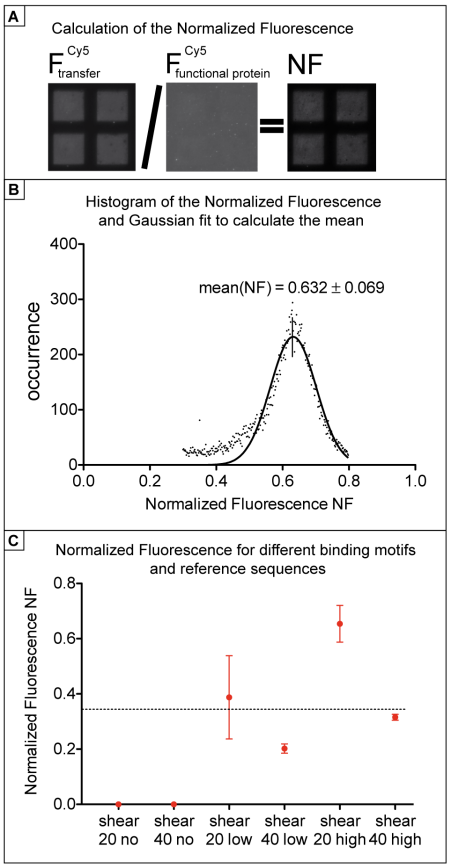

Figure 3. Quantification of the binding strength. (A) In order to quantify the binding strength, the fluorescence signal representing the DNA transfer has to be normalized to the number of available protein binding sites. For this purpose, a Cy5-labeled 40 bp DNA duplex harboring a high affinity binding motif is added subsequently to the force measurement in order to saturate all functional proteins. Following a washing protocol to remove all unbound DNA strands, the fluorescence intensity is measured a second time. After background subtraction, the fluorescence intensity of transferred DNA is divided by the signal corresponding to all functional proteins, yielding the Normalized Fluorescence NF. (B) Histograms of every pad on the PDMS stamp sum up the huge number of single-molecule experiments and are fitted by a Gaussian distribution in order to calculate an average NF and the standard deviation. Here, the histogram of the NF displayed in A is shown in detail. (C) One example measurement is displayed as a proof-of-principle. Details to the statistics are described in Supplement S1. The NF for the no binding sequences is too little to render fitting procedures possible. So we approximate the NF to be zero. Differences between low and high affinity binding motifs are very pronounced. A variation of the reference bond between 20 and 40 bp shear shows that the NF of the low affinity sequence against a 20 bp shear is about the same a the NF of the high affinity sequence against a 40 bp shear. This can be descriptively interpreted such that the difference in binding strength of the zinc finger protein with a low affinity sequence compared to a high affinity sequence corresponds to the stability of 20 bp DNA duplex.
doi:10.1371/journal.pone.0089626.g003

signal is used to place the protein spots below the stamp pillars functionalized with the different DNA sequences. After 10 minutes, the PDMS surface is retracted with constant velocity by a Piezo actuator. Thereby, a force is applied to the protein-sample complex as well as to the reference bond until the weaker one ruptures (Figure 1C). The fluorescence Cy5 signal on the glass slide is measured by an inverted epi-fluorescence microscope and indicates the number of intact protein-DNA complexes. Thus, the protein-DNA interaction is directly probed and compared to a well-characterized DNA double strand. In order to approximate the environment in a eukaryotic nucleus we designed our experiments as a competition assay and pre-incubated the zinc finger protein with low-molecular weight DNA from salmon sperm before the contact process. Details on the surface funtionalization, molecular constructs, contact and separation process as well as the fluorescence read-out are described in Supplement S1.

In a first test of our assay, we determined the binding of the zinc finger protein to a no binding sequence and a high affinity binding motif. The bond strength was compared to two reference sequences, a 20 bp double-stranded DNA and a 40 bp double-stranded DNA, both in shear geometry, by measuring the Cy5 fluorescence intensity of the transferred DNA after the contact and separation process. Figure 2 displays the results for all possible combinations of sample and reference bond. For the no binding sequence, only very little signal is measured. It hardly exceeds the background value of about 1000–2000 counts of pixel intensity so that false positives of unspecific interactions between the zinc finger protein with no binding sequences can be excluded in our assay. The high affinity sequence on the other hand clearly bound to the protein and the upper reference bond ruptured in most cases so that Cy5 labeled DNA was transferred to the glass slide. Additionally, a difference between the two reference bonds is evident. The weaker reference of 20 bp ruptured more often, yielding 17000 counts of transferred DNA on the slide. The stronger reference exceeds the binding strength of the protein-high affinity sequence interaction in more cases than the weaker reference, yielding distinctly less fluorescence signal of 13000 counts. These results of our first test confirm the specificity and feasibility of our approach for quantifying DNA-protein binding strength by means of the MFA and varying reference bonds.

In order to calculate a single, comparable number for the binding strength, environmental differences like the binding density of protein and oligonucleotide constructs on the surfaces have to be taken into account. In order to correct for differences in protein density on the glass slide, 0.5 μM of a Cy5 labeled 40 bp DNA duplex carrying a high affinity binding site for the protein in question is added subsequent to the force probe experiment to saturate all functional proteins bound to the surface. Calibration measurements confirmed a complete saturation after 30 min incubation time. After removing unbound fluorophores by a washing step, the fluorescence on the glass slide is determined again. It is a measure for the maximum number of functional proteins on the slide. Since the binding density of the DNA complexes on the PDMS always exceeds the number of functional proteins on the glass slide, further corrections are not necessary. The ratio of fluorescence signal on the glass slide directly after the rupture event $F_{transfer}$ to the maximal number of functional proteins $F_{intact\ protein}$ is defined as the Normalized Fluorescence, NF. The NF is calculated by dividing the pictures after background subtraction pixel-by-pixel (see Figure 3A), which cancels out inhomogeneities and renders this method robust. Histograms of the NF picture are generated and fitted by a Gaussian to yield the NF mean and standard deviation (Figure 3B).

Thus, every mean value of the NF is the result of several million tested molecular constructs (more details about the statistics can be found in Supplement S1). This number can be interpreted as the binding strength of the protein-DNA interaction in comparison to a certain reference bond. A variation of the reference bond will result in a different NF and refines the information of the DNA-protein interaction. We tested our zinc finger protein against three DNA double strands incorporating either a high affinity sequence, a low affinity sequence or a no binding sequence against two reference bonds, a 20 bp and a 40 bp DNA double strand and analyzed the data in the way just described (the exact sequences are shown in Figure S1). The result of one example experiment is depicted in Figure 3C. Due to the low DNA transfer for the no binding sequence, a calculation of the NF was not possible, so we set these values to zero. Differences are clearly visible for the NF values for the low and high affinity sequences as well as for the variations of the reference bond. As expected, we measured the highest value of 0.65 ± 0.07 for the high affinity sequence against the 20 bp reference bond compared to 0.39 ± 0.15 for the low affinity sequence against the same reference bond. The stronger reference bond lowers the values to 0.32 ± 0.01 and 0.20 ± 0.02 for high and low affinity DNA motifs, respectively. For both DNA binding motifs, the mean NF is reduced by half if the number of reference base pairs is doubled: 0.65 (20 bp) to 0.32 (40 bp) for the high affinity motif and 0.39 (20 bp) to 0.20 (40 bp). Hence, a linear relationship between the number of reference base pair and the mean NF can be assumed in this range of reference bond length. This result does not mean that the strength of the protein-DNA bond is altered by different reference bonds. The comparison of the protein-DNA bond with different reference bonds yields different NF values that draw a more detailed picture of the protein-DNA interaction and enables to adjust the setup to the biological problem. A linear relationship between the NF and number of base pairs in the reference duplex makes it possible to adjust the reference duplexes until the NF yields a value of 0.5 so that the reference duplex of a certain number of base pairs has the same stability as the protein-DNA bond. Thus, the protein-DNA bond strength can be directly quantified with the stability of a certain number of base pairs. In our proof-of principle experiment, we compare the stability of a protein-DNA interaction with varying affinities to the stability of two DNA duplexes of different lengths. Interestingly, the NF values for the low affinity sequence against the 20 bp reference bond, 0.39, and for the high affinity sequence against the 40 bp reference bond, 0.32, are equal within errors (see Figure 3C). This allows the interpretation of a difference in binding strength of the zinc finger protein with these two DNA motifs that corresponds to the average binding strength of a 20 bp DNA double strand. Thus, we demonstrated that the specificity of DNA-protein interactions can be quantified via the binding strength in a force-based assay in a single measurement. Further, we can characterize the binding strength in a simple picture by correlating it to the average binding strength of a certain number of DNA base pairs.

Conclusion

We described a new variant of the MFA that allows to directly detect the binding strength of protein-DNA interactions. This force-based format can test several DNA sequences against a protein in parallel with good statistics and can characterize the binding strength descriptively by correlating it to the average binding strength of a certain number of DNA base pairs. As a proof-of-principle, we could quantify the interactions of a zinc finger protein with three DNA sequences and compare them against two reference bonds. The resolution of the assay depends on the biological problem and the strength of the reference duplex. It was already demonstrated that the MFA can detect a single nucleotide polymorphism in a 20 base pair DNA duplex [19]. Shorter reference duplexes or a reference duplex in zipper geometry can discriminate between very small differences in the strength of the protein-DNA complexes invoked for example by a single base pair variation in the DNA target sequence. Further experiments will identify the capabilities and limitations of the assay for different DNA-protein complexes. For a complete characterization of a protein's binding specificity and affinity, it is necessary to probe the interactions with DNA sequences representative of a whole genome. This is, in principle, feasible with our force-based design. We have already shown that much smaller geometries for the DNA spots are sufficient to calculate the NF [27] and the fabrication of DNA microarrays is a standard procedure. Furthermore, our lab succeeded in integrating the MFA in a microfluidic chip [31]. The utilized surface chemistry also allows for the measurement of several proteins in a single experiment. Thus, our force-based assay can quantify protein-DNA interactions in a parallel format. It has the potential, with further developments in miniaturization and parallelization, to improve our understanding of transcriptional regulation.

Supporting Information

Figure S1 DNA sequences.
(TIF)

Supplement S1 Materials and Methods.
(DOC)

Acknowledgments

The authors thank Marcus Otten and Mathias Strackharn for helpful discussions. K.L. is grateful to the Elite Network of Bavaria (IDK-NBT) for a doctoral fellowship.

Author Contributions

Conceived and designed the experiments: KL DP DA HEG. Performed the experiments: KL. Analyzed the data: KL. Contributed reagents/materials/analysis tools: DP DA. Wrote the paper: KL DP DA HEG.

References

1. Badis G, Berger MF, Philippakis AA, Talukder S, Gehrke AR, et al. (2009) Diversity and complexity in DNA recognition by transcription factors. Science 324: 1720–1723.
2. Tanay A (2006) Extensive low-affinity transcriptional interactions in the yeast genome. Genome Res 16: 962–972.
3. Segal E, Raveh-Sadka T, Schroeder M, Unnerstall U, Gaul U (2008) Predicting expression patterns from regulatory sequence in Drosophila segmentation. Nature 451: 535–540.
4. Ren B, Robert F, Wyrick JJ, Aparicio O, Jennings EG, et al. (2000) Genome-wide location and function of DNA binding proteins. Science 290: 2306–2309.
5. Iyer VR, Horak CE, Scafe CS, Botstein D, Snyder M, et al. (2001) Genomic binding sites of the yeast cell-cycle transcription factors SBF and MBF. Nature 409: 533–538.
6. Park PJ (2009) ChIP-seq: advantages and challenges of a maturing technology. Nat Rev Genet 10: 669–680.
7. Bulyk ML, Huang X, Choo Y, Church GM (2001) Exploring the DNA-binding specificities of zinc fingers with DNA microarrays. Proc Natl Acad Sci U S A 98: 7158–7163.
8. Mukherjee S, Berger MF, Jona G, Wang XS, Muzzey D, et al. (2004) Rapid analysis of the DNA-binding specificities of transcription factors with DNA microarrays. Nat Genet 36: 1331–1339.

9. Berger MF, Philippakis AA, Qureshi AM, He FS, Estep PW, et al. (2006) Compact, universal DNA microarrays to comprehensively determine transcription-factor binding site specificities. Nat Biotechnol 24: 1429–1435.
10. Berger MF, Bulyk ML (2009) Universal protein-binding microarrays for the comprehensive characterization of the DNA-binding specificities of transcription factors. Nat Protoc 4: 393–411.
11. Fordyce PM, Gerber D, Tran D, Zheng J, Li H, et al. (2010) De novo identification and biophysical characterization of transcription-factor binding sites with microfluidic affinity analysis. Nat Biotechnol 28: 970–975.
12. Nutiu R, Friedman RC, Luo S, Khrebtukova I, Silva D, et al. (2011) Direct measurement of DNA affinity landscapes on a high-throughput sequencing instrument. Nat Biotechnol 29: 659–664.
13. Stormo GD, Zhao Y (2010) Determining the specificity of protein-DNA interactions. Nat Rev Genet 11: 751–760.
14. Koch SJ, Shundrovsky A, Jantzen BC, Wang MD (2002) Probing protein-DNA Interactions by Unzipping a Single DNA Double Helix. Biophysical Journal 83: 1098–1105.
15. Bartels FW, Baumgarth B, Anselmetti D, Ros R, Becker A (2003) Specific binding of the regulatory protein ExpG to promoter regions of the galactoglucan biosynthesis gene cluster of Sinorhizobium meliloti - a combined molecular biology and force spectroscopy investigation. Journal of Structural Biology 143: 145–152.
16. Kuhner F, Costa LT, Bisch PM, Thalhammer S, Heckl WM, et al. (2004) LexA-DNA bond strength by single molecule force spectroscopy. Biophys J 87: 2683–2690.
17. Bizzarri AR, Cannistraro S (2010) The application of atomic force spectroscopy to the study of biological complexes undergoing a biorecognition process. Chem Soc Rev 39: 734–749.
18. Moy VT, Florin EL, Gaub HE (1994) Intermolecular forces and energies between ligands and receptors. Science 266: 257–259.
19. Albrecht C, Blank K, Lalic-Multhaler M, Hirler S, Mai T, et al. (2003) DNA: a programmable force sensor. Science 301: 367–370.
20. Blank K, Mai T, Gilbert I, Schiffmann S, Rankl J, et al. (2003) A force-based protein biochip. Proc Natl Acad Sci U S A 100: 11356–11360.
21. Pavletich NP, Pabo CO (1991) Zinc Finger-DNA Recognition: Crystal Structure of a Zif268-DNA Complex at 2.1 A. Science 252: 809–817.
22. Kim J-S, Pabo CO (1998) Getting a handhold on DNA: Design of poly-zinc finger proteins with femtomolar dissociation constant. Proc Natl Acad Sci U S A 95: 2812–2817.
23. Elrod-Erickson M, Rould MA, Nekludova L, Pabo CO (1996) Zif268 protein-DNA complex refined at 1.6 A: a model system for understanding zinc finger-DNA interactions. Structure 4: 1171–1180.
24. Greisman HA, Pabo CO (1997) A general strategy for selecting high-affinity zinc finger proteins for diverse DNA target sites. Science 275: 657–661.
25. Carrion-Vazquez M, Oberhauser AF, Fowler SB, Marszalek PE, Broedel SE, et al. (1999) Mechanical and chemical unfolding of a single protein: a comparison. Proc Natl Acad Sci U S A 96: 3694–3699.
26. Ho D, Dose C, Albrecht CH, Severin P, Falter K, et al. (2009) Quantitative detection of small molecule/DNA complexes employing a force-based and label-free DNA-microarray. Biophys J 96: 4661–4671.
27. Severin PM, Ho D, Gaub HE (2011) A high throughput molecular force assay for protein-DNA interactions. Lab Chip 11: 856–862.
28. Ho D, Falter K, Severin P, Gaub HE (2009) DNA as a force sensor in an aptamer-based biochip for adenosine. Anal Chem 81: 3159–3164.
29. Limmer K, Aschenbrenner D, Gaub HE (2013) Sequence-specific inhibition of Dicer measured with a force-based microarray for RNA ligands. Nucleic Acids Res 41: e69.
30. Severin PM, Gaub HE (2012) DNA-Protein Binding Force Chip. Small.
31. Otten M, Wolf P, Gaub HE (2013) Protein-DNA force assay in a microfluidic format. Lab Chip 13: 4198–4204.
32. Yin J, Lin AJ, Golan DE, Walsh CT (2006) Site-specific protein labeling by Sfp phosphopantetheinyl transferase. Nat Protoc 1: 280–285.
33. Pedelacq JD, Cabantous S, Tran T, Terwilliger TC, Waldo GS (2006) Engineering and characterization of a superfolder green fluorescent protein. Nat Biotechnol 24: 79–88.
34. Wong LS, Thirlway J, Micklefield J (2008) Direct site-selective covalent protein immobilization catalyzed by a phosphopantetheinyl transferase. J Am Chem Soc 130: 12456–12464.
35. Wiegand G, Neumaier KR, Sackmann E (1998) Microinterferometry: three-dimensional reconstruction of surface microtopography for thin-film and wetting studies by interference contrast microscopy (RICM). Appl Opt 37: 6892–6905.

Supplement

Materials and Methods

Oligonucleotide constructs

The molecular complexes consist of three strands that are successively hybridized in shear geometry prior to usage. The uppermost strand which is covalently bound to the PDMS stamp is modified with an amino-group. Spacer18, a hexaethylene glycol chain of 18 atoms length, acts as an additional spacer between the amino-group and the oligonucleotides in order to avoid surface effects. Furthermore, poly-T stretches link the double-stranded sequences to the surfaces and each other. The cyanine dye Cy5 is attached by an N-Hydroxysuccinimide ester to the middle strand between the two duplexes.The reference bond is varied in length between 20 and 40 basepairs in order to test the protein-DNA bond against different strengths. The sample bond varies in its sequence in order to analyze the binding behavior of the protein against a high affinity DNA, `5'-caacaggtaac`**`aagggttca`**`g`**`gcgtgggcg`**`ttcgcgaagg-3'`, a low affinity DNA, `5'-caacaggtaac`**`aagtggtca`**`g`**`gcgaggtcg`**`ttcgcgaagg-3'`, and a no binding sequence, `5'-caacagtaacagagtgcaagccgtgagcttgccgcgaagg-3'`. The complete DNA constructs are dispalyed in Figure S1. All oligonulceotide constructs, including modified ones, were obtained from biomers.net GmbH, Germany.

Protein construct

A fusion protein construct consisting of an N-terminal ybbR-tag [1] (DSLEFIASKLA) followed by a superfolderGFP variant [2] and the six zinc finger protein construct Zif268/NRE (with an RQKDGERP linker sequence between the Zif268 and NRE moieties) [3] was cloned into pGEX6P2 between BamHI and XhoI sites similar to [4] . All construct fragments were amplified from synthetic templates (Mr.Gene or Geneart, Lifetechnologies, UK). The resulting fusion protein (ybbR-sfGFP-Zif268/NRE) harbored a GST-tag and was expressed in *E.coli* BL21 DE3 Codon Plus cells (Agilent Technologies, USA). One liter of SB medium was inoculated with 10ml of an overnight culture and grown at 37°C. When an OD_{600} of 0.7 had been reached, over night expression at 18°C was induced by adding 0.25mM IPTG. Cells were lyzed in 50mM TRIS-HCl (pH 7.5, 300 mM NaCl, 2mM DTT, 5% Glycerol, 10µM $ZnCl_2$) by a French pressure cell press. The ybbR-GFP-zinc finger construct was obtained in the soluble fraction

and purified by Glutathione affinity chromatography on GSTrap columns (GE Healthcare, Germany) according to standard procedures. After over night treatment with PreScission protease the GST-tag was removed and the protein further purified by Heparin cation exchange chromatography (HiTrap Heparin, GE Healthcare, Germany). Following preparative size exclusion chromatography on a HiLoad 16/60 Superdex 75 column (GE Healthcare, Germany) in 50mM TRIS-HCl (pH7.5, 150mM NaCl, 2mM DTT, 10µM $ZnCl_2$, 5% Glycerol) the protein construct was concentrated to 10µM by ultrafiltration in Amicon Ultra centrifugal filter units (Merck Millipore, USA) and stored at -80°C until further usage.

Stamp preparation

Micro-and macrostructured poly(dimethylsiloxane) (PDMS) stamps were fabricated by casting 1:10 crosslinker/base (Sylgard, Dow Corning, MI, USA) into a custom-made Pyrex/silicon wafer (HSG-IMIT, Germany) according to standard procedures [5]. The resulting PDMS stamps feature pillars of 1mm diameter and height with a spacing of 3mm in a square pattern on a 3mm thick basis and are cut in pieces of 4x4 pillars. The flat surface of the pillars is microstructured with 100µm x 100µm pads separated by 41µm wide and 5µm deep rectangular trenches enabling the drainage of liquid during the contact and separation process (Figure 1A). For the surface functionalization, the cleaned stamp surface was first activated in 12.5% HCl overnight and derivatized with (3-glycidoxypropyl)-trimethoxysilane (ABCR, Germany) in order to generate epoxide groups. After 30 minutes at 80°C in an Argon atmosphere, the functionalized stamp was allowed to cool down to room temperature. The amino-modified DNA strand, dissolved in water, was diluted 1:10 in a sodium borate-buffer (50mM H_3BO_3, 50mM $Na_2B_4O_7$•10 H_2O pH=9.0; Carl Roth GmbH & Co. KG, Germany) to a concentration of 10µM and 1.5µl was transferred to every pillar on the stamp. Overnight incubation of the stamp under humid conditions allowed the amino-groups to react with the epoxide-groups. Oligonucleotides that did not bind to the stamp were washed off the next day in an aqueous solution of 0.01% SDS (sodium dodecyl sulphate; Sigma-Aldrich GmbH, Germany). The other two DNA strands were pre-incubated in 5x SSC buffer (saline sodium citrate; 750mM sodium chloride, 75mM trisodium citrate; Sigma-Aldrich GmbH, Germany) in a concentration of 0.2µM. 1.5µl was transferred to every pillar of the stamp. After a minimum of 60 minutes incubation time the functionalized stamp was washed with 0.05% Tween 20 (VWR Scientific GmbH, Germany) in 1x SSC and gently dried with N_2 gas.

Slide preparation

Conventional glass slides for microscopy were aminosilanized in our lab: After thorough cleaning by sonication in 50% (v/v) 2-propanol in ddH20 for 15 min and oxidation in a solution of 50% (v/v) hydrogen peroxide (30%) and sulfuric acid for 30 min, they were washed with ddH2O and dried in a nitrogen stream. For the silanization, the glass slides were soaked for 1 h in a solution of 90% (v/v) ethanol, 8% ddH2O and 2% 3-aminopropyldimethylepoxysilane (ABCR, Germany). Subsequently they were washed twice in 2-propanol and ddH2O and dried at 80 °C for 40 min. They can be stored for several weeks in an Argon atmosphere at room temperature.

For further functionalisation, the amino-silanized glass slide was first deprotonated in a sodium borate buffer (50mM H_3BO_3, 50mM $Na_2B_4O_7$•10 H_2O pH=8.5; Carl Roth GmbH & Co. KG, Germany) for 30 minutes, then a heterobifunctional PEG crosslinker with N-hydroxy succinimide and maleimide groups (MW 5000, Rapp Polymere, Germany) was applied for 1 h at 30mM. The slide was thoroughly washed with ddH20 and gently dried with N2, before it was incubated another hour with Coenzyme A (Merck Millipore, USA) dissolved in coupling buffer (50mM $NaHPO_4$, 50mM NaCl, 10mM EDTA at pH=7.2). Again the slide was washed with ddH2O and gently dried with N_2. At this stage, the slide can be stored up to several days.

The Zif268/NRE protein aliquot at a concentration of 10µM is spun down in a table top centrifuge to remove agglomerates and the supernatant was diluted in a 50mM TRIS-HCl buffer (pH=7.5, 150mM NaCl, 10mM $MgCl_2$, 10µM $ZnCl_2$, 2mM DTT) to a final concentration of 2.5µM. Furthermore, low molecular weight DNA from salmon sperm (Sigma-Aldrich GmbH, Germany) was added in a concentration of 1g/ml. After a short incubation time of 15 minutes, 1,5 µl of Phosphopantetheinyltransferase Sfp was added to the sample and 2µl droplets of the mix were transferred to the functionalized glass slide in a 4x4 pattern. Sfp reacted the Coenzyme A on the glass slide to the ybbR-tag of the protein in humid atmosphere at room temperature during three hours incubation time. A PMMA mask with a well for the 4x4 pattern of spotted protein sample was fixed to the glass slide with a silicone lip seal. The mask prevented samples from drying out during following washing procedures and the MFA experiment. All protein that did not bind to the surface was washed off by 25ml 50mM TRIS-HCl buffer (pH=7.5, 150mM NaCl, 10µM $ZnCl_2$), 25ml 100mM TRIS-HCl buffer (pH=7.5, 300mM NaCl, 10µM $ZnCl_2$) and again 25ml 50mM TRIS-HCl buffer (pH=7.5, 150mM NaCl, 10µM $ZnCl_2$). The last buffer was also used for the MFA experiments. After the washing procedure, the samples were measured within 3 hours.

Contact process and fluorescence read-out

The functionalized stamp adhered upside-down to the glass block glued to a closed-loop piezoelectric actuator (PZ 400, Piezo Systems Jena, Germany) and a DC motorized translation stage (Physik Instrumente GmbH, Germany). The slide with the oligonucleotide constructs was fixed beneath the stamp on a stainless steel stage with permanent magnets. The fluorescence signal of the superfolderGFP fused between the ybbR-Tag and the zinc finger protein was used to place every protein spot beneath the right stamp pillar. The whole contact device is mounted on an inverted microscope (Axio Observer Z1, Carl Zeiss MicroImaging GmbH, Germany) with an xy-DC motorized high-accuracy translation stage (Physik Instrumente GmbH, Germany). Contact was made by means of the piezo and care was taken that each individual pillar is not compressed more than 3µm. The planar adjustment of stamp and slide as well as the contact process were controlled by reflection interference contrast microscopy [6]. In order to let the protein bind to the DNA sample sequence on the PDMS stamp, the contact between stamp and slide was maintained for 10 minutes. The piezo retracted the stamp with a velocity of 1µm/s in all experiments. A force buildt up in the molecular complexes until the weaker bond, either the protein-DNA complex or the reference bond, broke with higher probability. A Cy5 fluorophore conjugated to the linker sequence between the two DNA double strands indicated the intact bond. Hence, the Cy5 fluorescence intensity $F_{transfer}$ on the glass slide was measured with a CCD camera (ANDOR iXon, Andor, Northern Ireland) after the contact and separation process. In order to normalize the signal of the intact protein-DNA complexes to the protein density on the glass slide, the sample was subsequently incubated with a 40 bp double-stranded DNA sequence containing the high affinity binding site and labeled with a Cy5 fluorophore in a concentration of 0.5µM for 30 minutes. Unbound dsDNA was removed by the following washing procedure: 25ml 50mM TRIS-HCl buffer (pH=7.5, 150mM NaCl, 10µM $ZnCl_2$), 25ml 100mM TRIS-HCl buffer (pH=7.5, 300mM NaCl, 10µM $ZnCl_2$) and again 25ml 50mM TRIS-HCl buffer (pH=7.5, 150mM NaCl, 10µM $ZnCl_2$). The Cy5 fluorescence intensity was measured again and gives the number of possible protein binding sites. Since the binding density of the DNA complexes on the PDMS always exceeds the number of functional proteins on the glass slide, further corrections are not necessary. The ratio of fluorescence signal on the glass slide directly after the rupture event $F_{transfer}$ to the maximal number of functional proteins $F_{intact\ protein}$ is defined as the Normalized Fluorescence, NF. The NF is calculated by dividing the pictures after background subtraction pixel-by-pixel by a custom-built

software written in Labview. Histograms of the NF picture are generated and fitted by a Gaussian to yield the NF mean and standard deviation.

Statistics

In every experiment, every pillar of the PDMS stamp can be functionalized with a different combination of reference and sample complex. In our proof-of-principle measurements we usually bind the same combination of sample and reference bond to at least two pillars for better statistics. The contact area of a pillar is (100x100 μm^2 x 25)= $25x10^4$ μm^2. From the fluorescence signal of the functional protein we can estimate a lower bound for the density of functional protein on the glass slide of 10^3 per μm^2. Thus, every pillar tests around $25x10^7$ molecular complexes and the NF is the mean of $25x10^7$ tested molecular complexes. In order to demonstrate the validity of our approach to quantify the specificity of the protein-DNA interaction in a single measurement with good statistics, we show the result of one example measurement. Every data point is the average of two mean NF values. All NF values in this measurement are very close except the one for the low affinity binding motif against the 20bp reference. Other experiments yielded results in good agreement with the displayed experiment.

References

1. Yin J, Lin AJ, Golan DE, Walsh CT (2006) Site-specific protein labeling by Sfp phosphopantetheinyl transferase. Nat Protoc 1: 280-285.

2. Pedelacq JD, Cabantous S, Tran T, Terwilliger TC, Waldo GS (2006) Engineering and characterization of a superfolder green fluorescent protein. Nat Biotechnol 24: 79-88.

3. Kim J-S, Pabo CO (1998) Getting a handhold on DNA: Design of poly-zinc finger proteins with femtomolar dissociation constant. Proc Natl Acad Sci 95: 2812-2817.

4. Strackharn M, Pippig DA, Meyer P, Stahl SW, Gaub HE (2012) Nanoscale arrangement of proteins by single-molecule cut-and-paste. J Am Chem Soc 134: 15193-15196.

5. Xia Y, Whitesides GM (1998) Soft Lithography. Annu Rev Mater Sci 28: 153-184.

6. Wiegand G, Neumaier KR, Sackmann E (1998) Microinterferometry: three-dimensional reconstruction of surface microtopography for thin-film and wetting studies by interference contrast microscopy (RICM). Appl Opt 37: 6892-6905.

Figure S1

DNA sequences. The molecular constructs with all modifications are displayed. The reference bond comprises the same sequence for all six constructs, but differs in the length of the middle strand. The ZIF268/NRE high affinity sequence is shown in red. The mutations for the low affinity sequence and the no binding sequence are colored green.

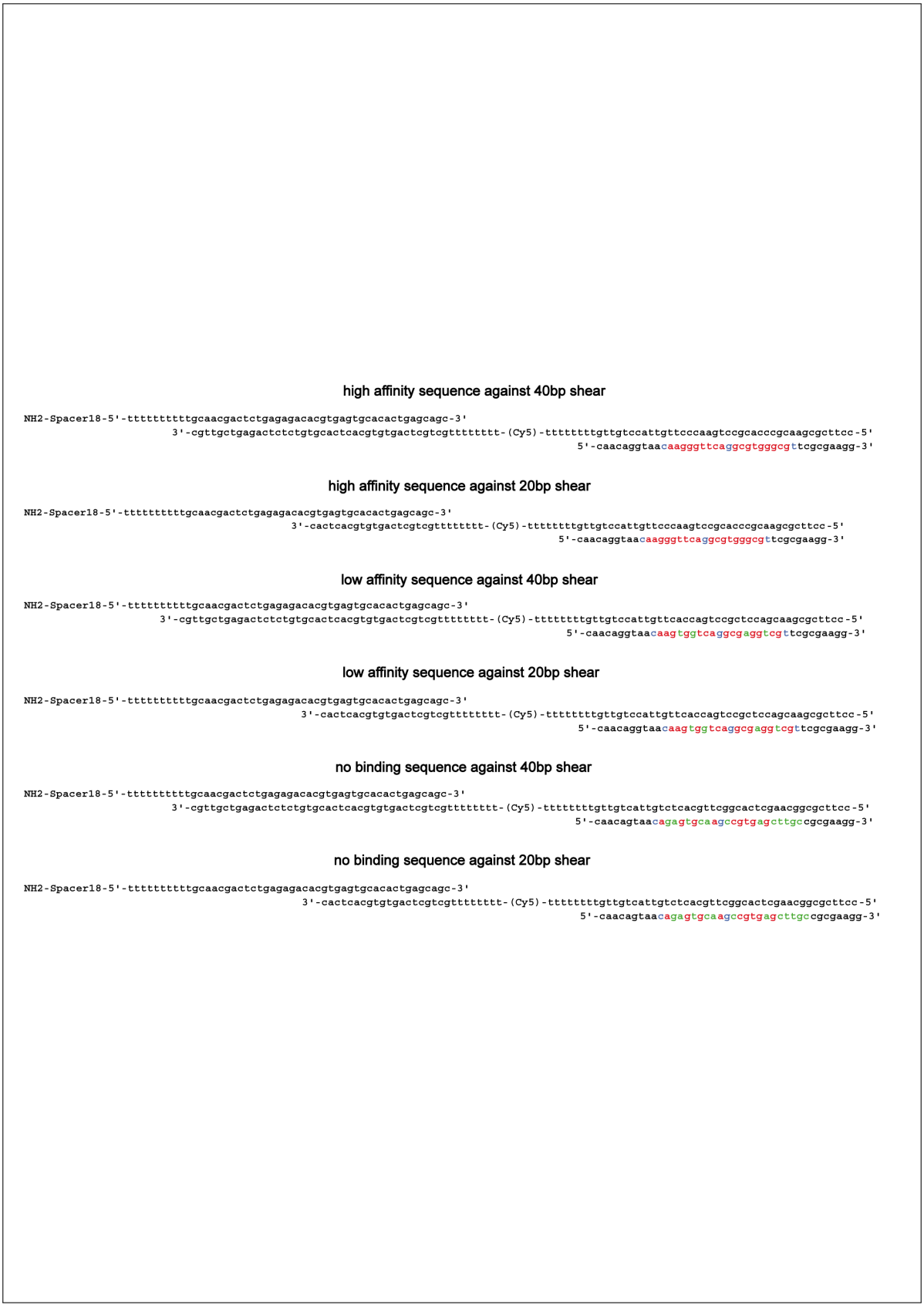
high affinity sequence against 40bp shear
NH2-Spacer18-5'-ttttttttttgcaacgactctgagagacacgtgagtgcacactgagcagc-3'
3'-cgttgctgagactctctgtgcactcacgtgtgactcgtcgttttttttt-(Cy5)-ttttttttgttgtccattgttcccaagtccgcacccgcaagcgcttcc-5'
5'-caacaggtaacaagggttcaggcgtgggcgttcgcgaagg-3'
high affinity sequence against 20bp shear
NH2-Spacer18-5'-ttttttttttgcaacgactctgagagacacgtgagtgcacactgagcagc-3'
3'-cactcacgtgtgactcgtcgttttttttt-(Cy5)-ttttttttgttgtccattgttcccaagtccgcacccgcaagcgcttcc-5'
5'-caacaggtaacaagggttcaggcgtgggcgttcgcgaagg-3'
low affinity sequence against 40bp shear
NH2-Spacer18-5'-ttttttttttgcaacgactctgagagacacgtgagtgcacactgagcagc-3'
3'-cgttgctgagactctctgtgcactcacgtgtgactcgtcgttttttttt-(Cy5)-ttttttttgttgtccattgttcaccagtccgctccagcaagcgcttcc-5'
5'-caacaggtaacaagtggtcaggcgaggtcgttcgcgaagg-3'
low affinity sequence against 20bp shear
NH2-Spacer18-5'-ttttttttttgcaacgactctgagagacacgtgagtgcacactgagcagc-3'
3'-cactcacgtgtgactcgtcgttttttttt-(Cy5)-ttttttttgttgtccattgttcaccagtccgctccagcaagcgcttcc-5'
5'-caacaggtaacaagtggtcaggcgaggtcgttcgcgaagg-3'
no binding sequence against 40bp shear
NH2-Spacer18-5'-ttttttttttgcaacgactctgagagacacgtgagtgcacactgagcagc-3'
3'-cgttgctgagactctctgtgcactcacgtgtgactcgtcgttttttttt-(Cy5)-ttttttttgttgtcattgtctcacgttcggcactcgaacggcgcttcc-5'
5'-caacagtaacagagtgcaagccgtgagcttgccgcgaagg-3'
no binding sequence against 20bp shear
NH2-Spacer18-5'-ttttttttttgcaacgactctgagagacacgtgagtgcacactgagcagc-3'
3'-cactcacgtgtgactcgtcgttttttttt-(Cy5)-ttttttttgttgtcattgtctcacgttcggcactcgaacggcgcttcc-5'
5'-caacagtaacagagtgcaagccgtgagcttgccgcgaagg-3'

B Accepted Manuscript

B.1 Manuscript 1: C-5 Propynyl Modifications Enhance the Mechanical Stability of DNA

C-5 Propynyl Modifications Enhance the Mechanical Stability of DNA

by

Daniela Aschenbrenner, Fabian Baumann, Lukas Milles, Diana Pippig and Hermann E. Gaub

accepted for publication in ChemPhysChem

COMMUNICATION WILEY-VCH

C-5 Propynyl Modifications Enhance the Mechanical Stability of DNA

Daniela Aschenbrenner,[a] Fabian Baumann,[a] Lukas F. Milles,[a] Diana A. Pippig,*[a][b] and Hermann E. Gaub[a]

Abstract: Increased thermal or mechanical stability of DNA duplexes is desired for many applications in nanotechnology or –medicine where DNA is used as a programmable building block. Modifications of pyrimidine bases are known to enhance thermal stability and have the advantage of standard base-pairing and easy integration during chemical DNA synthesis. Through single-molecule force spectroscopy experiments with Atomic Force Microscopy and the Molecular Force Assay we investigated the effect of pyrimidines harboring C-5 propynyl modifications on the mechanical stability of double-stranded DNA. Utilizing these complementary techniques, we show that propynyl bases significantly increase the mechanical stability if the DNA is annealed at high temperature. In contrast, modified DNA complexes formed at room temperature and short incubation times display the same stability as non-modified DNA duplexes.

In recent years, DNA has emerged as a prominent nanoscale building block. It exhibits unparalleled properties such as the ability to self-assemble depending on its sequence, which can be designed as required. Thus, two and three dimensional defined structures such as scaffolded DNA origami [1] can be created at the nanoscale. Another example are small "DNA bricks" [2], which can be assembled to larger structures in a LEGO-like fashion. However, materials that are prepared using DNA harbor the drawback of only limited thermal stability. In general, DNA structures cannot be employed at elevated temperatures in solution as they disassemble at high temperatures. In order to overcome this disadvantage, the heat tolerance of DNA structures can *e.g.* be improved by about 30°C by photo-cross-linking [3]. For other applications, the limiting factor is the mechanical stability of DNA structures. It is not directly correlated to the structures' thermal stability, as it largely depends on the orientation in which an external force is applied. A standard example is given by a short DNA duplex. Here, a higher rupture force is observed if the duplex is melted by applying a force load in shear geometry at opposing 5' termini than if the DNA is opened like a zipper from 5' and 3' termini of the same end [4]. In the latter case, one base pair at a time is loaded under force while in the first case all base pairs are stretched simultaneously. For the shearing of short DNA duplexes, the average rupture force is thus dependent on the number of base pairs (bp) [5]. At rupture forces of about 65 pN a force plateau is reached. This so-called BS-transition can be attributed to an overstretching of the DNA and is already observed for DNA duplexes as short as 30 bp [6]. Internal modifications of bases are capable of altering both thermal and mechanical stability of a DNA duplex. A prominent example is the methylation of the 5' position of cytosine [7]. Depending on the amount and position of modified bases in a DNA duplex the melting temperature [8] and the probability of strand dissociation under force are altered, as methylation can both stabilize and destabilize DNA duplexes [9]. Another alternative is *e.g.* the use of salicylic aldehyde nucleosides, which confers strong mechanical stabilization upon copper complexation [10].

In order to reach higher mechanical stability, integration of bases modified with a propynyl group at the 5' position of pyrimidines [11] is promising, as the apolar planar group extends into the major groove and enhances base-stacking. Graham *et al.* [12] determined the thermodynamic parameters for a 12 bp DNA duplex containing five propynyl bases compared to an unmodified duplex with UV-melting studies: the significant decrease in enthalpy is attributed to the electronic interactions in base-stacking and counteracts the entropy decrease likely resulting from more ordered water molecules normally found in the major groove. This results in a decrease in free energy ΔG and thus a stabilized complex [12]. Compared to other base modifications such as methylation, the incorporated propynyl bases lead to an even higher increase in melting temperature per base [13], number and position of the propynyl bases playing an important role [14]. Higher mechanical stabilities would be useful to render DNA nanostructures more stable in the presence of external forces, *e.g.* for techniques such as the Molecular Force Assay (MFA), where the mechanical stability of a molecular complex is determined by comparing it to a known DNA reference complex. An increase in mechanical stability of the DNA duplex broadens the dynamic range of the assay and enables *e.g.* the characterization of protein-protein interactions [15].

In the study presented here, the MFA technique is employed together with atomic force microscope (AFM) based force spectroscopy to characterize the difference in mechanical stability of short DNA duplexes with varying numbers of integrated propynyl bases. Thee different 40 base pair long oligonucleotides are investigated in shear mode, harboring no modification (0P), eight propynyl bases (8P) and 22 propynyl bases (22P), respectively (see scheme 1). The sequence is identical for all three strands, enabling binding to the same complementary DNA strand. A stabilization of the DNA complex to average rupture forces higher than the 65 pN that can be reached with unmodified DNA is desired. Therefore, the length of 40 bp is chosen for the duplexes. Two complementary force spectroscopy techniques are employed to characterize the DNA duplexes. The basic principle of the measurement with the atomic force microscope (AFM) [6, 16] is displayed in scheme 2a. The two strands are attached covalently *via* PEG spacers to the lower surface and the cantilever, respectively. Upon lowering the cantilever onto the glass slide, the DNA duplex to be

[a] D Aschenbrenner, F Baumann, LF Milles, Dr. DA Pippig, Prof. Dr. HE Gaub
Center for Nanoscience and Department of Physics
University of Munich, Amalienstrasse 54
80799 München (Germany)
E-mail: daniela.aschenbrenner@physik.uni-muenchen.de
[b] Dr. DA Pippig
Munich Center for Integrated Protein Science (CIPSM)
Butenandtstr. 5-13
81377 München (Germany)

Supporting information for this article is given via a link at the end of the document.

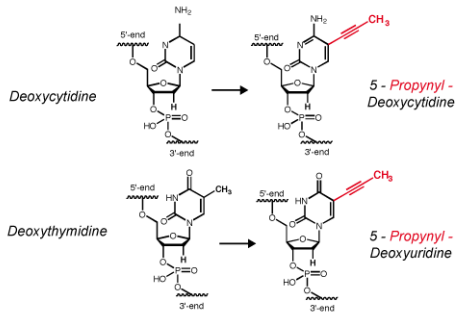

Scheme 1. Propynyl Bases and DNA Sequences. In order to obtain propynyl bases, the 5' position of the pyrimidines cytidine or thymidine is modified with an additional propynyl group, which extends into the major groove of the DNA helix. A stabilization of the DNA duplex harboring propynyl bases is thus expected to result from enhanced base-stacking. DNA oligonucleotides with the same sequence but a different amount of propynyl bases, namely none (*0P*, blue), 8 (*8P*, orange) and 22 (*22P*, purple) are investigated.

investigated is formed. Retraction of the force-calibrated cantilever stretches the PEG linker and the DNA duplex until it finally ruptures, as depicted in the resulting example force-distance curve (scheme 2a). The force resolution is limited due to thermal fluctuations by the size of the cantilever, which acts as the force sensor. In the technique of the Molecular Force Assay (MFA) [17], the size of the force sensor is minimized to a second DNA duplex. As shown in scheme 2b, this reference duplex is coupled in series with the duplex to be investigated and clamped between two surfaces. Retraction of the upper surface compares the mechanical stability of both complexes directly until, statistically, the weaker one ruptures. The outcome of the experiment is given by the position of the fluorophore dye on the linker after force load, as it stays with the stronger duplex. A second dye on the uppermost DNA strand forming a FRET pair with the dye on the linker allows for correction of constructs that did not couple to the upper surface and have thus not been under force load. The main advantage of the MFA technique lies in the parallelization of force-spectroscopy experiments. About 10^4 complexes per μm^2 are tested simultaneously [18]. An important difference between the two techniques is the incubation time and condition of the duplex to be investigated. While for the AFM experiment the incubation time of the duplex depends on the contact time of the cantilever with the surface, the duplex in the MFA experiment is pre-incubated over night and can also be annealed with a temperature ramp starting from denaturing temperatures.

In order to determine if integration of propynyl bases leads to average rupture forces higher than for unmodified DNA, AFM experiments were performed. To exclude calibration uncertainties, all measurements were conducted with the same cantilever harboring the complementary strand, while the strands 0P, 8P and 22P were covalently attached to the surface in three distinct populations. Representative histograms for data obtained with a retraction velocity of 1000 nm/s are displayed in figure 1. The histograms are fitted with the Bell-Evans-Model (see supporting information) and the most probable rupture forces were found to be 65.1 ± 4.5 pN (0P; N= 705 curves), 65.5 ± 4.4 pN (8P; N= 579) and 64.7 ± 4.5 pN (22P; N= 1079), respectively. Thus, the most probable rupture forces of 0P, 8P and 22P cannot be distinguished within the error bars. The same conclusion holds true for the other tested retraction velocities of the cantilever (the corresponding data can be found in the supporting information). However, although the most probable rupture forces were indistinguishable within error, we performed pair-wise two-sample Kolmogorov–Smirnov tests, in order to test the hypothesis whether the rupture force distributions are significantly different. For all retraction velocities besides 500 nm/s, the rupture force distributions for 8P and 22P were significantly different from the 0P distribution with a p-value below 0.05. Hereby, the p-values of the 22P distributions are considerably smaller than that those of the 8P distributions, when compared against the 0P distributions. This can also be seen in the width of the rupture force distribution, which increases with the number of propynyl modifications.

The Bell-Evans fits to the rupture force distributions confirm the validity of the model for this data and allow for the determination of the distance to the transition state in the binding energy landscape. We found for the three modified duplexes 0P, 8P and 22P a Δx of 0.582 ± 0.024 nm, 0.514 ± 0.019 nm, and 0.416 ± 0.010 nm respectively.

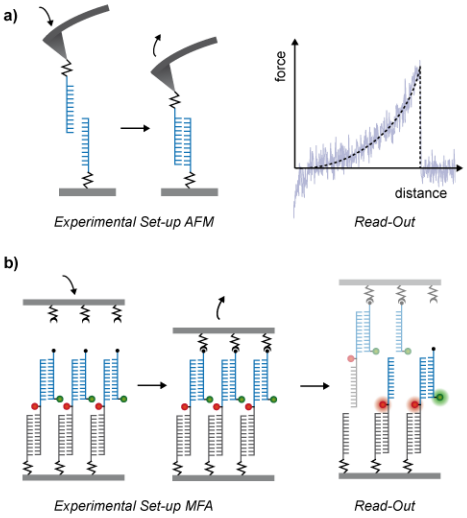

Scheme 2. Experimental Set-ups of AFM and MFA. The DNA duplexes are investigated with two complementary single-molecule force spectroscopy techniques. To this end, all three DNA strands are hybridized to the same, unmodified complementary strand and integrated into the experimental set-ups of the Atomic Force Microscope (AFM) (a) as well as the Molecular Force Assay (MFA) (b). In the well-established AFM force spectroscopy, the two DNA strands of the duplex are covalently attached to a lower glass surface and a cantilever, respectively. The duplex to be investigated (blue) forms when the cantilever is lowered onto the glass surface. Retraction of the force-calibrated cantilever yields a force-distance curve as the outcome of the experiment. The cantilever of the AFM experiment can be regarded as an elastic spring and acts as the force sensor. In contrast, in an MFA experiment, the force sensor is given by a second DNA duplex (grey), which is coupled in series with the duplex to be investigated (blue). Those DNA constructs are built up on a glass slide and then clamped between two surfaces *via* a Biotin-Streptavidin interaction (b). Retraction of the upper surface builds up a force acting on both molecular complexes until, statistically, the weaker one ruptures. The outcome of the experiment is read out *via* a fluorophore (red circle) attached to the linker between the two duplexes, which only gives a signal if the lower reference complex is still intact after rupture. A second fluorophore coupled to the upper strand (green circle) is necessary for the correction of the analysis if the molecular complexes did not couple to both surfaces and thus have not been under force load.

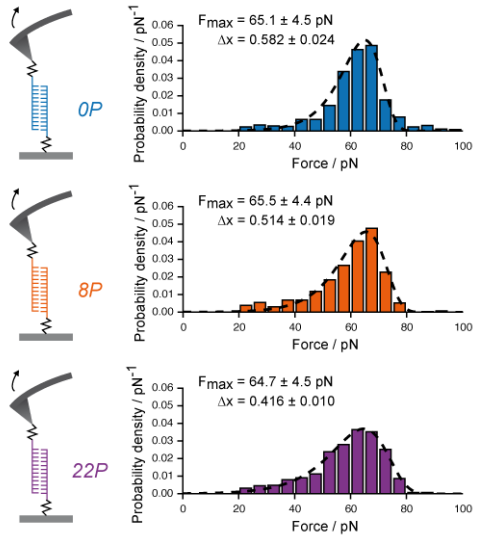

Figure 1. Investigation of DNA Duplexes containing Propynyl Bases with the Atomic Force Microscope. Representative histograms of the most probable rupture force for a retraction velocity of the cantilever of 1000 nm/s are shown for all three DNA complexes with a varying amount of propynyl bases. The most probable rupture forces F_{max} are all within error in the vicinity of the BS-transition (65pN). They were determined by fitting the histograms within the Bell-Evans formalism.

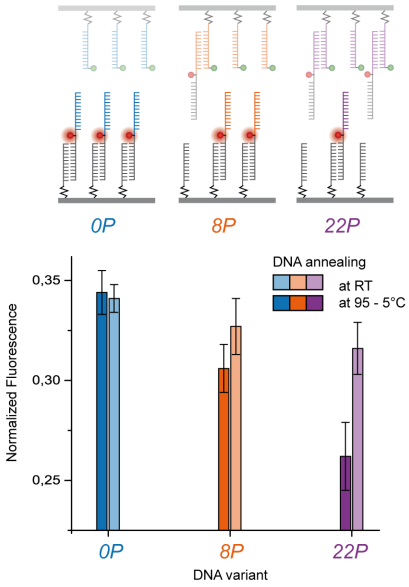

Figure 2. Investigation of DNA Duplexes containing Propynyl Bases with the Molecular Force Assay. In contrast to the AFM experiment, the DNA duplexes are not formed when the two surfaces are brought into contact, but instead the whole molecular construct consisting of both duplexes in series is build up in advance onto the lower glass slide. Hereby, the upper complex can be pre-incubated before attaching it to the surface. The more stable an upper complex is when compared to the same reference duplex, the less fluorescence signal remains on the lower glass slide after force load, as the fluorophore remains with the stronger duplex. This means that the Normalized Fluorescence (NF) value of the surface becomes smaller the higher the mechanical stability of the upper complex is. The NF values of all three DNA duplexes are displayed, with the upper complex pre-incubated by either heating up to 95°C and cooling it down very slowly (4 hours) to 5°C (left bars) or over night at room temperature (right bars) (all given with standard deviation error bars). Whereas the mode of pre-incubation does not influence the stability of the unmodified DNA strand *0P*, for *8P* and *22P* the stabilization trend depending on the number of propynyl bases is the same but statistically significant only for the slowly annealed DNA.

Figure 2 displays the characterization of the same sequences with the MFA. In order to make the data directly comparable, all duplexes in question are tested against identical reference DNA. The Normalized Fluorescence NF gives the ratio of still intact reference duplexes after force load in comparison to the initial amount of assembled molecular constructs after correction for background and complexes that have not been under force load. Thus, a decreased value of the NF results from a strengthened duplex in question. With the MFA, the duplexes with 0P, 8P and 22P oligonucleotides were tested in two variants: for one sample the duplexes were pre-incubated at room temperature (RT) over night, for the other they were annealed by heating to 95°C and cooling to 5°C over four hours. We determined the following results for the NF mean values and error bars: $NF_{RT}(0P)$ = (0.341±0.007), $NF_{RT}(8P)$ = (0.327±0.014), and $NF_{RT}(22P)$ = (0.316±0.013) for the incubation at RT as well as $NF_{95}(0P)$ = (0.344±0.011), $NF_{95}(8P)$ = (0.306±0.012), $NF_{95}(22P)$ = (0.262±0.017) for the annealed complexes. The respective results for the two samples are depicted in figure 2. For the duplexes incubated at RT (right bars), a slight stabilization depending on the number of modifications is discernible, although within standard deviation error bars. In contrast, for the duplexes annealed at high temperature (left bars), the stabilization effect is significant.

The MFA determines the relative stability of a DNA duplex in question by comparing it to a DNA reference duplex during strand separation. In comparison to the duplex with the unmodified DNA, 0P, the probability of strand separation in the annealed 8P sample is altered about (NF(8P) – NF(0P))/NF(0P) = - 11% and about - 24% for the annealed 22P duplex. The parallel measurement of the three samples with the MFA ensures identical measurement conditions and renders the obtained differences in rupture probability highly reliable. In the AFM measurements as well, care was taken to minimize measurement variations. In the characterization of the mechanical stability of methylated DNA conducted by Severin *et. al.* [9] with both AFM and MFA, the experiments led to the same results for stabilizing and destabilizing effects. We thus attribute the differing results of the AFM from the MFA measurements in this case of propynyl-modified DNA to different conformations of the DNA resulting from the very different incubation conditions, particularly the temperature and time span. In the AFM experiments, the duplex forms at RT during the contact time of the cantilever to the surface, which is below 0.1 s. Longer contact times enabling longer incubation times for the duplex are not feasible, as this reduces the probability to obtain single DNA binding events tremendously. The AFM measurements yield distinct populations of rupture force for all three samples, and sequence compatibility allows for one binding mode only. The slight broadening of the force distribution width with increasing number of base modifications leads to an elevated number of events both with lower and higher rupture force. The higher variance of the modified DNA distribution might be attributed to short lived perturbations in duplex formation caused by the propynyl modifications. However, this effect is very small. This leads to the assumption that even though the DNA duplex forms during the measurement the short contact time is not sufficient to acquire

a conformation in which the propynyl group can stabilize the DNA significantly. In support of this assumption the results for the MFA measurement with samples incubated at RT also only show a very slight, not significant, stabilization effect. This indicates a complex energy landscape and a high potential barrier that needs to be overcome in order to form the stabilized complex. The fact that the stabilized complex is formed upon annealing at high temperature might be due to an increase in kinetic degrees of freedom under these conditions. Double-stranded DNA harboring more G-C base pairs is thermally more stable due to base-stacking interactions [19] and it unbinds at a higher external force along the long axis of the DNA [4]. It is thus a valid assumption that enhanced mechanical stability of annealed propynyl DNA is due to its increase in base-stacking interactions.

In summary, we have demonstrated that the modification of pyrimidines with a propynyl group at their 5' position can have a significant stabilization effect on DNA duplex strand separation and thus on its mechanical stability. However, to obtain the conformation of higher stability, the DNA has to be pre-annealed at high temperature. Provided that heating of the sample is possible, propynyl-modified pyrimidines can be employed to enhance the mechanical as well as thermal stability of double-stranded DNA. For DNA origami structures that in general are also prepared by annealing, it has been shown that folding to the desired structure occurs at a narrow temperature range and can consequently also be achieved at constant temperatures specific for the structure [20]. In this context it might be possible to adjust the annealing process for propynyl-modified DNA for temperature sensitive samples. The propynyl modification offers the advantage of standard sequence recognition, easy availability and the lack of additional treatments such as irradiation with light. Notably, the characterization of the propynyl-modified DNA with the AFM alone would not have given the whole picture, as it is not possible to measure a statistically sufficient dataset with pre-annealed DNA. The additional measurement with the MFA technique provided crucial complementary information on the properties of the modified DNA.

Experimental Section

Atomic Force Microscope

AFM-based force spectroscopy has been applied for analyzing the unbinding forces of the described DNA oligonucleotides comparable to [6]. The DNA strands with different propynyl modification levels were covalently coupled *via* PEG spacers to the probed sample surface, whereas the complementary DNA oligonucleotides were attached in the same manner to a BL-AC40TS-C2 cantilever (Olympus, Tokyo, Japan). For probing the DNA, the functionalized cantilever is brought into contact with the surface and withdrawn at different retraction velocities, ranging from 200 to 10000 nm/s. A low molecular surface density prevents the formation of multiple bonds between surface and cantilever tip. All measurements of the shown dataset were conducted with the same cantilever on one surface to ensure high comparability for different retraction velocities and DNA modification levels. In order to obtain single DNA binding events, the experiments feature no additional contact time of the cantilever on the surface before retraction. Force curves representing multiple bonding, nonspecific adhesion of molecules to the cantilever tip, or lack of interaction, were filtered out using an automated pattern-recognition algorithm. Only single worm-like chain force responses with a persistence length in the range of 0.1 to 0.5 nm and a contour length matching that of the DNA strands were extracted for further analysis. Rupture forces for each distinct retraction speed were plotted in histograms and fitted with the Bell-Evans model [21] to determine the most probable rupture force analogous to the analysis described in [6]. To obtain measurements over a broad range of different loading rates, several experiments were carried out for five different retraction velocities. Additionally, the standard Bell-Evans model was applied to the force versus loading rate dependency yielding the natural dissociation rate at zero force and the potential width Δx of the investigated DNA duplex (the corresponding force-loading rate plots can be found in the supplement). Sample preparation and more detailed information on the measurement of rupture forces of DNA duplexes can be found *e.g.* in [6] and in the supporting information.

Molecular Force Assay

The MFA experiments have been performed as described previously *e.g.* in [17b]. For the measurements with the MFA, three oligonucleotide strands are assembled as displayed in scheme 2b to form two DNA helices, a reference duplex and a duplex to be investigated. The lowermost strand is attached covalently to the lower surface, a glass slide, and binds to the lower part of a longer strand harboring a Cy5 fluorophore dye at the linker between the two duplexes. The uppermost DNA strand, forming the second duplex with the longer middle strand, carries both a Biotin and a Cy3 dye, forming a FRET pair with the Cy5. The upper surface consists of a soft PDMS stamp coated with streptavidin. After initial measurement of the fluorophore intensities, the stamp is lowered onto the glass slide. The Biotin allows for the coupling of the uppermost strand to the stamp, so that the two DNA duplexes are clamped between both surfaces. Upon retraction of the stamp, a force builds up in the complexes and the mechanical stabilities of the duplexes are compared until, statistically, the weaker one ruptures. A second measurement of the remaining fluorescence intensities on the glass slide allows for the quantitative analysis of the experiment. The Cy5 dye attached to the linker stays with the stronger duplex. Thus, the higher the ratio of remaining intensity on the surface is to the initial intensity, the stronger the lower complex is in comparison to the upper duplex. If a molecular complex does not couple to the stamp, the DNA duplexes are not under force load and the Cy5 dye remains on the glass slide, yielding a false positive signal. This can be corrected by subtraction of the ratio of the FRET signal, which only remains if the complexes have not been under force load and the uppermost strand is still on the glass slide. The outcome of the experiment is thus given by the "Normalized Fluorescence" which denotes the ratio of still intact lower complexes in comparison to the initial amount of complexes that have been under load. In the current standard set-up, 16 different combinations of reference and sample complex can be tested in parallel, each of them statistically significant as about 10^4 molecular complexes per μm^2 are tested simultaneously. The derivation of the equation for the Normalized Fluorescence and more details of the preparation, measurement and analysis process can be found in the supplementary information.

In the measurements conducted here, the oligonucleotides including the modifications were integrated as the uppermost strand, so that the upper duplex is the complex in question. The lower complex consists of a 40bp long DNA duplex. It has a different sequence to prevent for cross-hybridization of the three strands. The sequences are given in the supporting information.

Acknowledgements

The autors want to thank Prof. Jan Lipfert for helpful discussions and Dr. Christopher Deck of biomers.net (Ulm, Germany) for excellent technical advice and the custom-synthesis of propynyl-modified DNA. Funding by the Deutsche Forschungs-gemeinschaft SFB 1032-A01 as well as a European Research Council Advanced Grant (Cellufuel Grant 294438) is gratefully acknowledged. The funders had no role in study design; collection, analysis and interpretation of data; in the writing of the report or the decision to submit the article for publication.

Keywords: biophysics • DNA mechanical stability • force spectroscopy • propynyl bases • single-molecule studies

[1] a) P. Rothemund, *Nature* **2006**, *440*, 297-302; b) E. Winfree, F. Liu, L. Wenzler, N. Seeman, *Nature* **1998**, *394*, 539-544; c) S. Douglas, H. Dietz, T. Liedl, B. Högberg, F. Graf, W. M. Shih, *Nature* **2009**, *459*, 414-418; d) R. Schreiber, J. Do, E. Roller, T. Zhang, V. Schüller, P. Nickels, J. Feldmann, T. Liedl, *Nat Nanotechnol* **2014**, *9*, 74-78.

[2] Y. Ke, L. L. Ong, W. M. Shih, P. Yin, *Science* **2012**, *338*, 1177-11783.

[3] A. Rajendran, M. Endo, Y. Katsuda, K. Hidaka, H. Sugiyama, *Journal of the American Chemical Society* **2011**, *133*, 14488-14491.

[4] M. Rief, H. Clausen-Schaumann, H. E. Gaub, *Nat Struct Biol* **1999**, *6*, 346-349.
[5] T. Strunz, K. Oroszlan, R. Schäfer, H. Güntherodt, *Proc. Natl. Acad. Sci. USA* **1999**, *96*, 11277-11282.
[6] J. Morfill, F. Kühner, K. Blank, R. A. Lugmaier, J. Sedlmair, H. E. Gaub, *Biophys J* **2007**, *93*, 2400-2409.
[7] A. Bird, *Cell* **1992**, *70*, 5-8.
[8] A. Lefebvre, O. Mauffret, S. Antri, M. Monnot, E. Lescot, F. S, *Eur. J. Biochem* **1995**, *229*, 445-454.
[9] P. Severin, X. Zou, H. Gaub, K. Schulten, *Nucleic Acids Research* **2011**, *39*, 8740-8751.
[10] B. M. Gaub, C. Kaul, J. L. Zimmermann, T. Carell, H. E. Gaub, *Nanotechnology* **2009**, *20*, 434002-434009.
[11] a) B. Froehler, S. Wadwani, T. Terhorst, S. Gerrard, *Tetrahedron letters* **1992**, *33*, 5307-5310; b) F. Seela, S. Budow, H. Eickmeier, H. Reuter, *Acta Cryst.* **2007**, *C63*, o54-o57; c) S. Budow, H. Eickmeier, H. Reuter, F. Seela, *Acta Cryst.* **2009**, *C65*, o645-o648.
[12] D. Graham, J. Parkinson, T. Brown, *J. Chem. Soc., Perkin Trans. 1* **1998**, 1131-1138.
[13] M. Terrazas, E. Kool, *Nucleic acids research* **2009**, *37*, 346-353.
[14] T. Barnes, D. Turner, *Journal of the American Chemical Society* **2001**, *123*, 4107-4118.
[15] D. Aschenbrenner, D. Pippig, K. Klamecka, K. Limmer, H. Leonhardt, H. E. Gaub, *PLoS ONE* **2014**, *e115049*.
[16] G. Binnig, C. Quate, C. Gerber, *Physical Review Letters* **1986**, *56*, 930-933.
[17] a) C. Albrecht, K. Blank, M. Lalic-Mülthaler, S. Hirler, T. Mai, I. Gilbert, S. Schiffmann, T. Bayer, H. Clausen-Schaumann, H. E. Gaub, *Science* **2003**, *301*, 367-370; b) P. M. D. Severin, D. Ho, H. E. Gaub, *Lab Chip* **2011**, *11*, 856-862.
[18] a) D. Ho, C. Dose, C. H. Albrecht, P. Severin, K. Falter, P. B. Dervan, H. E. Gaub, *Biophys J* **2009**, *96*, 4661-4671; b) P. M. D. Severin, H. E. Gaub, *Small* **2012**, *8*, 3269–3273.
[19] P. Yakovchuk, E. Protozanova, M. D. Frank-Kamenetskii, *Nucleic Acids Res* **2006**, *34*, 564-574.
[20] J. Sobczak, T. Martin, T. Gerling, H. Dietz, *Science* **2012**, *338*, 1458-1461.
[21] E. Evans, K. Ritchie, *Biophys J* **1997**, *72*, 1541-1555.

Supporting Information

1. Supplementary Materials and Methods

DNA Oligonucleotides

Propynyl bases can be obtained from pyrimidines, which are modified with an additional propynyl group at the 5' position of the base (see scheme 1). In desoxycytidines, this is achieved by replacing the H- group with the propynyl group. Desoxythymidines are replaced by desoxyuridines modified with the propynyl group, as uracil does not already harbor a methyl group at its 5' position as thymidine.
Experiments were performed with three degrees of propynyl bases: one strand contained no base modification (0P), one eight propynyl-desoxycytidines (8P) and the last 13 propynyl-desoxycytidines as well as nine propynyl-desoxyuridines yielding 22 propynyl bases (22P). The modifications are distributed over the same sequence of 40 bases. The unchanged base-recognition for propynyl-modified bases yields binding of all examined oligonucleotides to the same complementary strand. All measurements in this study are performed at room temperature and physiological salt concentrations in 1xPBS buffer.

MFA Preparation

The lower surface with the two DNA duplexes in series was prepared as described previously *e.g.* [1] except for small modifications. The DNA oligomers were purchased including all modifications from biomers.net GmbH (Ulm, Germany) and IBA GmbH (Göttingen, Germany).
The lowermost oligonucleotide strand was coupled covalently *via* its NH_2-group at the 5' end to the aldehyde-functionalized glass slide (Schott GmbH, Jena, Germany). Five hexaethyleneglycol (HEGL) linkers acted as additional spacers. In the middle strand, a Cy5 fluorophore is attached to the poly-t-linker connecting the sequences for the two complexes. The direction of the middle strand is inverted in the linker, ensuring that both complexes are probed from the 5' ends. The three different uppermost strands harbor varying amounts of propynyl modification. Additionally, each strand carries a Cy3 fluorophore forming the FRET pair with the Cy5 dye in the middle strand as well as a biotin on the 5' end for coupling to the upper surface.

Lower Strand
NH2 - 5xHEGL - 5'- $(t)_{10}$ – ctg atg agt cga caa cgt atg cac tac gct cgc tta cta g
Middle Strand
3' - gac gac tgg tgg tgc tga cta tct aag tgg cta act tga g - $(t)_7$ - 5' - **(Cy5)** - 5' - $(t)_7$ - cta gta agc gag cgt agt gca tac gtt gtc gac tca tca g -3'
Upper Strands
(0P) Biotin - 5' - $(t)_{10}$ - ctg ctg acc acc acg act gat aga ttc acc gat tga act c - 3' - **(Cy3)**
(8P) Biotin - 5' - $(t)_{10}$ - ctg ctg acc acc acg act gat aga ttc acc gat tga act c - 3' - **(Cy3)**
(22P) Biotin - 5' - $(t)_{10}$ - ctg ctg acc acc acg act gat aga ttc acc gat tga act c - 3' - **(Cy3)**

The lower strand was spotted in 1 µl droplets of 25 µM in 5xPBS (Roche Life Science, Indiana, USA) in a 4x4 pattern on the functionalized glass slide and incubated in a saturated NaCl ddH_2O atmosphere overnight. The resulting Schiff Bases were reduced with 1% aqueous $NaBH_4$ (VWR Scientific GmbH, Darmstadt, Germany) for 90 minutes to render the attachment covalent. After a washing step with ddH_2O the slide was incubated in 1xPBS with 4% BSA (bovine serum albumin; Sigma-Aldrich GmbH, Munich, Germany) to reduce unspecific binding. A custom-made silicone isolator with 16 wells (Grace-Biolabs, OR, USA) was positioned on top of the spotted pattern of the lower DNA strand. A pre-incubated mix of middle and respective upper strand was spotted in the wells and incubated for 1h. The ratio of middle to upper strand was 1:2 (100nM:200nM) in 5xPBS to ensure a saturation of middle strands with bound upper strands. The mix was either incubated over night at room temperature (RT) or annealed by heating to 95°C and cooling slowly over 4 hours to 5°C. In order to remove free unbound DNA, the slide was rinsed carefully in washing steps with 2x, 0.2x and 1xPBS after removal of the isolator.

The upper surface, a soft PDMS (polydimethylsiloxane) stamp with 16 pillars matching the pattern of DNA constructs on the glass slide, is custom-made and functionalized in our lab as described in detail *e.g.* in [1]. The pillars are 1 mm in height and 1.1 mm in diameter on a 3mm thick basis and harbor a microstructure on the top. The pads of 100 µm x 100 µm are separated by trenches of 41 µm in width and 5 µm in depth to ensure liquid drainage during the contact and separation process to the lower glass slide. For the experiment, the stamps are functionalized with a 1:1 mix of NH_2-PEG-biotin (MW 3400) and NH_2-PEG-CH_3 (MW 2000; Rapp Polymere, Tübingen, Germany) and subsequently with 1mg/ml streptavidin (Thermo Fisher Scientific, Bonn, Germany) in 1xPBS containing 0.4% (w/v) BSA. Prior to the measurement, they were rinsed with 0.05% Tween 20 (VWR Scientific GmbH, Germany) in 0.2xPBS and gently dried with N_2 gas.

MFA Contact Process, Readout and Analysis

A detailed description of the measurement and analysis process of the MFA can *e.g.* be found in [1]. In short, a custom-build contact device is mounted on an inverted epi-fluorescence microscope, permitting fluorescence readout of the glass slide. A piezoelectric actuator enables the contact and separation process between slide and PDMS stamp which is controlled using reflection interference contrast microscopy [2]. The initially separated surfaces are left in contact for 10 minutes to allow for the coupling of the molecular complexes on the slide to the stamp *via* the Biotins on the uppermost DNA strand. Retraction of the stamp occurs at constant velocity of 1 µm/s. Before and after the contact of the stamp to the lower glass slide, the fluorescence intensity of the Cy5 ("RED_{Start}" and "RED_{Final}") and the FRET signal ("$FRET_{Start}$" and "$FRET_{Final}$") are recorded for each spot of molecular complexes on the slide.

In the analysis, the ratio of RED_{Final} to RED_{Start} gives the amount of intact lower bonds after stamp retraction in comparison to the initial amount of complexes: $Ratio_{RED} = RED_{Final} / RED_{Start}$. In order to correct for the complexes that have not been under load, the ratio of FRET signal is being subtracted, as a FRET signal only remains if the complexes are still fully assembled: $Ratio_{FRET} = FRET_{Final} / FRET_{Start}$. Normalization to the Coupling Efficiency CE = 1- $Ratio_{FRET}$ of complexes to the stamp yields the Normalized Fluorescence:

$NF = (Ratio_{RED} - Ratio_{FRET}) / CE$.

Hence, the NF gives the ratio between broken upper complexes in question and total amount of complexes that have been under force load. This means that the closer the NF to 0, the more stable the complex in question in comparison to the reference DNA duplex and *vice versa* for a NF closer to 1. Ideally, if the mechanical strength of both complexes is identical, the NF would be 0.5. The deviation from 0.5 in the case of the unmodified duplex against the reference of identical length and GC content can be attributed to the different positions of the GC pairs stabilizing the sequence more than AT pairs. The difference in the sequence is necessary to prevent for cross-hybridization. Additionally, the symmetry break due to the different surfaces to which the oligonucleotides are attached can play a role. The minor imbalance does not affect the result, as all samples are tested against the same reference and the effect thus cancels out.

The analysis is performed automatically using a customized LabView software which divides the original fluorescence images after background correction pixel-by-pixel according to the equation for NF and corrects for bleaching effects. The NF is then determined by fitting a Gaussian to the resulting histogram of counts.

AFM Sample Preparation

Samples for the measurement with the atomic force microscope were prepared with small changes as described previously [3]. In short, the oligonucelotides were immobilized on the amino-modified cantilever and glass surface (3-aminopropyldimethylethoxysilane; ABCR GmbH, Karlsruhe, Germany) at their 5'-termini *via* heterobifunctional NHS-PEG-Maleimide spacers (MW 5000; Rapp Polymere, Tübingen, Germany). The PEG was dissolved in a concentration of 25 mM in borate buffer at pH 8.5 and incubated for 1h. Possible disulfide bonds between oligonucleotides were reduced by TCEP incubation (Thermo Fisher Scientific, Bonn, Germany) and subsequent ethanol precipitation. The reduced DNA strands were incubated in concentrations of 5µM (surface) and 15 µM (cantilever) for 1h before a final washing step and storage in 1xPBS until use. For a parallel characterization of the individual unbinding forces in a single experiment, three distinct populations of the investigated DNA strands with propynyl modifications were incubated on one glass surface.

For all measurements, BL- AC40TS-C2 cantilevers (Olympus, Tokyo, Japan) were employed. The DNA oligomers were purchased including all modifications from biomers.net GmbH:

Cantilever Strand
SH - 5' - $(t)_{10}$ - tag gta gtg gag ttc aat cgg tga atc tat cag tcg tgg tgg tca gca g - 3' - **(Cy5)**
Surface Strands
(0P) SH - 5' - $(t)_{10}$ - ctg ctg a**(Cy3)**cc acc acg act gat aga ttc acc gat tga act c - 3'
(8P) SH - 5' - $(t)_{10}$ - ctg ctg a**(Cy3)**cc acc acg act gat aga ttc acc gat tga act c - 3'
(22P) SH - 5' - $(t)_{10}$ - ctg ctg a**(Cy3)**cc acc acg act gat aga ttc acc gat tga act c - 3'

AFM Measurement and Analysis

Single-molecule AFM experiments were carried out on a custom built atomic force microscope, controlled by an MFP-3D controller from Asylum Research (Santa Barbara, CA, USA), which provides ACD and DAC channels as well as a DSP board for setting up feedback loops. The protocol for data recording was executed by a custom written Igor Pro (Wave Metrics, Lake Oswego, USA) software and cantilever actuation in the z direction was performed by a LISA piezo-actuator (Physik Instrumente, Karlsruhe, Germany) driven by the AFM controller. During surface approach, an indentation force of typically around 180 pN was used. The conversion from photodiode voltages into force values was performed after cantilever spring constant calibration by the thermal method using the equipartition theorem [2]. A typical spring constant in the range of 100 pN/nm and a resonance frequency of 25 kHz were obtained. After each force-extension trace the probed surface was moved by an actuated x-y stage for 100 nm to expose the DNA anchor on the cantilever to a new binding partner.
The obtained data sets for each pulling speed typically showed a yield of about 10% to 25% specific interactions of a total of 68800 curves recorded. Curves were sorted to contain exclusively single peak events with a worm-like chain behavior. The loading rate for each peak was determined as a linear fit to the in force over time in the last 4 nm before a rupture event.
Importantly, to allow for direct comparability and exclude calibration effects, the data given here have been obtained with one single cantilever. However, further experiments have reproducibly shown that the most probable rupture force cannot be distinguished for different DNA modifications in AFM experiments.

Sample AFM force-distance curve

Force-distance curves of single-binding events display a behavior that allows to preselect them using the WLC model as a criterion. However, no information is deduced from this fit. The short persistence length of 0.1-0.5 nm is a general feature of DNA measurements with AFM and consistent with previous studies. It is dominated by the very short persistence length of the PEG linkers used to attach the oligonucleotides to cantilever and surface, as they are the longest components of the system, which are stretched.

AFM sample curve for 0P at cantilever retraction of 500 nm/s

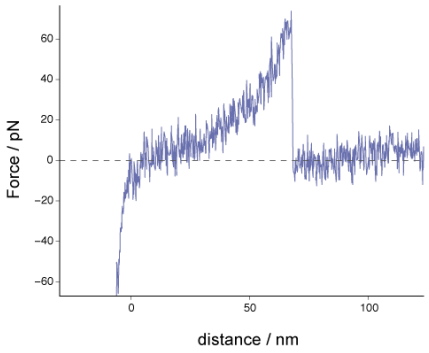

2. Supplementary Data

Force - Loading Rate Plots of AFM Measurements

The force-loading rate plots assembled below were fitted with an elliptical two-dimensional Gaussian to determine their respective population means and standard deviation for each retraction speed. As can be seen comparing the force-loading rate plots for 0P, 8P and 22P, the most probable rupture force for each retraction velocity are indistinguishable within error. Additionally, the rupture forces for the different retraction velocities for each variant display no significant loading rate dependence.

Force - Loading Rate Plot for 0P

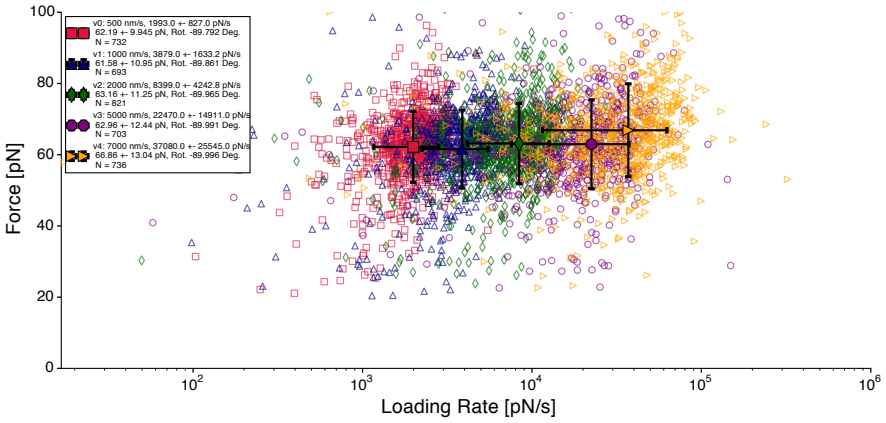

Force - Loading Rate Plot for 8P

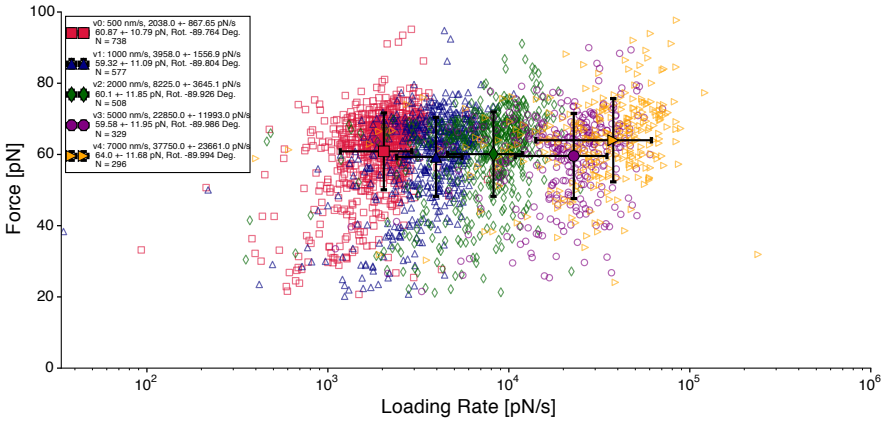

Force - Loading Rate Plot for 22P

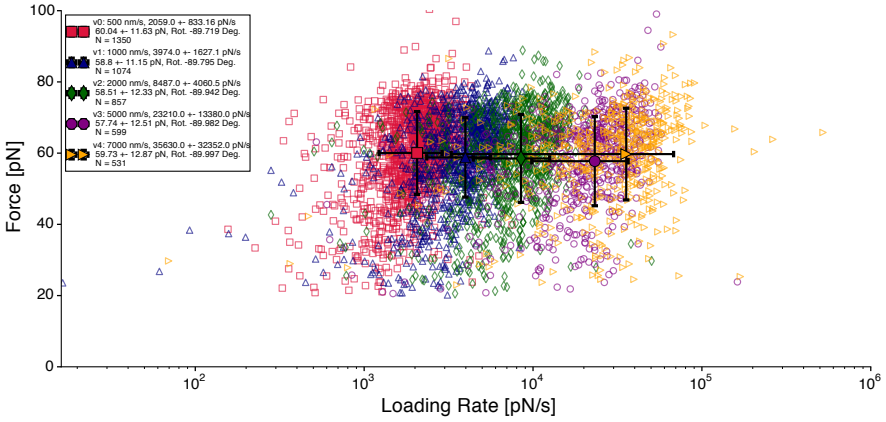

References

1. Severin PMD, Ho D, Gaub HE (2011) A high throughput molecular force assay for protein-DNA interactions. Lab Chip. pp. 856-862.
2. Hutter, J L, Bechhoefer, J (1993) Calibration of atomic-force microscope tips. Review of Scientific Instruments, *64*(7), pp. 1868-1873.

Bibliography

[1] Watson, J.D. and Crick, F.H. (1953). Molecular structure of nucleic acids; a structure for deoxyribose nucleic acid. *Nature*, **171**(4356), 737–8.

[2] Crick, F. (1958). On protein synthesis. *Symposia of the Society for Experimental Biology, The Biological Replication of Macromolecules*, pp. 138–163.

[3] Crick, F. (1970). Central dogma of molecular biology. *Nature*, **227**, 561–563.

[4] Blackstock, W. and Weir, M. (1999). Proteomics: quantitative and physical mapping of cellular proteins. *Trends in biotechnology*, **17**, 121–127.

[5] Werther, M. and Seitz, H., eds. (2008). *Protein-Protein Interaction*. Springer.

[6] Collas, P. (2010). The current state of chromatin immunoprecipitation. *Molecular biotechnology*, **47**, 87–100.

[7] Iioka, H., Loiselle, D., Haystead, T.A., and Macara, I.A. (2011). Efficient detection of RNA–protein interactions using tethered RNAs. *Nucleic Acids Res*, **39**(8), e53.

[8] Uetz, P., Giot, L., Cagney, G., Mansfield, T., Judson, R., *et al.* (2000). A comprehensive analysis of protein–protein interactions in Saccharomyces cerevisiae. *Nature*, **403**(6770), 623–7.

[9] Moffitt, J., Chemla, Y., Smith, S., and Bustamante, C. (2008). Recent advances in optical tweezers. *Annu. Rev. Biochem.*, **77**, 205–28.

[10] Binnig, G., Quate, C., and Gerber, C. (1986). Atomic force microscope. *Physical review letters*, **56**(9), 930–933.

[11] Florin, E., Moy, V., and Gaub, H. (1994). Adhesion forces between individual ligand-receptor pairs. *Science*, **264**(5157), 415–7.

[12] Moy, V.T., Florin, E.L., and Gaub, H.E. (1994). Intermolecular forces and energies between ligands and receptors. *Science*, **266**(5183), 257–9.

[13] Lin, S., Chen, J., Huang, L., and Lin, H. (2005). Measurements of the forces in protein interactions with atomic force microscopy. *Current Proteomics*, **2**, 55–81.

[14] Bujalowski, P. and Oberhauser, A. (2013). Tracking unfolding and refolding reactions of single proteins using atomic force microscopy methods. *Methods*, **60**(2), 151–160.

[15] Rief, M., Clausen-Schaumann, H., and Gaub, H.E. (1999). Sequence-dependent mechanics of single DNA molecules. *Nat Struct Biol*, **6**(4), 346–9.

[16] Morfill, J., Kühner, F., Blank, K., Lugmaier, R.A., Sedlmair, J., *et al.* (2007). B-S transition in short oligonucleotides. *Biophys J*, **93**(7), 2400–9.

[17] Albrecht, C., Blank, K., Lalic-Mülthaler, M., Hirler, S., Mai, T., *et al.* (2003). DNA: a programmable force sensor. *Science*, **301**(5631), 367–70.

[18] Ho, D., Dose, C., Albrecht, C.H., Severin, P., Falter, K., *et al.* (2009). Quantitative detection of small molecule/DNA complexes employing a force-based and label-free DNA-microarray. *Biophys J*, **96**(11), 4661–71.

[19] Severin, P.M.D. and Gaub, H.E. (2012). DNA-Protein Binding Force Chip. *Small*, **8**(21), 3269–3273.

[20] Mello, C. and Conte, D. (2004). Revealing the world of RNA interference. *Nature*, **431**(7006), 338–342.

[21] Lau, P., Guiley, K., De, N., Potter, C., Carragher, B., *et al.* (2012). The molecular architecture of human Dicer. *Nat Struct Mol Biol.*, **19**(4), 436–440.

[22] Friedman, J. and Jones, P. (2009). MicroRNAs: critical mediators of differentiation, development and disease. *Swiss medical weekly*, **139**(33–34), 446–472.

[23] Dietz, H. and Rief, M. (2006). Protein structure by mechanical triangulation. *Proc Natl Acad Sci USA*, **103**(5), 1244–7.

[24] Stephanopoulos, N. and Francis, M.B. (2011). Choosing an effective protein bioconjugation strategy. *Nat Chem Biol*, **7**(12), 876–84.

[25] Yin, J., Straight, P.D., McLoughlin, S.M., Zhou, Z., Lin, A.J., *et al.* (2005). Genetically encoded short peptide tag for versatile protein labeling by Sfp phosphopantetheinyl transferase. *Proc Natl Acad Sci USA*, **102**(44), 15815–20.

[26] Yin, J., Lin, A.J., Golan, D.E., and Walsh, C.T. (2006). Site-specific protein labeling by Sfp phosphopantetheinyl transferase. *Nat Protoc*, **1**(1), 280–5.

[27] Quadri, L.E., Weinreb, P.H., Lei, M., Nakano, M.M., Zuber, P., *et al.* (1998). Characterization of Sfp, a Bacillus subtilis phosphopantetheinyl transferase for peptidyl carrier protein domains in peptide synthetases. *Biochemistry*, **37**(6), 1585–95.

[28] Jongsma, M.A. and Litjens, R.H.G.M. (2006). Self-assembling protein arrays on DNA chips by auto-labeling fusion proteins with a single DNA address. *Proteomics*, **6**(9), 2650–5.

[29] Giot, L., Bader, J., Brouwer, C., Chaudhuri, A., Kuang, B., *et al.* (2003). A protein interaction map of Drosophila melanogaster. *Science*, **302**(5651), 1727–1736.

[30] Kirchhofer, A., Helma, J., Schmidthals, K., Frauer, C., Cui, S., *et al.* (2010). Modulation of protein properties in living cells using nanobodies. *Nat Struct Mol Biol*, **17**(1), 133–8.

[31] Dervan, P. and Edelson, B. (2003). Recognition of the DNA minor groove by pyrrole-imidazole polyamides. *Curr Opin Struct Biol*, **13**, 284–299.

[32] Froehler, B., Wadwani, S., Terhorst, T., and Gerrard, S. (1992). Oligodeoxynucleotides containing C-5 propyne analogs of 2-deoxyuridine and 2-deoxycytidine. *Tetrahedron letters*, **33**(37), 5307–5310.

[33] Leckband, D. (2000). Measuring the forces that control protein interactions. *Annu Rev Biophys Biomol Struct*, **29**, 1–26.

[34] Israelachvili, J.N. (2011). *Intermolecular and Surface Forces, 3rd edition.* Academic Press.

[35] Leckband, D. and Sivasankar, S. (1999). Forces controlling protein interactions: theory and experiment. *Colloids and surfaces B: Biointerfaces*, **14**, 83–97.

[36] Alberts, B., Johnson, A., Lewis, J., Raff, M., Roberts, K., *et al.* (2008). *Molecular Biology of the Cell, 5th edition. Extended version.* Garland Publishing.

[37] Seifert, C. and Gräter, F. (2013). Protein mechanics: How force regulates molecular function. *Biochimica et Biophysica Acta (BBA)-General Subjects*, **1830**(10), 4762–8.

[38] Vogel, V. and Sheetz, M. (2009). Cell fate regulation by coupling mechanical cycles to biochemical signaling pathways. *Current opinion in cell biology*, **21**, 38–46.

[39] Zhang, X., Halvorsen, K., Zhang, C.Z., Wong, W.P., and Springer, T.A. (2009). Mechanoenzymatic cleavage of the ultralarge vascular protein von Willebrand factor. *Science*, **324**(5932), 1330–4.

[40] Langenhan, T., Aust, G., and Hamann, J. (2013). Sticky signaling–adhesion class G protein-coupled receptors take the stage. *Science signaling*, **6**(276), re3.

[41] Kong, F., García, A.J., Mould, A.P., Humphries, M.J., and Zhu, C. (2009). Demonstration of catch bonds between an integrin and its ligand. *The Journal of Cell Biology*, **185**(7), 1275–84.

[42] Manibog, K., Li, H., Rakshit, S., and Sivasankar, S. (2014). Resolving the molecular mechanism of cadherin catch bond formation. *Nat Commun*, **5**, 3941.

[43] Sims, P. and Xie, X. (2009). Probing dynein and kinesin stepping with mechanical manipulation in a living cell. *Chemphyschem*, **10**(0), 1511–1516.

[44] Hinterdorfer, P. and Dufrêne, Y. (2006). Detection and localization of single molecular recognition events using atomic force microscopy. *Nature Methods*, **3**(5), 347–355.

[45] Allis, C.D., Jenuwein, T., and Reinberg, D., eds. (2009). *Epigenetics*. Cold Spring Harbor Laboratory Press.

[46] Limmer, K., Pippig, D.A., Aschenbrenner, D., and Gaub, H.E. (2014). A Force-Based, Parallel Assay for the Quantification of Protein-DNA Interactions. *PLoS ONE*, **9**(2), e89626.

[47] Limmer, K.M. (2013). *Analysis of DNA - ligand interaction in a parallel force-based assay*. Ph.D. thesis, Ludwig-Maximilians-Universität München.

[48] Rinn, J. and Ule, J. (2014). 'Oming in on RNA-protein interactions. *Genome Biol*, **15**(1), 401.

[49] Bloomfield, V.A., Crothers, D.M., and Tinoco, I. (2000). *Nucleic Acids - Structures, Properties, and Functions*. University Science Books.

[50] Stefl, R., Skrisovska, L., and Allain, F. (2005). RNA sequenceand shapedependent recognition by proteins in the ribonucleoprotein particle. *EMBO Rep*, **6**(1), 33–38.

[51] "The 2006 Nobel Prize in Physiology or Medicine - Advanced Information". Nobel Media AB 2014. Web. 22 Jan 2015. `http://www.nobelprize.org/nobel_prizes/medicine/laureates/2006/advanced.html`.

[52] Carthew, R.W. and Sontheimer, E.J. (2009). Origins and mechanisms of miRNAs and siRNAs. *Cell*, **136**(4), 642–655.

[53] Deiters, A. (2010). Small molecule modifiers of the microRNA and RNA interference pathway. *AAPS J*, **12**(1), 51–60.

[54] Bernstein, E., Caudy, A., Hammond, S., and Hannon, G. (2001). Role for a bidentate ribonuclease in the initiation step of RNA interference. *Nature*, **409**(6818), 363–6.

[55] Macrae, I.J., Zhou, K., Li, F., Repic, A., Brooks, A.N., *et al.* (2006). Structural basis for double-stranded RNA processing by Dicer. *Science*, **311**(5758), 195–8.

[56] Vermeulen, A., Behlen, L., Reynolds, A., Wolfson, A., Marshall, W.S., *et al.* (2005). The contributions of dsRNA structure to Dicer specificity and efficiency. *RNA*, **11**, 674–682.

[57] Nussinov, R. and Schreiber, G., eds. (2009). *Computational Protein-Protein Interactions*. CRC Press.

[58] Reichmann, D., Rahat, O., Cohen, M., Neuvirth, H., and Schreiber, G. (2007). The molecular architecture of protein-protein binding sites. *Curr Opin Struct Biol*, **17**(1), 67–76.

[59] Perkins, J.R., Diboun, I., Dessailly, B.H., Lees, J.G., and Orengo, C. (2010). Transient protein-protein interactions: structural, functional, and network properties. *Structure*, **18**(10), 1233–43.

[60] Dobson, C. (2002). Protein-misfolding diseases: getting out of shape. *Nature*, **418**(6899), 729–30.

[61] Gregersen, N., Bross, P., Vang, S., and Christensen, J.H. (2006). Protein misfolding and human disease. *Annu. Rev. Genomics Hum. Genet.*, **7**, 103–24.

[62] Stumpf, M.P.H., Thorne, T., de Silva, E., Stewart, R., An, H.J., *et al.* (2008). Estimating the size of the human interactome. *Proc Natl Acad Sci USA*, **105**(19), 6959–64.

[63] Schreiber, G. (2002). Kinetic studies of protein-protein interactions. *Curr Opin Struct Biol*, **12**(1), 41–7.

[64] Shoemaker, B.A. and Panchenko, A.R. (2007). Deciphering protein-protein interactions. Part I. Experimental techniques and databases. *PLoS Comput Biol*, **3**(3), e42.

[65] Zhu, H., Bilgin, M., and Snyder, M. (2003). Proteomics. *Annual review of biochemistry*, **72**, 783–812.

[66] Gerber, D., Maerkl, S.J., and Quake, S.R. (2009). An in vitro microfluidic approach to generating protein-interaction networks. *Nat Methods*, **6**(1), 71–4.

[67] Kornreich, M., Avinery, R., and Beck, R. (2013). Modern X-ray scattering studies of complex biological systems. *Current Opinion in Biotechnology*, **24**, 716–723.

[68] Truong, K. and Ikura, M. (2001). The use of FRET imaging microscopy to detect protein–protein interactions and protein conformational changes *in vivo*. *Curr Opin Struct Biol*, **11**, 573–578.

[69] Karlsson, R. (2004). SPR for molecular interaction analysis: a review of emerging application areas. *Journal of Molecular Recognition*, **17**, 151–161.

[70] Tsien, R. (1998). The green fluorescent protein. *Annual review of biochemistry*, **67**, 509–44.

[71] Pédelacq, J.D., Cabantous, S., Tran, T., Terwilliger, T.C., and Waldo, G.S. (2006). Engineering and characterization of a superfolder green fluorescent protein. *Nat Biotechnol*, **24**(1), 79–88.

[72] Heim, R., Cubitt, A., and Tsien, R. (1995). Improved green fluorescence. *Nature*, **373**(6516), 663–4.

[73] Rothbauer, U., Zolghadr, K., Muyldermans, S., Schepers, A., Cardoso, M.C., *et al.* (2008). A versatile nanotrap for biochemical and functional studies with fluorescent fusion proteins. *Mol Cell Proteomics*, **7**(2), 282–9.

[74] Tang, J.C.Y., Szikra, T., Kozorovitskiy, Y., Teixiera, M., Sabatini, B.L., *et al.* (2013). A nanobody-based system using fluorescent proteins as scaffolds for cell-specific gene manipulation. *Cell*, **154**(4), 928–39.

[75] Rothemund, P. (2006). Folding DNA to create nanoscale shapes and patterns. *Nature*, **440**(7082), 297–302.

[76] Winfree, E., Liu, F., Wenzler, L., and Seeman, N. (1998). Design and self-assembly of two-dimensional DNA crystals. *Nature*, **394**(6693), 539–544.

[77] Schreiber, R., Do, J., Roller, E., Zhang, T., Schüller, V., *et al.* (2013). Hierarchical assembly of metal nanoparticles, quantum dots and organic dyes using DNA origami scaffolds. *Nat Nanotechnol*, **9**(1), 74–78.

[78] Ke, Y., Ong, L.L., Shih, W.M., and Yin, P. (2012). Three-dimensional structures self-assembled from DNA bricks. *Science*, **338**(6111), 1177–83.

[79] Krishnan, Y. and Simmel, F. (2011). Nucleic acid based molecular devices. *Angewandte Chemie International Edition*, **50**, 3124–3156.

[80] Chemical structure of DNA. `http://en.wikipedia.org/wiki/DNA`.

[81] Yakovchuk, P., Protozanova, E., and Frank-Kamenetskii, M.D. (2006). Base-stacking and base-pairing contributions into thermal stability of the DNA double helix. *Nucleic Acids Res*, **34**(2), 564–74.

[82] Leontis, N.B., Stombaugh, J., and Westhof, E. (2002). The non-Watson-Crick base pairs and their associated isostericity matrices. *Nucleic Acids Res*, **30**(16), 3497–531.

[83] Strunz, T., Oroszlan, K., Schäfer, R., and Güntherodt, H.J. (1999). Dynamic force spectroscopy of single DNA molecules. *Proc. Natl. Acad. Sci.*, **96**, 11277–82.

[84] Albrecht, C.H., Neuert, G., Lugmaier, R.A., and Gaub, H.E. (2008). Molecular force balance measurements reveal that double-stranded DNA unbinds under force in rate-dependent pathways. *Biophys J*, **94**(12), 4766–74.

[85] Kufer, S., Puchner, E., Gumpp, H., Liedl, T., and Gaub, H. (2008). Single-molecule cut-and-paste surface assembly. *Science*, **319**(5863), 594–6.

[86] Strackharn, M., Pippig, D.A., Meyer, P., Stahl, S.W., and Gaub, H.E. (2012). Nanoscale arrangement of proteins by single-molecule cut-and-paste. *Journal of the American Chemical Society*, **134**(37), 15193–6.

[87] Lefebvre, A., Mauffret, O., Antri, S., Monnot, M., Lescot, E., *et al.* (1995). Sequence dependent effects of CpG cytosine methylation. *Eur. J. Biochem.*, **229**, 445–454.

[88] Severin, P., Zou, X., Gaub, H., and Schulten, K. (2011). Cytosine methylation alters DNA mechanical properties. *Nucleic Acids Res*, **39**(20), 8740–8751.

[89] Shen, L., Siwkowski, A., Wancewicz, E., Lesnik, E., Butler, M., *et al.* (2003). Evaluation of C-5 propynyl pyrimidine-containing oligonucleotides in vitro and in vivo. *Antisense and Nucleic Acid Drug Development*, **13**, 129–142.

[90] Terrazas, M. and Kool, E. (2009). RNA major groove modifications improve siRNA stability and biological activity. *Nucleic acids research*, **37**(2), 346–353.

[91] Graham, D., Parkinson, J., and Brown, T. (1998). DNA duplexes stabilized by modified monomer residues: synthesis and stability. *Journal of the Chemical Society*, **1**, 1131–1138.

[92] Wiegand, G., Neumaier, K.R., and Sackmann, E. (1998). Microinterferometry: Three-Dimensional Reconstruction of Surface Microtopography for Thin-Film and Wetting Studies by Reflection Interference Contrast Microscopy (RICM). *Appl Opt*, **37**(29), 6892–905.

[93] Severin, P.M.D., Ho, D., and Gaub, H.E. (2011). A high throughput molecular force assay for protein-DNA interactions. *Lab Chip*, **11**(5), 856–62.

[94] Limmer, K., Aschenbrenner, D., and Gaub, H. (2013). Sequence-specific inhibition of Dicer measured with a force-based microarray for RNA ligands. *Nucleic Acids Res*, **41**(6), e69.

[95] Merkel, R., Nassoy, P., Leung, A., Ritchie, K., and Evans, E. (1999). Energy landscapes of receptor–ligand bonds explored with dynamic force spectroscopy. *Nature*, **397**(6714), 50–53.

[96] Otten, M., Wolf, P., and Gaub, H.E. (2013). Protein-DNA force assay in a microfluidic format. *Lab Chip*, **13**(21), 4198–4204.

[97] Wienken, U. and Gaub, H. (2013). Stamping Vital Cells–a Force-Based Ligand Receptor Assay. *Biophys J*, **105**, 2687–2694.

[98] Aschenbrenner, D., Pippig, D., Klamecka, K., Limmer, K., Leonhardt, H., *et al.* (2014). Parallel Force Assay for Protein-Protein Interactions. *PLoS ONE*, **9**(12), e115049.

[99] Hutter, J. and Bechhoefer, J. (1993). Calibration of atomicforce microscope tips. *Review of Scientific Instruments*, **64**(7), 1868–1873.

[100] Butt, H., Cappella, B., and Kappl, M. (2005). Force measurements with the atomic force microscope: Technique, interpretation and applications. *Surface science reports*, **59**, 1–152.

[101] Viani, M., Schäffer, T., Chand, A., and Rief, M. (1999). Small cantilevers for force spectroscopy of single molecules. *Journal of Applied Physics*, **86**(4), 2258–2262.

[102] Recht, M., Fourmy, D., and Blanchard, S. (1996). RNA sequence determinants for aminoglycoside binding to an A-site rRNA model oligonucleotide. *J. Mol. Biol*, **262**, 421–436.

[103] Anderson, P.C. and Mecozzi, S. (2007). Minimum sequence requirements for the binding of paromomycin to the rRNA decoding site A. *Biopolymers*, **86**(2), 95–111.

[104] Pippig, D.A., Baumann, F., Strackharn, M., Aschenbrenner, D., and Gaub, H.E. (2014). Protein-DNA Chimeras for Nano Assembly. *ACS Nano*, **8**(7), 6551–6555.

[105] Schaeffer, P. and Dixon, N. (2009). Synthesis and applications of covalent protein-DNA conjugates. *Australian journal of chemistry*, **62**(10), 1328–1332.

[106] Bauer, D., Rogge, A., Stolzer, L., Barner-Kowollik, C., and Fruk, L. (2013). Light induced DNA–protein conjugation. *Chem. Commun.*, **49**, 8626–8628.

[107] Rosen, C., Kodal, A., Nielsen, J., Schaffert, D., Scavenius, C., *et al.* (2014). Template-directed covalent conjugation of DNA to native antibodies, transferrin and other metal-binding proteins. *Nature Chemistry*, **6**(9), 804–9.

[108] Otten, M., Ott, W., Jobst, M., Milles, L., Verdorfer, T., *et al.* (2014). From genes to protein mechanics on a chip. *Nature Methods*, **11**(11), 1127–1130.

[109] Baird-Titus, J.M., Clark-Baldwin, K., Dave, V., Caperelli, C.A., Ma, J., *et al.* (2006). The solution structure of the native K50 Bicoid homeodomain bound to the consensus TAATCC DNA-binding site. *Journal of molecular biology*, **356**(5), 1137–51.

[110] Rajendran, A., Endo, M., Katsuda, Y., Hidaka, K., and Sugiyama, H. (2011). Photo-cross-linking-assisted thermal stability of DNA origami structures and its application for higher-temperature self-assembly. *Journal of the American Chemical Society*, **133**(37), 14488–91.

[111] Sobczak, J., Martin, T., Gerling, T., and Dietz, H. (2012). Rapid folding of DNA into nanoscale shapes at constant temperature. *Science*, **338**(6113), 1458–61.

[112] Maerkl, S.J. and Quake, S.R. (2007). A systems approach to measuring the binding energy landscapes of transcription factors. *Science*, **315**(5809), 233–7.

[113] Maerkl, S.J. (2011). Next generation microfluidic platforms for high-throughput protein biochemistry. *Current Opinion in Biotechnology*, **22**(1), 59–65.

[114] Otten, M. (2014). *Microfluidic & microrheological studies of protein interactions at the single–molecule & single–cell level.* Ph.D. thesis, Ludwig-Maximilians-Universität München.

List of Figures

Lebenslauf

Daniela Solveig Raphaela Aschenbrenner

Danksagung

An dieser Stelle möchte ich mich ganz herzlich für die großartige Unterstützung bedanken, die ich in den letzten Jahren von meinen Kollegen, meinen Freunden und meiner Familie bekommen habe.

Mein besonderer Dank gilt

- meinem Doktorvater **Prof. Hermann Gaub** für viele motivierende und inspirierende Diskussionen, seine stete Unterstützung sowie die phantastische Atmosphäre an seinem Lehrstuhl. Und für seine unvergleichlichen Spaghetti vongole.
- **Prof. Jan Lipfert** für sein stets offenes Ohr und die tolle Motivation auf den letzten Metern.
- **Dr. Katja Limmer**, die mich vom allerersten bis zum allerletzten Tag meiner Arbeit begleitet und unterstützt hat. Danke für unsere tolle Zusammenarbeit, unsere Teestunden, die intensiven Gespräche und vor allem unsere Freundschaft!
- **Dr. Marc Otten** für all die Stemplerrunden, Opernbesuche und interessanten Gespräche, nicht nur über die Physik! Vor allem auch für seine große Hilfe bei der übersichtlichen Darstellung wissenschaftlicher Zusammenhänge.
- meinen Vorgängern und Mitstreitern bei den Stemplern: **Dr. Philip Severin**, **Dr. Uta Wienken** und **Anita Ladenburger**.
- **Dr. Diana Pippig** für ihre unendliche Geduld mir Fragen im Chemielabor zu beantworten, ihre phantastischen Kuchen und die gemeinsamen Projekte!
- **Kamila Klamecka**, **Fabian Baumann** und **Lukas Milles** für ihre Hilfsbereitschaft bei unseren gemeinsamen Projekten und die tolle Zusammenarbeit bei den Papern.
- meinen Lieblingsjungs im Büro: **Philipp Walker**, **Jacques Scheller**, **Thomas Zettel** und **Jürgen Kreiter**.

- **Constantin Schöler** für seine Hilfe, wann immer ich meinen Computer am liebsten aus dem Fenster geworfen hätte.
- **Katy Ehrlich** für ihre Hilfsbereitschaft bei jeder Frage zur englischen Sprache!
- **Angelika Kardinal** und **Thomas Nikolaus** für all die Unterstützung im Chemielabor.
- **Dr. Christopher Deck** von biomers.net, für die großartige Hilfe bei der Auswahl und Synthese von speziellen DNA Oligonucleotiden.
- **meinen Freunden**, die in den letzten Jahren mehrfach bewiesen haben, dass sie immer für mich da sind. Ihr seid die Besten!
- meinen "Fast-Schwiegereltern" **Hermann** und **Christine Drube** für die nordhessischen Care-Pakete, die mich die letzen Monate bei Laune gehalten haben.
- min kjære **Mormor**, som hadde alltid tro på meg.
- meiner Schwester **Stephanie Aschenbrenner** und meinen Eltern **Reidun** und **Max Aschenbrenner** für ihre liebevolle Unterstützung in allen Lebenslagen. Kjempe glad i dere!
- meinem Verlobten **Dr. Fabian Drube** für seine unendliche Geduld, Wärme und Zuversicht. Ganz besonders dafür, dass ich mich immer auf ihn verlassen kann. Wir haben es geschafft!

Ich versichere, diese Arbeit selbstständig angefertigt und dazu nur die im Literaturverzeichnis angegebenen Quellen benutzt zu haben.

München, den 4. März 2015